VERIFICATION OF HARDWARE-IN-THE-LOOP AS A VALID TESTING METHOD FOR SUSPENSION DEVELOPMENT

by

WERNER EKHARD MISSELHORN

Submitted in partial fulfilment of the requirements for the degree

MASTER OF ENGINEERING
(Mechanical Engineering)

in the

Faculty of Engineering, Built Environment and Information Technology

University of Pretoria

1 November 2004

Abstract

Title: Verification of hardware-in-the-loop as a valid testing method for suspension development

Student: Werner Ekhard Misselhorn
Study leader: Prof. N.J. Theron
Co-Leader: Mr. P.S. Els
Degree: Master of Engineering

A need for a cost effective, versatile and easy to use suspension component testing method has arisen, following the development of a four-state hydro-pneumatic semi-active spring-damper system. A method known as hardware-in-the-loop (HiL) was investigated, in particular its use and compatibility with tests involving physical systems – previously HiL was used predominantly for Electronic Control Unit (ECU) testing. The suitability of HiL in the development of advanced suspension systems and their control systems, during which various vehicle models can be used, was determined.

A first step in vehicle suspension design is estimating a desired spring and damper characteristic, and verifying that characteristic using software simulation. The models used during this step are usually low-order, simple models, which hampers quick development progress. To predict vehicle response before vehicle prototype completion, many researchers have attempted to use complex and advanced damper models to simulate the vehicle's dynamics, but these models all suffer from some drawback – it is either based on empirical data, giving no indication of the physical parameters of the design sought; it may be overly complex, having many parameters and thus rendering software impractical; or it may be quick but based on the premise that there is no hysteresis in the damping character.

It can be seen that an obvious answer exists – use a physical commercially available or prototype damper in the software simulation instead of the mathematical model. In this way the suspension deflection, i.e. the true motion of the damper is used as excitation, and the true damper force is measured using a hydraulic actuator and load cell. The vehicle mass motions are simulated in a software environment. This is basically what HiL simulation does.

The HiL method was verified by comparing HiL simulations and tests to globally accepted testing methods, employing widely-used vehicle models: linear single-degree-of-freedom (SDOF) and two-degrees-of-freedom (2DOF) or quarter-car models were used. The HiL method was also compared to a non-linear physical system to verify that the method holds for real vehicle suspension geometries. This meant that HiL had to perform adequately at both ends of the suspension-testing spectrum – base software and real system simulation.

The comparison of the HiL and software/real system simulation was done using the "Error Coefficient of Variance" (ECOV) between the compared signals; this quantitative measure proved very sensitive and performed dubiously in the presence of signal offsets, phase lags and scaling errors, but remains a tangible, measurable parameter with which to compare signals. Visual confirmation was also obtained to back the ECOV values.

It was found that even using a relatively low-force actuator, the HiL simulation results followed the software/real system responses well. Phase lags and DC offsets in the HiL simulation's measured signals (as well as the real systems responses) has an adverse effect on the performance of the HiL simulation. Special attention must thus be paid to the zeroing of equipment and the amount/type of filters in the system, as these affect the HiL results dramatically. In all, HiL was proven to be a versatile and easy to use alternative to conventional mass-based suspension testing.

Keywords: hardware-in-the-loop, suspension design, SDOF, 2DOF, ECOV, non-linear physical system, phase lags, DC offsets, filters, mass-based suspension testing

Opsomming

Titel: Verifikasie van hardeware-geïntegreerde simulasie as juiste toetsmetode vir gebruik in suspensiestelselontwikkeling

Student: Werner Ekhard Misselhorn
Studieleier: Prof. N.J. Theron
Mede-leier: Mnr. P.S. Els
Graad: Meester van Ingenieurswese

Met die ontwikkeling van ‘n vier-toestand, hidro-pneumatiese semi-aktiewe veer-demper stelsel, het daar ‘n behoefte ontstaan vir ‘n goedkoop, veelsydige en gebruikersvriendelike veerstelsel toetsmetode. ‘n Hardeware-geïntegreerde simulasie metode (Engels: Hardware-in-the-loop) is ondersoek, spesifiek in terme van die gebruik en aanpasbaarheid met die simulasie van meganiese stelsels – die metode is alreeds gebruik vir die toets van elektroniese beheereenhede. Die toepaslikheid van hardeware-geïntegreerde simulasie in die ontwikkeling van gevorderde veerstelsels en hul beheerstelsels, waartydens verskeie voertuigmodelle gebruik word, is bepaal.

Die eerste stap in suspensieontwerp is om die gewensde veer en demper karakteristieke te bepaal, en dit te verifieer deur sagtewaresimulasies. Hierdie wiskundige modelle is gewoonlik eenvoudige lae-orde modelle, wat verdere ontwikkeling kortwiek. Ten einde voertuigdinamika te voorspel, voordat ‘n voertuig prototipe beskikbaar is, het verskeie navorsers al probeer om gevorderde, komplekse dempermodelle te gebruik tydens simulasie. Hierdie modelle het egter nadele. Van hulle is gebaseer op eksperimentele data, en gee geen aanduiding van die fisiese aard van die demper ontwerp nie. Die meerderheid modelle is te ingewikkeld, en het te veel veranderlikes. Gebruik in ‘n simulasie-omgewing is dus onprakties. Van die modelle is maklik en vinnig om te implementeer, maar werk op ‘n aanname van geen histerese in die demper karakteristiek.

‘n Voor-die-hand-liggende oplossing bestaan egter – ‘n komersieel beskikbare of prototipe demper kan in die simulasie gebruik word, in plaas van die wiskundige demper model. Die demper se snelheid word as insetsein gegee, terwyl die ware demperkrag gemeet word wanneer ‘n hidrouliese aktueerder en lassel gebruik word. Die voertuig se beweging word in ‘n sagteware-omgewing gesimuleer. Hardeware-geïntegreerde simulasie berus hierop.

Die hardeware-geïntegreerde metode is geverifieer deur dit te vergelyk met algemeen-aanvaarde toetsmetodes, waartydens verskeie algemene voertuigmodelle gebruik is: lineêre enkelvryheidsgraad en tweevryheidsgraad (kwart-voertuig) modelle is gebruik. Die metode is ook vergelyk met ‘n werklike, fisiese stelsel om te bevestig dat die metode geldig is vir werklike voertuig veerstelseluitlegte. Dit beteken dat die hardeware-geïntegreerde simulasie metode goed genoeg moes presteer aan beide kante van die spektrum – basiese sagteware simulasies en werklike stelsel bewegings.

Die vergelyking tussen die hardeware-geïntegreerde simulasie en die sagteware simulasie is getref met behulp van ‘n foutskattingsvergelyking, genoem die ECOV (vanaf Engels: “Error Coefficient of Variance”). Die kwantitatiewe vergelyking blyk baie sensitief te wees wanneer skaalverskille, faseverskuiwings en nulpuntverskille teenwoordig is, maar dit verskaf tog ‘n duidelike, meetbare waarde waarmee data vergelyk kan word. Visuele vergelykings is ook gemaak om die ECOV waardes mee te staaf.

Daar is gevind dat hardeware-geïntegreerde simulasie die sagteware/werklike beweging goed volg, selfs al is ‘n relatief lae-krag aktueerder gebruik. Fase skuiwings en nulpuntverskille het ‘n nadelige uitwerking op die metode se resultate, en klem moet gelê word op die verwysingsvlakke en seinfilters in die stelsel. Daar is bewys dat hardeware-geïntegreerde veringstoetse ‘n veelsydige en maklik bruikbare alternatief is vir die konvensionele massa-gebaseerde suspensietoetse.

Sleutelwoorde: hardeware-geïntegreerde simulasie, suspensieontwerp, enkelvryheidsgraad, tweevryheidsgraad, ECOV, fisiese stelsel, fase skuiwings, verwysingsvlakke, seinfilters, massa-gebaseerde suspensietoetse

Table of Contents:

List of Tables

List of Figures

List of Abbreviations

2DOF	-	Two-degrees-of-freedom
A/D	-	Analogue-to-Digital
AAC	-	ARMARKOV Adaptive Controller
ABS	-	Automatic Braking System
ARMARKOV	-	Auto-Regressive Markov
AYC	-	Active Yaw Control
CAE	-	Computer Aided Engineering
CDAS	-	Continuous Data Acquisition System
CPU	-	Central Processing Unit
D/A	-	Digital-to-Analogue
DC	-	Direct Current
DEC Alpha	-	Digital Electronics Company, Alpha processor model
DOF	-	Degree(s) of Freedom
DSC	-	Direct Stability Control
DSK	-	DSP Starter Kit
DSP	-	Digital Signal Processor
DYC	-	Direct Yaw Control
ECOV	-	Error Coefficient of Variance
ECU	-	Electronic Control Unit
EMP	-	Electro-Magnetic Pulse
ER	-	Electro-Rheological
ERM	-	Electro-Rheological Magnetic
FFT	-	Fast Fourier Transform
FLOPS	-	Floating Point Operations Per Second
HBM	-	Hottinger-Baldwin-Messtechnik
HiL	-	Hardware-in-the-Loop
I/O	-	Input/Output
ISA	-	Industry Standard Association
LVDT	-	Linear Variable Differential Transformer
MDOF	-	Multiple-degrees-of-freedom
MIMO	-	Multiple Input Multiple Output
MR	-	Magneto-Rheological
MSC.ADAMS	-	Dynamic modelling software by McNeil-Schwendler Corporation

NEWEUL	-	Euler-equations based dynamic modelling software
NI	-	National Instruments
ODE	-	Ordinary Differential Equations
ODE45	-	ODE solver function utilised in MatLab
OS or OS9	-	Operating System; OS9 refers to OS version 9
PC	-	Personal Computer
PID	-	Proportional-Integral-Derivative
PSD	-	Power Spectral Density
PWM	-	Pulse Width Modulation
RAM	-	Random Access Memory
RCP	-	Rapid Control Prototyping
RMS	-	Root Mean Square
RTW	-	Real-Time Workshop
SDOF	-	Single-degree-of-freedom
SDRAM	-	Synchronous Dynamic Random Access Memory
SISO	-	Single Input Single Output
SL	-	Simulink
SM	-	Spring-Mass
SMD	-	Spring-Mass-Damper
TI	-	Texas Instruments
UAV	-	Unmanned Aerial Vehicle
UP	-	University of Pretoria

List of Symbols

α	-	Angular Acceleration / Exponent / Phase Shift
A	-	Amplitude
$a,\ \ddot{x}$	-	Acceleration
C, c	-	Damping Coefficient
δ	-	Logarithmic Decrement
d	-	Distance
Err	-	Error
F	-	Force
f	-	Function
θ	-	Angular Displacement
G	-	Transfer Function
γ	-	Wave Number
g	-	Gravity Acceleration Constant
η	-	Dimensionless Exponent
κ	-	Roughness Coefficient
K, k	-	Spring Stiffness Coefficient
l	-	Length
m	-	Mass
M	-	Moment(s)
M, F, G	-	Coefficients used in Equations of Motion
p	-	Parameters
S	-	PSD Function
s	-	Laplace Operator
S_1, U_1	-	Coefficients used for Simulink Model
t	-	Time
$v,\ \dot{x}$	-	Velocity
Ω	-	Spatial Frequency [radians/m]
w	-	Wave Number
ω	-	Rotational Velocity
W	-	Weight
x, y	-	Displacement

X	-	Laplace Transform of "x"
ζ	-	Damping Ratio

List of Subscripts

0	-	Initial or Reference
a	-	Sprung Mass
ave	-	Average
b	-	Unsprung Mass
c	-	Damping
cg	-	Centre of Gravity
com	-	Centre of Mass
cs	-	Transducer Cable
d	-	Damper
i, j	-	Counters
k	-	Stiffness
n	-	Natural
r	-	Road
s	-	Spring / Sprung
sd	-	Spring-Damper Unit
sp	-	Road Roughness
su	-	Swingarm
t	-	Tyre
u	-	Unsprung
w, wm	-	Wall-mount
ζ	-	Ground Roughness

1. Introduction

Suspension systems have been in use since before the invention of the internal combustion engine. These first suspensions consisted primarily of springs, as the leaf springs found on horse-drawn carts, or employed a system whereby a cabin was suspended between two posts. With the advent of the automobile, suspension systems became increasingly important, and also increasingly complex. This was necessary, as the evolution of the other automotive technologies (especially those related to speed and performance) called for the suspension to evolve as well.

There exists a classic paradox when one considers the task of the primary suspension – on the one hand, one wishes to have a "soft ride" (comfortable) so that the trip one undertakes will be as comfortable as possible, and so that the occupants and the vehicle itself aren't overly fatigued. On the other hand, a "hard ride" (good handling) is also required so that the wheels stay in contact with the ground during extreme manoeuvres, increasing the handling and safety characteristics of the vehicle. These two ride characteristics stand in direct contrast to each other, particularly when considering a suspension system utilising only passive elements, because a "soft ride" is realised by using a damper with a relatively low damping coefficient; a "hard ride" is implemented with the aid of a damper having a relatively large damping coefficient. Since both coefficients aren't realisable simultaneously, damper manufacturers usually make a compromise. The springs also play a role in the ride quality of a vehicle – springs with relatively high spring rates provide good handling but a harsh ride, and thus discomfort. On the other hand, springs with a relatively low stiffness coefficient provide good ride comfort, but inferior handling.

Dampers are usually the complex part of a suspension package – springs are easier to design, model and manufacture, and their behaviour is easier to predict. There exist some systems employing devices that act as spring-damper combinations, using air and oil. The spring elements of a suspension system can be implemented in a variety of ways – as coil springs, leaf springs, torsion bars, or rubber bushings that include damping. The spring rate and linearity of the spring characteristic can be determined in various ways. The material, amount and thickness of the coils and the end finish of coil springs are the main elements determining a coil spring's characteristics. Likewise, the amount, thickness, length, and material used in leaf springs, as well as the leaf blade configuration, determines leaf spring characteristics.

From the above discussion one can begin to get an idea of the importance of good damper design. Suspension design is also a continuous process – it involves iterative processes, testing and improvements. It would stand to reason, then, that a quick and cost effective method to develop and test dampers with, to develop variable damper control systems on, and to predict vehicle behaviour with, will be of great importance to any party interested in designing and manufacturing dampers.

In this introduction an overview will be given of different types of dampers used in vehicles, factors that affect their performance, and how said performance is quantified. A literature study was also undertaken, and findings will be discussed in this chapter. This includes a study of work done using hardware-in-the-loop, deriving mathematical damper models, and testing methods used by other authors.

The hardware used in this study will also be discussed in this chapter. This will include an overview of the control and measuring equipment used and the actuator-controller hardware employed in the test setup.

1.1. Hardware-in-the-Loop as a Design Tool

It is stated that a quick, easy method for developing suspension components is necessary. **Such a method is the subject of this thesis – the verification of hardware-in-the-loop as an easy to use, reliable, repeatable, quick and cost effective method of suspension testing.** This method incorporates physical hardware

into a mathematical model for testing; thus a possibly complicated model of the component's behaviour is not needed as the hardware itself is used in the test. It will be discussed in more detail at a later stage.

1.2. Damper Designs and What Makes Them Work

Dampers or shock absorbers are coupled with spring elements in suspension systems, each with its own task. While springs are energy-storage devices, dampers are energy-dissipating devices. Simply, this can be described in the following way. Springs ensure that a reasonable ride height is maintained and that some energy due to wheel motion (the unsprung mass) caused by road disturbances is stored so that a return to equilibrium is achieved without much delay. Dampers, on the other hand, tend to dissipate the energy stored by unsprung mass motion, so that the velocity component of the wheel (the unsprung mass), normal to the road, as well as that of the vehicle body (the sprung mass) are returned to zero.

While there are various types of dampers, there are also different configurations. Most notably, dampers have either a linear motion character or a rotary motion character. The most common, as used on almost all automobiles, is the linear motion damper, whereby the damper unit is placed between the unsprung and sprung masses, and shortens and lengthens with wheel and body motion. Rotary dampers are either placed directly at the hinge connecting the suspension swing arm to the chassis, or on the body connected to the unsprung mass with some structure. Three mounting configurations are shown in Figure 1-1.

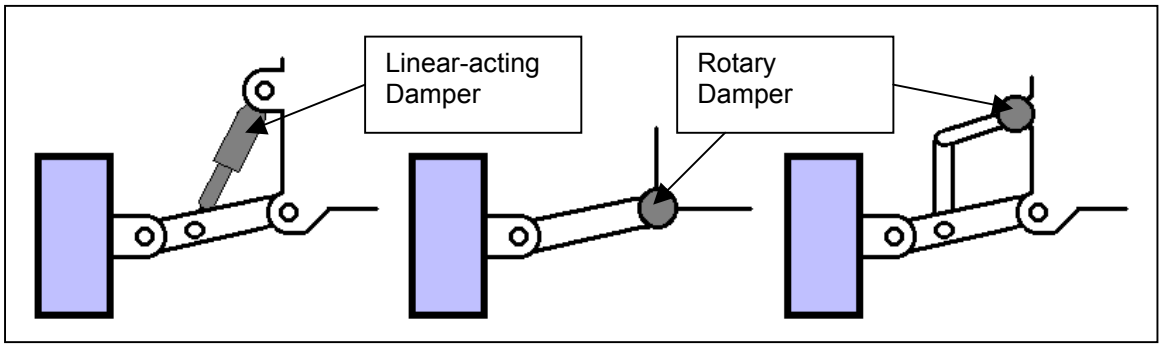

Figure 1-1: Different damper configurations

Some of the main types of damper designs will be discussed in the next section. These dampers are predominantly employed in the primary suspension systems of vehicles (connecting the sprung and unsprung masses) but some can be found in other suspension applications such as load bed dampers, seismic damping and seat suspensions.

1.2.1. Passive Dampers

Passive dampers are dampers that have fixed characteristics and architectures. That is, the damper is for most part a sealed unit that has no external input to change its characteristics with. Some passive dampers have different settings, changeable through mechanical manipulation of the damper when it is not in use, therefore considered passive.

1.2.2. Mono Tube Passive Damper

As the name implies, the outer wall of this damper consists of a single tube, containing the inner workings in a single tubular space, as shown in Figure 1-2. The working of the mono tube damper is straightforward. During compression, oil is forced from the compression chamber, through the valves in the piston, into the rebound chamber. The friction caused by the oil flowing through the valve restriction, i.e. viscous losses, dissipates energy. The gas volume is there to account for the volume change of oil, because the rod causes a smaller volume change in the rebound

chamber than in the compression chamber. This gas volume adds to the non-linear nature of dampers, because the dividing piston (also called a floating piston) may move downward with little resistance if the gas pressure is too low, causing a vacuum in the rebound chamber during compression. A drawback of this design is the possibility that some gas (usually nitrogen) may leak into the compression chamber, increasing the non-linearity due to gas flow, solubility and foaming.

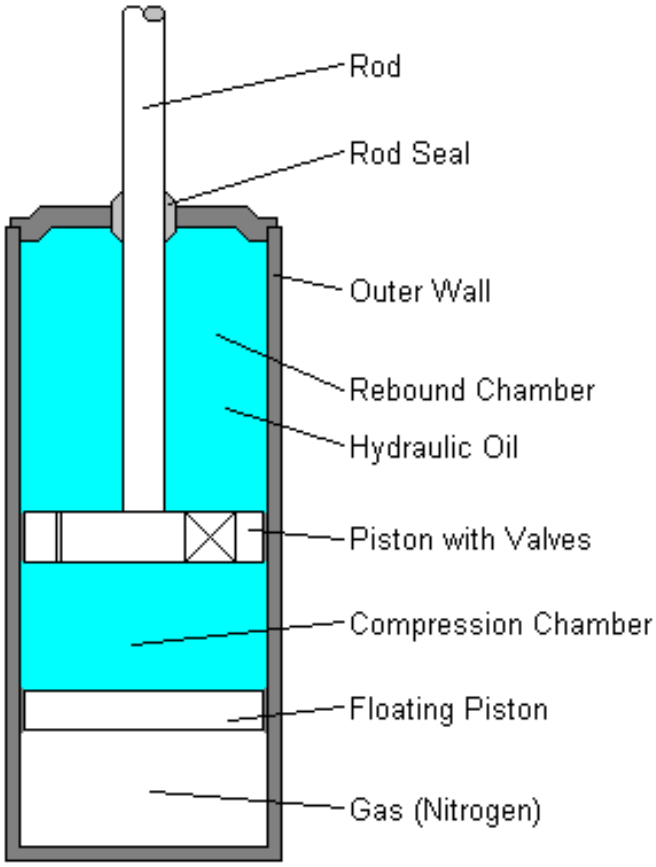

Figure 1-2: Schematic of a mono tube damper

1.2.3. Dual Tube Passive Damper

The dual tube passive damper operates in much the same way as the mono tube damper, but it has a different architecture. In this scheme, oil flows through the piston valves and the bottom valves during compression and rebound, as the volume-compensating gas is stored in the outer tubular cavity surrounding the inner tube. The schematic is shown in Figure 1-3.

This configuration has the advantage that there is no seal required between the gas and oil volumes while the damper is operated in an upright fashion. The obvious drawback is that it cannot be operated at large lean angles, precisely because there is no seal. It is also more complex than an equivalent mono tube damper, increasing its development and manufacturing cost.

The volume of oil displaced during compression and rebound is the same as the volume change in the rebound chamber. Since this volume change is dependent on the piston size, rod diameter and damper motion, mono tube, dual tube and quad tube dampers can all displace the same volume of oil during operation if designed to do so. The volume of oil displaced influences the sensitivity of the damper.

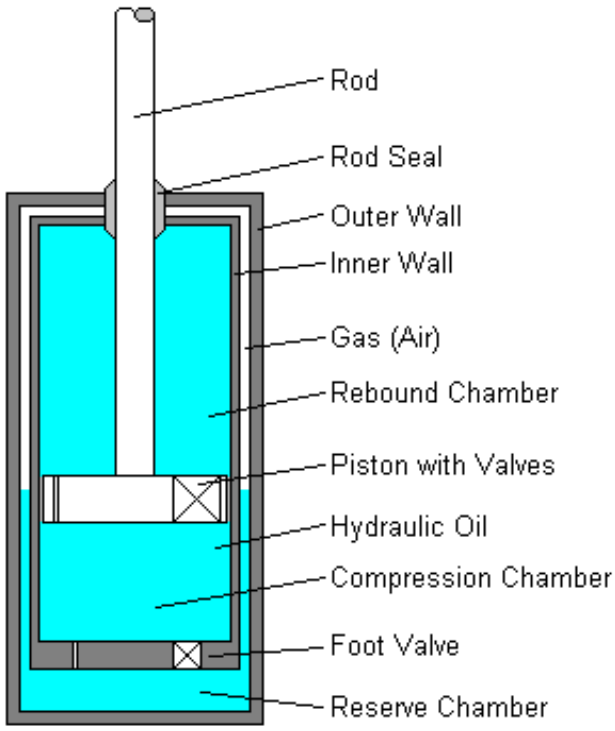

Figure 1-3: Schematic of a dual tube damper

1.2.4. Motorcycle Damper

Motorcycle dampers are usually mono tube passive dampers, but with two major differences in comparison to conventional mono tube dampers. Firstly, the valve architecture is set up in such a way that the compression force is as small as possible, that is, the compression-damping coefficient is close to zero. This is so that the motorcycle wheel can move out of the way quickly when an obstacle is encountered (to minimise the chance of the rider being thrown off due to sudden upward acceleration), and prevents the wheel from being damaged. Rebound damping is normal and dissipates energy. The second difference is that due to the nature of motorcycle design, its operation and accessibility of the damper, many motorcycle dampers are adjustable. This is done by changing the gas volume/pressure inside the damper with the aid of some small external reservoir, as shown in Figure 1-4.

Figure 1-4: A CAD drawing of a racing motorcycle suspension unit developed for a Suzuki GSXR-600

An example of the characteristic of a motorcycle damper is shown in Figure 1-7 when the characteristic diagram of a damper is discussed.

One drawback of the mono tube nature of the motorcycle damper (or any mono tube damper, for that matter) is that it has a severe lockup failure mode when an object like a stone damages its outer wall. This failure mode is not as prevalent in dual tube dampers.

1.2.5. Valve Architecture and Influences

The characteristic of a passive damper is mainly attributable to the architecture and parameters of the valves in the piston, and the valves separating the compression and reserve chambers in dual-tube dampers. The valves and restrictions used have definite effects on the character of the damper, and can be seen in the characteristic diagram of the damper. Physically larger restrictions and valve openings decrease the viscous friction losses and thus leads to lower damping coefficients; conversely, smaller restrictions lead to higher damping coefficients. Also, the pressure at which blow-off valves open to change the damping coefficient plays a role, as well as the layout – some dampers have blow-off valves for compression only, while others have blow-off valves in rebound as well. Figure 1-5 shows some valve configurations, and the effect they have on the characteristics of a damper will be shown in Figure 1-8.

The blow-off valves and restrictions are utilised in such a way that a bilinear or trilinear idealised characteristic is obtained, that is a direct result of the trade-off between handling and ride quality. Also, the way in which the valves are realised differs – some dampers use only shims as valve elements (spring steel washers which deform during operation), while more complex dampers use small springs and washers in their design (whereby only the spring deforms during operation).

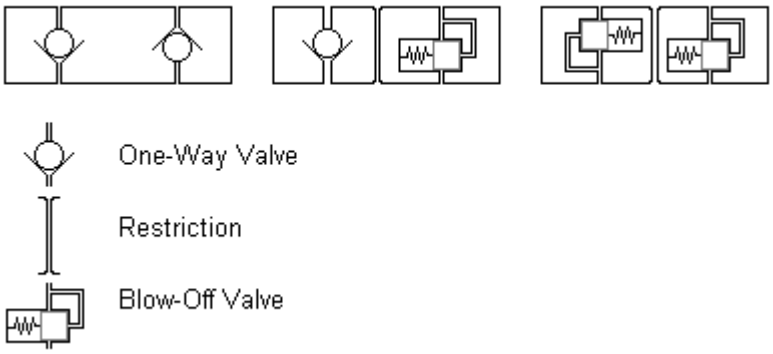

Figure 1-5: Examples of different valve configurations

The effect of restrictions and blow-off valves will be shown in more detail when the characteristic diagram of a damper is discussed in Section 1.2.6. It is important to note the valve types and their effects, as a lot of scientists attempt to use this data in theoretical mathematical damper models. Such models will be discussed in Section 1.3.2.

1.2.6. Characteristic Diagram (Force-Velocity Diagram)

As mentioned previously, there exist a definite correlation between the valves inside the damper and the characteristics of the damper. The characteristic diagram best illustrates this, and is also the standard diagram with which to identify a damper's capabilities. The characteristic diagram is basically a plot of damping force versus relative damper velocity (the velocity of the piston internal to the damper), as shown in Figure 1-6. There are various ways to produce this diagram – a simple, accurate and effective method is to excite a damper at several velocities and measure the force at each. The effects of the blow-off valves and restrictions can then be seen. Examples of the measured responses of spring-damper units are shown in Figure 1-7, where the effect of hysteresis is also shown. In Figure 1-10 the addition of the spring force is shown as well, this time in the work diagram. The damping force can be determined in the case of spring-damper combinations by determining the spring force (rate) at different displacements, and subtracting from the measured, excited

force. This can be done since the actuator displacement (and thus spring deflection) is measured during the damping test, and it is used to determine the damper velocity through numerical differentiation.

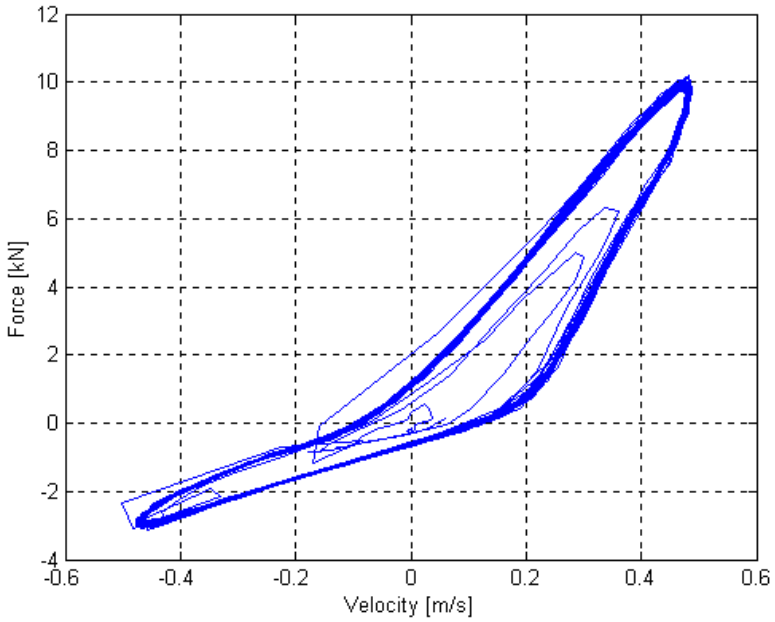

Figure 1-6: A typical passive damper's characteristic diagram

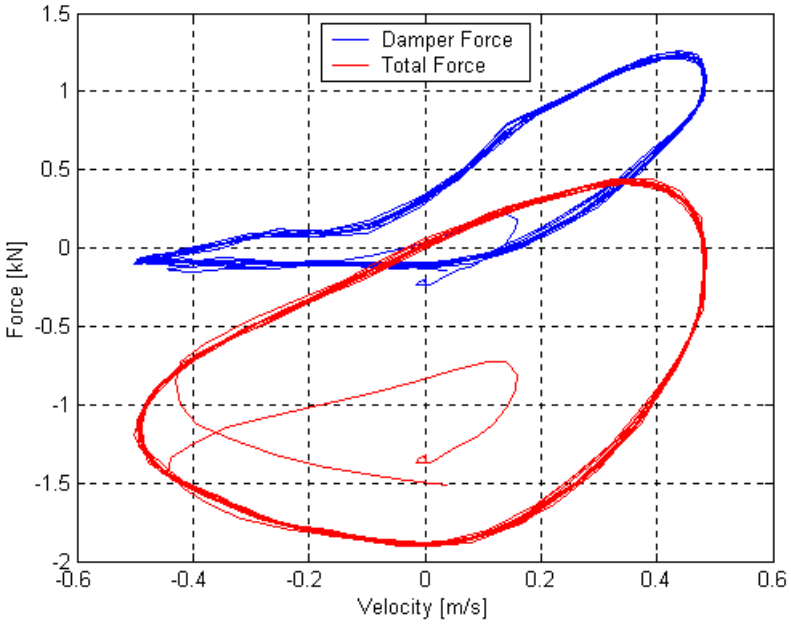

Figure 1-7: A motorcycle damper's characteristic diagram. Note that compression force is kept to a minimum, and that the damper force is extracted from the measured data by subtracting spring force. (See also Figure 1-13)

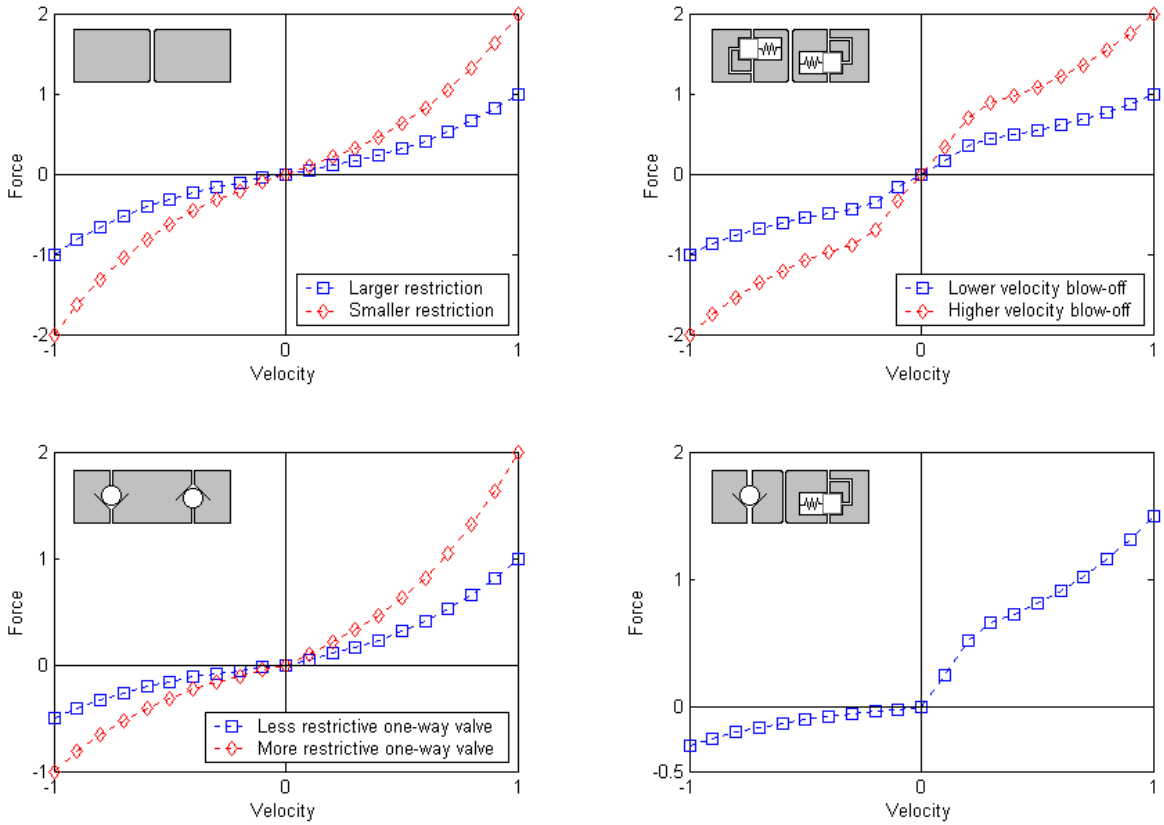

Figure 1-8: Various valve arrangements and their influence on the characteristic diagram

The restrictions in the piston are facilitated by channels or holes, which allow the passage of oil. The size or diameter of the hole directly influences the fluid friction it causes – the smaller the hole, the larger the friction and the steeper the characteristic's slope. Blow-off valves are placed in the piston to give a multi-linear characteristic diagram. These valves work by opening when the pressure in the damper reaches a certain value – this changes the slope of the diagram at the velocity corresponding to that particular pressure. This is because a new restriction is opened when the valve opens, and the addition of flow resistances in parallel tend to lessen the overall flow resistance. This is analogous to electrical resistors placed in parallel in an electrical circuit. Figure 1-8 shows different idealised characteristic diagrams and their valve schematics, featuring combinations of restrictions and/or blow-off valves and/or one-way valves.

1.2.7. Work Diagram (Force – Displacement Diagram)

A secondary diagram sometimes used to identify a damper with is the work diagram, an example of which is shown in Figure 1-9. This diagram is most suited when generated using a harmonic displacement input as damper excitation during the characterisation tests, so that a zero displacement corresponds to maximum velocity, and maximum displacement to zero velocity. A perfectly linear, non-hysteretic damper will then give an oval diagram, because force is directly proportional to velocity, giving a scaled velocity-displacement diagram – i.e. sine vs. cosine or cosine vs. sine. Deviation from this zero-centred oval shape can give an indication of the non-linear characteristic of the damper.

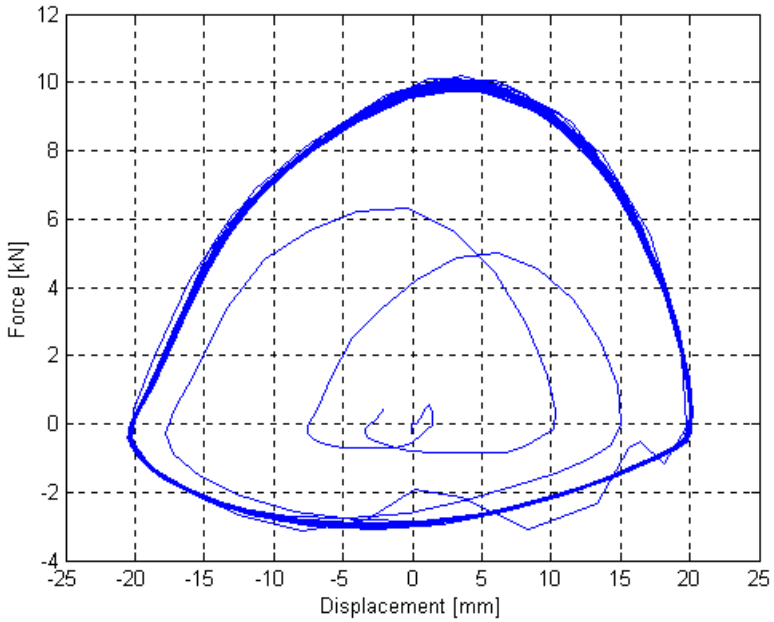

Figure 1-9: Example of a work diagram

Figure 1-10 shows the work diagram for a motorcycle suspension unit. The spring that forms part of this unit is preloaded, so that it doesn't give a zero force at maximum damper length. This is done so that some static deflection of the motorcycle can be absorbed without unnecessarily long suspension travel. Knowing the spring's characteristics enables one to determine the damper's characteristic.

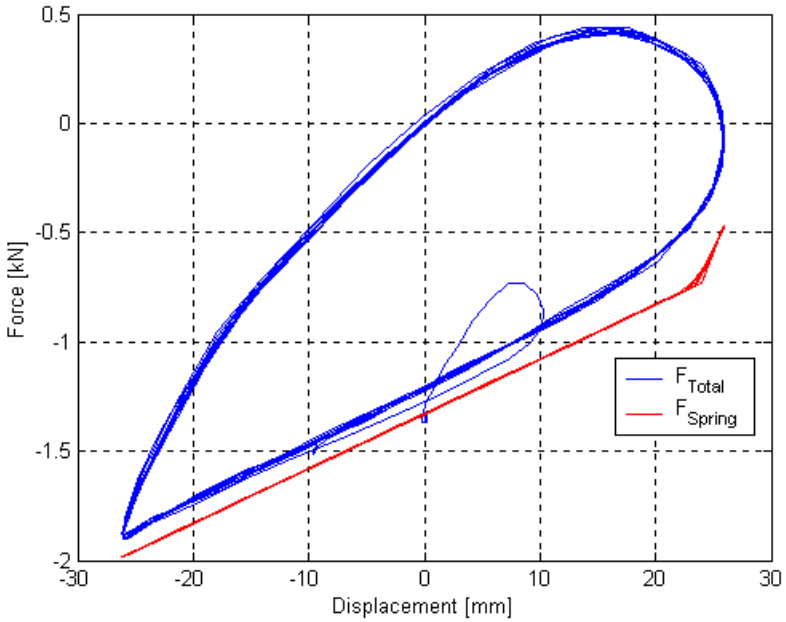

Figure 1-10: Work diagram of a motorcycle spring-damper unit

1.2.8. Semi-Active Dampers

Semi-active, slow-active and active dampers fall in the realm of controllable dampers and suspension systems (also called adaptive or adjustable suspension). Variable suspension systems enjoyed mainstream applications since the 1950's, an example being the Citroën DS range that featured hydro-pneumatic suspension with ride height control. Controllable suspension systems were developed to minimise or

eliminate the effect of the suspension trade-off between ride quality and handling – it seeks the best of both worlds, so to speak.

Semi-active dampers are dampers with changeable damper coefficients. The coefficients may be continuously variable throughout a certain range, or may have discrete settings. The operational range is shown schematically in Figure 1-11, where the force attainable for a real and ideal damper is shown.

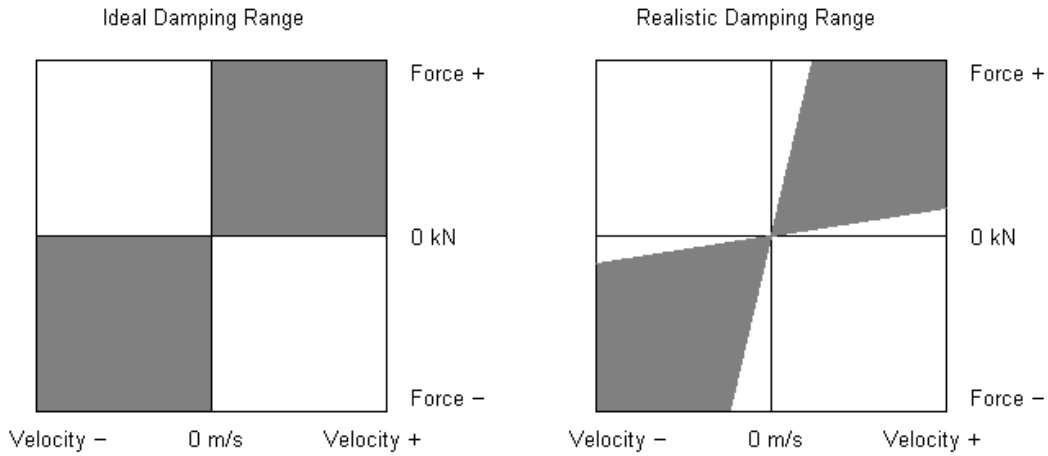

Figure 1-11: The ideal linear damping range of a semi-active damper (Left) and a more realistic, achievable damping range (Right).

Because of some leakage through valves or past the piston, high forces at low velocities aren't practically realisable. In the same way friction forces in the rod seal and between the piston and wall, and minor flow losses through open valves, cause some force at high velocities, meaning that a zero force during motion cannot be attained. The coefficient(s) are selectable using valves and orifices, switched by some control system. Because these are still dampers, they can only dissipate energy. However, switching to a high damping coefficient gives the desired handling characteristics, while a low damping coefficient gives suitable ride performance. Semi-active dampers are becoming the performance norm in luxury and sports cars, as these dampers require little engine power to operate. Their complexity and cost still inhibits their application in smaller, cheaper vehicles.

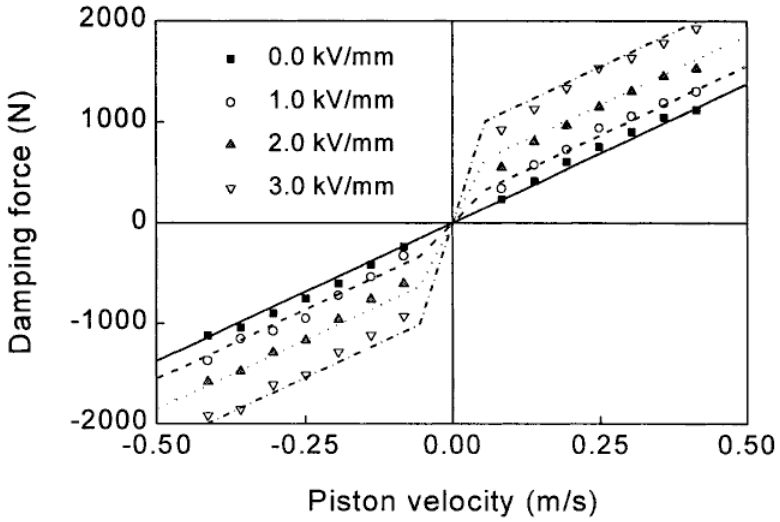

Figure 1-12: Characteristic diagram of Electro-Rheological semi-active damper [1]

Figures 1-12 and 1-13 show the characteristic and work diagrams for a semi-active damper, the schematic of which is shown in Figure 1-15. The different lines on the diagrams indicate the different characteristics that the damper assumes when

switched – different damper designs use different switching methods. The diagrams shown in Figures 1-12 and 1-13 (from Choi, Lee and Chang [1]) are measured using a rheological damper, which will be discussed in Section 1.2.10.

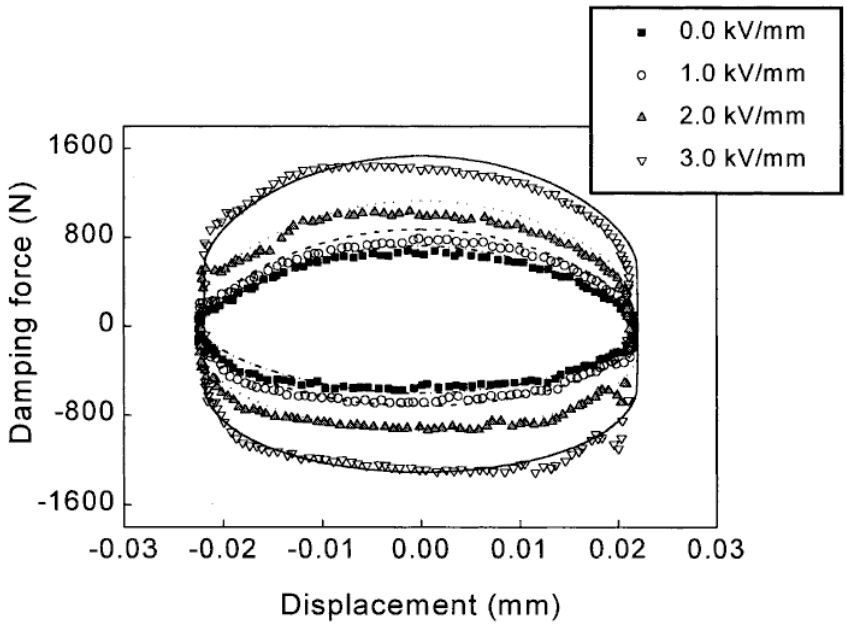

Figure 1-13: Work diagram of Electro-Rheological semi-active damper [1]

It should be noted here that adjustable suspensions, i.e. where the character of the suspension is either directly chosen by the vehicle operator, or determined using a trend sensed in the road input, can be realised using semi-active suspension systems. Obviously, this kind of manual control is inferior to the control as done by ECUs for real-time semi-active and active suspensions, as the operator wouldn't be able to adjust the system to respond to transient phenomena like potholes, turns, etc, and the control system implemented in adaptive damping switches much slower than that used in semi-active damping.

1.2.9. Active and Slow-Active Suspension

Active and slow-active suspension systems are also controllable, allowing damping at variable rates, but because they also facilitate the introduction of energy into the system, they can no longer be described as dampers. Active suspension systems are the most complex and costly suspension systems available. It basically entails an actuator - usually hydraulic - mounted between the sprung and unsprung masses of the vehicle, giving it the ability to do more than semi-active suspensions. The force actuator can apply some force between the connecting elements irrespective of relative displacement or velocity. Some active suspension configurations are shown in Figure 1-14. A combination of the actuator and/or spring and damper is used to realise this suspension system.

Due to the possibility of failure of one or more components of the active suspension, it is advisable that there exist some damping and spring effect when the actuator is not working. (Failure is of course possible through control system failure, hydraulic oil leakage, actuator damage and even something as menial as pump drive belt breakage leaving no oil pressure!) It is possible to have an active suspension configuration which leaves the car undamped and/or unsprung when it fails.

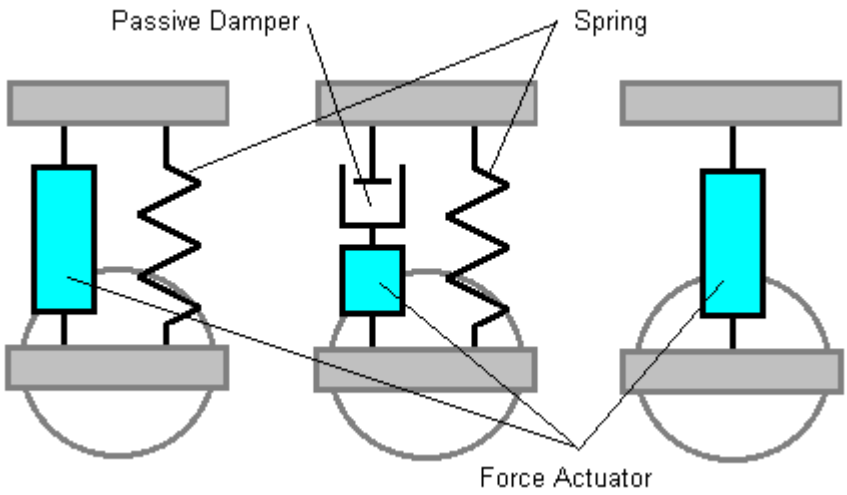

Figure 1-14: Active suspension system configurations

Even though the design and control of active suspension systems are complex, it has been implemented in various forms. Most notably is the Nissan Skyline GTR sedan which features active suspension, coupled with chassis control, active yaw control, active roll control and stability control. A drawback of the system on this car is that the hydraulic power pack requires considerable engine power to operate, and the system requires high maintenance.

Slow-active suspensions differ from normal active suspensions in that the actuator is placed in series with a passive spring element. The actuator usually has a much lower frequency bandwidth than its fully active counterpart (typically in the vehicle body natural frequency range, i.e. 1 – 3 Hz), and follows a displacement demand signal instead of the force demand signal. When the frequency limit of the actuator is reached, it acts as a solid body, and the passive spring handles further motion. Another passive spring is usually used in parallel with the actuator as well, to support the weight of the vehicle sprung mass and to lower the actuator's power requirements. Both slow-active and fully active suspension systems can add energy to the suspension system, and this fact allows them to perform better than both semi-active and passive dampers.

1.2.10. Controllable Materials Dampers

Recently, more interest has been shown in controllable material dampers. The materials used are rheological in nature, meaning that the operating fluid (which replaces the conventional oil) contains solid particles that align when an appropriate energy field is applied to it. As the particles align the ability to flow or shear is reduced; that is, the viscous losses attained through damper motion is increased. The two main types of energy fields used are electric and magnetic fields, from whence the names are derived: Electro-rheological (ER) and Magneto-rheological (MR) dampers. The latter is also referred to as Electro-rheological Magnetic (ERM) in some texts.

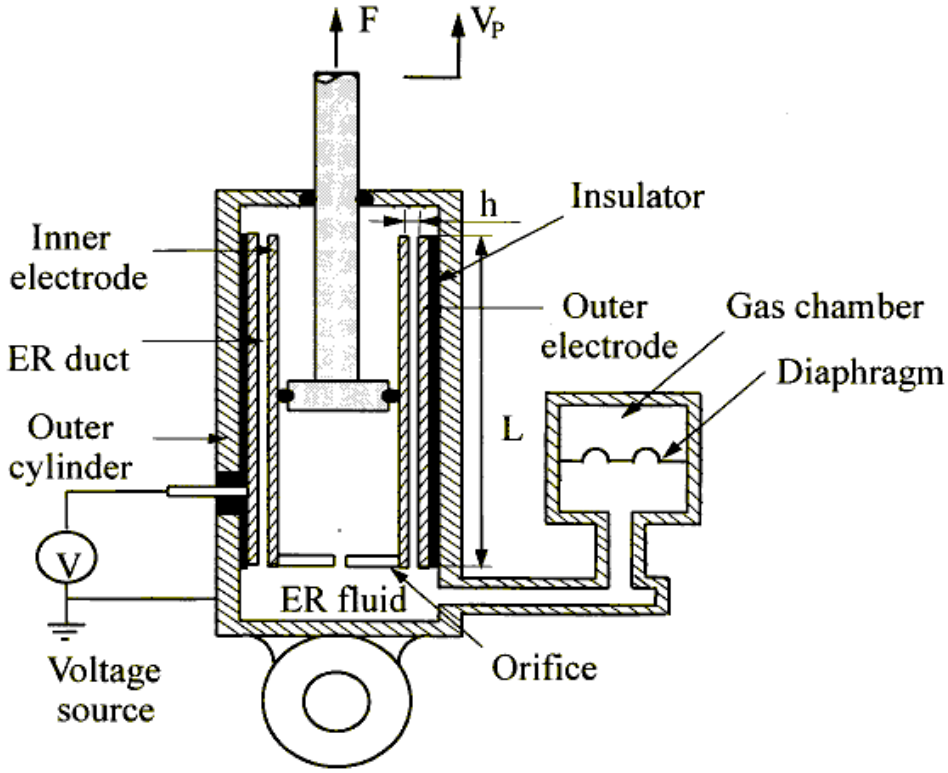

Figure 1-15: Schematic of an Electro-Rheological damper
(As developed by Choi et al. [1])

The major advantage in using rheological fluids in the dampers is that no externally controllable valves are necessary as in semi-active and active suspension systems, as the valve architecture is constant throughout operation. Applying the appropriate field attains various damping rates, with field strength determining the damping coefficient. For ER dampers this is somewhat of a drawback, as their operation requires a several kV/mm electrical field, while low shear stresses are attained. This hampers ER dampers' use due to safety and packaging concerns. MR dampers, on the other hand, can generate high shear stresses while being operated on a normal vehicle battery. This makes magneto-rheological fluid suitable for use in in-line and rotary dampers, clutches, bushings, engine mountings etc. in vehicles, and in the damping of structures for seismic inputs. Typical fluid characteristics for such uses include low viscosity at zero field, high viscosity at maximum applied field, low hysteresis, chemical inertness, temperature stability, and fast response time. Also, the solid particles must stay in an evenly distributed suspension throughout the fluid.

1.3. Literature Study

Published documentation referring to Hardware-in-the-Loop simulation and testing is not readily available. However, it is by no means a new concept. Hardware-in-the-loop (HiL) has been used extensively for the testing of, amongst others, control electronics. The main premise of HiL testing is the replacement of some mathematical model in a software simulation with that particular model's real hardware counterpart. In this way a piece of hardware replaces an inaccurate or overly complicated model. In the case of this project, a real, physical damper and/or spring was incorporated into a software-based vehicle simulation, thus negating the need for a mathematical model for the damper or spring.

1.3.1. Origins of HiL: Testing of ECU's

The testing of electronic control units is where hardware-in-the-loop simulation first made its mainstream appearance. HiL simulations are run exclusively in real-time;

otherwise realistic simulation results will not be obtained. There are two options when attempting a real-time simulation: use a dedicated computer running a real-time operating system, or let a standard computer act like a real-time computer. The former option has several drawbacks, the most prominent of which is the relatively low performance of such computers and the difficulty in porting software code other than C or C++ to the computer. Fortunately, there exist some computer applications that incorporate a real-time component to aid simulation, like The Mathworks' Real-Time Workshop (RTW), that can be used in conjunction with Simulink. Also, National Instruments I/O boards comply with LabView, a user-friendly graphic user interface that can also run in real-time.

As with any new testing technique or process, there are advantages and disadvantages. In the case of ECUs (like ABS systems, Engine management, aircraft autopilot, etc.) the control systems implemented in these units can be developed and tested using HiL, which leads to the following advantages:

- Mathematical plant models used during development are readily usable during production and quality assurance testing;
- ECU software changes can easily be checked for consistency with the design parameters;
- Tests are repeatable as the software can be reused as necessary, and plant parameters can be easily altered to simulate different models;
- There is no extra learning curve for the user;
- ECU development can run concurrently with the controlled object's development, even if only preliminary parameters of said object is known.

Until recently, rapid control prototyping (RCP) was used extensively (instead of HiL) for the development of control systems. That is, the control system is written as a software model and implemented in real-time using a suitable computer and I/O device; the plant (or object to be controlled) is realised as a physical, working model. This also means that control system development takes place after plant development, placing time constraints on the development of both. In contrast, HiL testing of ECUs uses a physical control system while the plant is mathematically modelled, which means concurrent development of the control and plant parts are possible. In other words, the I/O channels of HiL, compared to RCP, are reversed. This is shown schematically in Figure 1-16.

Of course, there are disadvantages to HiL-based ECU development, some of which are highlighted below:

- Measuring certain parameters becomes more tedious as ECUs may have built-in error checking, ground detection or short-circuit protection, all of which needs to be considered;
- Many times the ECU reads input signals either at random intervals, or at certain trigger points, which may be difficult or impossible for the plant model to predict. To circumvent this problem, the plant's resolution (output update frequency) must be much higher than the ECU's frequency. For instance, knock in an automobile engine is time-variant in severity and interval, and is thus difficult to control;
- HiL is often computationally more complex and demanding than rapid control prototyping, due to the fact that high resolution is needed and high precision is necessary. Also, integration and derivation algorithms are often recursive, iterative and have variable step sizes and are difficult to implement in real-time.

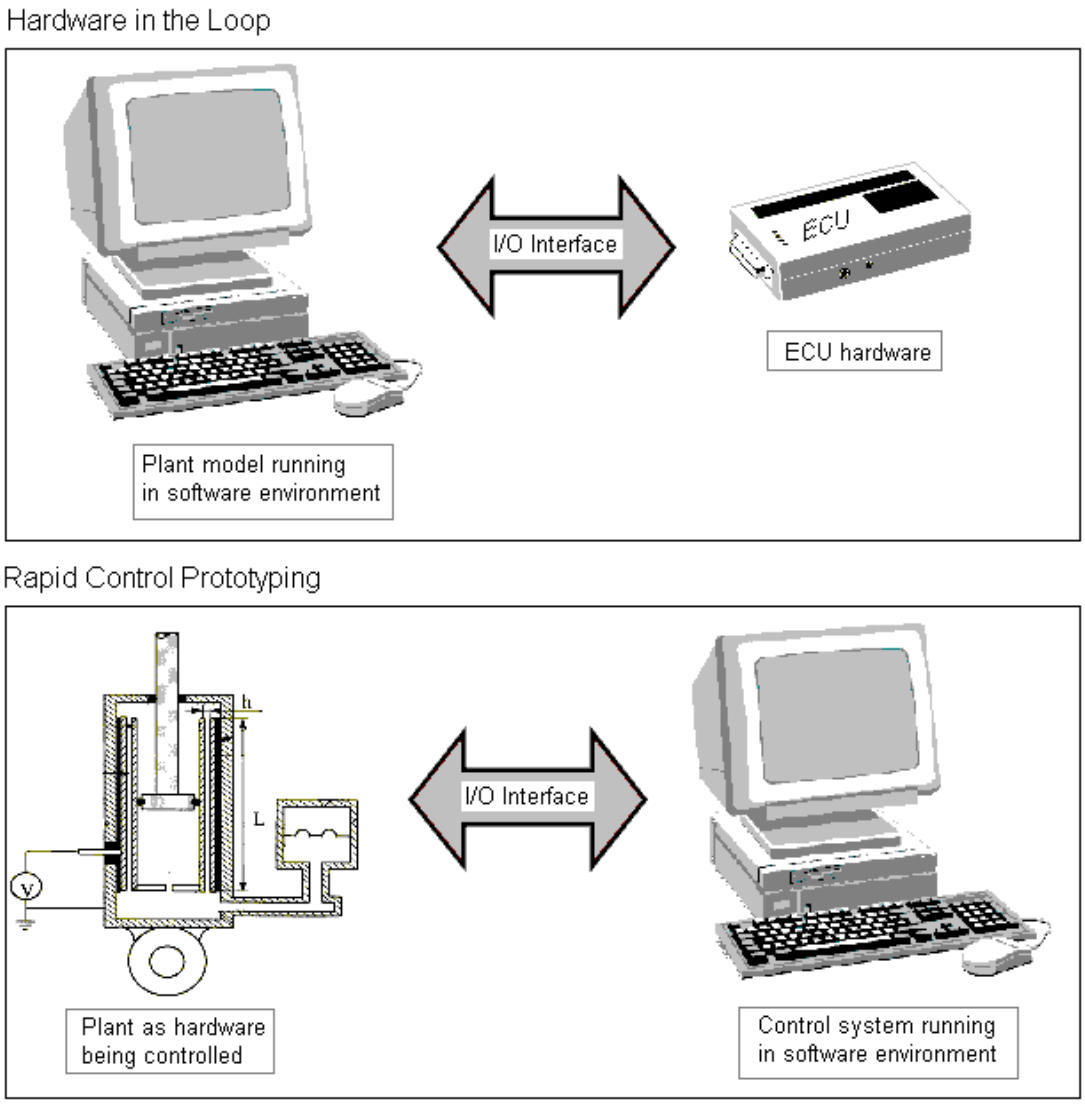

Figure 1-16: HiL vs. RCP

When considering ECU simulations, it must be said that the intention is not so much to check the coding of a control system – this must still be done using a software debugger, since a HiL ECU test would involve the code already downloaded to its final platform. Since one cannot monitor the part of code being executed in the ECU without excessive intrusions through pauses or breakpoints (that wouldn't be a true reflection of the units being shipped) it is clearly not the function of HiL to detect coding errors, but rather to determine how the unit would fare in real-world application.

An important consideration in HiL testing is the digitising and iteration rate. Martin Gomez [2], a software engineer at John Hopkins University, developed HiL systems in the past. He found that the "twice the rate of the highest frequency component" rule is actually inappropriate, as it is based on an incomplete reading of the sampling theory. This theory requires that you take each sample and multiply it by a scaled and shifted function. In practice one should sample at five to ten times the highest frequency component.

To show the impact of vehicle models on computation time as an example, Hanselmann [3] compared three processors while running a vehicle model with 50 degrees of freedom, including a complex tyre model and elasto-kinematic axles. He found that a Texas Instruments TMS320C40 DSP chip running at 50MHz completed a step every 2100 μs, a PowerPC604 at 100 MHz took 770 μs, and a DEC Alpha

AXP21164 workstation took just 290 μs. This shows that, for the kind of speed ECUs run at, fast computing hardware is necessary for complex plant models. It also gives an idea of the computing power necessary to run HiL simulations of mechanical systems, because although the mechanical systems operate in a frequency range much lower than electronic systems, the sampling rates and times must be such that both the mechanical system's frequency and magnitude behaviour can be predicted and monitored.

Jedrkowiak, Hesselbarth, Bartels and Miller [4] studied the implementation of HiL simulations utilising a computer having sufficient power to handle complex plant models, coupled with a real-time computer dedicated to handling the real-time I/O of the system. The real-time computer used was based on the Motorola 68040 CPU, with dedicated real-time OS9 operating system. This computer was in charge of I/O management. The workstation housing the mathematical models was a DEC Alpha workstation utilising a 500 MHz CPU. The computers were coupled using bus-to-bus connector cards, which need minimal overhead CPU usage. This combination proved to be sufficient for 0.1ms time steps for the plant model, and facilitated the testing of ECUs. From this, one can also see that it is more than adequate for the testing of mechanical systems with maximum frequency components in the order of 20Hz.

Another useful characteristic of HiL testing is that the tests can be automated. While this may not be as important in function verification and development, it is imperative during quality assurance and routine testing. A piece of software may do all the administrative tasks while ECU tests are run sequentially or sporadically, and when a certain occurrence is detected, the tests are stopped and a time history of events leading up to the fact is available. Also, between tests, the data can be analysed to spot certain phenomena, and the test modified automatically, until a certain criteria is identified. (For instance, an ABS ECU can be tested using progressively larger noise disturbances superimposed on the control signals to determine if the unit can tolerate it, when the control method breaks down and when the unit malfunctions.) Due to the nature of ECU tests, catastrophic failures aren't possible and the test automation can thus be left unsupervised.

It was stated earlier that one of the advantages of HiL simulations is that not all the hardware to be used in the plant need to be developed or available. For instance, Jackson, Brown, Crolla, Woodhouse and Parsons [5] published a preliminary report on the development of mobility control, with the focus on Direct Yaw Control (DYC), for a 6x6 off-road vehicle with hub-mounted electric drives. The individual wheel control to be used on the vehicle has not yet been realised. Possible controllers (both a PID and a fuzzy logic controller were studied) were developed and implemented using software simulations only; no compatibility or hardware studies were done. Implementing the final DYC in an ECU would have allowed much easier development of the other control systems that would follow, like a traction control system. This kind of ECU testing is well suited to hardware in the loop tests, whereby the physical, real controller can be interfaced with a computer running the vehicle model and any other control systems in a software state. This will not only verify the control system, but give an indication of the hardware's potential as well, like compatibility, power consumption, noise sensitivity, EMP resistance, and signal limits.

It must be mentioned at this time that HiL is a very versatile testing method. For instance, Ferreira, de Oliveira and Costa [6] investigated the application of control in hydraulic systems utilising electro-hydraulic components. In order to test the control of hydraulic systems, a hardware-in-the-loop method is chosen, which entails the creation of a detailed library of hydraulic components. A hydraulic system can then be constructed from this library of "building blocks", which can be run on a DSP and be controlled by a real ECU. Different complexity components were modelled so that the model complexity in question, which varies from one hydraulic system to the next, can be accurately described without being overly complex or vague. The ECU must think it is working with real hardware and thus, to obtain accurate simulation results, the model accuracy must be sufficient. (Maclay [7] also stated this.)

1.3.2. Damper Models Used

As stated before, there exists a definite trade-off when it comes to the ride and handling characteristics of passive suspension systems. A first iteration in the suspension design and selection process usually includes a full vehicle model simulated with a mathematical spring-damper model, and this data is used to obtain an idea about the quality of the chosen suspension. However, it must be noted that the reliability of the data is greatly influenced by the choice of damper model, as real dampers are usually non-linear and time-variant, and the damping fluid (the oil) has a viscosity dependent on temperature (Viscous losses heat up the fluid, which in turn influences viscosity).

A typical passive damper's characteristic will include hysteresis and non-linearity. Mostly, as a ride-handling compromise, a bilinear or multi-linear non-linearity is built in. Also, at low frequencies and velocities, the effect of friction between the piston rod and the seal and the piston and the cylinder wall plays a part. This is usually not seen for higher velocities and frequencies. At higher damper velocities, the break frequency can be seen, meaning that a blow-off valve has opened inside the damper (this is part of the built-in non-linearity). As the damper velocity increases, the amount of hysteresis also increases – superimposing tests done for different excitations will hardly ever "line up" over each other because of this. It is therefore clear that the characteristic diagram cannot accurately describe the behaviour of a damper, but can merely give a ballpark indication of some of the parameters. From this initial discussion one can see that modelling a damper's behaviour is not a trivial task.

Duym, Stiens and Reybrouck [8] refer to Lang [9] who used a mechanistic model to calculate damping force from a system of differential equations. Although the model was developed for a broad range of operating conditions, it did not, in fact, use the measured force data from an identification test in determining the model parameters, but rather the internal pressures. This requires specialist equipment or time consuming procedures, and if one considers that the iterative identification procedure requires solution of a system of differential equations, the whole process becomes quite time consuming. (Duym lists an example in which the simulation of one time step took seven hours!)

Duym also considers an explicit physical model developed by Reybrouck – this model requires 14 parameters, and gives the damping force as a function of displacement, velocity and acceleration. The parameters used are mostly flow discharge coefficients and empirical coefficients, so characterisation and usage of the model is hampered by the need to run numerous tests to determine such coefficients. Also, it is admitted that some of the empirical equations were fitted by trial and error from predetermined excitations. Even though the low velocity data correlates well between the measured and computed damper characteristic, at higher velocities the mathematical model shows significantly less hysteresis than the real damper, and the model becomes redundant. Considering the amount of tests that need to be done to characterise the damper model coefficients (if the starting values aren't suitably close), and the complexity of the model itself, this method is not suited as a first iteration in the suspension design process, but with the advent of even faster and more readily accessible PC's, Reybrouck's model could provide a good damper model for use in simulations. One must bear in mind that this model was developed for a specific valve assembly and damper type, and valve assemblies and damper types other than the ones considered might require major changes to the model.

Another model put forward by Duym et al [8] is a physical model without hysteresis – the damping force is thus a function of internal pressures, valve characteristics and damper geometry; a complete theoretical derivation of the equations is given in the reference. To identify the parameters, an exponential sweep is used as excitation to decrease the high-velocity component of the test, as one would find in a linear sweep. The simple non-hysteretic model performed similarly to the Reybrouck model, except for an overly accentuated break frequency with a very sharp corner. In contrast to the Reybrouck model, the physical model is quick to fit, albeit without hysteresis.

Duym et al [8] also considers various models based on basic elements – springs, dashpots, friction elements and even backlash elements. The basic problem found with the majority of these models was the need to compute non-linear differential equations. Fast simulation and identification is therefore ruled out (once again, faster computers may negate this effect to some extent, but identification would remain tedious). Also, the fits are only decent for models without hysteresis – they under-perform when hysteresis is included.

Duym et al also investigated non-parametric models – these are models with an elevated number of parameters, which are empirically correlated. Some mathematical models contain both parametric and non-parametric elements. In order to provide a fast identifiable damper model that includes hysteresis identification, a non-parametric model based on restoring force was introduced:

$$F_{damper}(x,\dot{x}) = \sum_{i,j} a_{i,j} x^i \dot{x}^i$$

Unfortunately, these models proved unsuccessful in broadband operation – they could only be used in the operating environments in which they were tested. While some work went into finding the problem (thermodynamic state variables and inertial effects were suggested), it turned out that this model was only suited for constant-frequency variable-amplitude identification. The number of maps or lookup tables produced, made this method impractical.

Another non-parametric model is suggested, one that uses velocity and acceleration as state variables:

$$F_{damper}(x,\dot{x}) = \sum_{i,j} a_{i,j} \dot{x}^i \ddot{x}^i$$

While this model is considerably faster and produces less error than the previously described non-parametric model, it changes the direction of the hysteresis from counter-clockwise to clockwise. In its defence, it is the fastest model to reliably implement.

A common thread throughout the model investigation is that hysteresis is very difficult to describe mathematically. This is also echoed in the fact that the RMS errors, obtained by the fitting of the modelled data to the measured data, are three times less for models without hysteresis compared to models with hysteresis. It would appear that attempting to model hysteresis, in some cases, appears to give more erroneous predictions!

Lastly curvilinear models are mentioned, but these also require the solution of a first order non-linear differential equation, and are thus slow to implement.

Lang and Sonnenburg [10] investigated a model to describe a double tube pressurized damper for use with the MSC.ADAMS dynamic simulation software package, as the absorber model has a perceptible influence on the simulation results. The damper in question consists of a system of small spring washers, coil springs and machined valve bodies. A theoretical approach is followed in deriving the damper model, while an extensive database on pressure-flux characteristics of different valves is used instead of theoretical flux expressions and assumptions. The company for which Lang worked developed this database.

Hysteresis is accounted for by noting that the gas pressure in the absorber continually changes when using the adiabatic state equation; this change in gas pressure is due to the movement of the piston and rod, and results in hysteresis at all excitation frequencies of the damper. Because of the tight sealing of the rod, friction forces also have to be accounted for, as these can be very high; using a momentum-balance equation, these were incorporated into the model. Also included in the model is the effect of stick-slip (also called sticktion; see Appendix C: Determination of Stick-Slip Effect), which is implemented in the model using an analytical equation. Due to

similarities in the stick-slip effects and tyre-road contact patch physics, a first version of the "Magic Tyre Formula" was used.

The resulting model is quite complex, and even though low velocity forces can be accurately predicted (including hysteresis), a lot of high velocity effects are omitted due to the limitations of the model. Also, it should be noted that the oil flux through the internal valves is implemented using empirical lookup tables; it is impractical to implement this model (or a similar model) if one doesn't have an adequate database of oil flow through valves.

Because of the importance of dampers in automotive handling and ride comfort, it is imperative to know what the characteristics of a damper are. Several models have been developed and implemented into quarter-car models, pitch vehicle models and full vehicle models with differing degrees of success. This is due to the fact that some physical parameters or components like massless springs and body masses can quickly and efficiently be implemented into simulations and dynamic equations, with good accuracy and reliability. However, components like dampers, which tend to have strong non-linear and time and history dependent characteristics, cannot be readily implemented. Real damper characterisation thus also enjoys some attention.

Schiehlen and Hu [11] use Hardware-in-the-Loop simulation to characterise a damper using Monte Carlo Simulation and random road inputs. Ground roughness is characterised by a Gaussian, ergodic and stationary process with zero mean value, a standard model of which is used by Schiehlen and is given below

$$S_\zeta(\Omega) = S_0\left(\frac{\Omega_0}{\Omega}\right)^w$$

with Ω being the spatial frequency [radians/m] and w the wave number. The spatial frequency ratios used are in a range of

$$0.05 \le \Omega \le 500$$

with limits set, and the reference spatial frequency is set at Ω_0 = 1 radians/m; it was found that for frequencies outside of the bounds mentioned above, there are only minor influences on the dynamic behaviour of vehicles. Because the excitation is in the frequency domain, the roughness models are transformed to the time domain. The actuator providing the real damper motion is excited using the projected damper deflection (determined numerically), while the damper force is fed back into the simulation. Characterisation simulation is done using Euler integration and 0.001s time steps.

Statistical analysis suggests that there is no correlation between the displacement of the piston and the damping force, and the latter is only a function of piston velocity. (This assumption is very limiting, as shown in various mathematical models considered above.) Using the data extracted from the HiL simulation results, a piecewise linear model of the damper is set up using both a least squares and a correlation-based approach. This enables Schiehlen to determine both the body vibration and characterise the damper during the same experiment. The drawbacks are, of course, the simplified damper characteristic, that can be obtained using successive harmonic tests, and the fact that body excitation is only determined in one way (HiL) while pure numerical simulation using the newly extracted damper characteristics is bound to be erroneous.

Besinger, Cebon and Cole [12] investigated damper models with the focus on heavy vehicles. Utilising a HiL test bench, they also investigated the accuracy of their setup, so as to develop a mathematical damper model and test its accuracy compared to physical measurements (the HiL tests). The damper model is developed because Hall and Gill [13] found that using a linear or bilinear model gave optimistically inaccurate results when compared to a more advanced model, like the 82 parameter model of Segel and Lang [14], which for more practical applications is too complex. Likewise, a model described by Karadayi and Masada [15] was also considered, but because only low-speed results were given, the model was discarded. (The model was

developed using two dampers from passenger cars, and contained hysteresis due to fluid compressibility, and backlash.)

A quarter car model was used during model verification, as it gives good results through appropriate amplitude and frequency content, so as to test suspension systems under relatively realistic conditions. Unfortunately it doesn't make provision for suspension non-linearities due to geometry, or to mass motion like the trailing arms, side shafts and dampers itself. The road input was again a random signal, generated using Robert's formula (which will be given later).

A damper model derived by Besinger [12] was compared to a real damper characterised with the HiL test setup. Good agreement between the measured and calculated characteristics was obtained for low damper velocities (low frequency high amplitude and high frequency low amplitude), but for high velocities the hysteresis of the measured characteristics far exceeded that of the calculated characteristic. This was possibly because of foaming of the hydraulic fluid, which wasn't considered in the model. There were also fluctuations in the measured data, in the form of ripples, which were due to the internal valves of the damper – these effects were also not modelled. This damper model was subsequently used to validate the HiL setup used in other tests. An "Error Coefficient of Variance" (ECOV) was used to quantify the difference error between the HiL simulation and the computation; this equation has the following form:

$$ECOV = \sqrt{\frac{\int_0^T \left(x(t) - y(t)\right)^2 dt}{\int_0^T x(t)^2 dt}} \times 100\%$$

Here, x is a reference signal and y a comparative signal. This quantitative measure is extremely sensitive, and the small phase lags between the computed and measured signals caused errors of 13.1%, 20.4%, 9.4% and 44.8% for body acceleration, tyre force, suspension deflection and damping force, respectively. The ECOV values were able to give an indication of the quality of the damper model, and its application in simulations. Tests showed that the model is very parameter sensitive, and that it only has applications with road input spectra frequencies of below 15 Hz, so as to eliminate large velocities and high-frequency phenomena. In general, good agreement between the HiL and computer simulations was obtained, and this was visually confirmed, despite the apparently large ECOV values. (The "Error Coefficient of Variance" check will be discussed further in Chapter 2.)

It was concluded by Besinger that a damper model must make provision for saturation, as rough roads or low damping ratios cause large errors when it is neglected. HiL performed well for a wide range of operating conditions, and up to 20Hz. It was found that HiL offered a versatile, easy to use damper testing and model verification tool.

Rao and Gruenberg [16] describes a method for obtaining linear suspension models for use in Computer Aided Engineering (CAE) problems, as system-level CAE models are linear in nature. However, instead of using a conventional actuator in suspension testing, an electrodynamic shaker was selected, as the conventional hydraulic actuator had inherent noise at higher testing frequencies. While Lang, Morman [17] and Reybrouck [18] all attempt to create models using spring-dashpot models, flow equations, pressure differences, etc., and attempt to account for hysteresis and backlash (like Karadayi), they all end up with models consisting of a set of non-linear differential equations requiring time-consuming numerical solution. However, parametric modelling is much more suited to the I/O based CAE models. In this parametric approach, the damper is seen as a black box, and subjecting the damper to different inputs while the outputs are measured sets up an input-output relation. The physical coefficients obtained in this way usually have no accurate physical

bearing on the damper in question, but are strongly correlated to the experimental readings. Of course, the drawbacks of this method is that the model is only valid for the conditions for which it was tested, and equipment for the testing and data recording of the damper data is needed; hence, the damper must be "characterised" before application is possible. That is why the two model types, parametric and non-parametric, have different uses. The former is used when a damper needs to be used in a software simulation and no modification or verification of said damper is the object. The latter is used when developing and tuning the damper layout, control system or suspension geometry, and the changes need to be investigated before production of the components.

The electrodynamic actuator used in this test is a 50-pound force actuator by MB Dynamics, similar to the Modal 50 actuator available in the UP's Sasol Laboratory. Using the data measured from a 25 to 300 Hz bandwidth, at an amplitude of 0.05mm, a parametric model was constructed using curve-fitting techniques. These experiments showed that an electrodynamic shaker can in fact be used to obtain equivalent dynamic properties of dampers, however, it has been mentioned before that there exists phenomena that only appears at high stroking displacements and velocities.

Duym, Stiens, Baron and Reybrouck [19] represent an alternative formulation for a physical model of a damper including hysteresis, modelling the internal architecture like valve parameters together with hysteresis effects. Apart from the compressibility of oil (which is usually seen as an incompressible fluid in most other applications), gases also form part of the hysteresis problem with a variable gas phase caused by either gas bubbles being present in the working fluid, or by dissolved gas. Owing to the nature of the damper and its application, the soluble gas is found as bubbles that appear and disappear with pressure fluctuations, changing the fluid characteristics.

Dampers have certain inherent characteristics, determined to a large extent by damper design, but which are nonetheless prevalent in almost all dampers. Firstly, dampers have a strong non-linear nature, due to non-linear pressure drops during its operation. Also, designers usually strive for a multi-linear characteristic, whereby the rebound-damping constant is higher than the compression constant, and there is usually a break point in the compression phase where blow-off valves open to ease the damping constant. Second is the temperature-dependence of the damper, due to its reliance on a working fluid that has temperature-dependent viscosity. Viscous losses and internal friction may increase the heat of the damper unit, lowering the viscosity and thus changing the characteristics. It is not too uncommon to see damping force decrease as the oil's temperature increases. Thirdly, hysteresis is present due to compressibility effects and friction force in the damper.

Morman [20] also elaborated on the work of Lang [9] and Segel [14] (who collaborated with Lang), and implemented the gas as a separate volume that is alternatively compressed and expanded in compliance with the isentropic law. Lang stated in his thesis that the gas present in the absorber is evaporated damper oil, and modelled this phenomenon with some heuristic rules. Together with Segel, however, Lang stated that a more plausible explanation for the presence of gas in the damper is that it is nitrogen gas emanating from the reserve chamber – this occurrence is known as frothing. This work did not, however, explain the sudden appearance and disappearance of gas bubbles when studying transparent dampers.

After considering this, Duym et al [19] proceeds to attempt to include these effects into their model. As in other studies, valve dynamics and properties and damper dynamics are mathematically modelled. Now, however, the dual tube damper's rebound and compression chambers are filled with oil and gas bubbles, and the reserve chamber is filled with oil, bubbles and nitrogen gas. Identifying the model parameters using force data instead of pressure measurements, parameter-sensitivity functions (whereby parameters are found using a gradient method, and gradients are determined from a related set of differential equations) are employed along with some

basic assumptions. They discovered some interesting results when utilising their model. Firstly, the pressures at which the bubbles appear and disappear are not the same – the bubbles disappear at a pressure higher than the pressure at which the bubbles form. This can be due to the finite diameter of the bubbles, and the fact that they aren't evenly dispersed within the hydraulic oil. Secondly, friction plays a definite part in the model, and can be brought about due to the suspension geometry. McPherson struts, for instance, allow a moment to be placed on the damper unit, and this can mean that large friction forces are generated. Residues and variances in the readings determined the quality of the fit – it was found that the model gave relatively accurate results. The model discussed is said to be easy to implement in identification and simulation, however, the internal geometries and architecture of the damper must be known and thus it doesn't lend itself to the software modelling of unknown dampers.

Hydraulic oil typically contains 8 to 9% by volume of dissolved air, as stated in the Shell publication "Compression, bulk modulus and related properties". The dissolved air has little or no effect on the oil's bulk modulus, but excessive trapped air can result in severe modulus reductions. This is but another obstacle in the development of damper models.

All the damper models discussed up to now have some drawback – they either have limited applications, are inaccurate, computationally too complex, or are too vague to implement with confidence. This is one of the reasons why HiL suspension testing and simulation is so attractive – it uses the real damper instead of these inadequate models.

1.3.3. HiL Setups Employed and Conclusions On Their Use

As mentioned before, HiL has been used before for the testing and simulation of mechanical components. In this section, an overview will be given of various authors' work pertaining to HiL.

Besinger [12] developed a HiL test rig to verify damper models with. The HiL setup used consisted of an actuator securely mounted in a reconfigurable test rig, with a strain-gauge load cell fitted between the actuator and the damper. The actuator controller conditioned both the load cell and actuator LVDT signals. An accelerometer with low cut-off frequency was also used to measure the vertical acceleration of the load cell. A 386 PC utilising a 12-bit A/D interface card supplied the computing power. To minimise phase lags, no external filtering was employed. The actuator bandwidth was 40Hz. (While testing the dampers, it was found that when testing large damping ratios, it is more stable to scale down the vehicle parameters than to scale up the damper force.)

The choice of integration algorithm is an important one, since computing power is usually limited when using a PC. The vehicle model can be described as

$$\frac{dx}{dt} = f(t, x)$$

with time t, x the state vector and f a derivative function. Numerical integration is used to solve this equation. Because A/D and DSP cards operate at a pre-set sampling frequency, it is necessary to use a fixed-step integration routine to achieve the best possible accuracy. When considering Euler and 2nd, 3rd and 4th order Runge-Kutta integration algorithms in a software environment, it was found that the Euler integration scheme gave unacceptable errors at all time step sizes above 0.5 ms; this is due to the low order of the scheme, and hence it lacks accuracy. The Runge-Kutta algorithms fared better in this respect, with low errors for all three schemes when the time steps were below 4 ms. In fact, the 3rd and 4th order algorithms give almost identical, low errors up to 10 ms. Above 10ms time steps all integration schemes give unacceptable errors, but since steps so large are impractical anyway, this poses no problem. Integration becomes unstable above 25ms. (Remember that a sampling rate of more than ten times the highest frequency of interest is preferable.) The errors

mentioned were obtained considering a step input, and calculated using the exact theoretical solution using an idealised linear damper in the simulation:

$$Err = \frac{Deflection_{Theoretical,RMS} - Deflection_{Integration,RMS}}{Deflection_{Theoretical,RMS}} \times 100\%$$

The computational load of the integration scheme was found by investigating the amount of floating point operations (FLOPS) achieved by the derivative function. As the time step decreases, the amount of operations possible in each step decreases. This also indicates the error that can be incurred. As can be expected, the Euler scheme fared worst, while the 2nd, 3rd and 4th order Runge-Kutta schemes performed progressively better. It should be noted at this point that in a single time step, different integration schemes may do multiple A/D and D/A conversions, and this must be accounted for in the selection of scheme and time step size. For instance, if one A/D conversion takes 0.1ms it would be unwise to specify a time step of the same size; rather, a time step five to ten times larger is advised. It was found by Besinger et al [12] that modifying the Runge-Kutta integration software to update the actuator output more frequently resulted in improved HiL system accuracy. They were able to do this as they were running custom C code on their test computer. The errors and integration times are summarised in Figure 1-17.

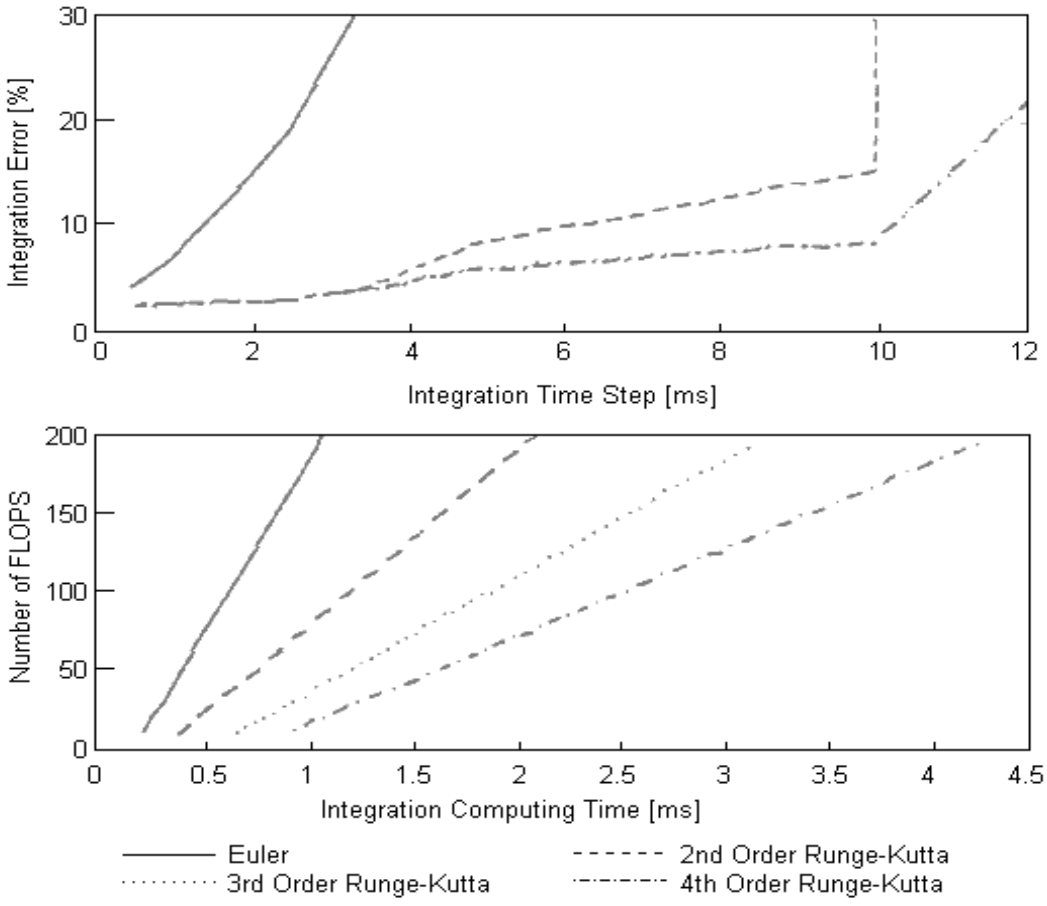

Figure 1-17: Effect of integration time step size and computing time (From Besinger [12])

To determine the effect of the actuator dynamics on the HiL simulation, a model of the actuator and its components (PID controller, servo valve and hydraulic actuator) were investigated, and compared to a simulation without said components. An actuator system transfer function was used:

$$G_{actuatorsystem} = \frac{G_{PID}(s)G_{Valve}(s)G_{Actuator}(s)}{1 + G_{PID}(s)G_{Valve}(s)G_{Actuator}(s)}$$

The parameters for the transfer function were determined experimentally. It was found that using body acceleration, tyre force and suspension deflection as measurements, there was absolutely no difference between the system utilising the transfer function and the original system (without transfer function) for frequencies below 8 Hz, as can be seen in Figure 1-18. The ideal actuator used in Figure 1-18 refers to a "perfect" actuator, i.e. an actuator that immediately follows the input signal perfectly.

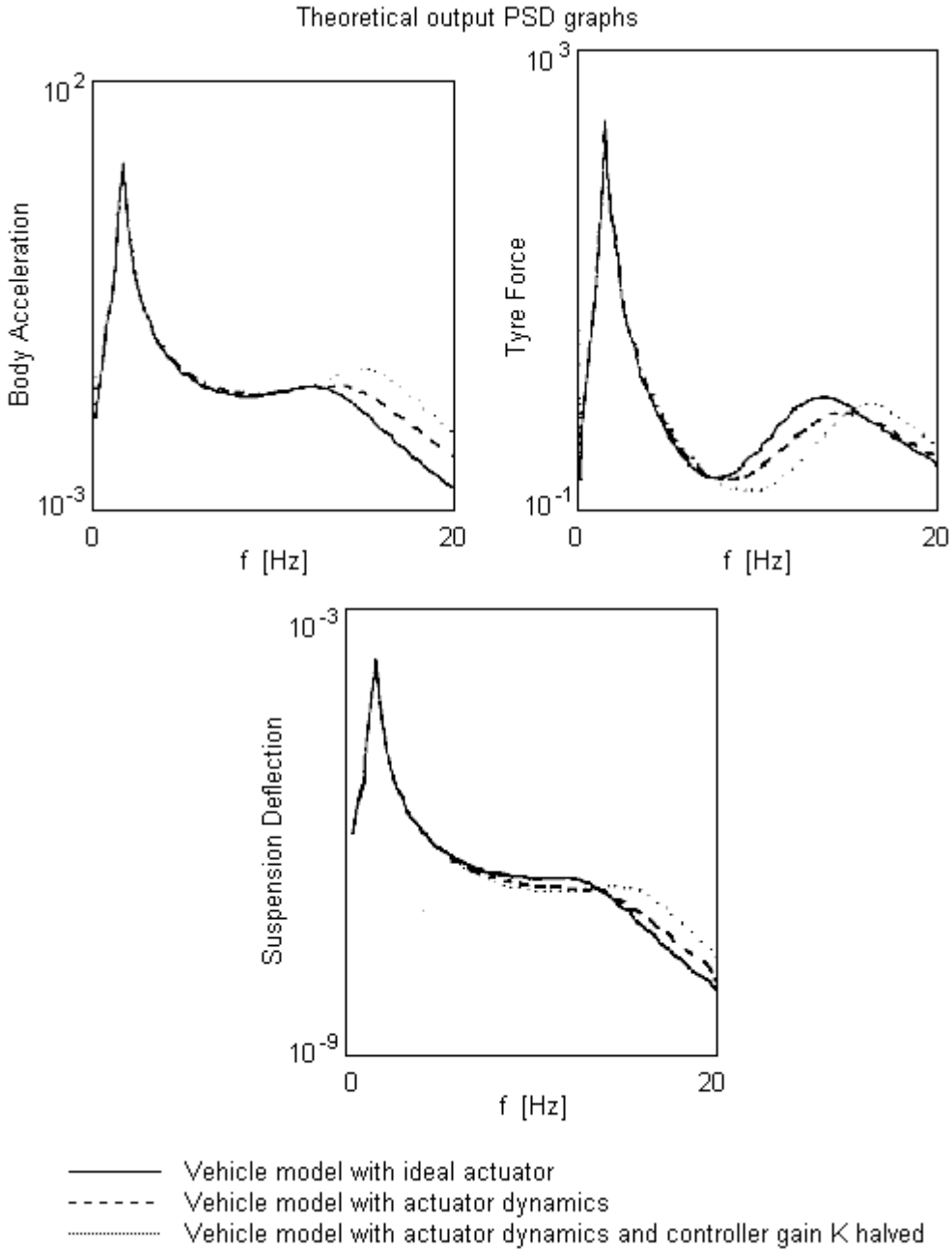

Figure 1-18: Vehicle response comparison using different actuator models. Y-values plotted on a logarithmic axis, X-values on linear axis (From Besinger [12])

The frequencies considered comfortably includes the sprung mass mode. Above 8 Hz, small deviations in the measurements were seen, but the relative amplitude of the deviations was small enough not to influence the simulation adversely. It was found,

however, that the proportional gain of the controller had a large effect on the simulations, and should thus be selected carefully. Halving the gain during this investigation caused the errors to more than double.

In their investigation into the control of a semi-active damper to track a prescribed force, Besinger, Cebon and Cole [21] continued to use a HiL test method to measure the open loop and force feedback (closed loop) performance of their suspension controllers under realistic conditions. The hardware-in-the-loop setup has advantages over conventional test methods, like low hydraulic power requirements, flexibility and short implementation time, as well as ease of changing model parameters. The setup once again utilises a quarter car model, which for heavy vehicles lacks the complexities of sprung mass motion, however suspension deflection amplitude and frequency content are sufficient for testing under realistic conditions. Road inputs used were random, similar to those used by Kitching, Cole and Cebon [22] (Power spectral density equation).

Besinger used an automobile damper in the tests, implemented by scaling the measured force to a sufficient value. This way, the automotive damper emulated a realistic truck damper, and its proven design ensured stability. Even though lags in the system due to flow in the damper, damper valve switching and response are significant, the lag due to the actuator and its controller was neglected, an action that was already verified as permissible. This could prove to be a risky assumption, and the lags should be determined to see if the assumption is justified. However, Besinger warns that lags in the HiL setup may cause instability, and that the overshoot induced when using larger gains are also not wanted. That is why a scaling down of the plant model is suggested, instead of a scaling up of the damper force.

In a previous paper Besinger, Cebon and Cole [23] published research into advanced suspension systems for heavy vehicles. They chose to use HiL because it gives results under realistic and repeatable conditions. Because no simple, accurate damper models exist, Segel et al [14] gives an 82-parameter damper model based on pressure-flow phenomena. Other models have been described earlier. Thus, to accurately and efficiently test suspension systems, HiL is employed.

Besinger et al checked the HiL process by comparing it to a numerical solution utilising a simple piecewise linear damper model. The force is thus given in a 7-parameter model, the coefficients of which is chosen so as to give best agreement with the measured characteristic, which had to be determined beforehand. (Hysteresis is obtained through damper compliance and the inclusion of the damper bushings.) The model gave good fits through a limited operating region.

Also considered is the actuator dynamics, and the errors introduced by it (This work was detailed more thoroughly by Besinger at a later date [12]). By using a transfer function to describe the actuator, tests were done to determine the introduced errors. It was found that only at the wheel hop frequency (typically 10 – 15 Hz) are there large differences between the system utilising an actuator model and those that don't. Road displacement amplitude also decreases rapidly, meaning that the difference is less important for typical load conditions. Tyre force and body acceleration discrepancies are typically less than 1%. They also thoroughly verified the HiL system by comparing it to a purely numerical solution, and comparing the PSDs. These showed that the HiL simulation is indeed suitable, and that it is in fact superior to numerical simulation incorporating a damper model.

A semi-active damper that was used in this experiment (provided by Lord Corporation) was tested in the resulting HiL test rig with good, predictable results, and the purely numerical software and HiL time histories were in good agreement. Once HiL was verified as working correctly for the given actuator and PC interface, more advanced tests like on-off control and switching frequency could be performed.

Rieger and Schiehlen [24] looked at hardware-in-the-loop as a testing method to determine if the performance of an active suspension system is financially viable compared to passive suspension, and also used it as a method of reliability testing, due to the realism afforded by it. The dynamics of the vehicle is handled through the use of multi-body system dynamics, aided by computer dynamics packages and formalisms such as NEWEUL (a dynamic modelling software package). The HiL setup is implemented without considering the actuator and its controller's dynamics, but the suspension control system implements a linear quadratic regulator and a phase lag compensator, resulting in a test setup having excellent phase behaviour. The suspension considered is a simple McPherson suspension, with geometry shown in Figure 1-19.

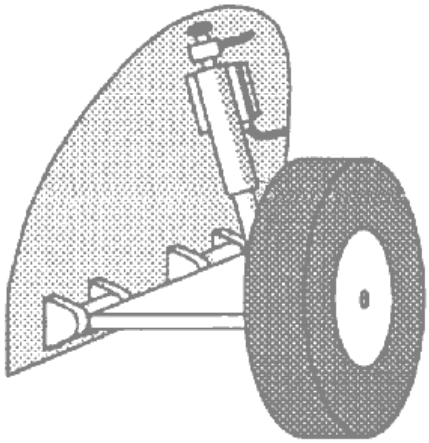

Figure 1-19: Simple McPherson suspension schematic

HiL tests were used to compare passive and active controlled suspension systems, and good agreement between the HiL tests and theoretical predictions were obtained. This research showed that the application of HiL can be predictable as well, and advises the application of HiL as a simple checking mechanism when theoretical predictions are either scant or unclear.

Kitching et al [22] developed, modelled and tested a continuously variable semi-active damper for heavy vehicles using a quarter-car HiL test rig.

A HiL setup was used to examine the behaviour of the damper. To determine a passive suspension optimum, the HiL model was fitted with a passive damper from an Iveco-Ford tractor, and the force measured was scaled before being fed back to the numerical simulation. Kitching conducted the HiL simulations using random road inputs as given by the equation representing a power spectral density function:

$$S_r(\gamma) = \frac{\kappa}{\gamma^{\eta}}$$

where κ is the roughness coefficient, η is a dimensionless exponent, and γ is the wave number. Also, two transient or discrete inputs were used to measure suspension performance – a smoothed-step input of 10mm, which is preceded by a linear ramp as long as a typical heavy vehicle tyre contact patch, and a bump input which is essentially a half sine wave of 300mm long and 10mm high. These inputs, along with random road inputs, were used to compare a modified skyhook damping control law damper with a passive damper.

Kitching also found, as will be shown in a later chapter, that the wheel hop frequency of the HiL predicted model is significantly higher than the theoretical value. (Besinger [25] first documented this fact in his PhD thesis.) This is what prompted the use of 10mm high transient inputs. Also, it was found during the HiL simulation that the damper supplied energy to the suspension. This is contrary to the fundamentals of semi-active suspension, and may be because of lags in the experimental setup or

due to elastic energy stored internally in the damper unit and damper mounts. The precise cause is quantitatively unknown.

Deakin, Crolla, Roberts, Holman and Woodhouse [26] developed and tested a novel semi-active suspension system for a combat support vehicle. The testing was done in three phases – damper characterisation, HiL testing and single degree of freedom testing. It was found during the HiL testing that the experiment showed unstable behaviour. It was suspected that due to the size and mass of the actuator, it didn't possess a sufficiently high cut-off frequency. Three proposals were made to increase the HIL setup's stability – firstly, an actuator with more favourable frequency characteristics should be used, but this is impractical; secondly, a phase compensator should be employed within the controller, and thirdly, the model's parameters should be changed to obtain stability. The phase compensator did improve stability, although coupled with a 10Hz bandwidth actuator the improvement was insufficient. Using the equipment available to the authors, they were unable to test the damper using HiL simulation, as even with phase compensation and a simplified, SDOF spring-mass-damper model the test showed a 50% higher response than the pure numerical simulation showed. Thus, they tested the suspension using a SDOF setup with a physical mass in place, shown in Figure 1-20. They concluded that an actuator with bandwidth of 10Hz is insufficient in HiL testing.

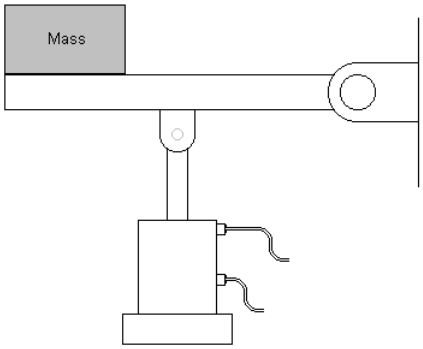

Figure 1-20: Non-linear SDOF test setup

Kitching, Cebon and Cole [27] investigated the use of preview control in the application of semi-active dampers for heavy vehicles, since it has been shown that preview control is superior to non-preview control for adaptive suspension. The testing method employed was, again, hardware-in-the-loop. The flexibility of this testing method enabled the modelling of a four-DOF pitch vehicle model, even though only one servo-controlled actuator was available for testing. The drive axle was thus incorporated into the model using HiL, while the steer axle was damped using a mathematically modelled linear damper. It was found that a time step of 2ms was sufficient for the tests. Road inputs were again given by a PSD function.

Random road inputs were used as preview control lends itself to best performance in these situations. However, because of the use and repeatability of transient obstacles, a 10mm step was also used. (The maximum step height was 10mm, due to limitations in the experimental equipment in this case.)

One of the problems associated with preview control simulation is also one of HiL simulation's strong suites – due to time lags between damper setting demand and execution due to physics, sensors, etc. a time penalty must be imposed or added to the theoretical control system. In HiL simulation, with its flexible parameters, this is not a problem and merely an addition to the vehicle model. Indeed, Kitching implemented phase lag compensation during the tests, necessitating the prediction of the future states of the HiL vehicle. This can be done in two ways: open-loop prediction, during which a vehicle model runs ahead of the HiL model, so that the demanded damping force required by the HiL vehicle drive damper can be predicted by the model, and run-ahead prediction, using current HiL states as the initial conditions for a short theoretical model simulation to determine demanded force. The

latter process is far more robust, as the HiL vehicle is dependent on the real, physical damper all the time and is thus giving the correct states during each HiL simulation step. The former method depends heavily on the accuracy of the theoretical vehicle model without the real damper, circumventing the reason for using HiL simulation – to use the real component instead of a flawed or inaccurate model. It is, however, not nearly as computationally complex as the run-ahead prediction scheme, and is thus used. Faster computers will enable the use of run-ahead prediction, leading to even more accurate HiL simulations incorporating phase compensation. (The tests were done using an 180Mhz Pentium Pro PC; PCs more than 20 times faster are available today!) Using open-loop prediction also worked because of the relatively short-timed road disturbance signals, for example, the step input test lasts only 1 second. This negated the need for long time histories and kept numerical integration errors in check.

According to Hwang, Heo, Kim and Lee [28] electronically controlled adaptive suspension systems cannot offer real ride quality benefits and be as safe as passive suspensions when utilising open-loop control. Improvements can only be seen when closed-loop control is implemented. Also, due to the complexity, power requirements and cost of active suspensions, variable-damping suspension systems will become the high-performance suspension system of choice in the future. The control system that was proposed was implemented and tested using a HiL setup. In fact, the compared control systems (e.g. bang-bang or on/off control, proportional control and skyhook control) were all dynamically tested using the HiL test bench, while the software vehicle was once again a quarter car model. It is stated that the proposed actuator to be used should have a maximum velocity of 1.5 m/s and have a response time of less than 10ms. The frequencies of interest are below 20 Hz. The experimental damper developed by the authors was not only tested using the HiL setup; it was also characterised by tuning it to a known passive damper. It was found that a continuous control method gave improved ride comfort, while bang-bang control provided superior handling (although this conclusion is strangely reversed in the paper). It was suggested that a controller utilising both an on/off element and a continuous element should be investigated, since it is thought that it would deliver the best all-round performance.

1.3.4. Background to Skyhook Damping

In the middle 1960's D Karnopp and a graduate student, Bender, initiated a study attempting to apply optimal control to automobile suspensions [29]. Before that time, some work was done in the field of active suspensions and control systems respectively, but without much technology sharing. Each was considered a science in its own right. When considering the problem of control applied to active and semi-active suspension systems, they found an optimal damping layout, which they called "Skyhook Damping". Obviously, this layout was impractical in real life, but the use of active and semi-active elements in a suspension configuration enabled implementation.

Skyhook damping theory states that the optimal layout for a sprung mass is that the damper, with a damping ratio of $\zeta = 0.707$, should be connected so that the velocity of the damper is essentially the sprung mass velocity; the damper should thus connect the sprung mass directly to a stable, constant height level. Control laws for skyhook damping states that an actuator placed between the sprung mass and the road (the intermediary being the unsprung mass or wheel) must produce the force that the idealised damper would have produced.

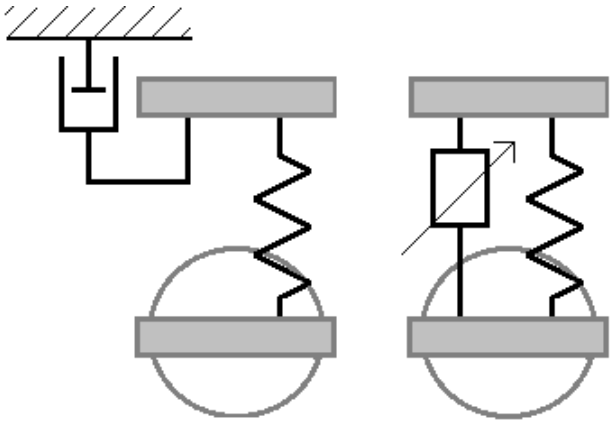

Figure 1-21: Skyhook damping schematic, and its realisable counterpart.

In the absence of an actuator, a 2-state semi-active damper can take the role of a skyhook damper by conforming to the control law

$$C = C_{Soft} \quad when \quad (\dot{x}_a)(\dot{x}_a - \dot{x}_b) < 0$$
$$C = C_{Hard} \quad when \quad (\dot{x}_a)(\dot{x}_a - \dot{x}_b) > 0$$

Here, x_a is the sprung mass displacement and x_b the unsprung mass displacement. This control law is shown schematically in Figure 1-22.

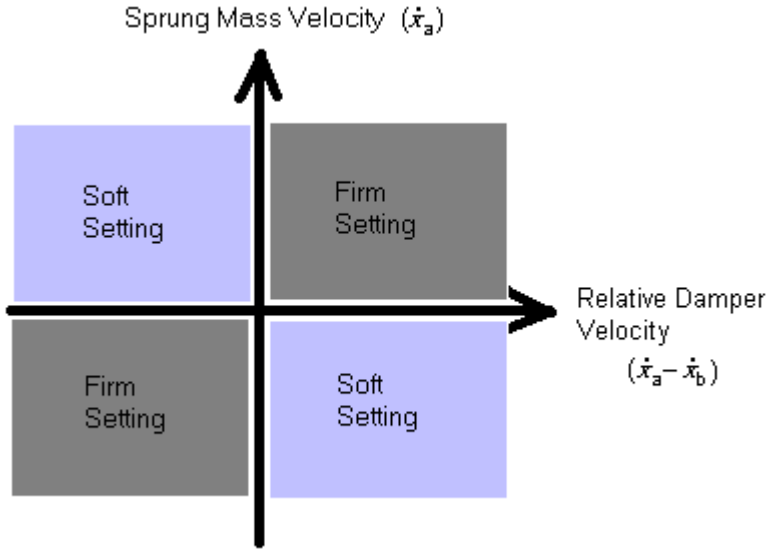

Figure 1-22: Skyhook control law for semi-active dampers

Because the semi-active damper cannot put energy into the equation, it doesn't perform as well as an active suspension system would. There are, however, other ways in which semi-active suspension systems are superior to active suspension systems.

Skyhook damping proved more influential than most originally thought. Even though it was derived through optimal linear control theory using a single degree of freedom model and white noise as input, its form is still prevalent in many other scenarios. Consider, for example, the control law proposed by Hölscher and Huang (as quoted by Nell [30]):

$$C = C_{Soft} \quad when \quad (\ddot{x}_a)(\dot{x}_a - \dot{x}_b) < 0$$
$$C = C_{Hard} \quad when \quad (\ddot{x}_a)(\dot{x}_a - \dot{x}_b) > 0$$

Rakheja and Sankar propose a similar control law (also from Nell [30]):

$$C = C_{Soft} \quad when \quad (\dot{x}_a - \dot{x}_b)(x_a - x_b) > 0$$
$$C = C_{Hard} \quad when \quad (\dot{x}_a - \dot{x}_b)(x_a - x_b) < 0$$

It is clear that skyhook damping is an important concept when working with active and semi-active suspension systems and their control.

1.3.5. Tests Used By Various Authors in Their Work

In developing a road-sensing system to be used in active suspension preview control (look-ahead control), Kim, Yang and Park [31] used simulations as well as real road tests to determine the suitability of the system. These road tests were done in a vehicle equipped with various measuring and sensing tools, including a data capturing device, preview composite-sensor system, and vehicle body vibration measurement equipment. The vehicle was driven over deterministic and random road sections in a testing ground, at velocities of between 10 and 80 km/h. (The deterministic road inputs were 0.1m deep, 6m long concave bumps which were traversed at 10km/h, while the random road inputs were PSD functions with road roughness coefficient values between C_{sp} = 2.2x10^{-2} and C_{sp} = 3.1x10^{-5})

Lab simulations were also run during the suspension system's development. If suitable random road inputs are not available for the simulations, they were constructed by filtering white noise with a shaping filter, to obtain these inputs. The simplified road model is expressed as

$$S(w) = C_{sp} w^{\alpha}$$

with C_{sp} the road roughness coefficient, α the exponent and w the wave number [cycles/m]. This equation is essentially a PSD formulation. Kim et al considered this road input mechanism with α between -2 and –1.5, however, this type of road input did not give the desired random signal frequency range, and so they decided on a more complex PSD related method,

$$S(w) = \left(\frac{\alpha_1^2}{\pi}\right)\left(\frac{\alpha_1 v}{w^2 + \alpha_1^2 v^2}\right) + \left(\frac{\alpha_2^2}{\pi}\right)\left(\frac{\alpha_2 v(w^2 + \alpha_2^2 v^2 + \beta^2 v^2)}{(w^2 + \alpha_2^2 v^2 + \beta^2 v^2)^2 + 4\alpha_2^2 \beta^2 v^4}\right)$$

with w the angular velocity, v the vehicle velocity, while the coefficients α_1, α_2, β_1 and β_2 are dependent on the road type. It is clear from the complexity of this equation that a more realistic way of simulation is the application of the measured road input data.

Also, the development and usage of a hardware-in-the-loop experimental setup is suggested by the authors (but not used) due to the nature of the tests and the repeatability of the HiL setup. For the type of accuracy required the actuator dynamics will form part of the DSP/FFT chipset housing the control system and motion algorithms. Of course, a benefit of this type of testing is that even if the sensors required for preview control may technologically not be feasible, or too expensive, the control system can be thoroughly tested and optimised without being hampered by the shortcomings of the road sensor. In fact, the development of a suitable road sensor is what hampered previous research into such a preview control system as undertaken by various other scientists.

Choi, Lee and Chang [1] developed an electro-rheological damper for use in a mid-sized passenger car, controlled using skyhook control theory. The development of the suspension system began with the production of four ER dampers, which were then characterised and fitted to the test vehicle. Some work has previously gone into design and characterisation of ER dampers for quarter car experiments, but the rarity of full vehicle tests prompted this research. The tests required not just the dampers, but a DSP-board equipped microcomputer, accelerometers for the suspension and body movements, and high-voltage amplifiers.

Hardware-in-the-loop is ideally suited to this kind of test, as all four wheel stations can be simulated at once in real-time, and the need for special high-voltage amplifiers is

negated. During the pitch test, only two actuator/damper combinations need to be active, and should something go wrong with one of the dampers or it needs an adjustment, it can just be removed from the actuator and replaced without problem.

The tools used in HiL test setups are found in other tests as well. Venugopal, Beine and Ruekgauer [32] used dSpace development tools to implement an ARMARKOV adaptive controller (AAC) in real time utilising a MIMO model. The dSpace system used is a dual processor setup, one processor to simulate the full vehicle model, and the other to run the controller. Adaptive control is superior to general robust control in that it adjusts controller gains during operation, allowing greater uncertainty levels to be tolerated than robust control, and to improve system performance during operation. Its inherently non-linear character allows it to even control some time-variant systems with success.

The power of the dSpace system is illustrated here – the vehicle model is implemented in Fortran as a 58 DOF system, which is translated to C code for implementation in a Simulink S-function block. The Simulink model is easy to implement in real-time, and due to the processing power of the dSpace boards, a sampling time of 0.1 ms is achievable. This allows real-time simulation of intensive models while adaptive control is applied.

Roberts, Deakin and Crolla [33] developed a semi-active damper controller using rapid control prototyping methods – implementing the control system as software in a pure software computer simulation. This enables the modification and improvement of the control system without the need to alter hardware, and also decreases development time, as algorithm and software design is completed in one operation when using a suitable microchip emulator. The semi-active damper is intended for use in a combat support vehicle. RCP has an advantage over traditional control design in that the software can also control the hardware on which it is to be implemented – the control software can be loaded onto various configurations of computers and I/O boards, and compatibility can be checked. This method usually utilises a real damper that is controlled, and it follows the damper's development and production.

To develop the control system, the real hardware was modelled mathematically as a quarter-car using two equations of motion derived from Newton's second law. In this instance, the variable damper was modelled in the simplest fashion available, which is linear damper with variable rate. A penalty function was derived so as to optimise the control system parameters. After offline, non-real-time simulations gave an indication of a suitable model, hardware tests were conducted using a single DOF setup. This setup utilised a lever supported by an actuator, with a mass at the lever's tip. The advantage of this setup is that there are no linear bearings, however, geometric non-linearities are introduced. As predicted by Besinger [12], overly optimistic results were obtained. It is worth noting that the computer simulation employed a 4^{th} order Runge-Kutta integration algorithm, with a step size of 3ms.

1.4. Characterisation of Suspension Components

Before the suspension components used in this study was employed in the HiL setup, they were characterised using conventional methods. Various springs and dampers were available for use, and suitable units were selected after their applicability was determined. Different units were also used for different tests – the equipment used will be discussed when the appropriate test is discussed.

Springs are easily characterised. An actuator compresses the spring while the force output of the spring is measured via a load cell. The force and displacement data are all that is needed for a spring characterisation diagram, which is a force-displacement curve. The slope or gradient of the curve at a certain displacement gives the spring's rate or stiffness coefficient. One must remember that not all springs used are linear, although the nature of the non-linear springs is usually bilinear, with negligible hysteresis due to either

internal or external friction. The input excitation used during static deflection tests was a very long period triangular wave, the long period (low frequency) approximating static conditions. (Periods were typically in the range of 300 seconds for 100mm peak-to-peak excitations.)

Characterising the damper is somewhat more work, but still relatively simple. The needed data for a damper's characteristic diagram is velocity and force data; a load cell supplies the latter, while the former is simply taken as the derivative of the displacement. The data is recorded while the damper is excited with successive harmonic signals, with the frequency of said signal increasing to increase velocity. For the dampers used in this study, a maximum velocity of approximately 0.8m/s was sufficient. Other dampers may be tested at velocities up to and exceeding 1.5m/s. The velocity can be achieved using 50mm peak-to-peak sine waves, with a maximum frequency of 7.5Hz, which translates into a maximum velocity of 1.18m/s.

The motorcycle tyre used in the HiL test of Chapter 4 posed more of a problem than the springs and dampers did. Characterisation of the tyre was done in three steps: Determining the spring component of the tyre through static deflection tests; determining the damping of the tyre through impulse excitation response; and determining the transfer function between the wheel hub and road input (the reference point) through random excitation.

Static deflection tests were done by securing the wheel spindle to the actuator frame posts. A strain gauge type load cell was placed between the actuator and the tyre. Displacement was measured using a small, spring-loaded strain-gauge type displacement transducer, which differed from the actuator's internal LVDT used for displacement control. Both sensors were amplified using a digital bridge amplifier (an HBM amplifier, model MGC, commonly called by its model name), and the results were measured. The strain-gauge type displacement transducer was used because it offers considerable more accuracy than the LVDT of the actuator. The tyre was characterised using discrete static deflections as well as a long period triangular wave, the results of which are shown below. Air pressure inside the tyre was 100 kPa above atmosphere. The results of the characterisation tests are shown in Figure 1-23.

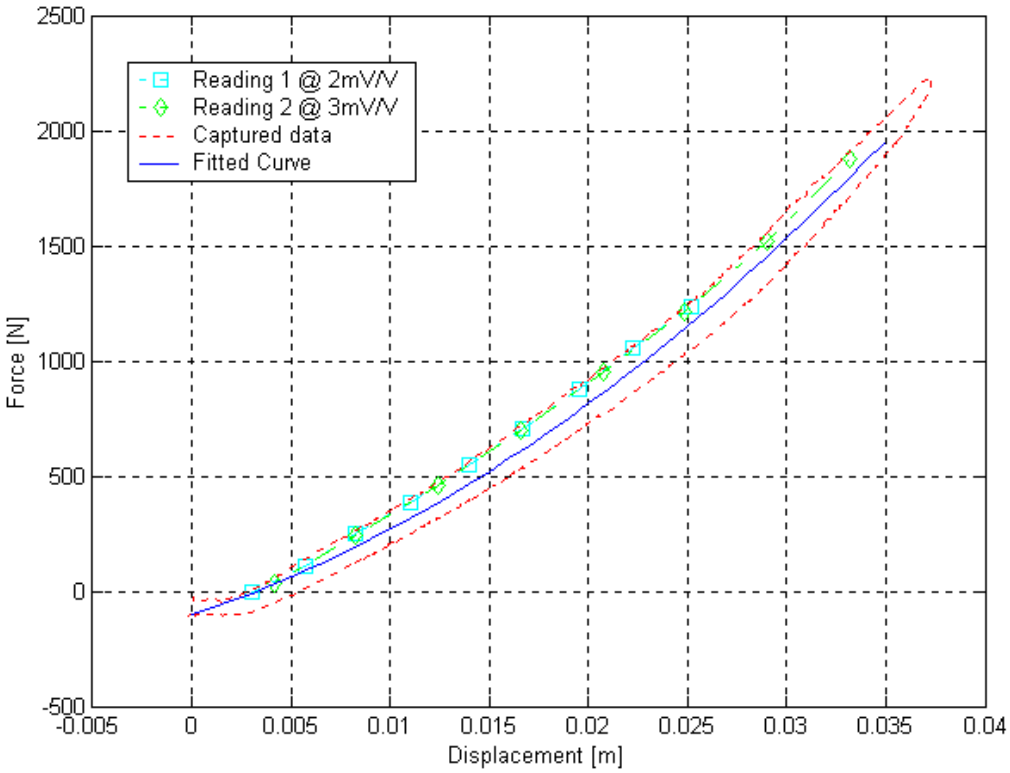

Figure 1-23: Tyre stiffness test results

The stiffness characteristic of the tyre shows a clear non-linear behaviour, which is easily explained when considering that the gas pressure inside the tyre, which increases as deflection increases, adds to the tyre-wall force when measuring the tyre stiffness. Two tests were done for different bridge amplifier settings, named “Reading 1” and “Reading 2”. These tests were done measuring the tyre force at static positions. The curve called “Captured data” was created using a continuous motion input slow enough to be considered static, compressing and relaxing the tyre. A very low frequency triangular wave supplied this input. The hysteresis shown in the figure is due to the tyre friction as it deforms on the contact patch below it (the load cell). Fitting a polynomial function through the measured data, the tyre force equation was determined as

$$F_{tyre} = 8.63 \times 10^5 x^2 + 2.85 \times 10^4 x$$

with x the tyre deflection in meters and the constant force term (due to inaccurate zeroing of the load cell) neglected. Of course, the slope of the curve gives the tangent stiffness; in this case, the tyre’s tangent stiffness is (with x again the deflection)

$$K_{tyre} = 17.26 \times 10^5 x + 2.85 \times 10^4$$

The damping of the tyre was determined using an impulse input to excite the tyre with, and then monitoring its response. The impulse given was a compressive force, allowing the tyre to “bounce” as its first free motion, without losing contact with the supporting surface (Tyre bounce in which contact is lost will give bad results due to heavily non-linear motion). A logarithmic decrement method was then used to determine the damping ratio and the damped natural frequency of the tyre. (For this test, the tyre was attached to a swingarm long enough to ensure that geometrical non-linearities are insignificant.) The logarithmic decrement, δ, leads to the damping ratio ζ in the following manner:

$$\delta = \ln\left(\frac{x_0}{x_1}\right) \qquad \zeta = \frac{\delta}{\sqrt{(2\pi)^2 + \delta^2}}$$

As can be seen from Figure 1-24, numerous inputs were run successively and the damping ratio and damped natural frequency was computed for certain intervals – the stars show the successive oscillation maximums used in the logarithmic decrement computations, and the circles show the intervals used to search for said maximums. A close-up of the response of one impulse motion is given in Figure 1-25 for clarity. (Note: To determine the logarithmic decrement, only relatively large displacement responses were used. The higher responses are those higher than a baseline, which is shown by the checking intervals, marked by a circle on the figure – a circle where the signal is rising, i.e. a positive slope, signifies the start of the interval. The interval ends at the next circle where the signal is falling, i.e. a negative slope.)

The damping ratio determined from the data is 0.054; this is very low, as can be expected from a tyre. In fact, most authors using a quarter-car model in their simulations and tests, albeit HiL or pure computer simulations, model the tyre as a spring only – the damping of the tyre is neglected. The results given by the tyre in question here supports the practice of neglecting tyre damping. For the purpose of this study, however, it will be implemented in the model.

With the damping ratio known, one can determine the damping coefficient *C* of the tyre when given the tyre assembly weight. Also determined during the test was the damped natural frequency of the tyre – it was found to be about 12 Hz. This value must be viewed in perspective, however; it seems that the damping of the tyre is indeed not constant (one would expect this) and the periods measured between the successive peaks, giving the frequency, aren’t constant. The damped frequency given is close to the expected frequency. Even though the logarithmic decrement method was derived for linear damping systems, it is applicable in this case. Only the first few maximums of each data set was used, while the damping behaved linearly – this is echoed in the fact that the damping ratios predicted by the successive peaks were very close to each other magnitude-wise. At the low-amplitude local maximums, there was a strong non-linear effect, and hence these readings weren’t used.

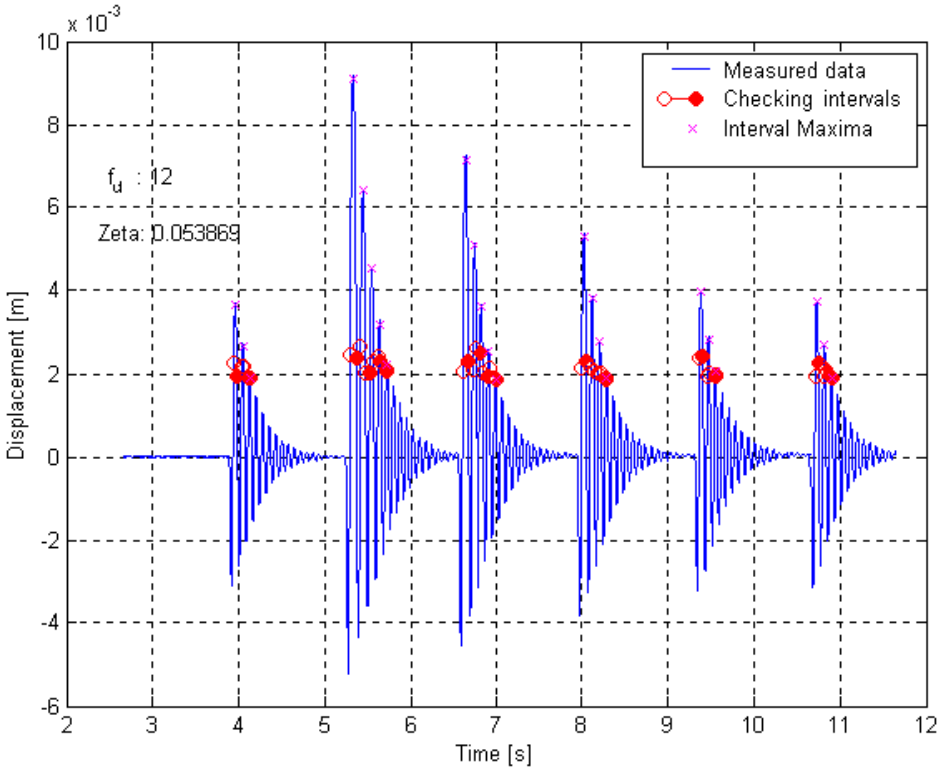

Figure 1-24: Measurements to compute damping of tyre

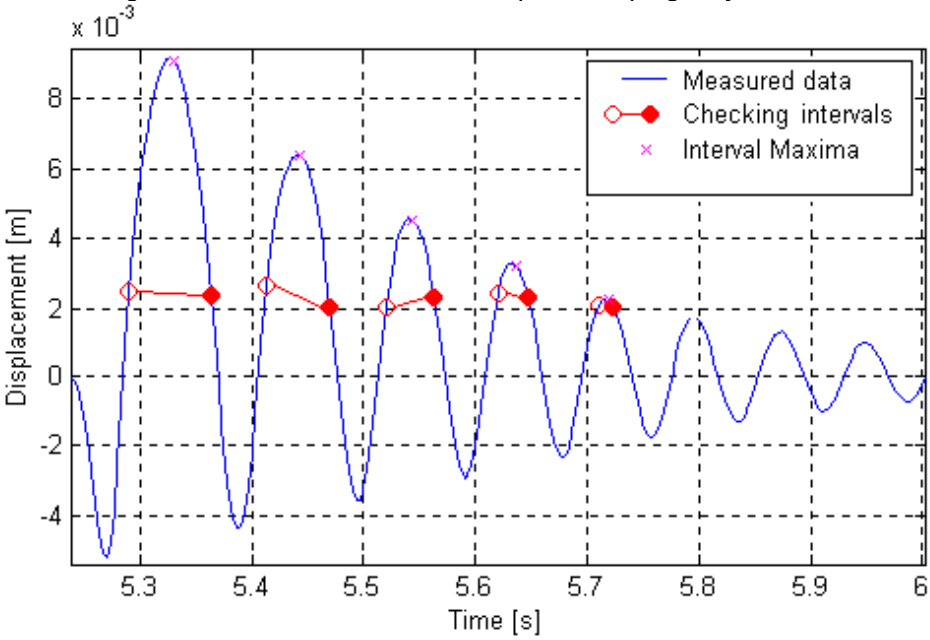

Figure 1-25: Close-up of measured data, for logarithmic decrement

The third stage of tyre characterisation was undertaken as a check to see if the previous tests yielded believable results. As such, a transfer function was determined between points on the tyre contact level and the wheel spindle. This was done by measuring accelerations at these points. Accelerometers were used to measure the accelerations, and a Siglab A/D & D/A unit and its software were used to determine the transfer function. The Siglab was also used to generate a suitable random excitation signal for the actuator.

The results of the transfer function analysis are shown in Figures 1-26 and 1-27 for different RMS acceleration magnitudes; this is as one would expect, since both excitations were well below the amplitude which induced wheel hop (which was,

incidentally, at 70 mV RMS; this corresponds to a displacement input with an RMS value of 0.35mm). Using the fitted curves for several different bandwidths and excitation amplitudes, a mean value for the tyre stiffness and damping could be determined. The data is summarised in Table 1-1. For the purpose of fitting a curve through the measured data, a SDOF spring-mass-damper transfer function was used, which can be determined with the aid of a Laplace transform of the equation of motion:

$$m\ddot{x}_s = k(x_r - x_s) + c(\dot{x}_r - \dot{x}_s)$$

$$L\left(m\ddot{x}_s - k(x_r - x_s) - c(\dot{x}_r - \dot{x}_s)\right) = mX_s s^2 - kX_r + kX_s - cX_r s + cX_s s$$

$$\therefore G = \frac{cs + k}{ms^2 + cs + k}$$

Also, a constant mass value of 9.9 kg (equivalent mass) was used for the fitment calculations.

Table 1-1: Curve fitting parameters

Mass	Damping	Stiffness
9.9	65	79992
9.9	70	83490
9.9	59	77897
9.9	57	80624
9.9	64	82005
9.9	62	79476
9.9	57	66149
9.9	64	78135
9.9	59	75254
9.9	72	76862
9.9	55	80413
9.9	72	76991
9.9	57	73879
9.9	54	80276
9.9	60	71128
9.9	57	73909
9.9	71	61660
Average Values:		
9.9 kg	62 Ns/m	76361 N/m

A quick comparison of the two stiffness and two damping values obtained through the two methods follows. When considering a wheel and tyre combination mass of 9.9kg, it seems that the tyre deflects statically under a weight of just under 100N. This corresponds to between 3mm and 4mm static deflection, at which point the tyre stiffness is 35kN/m. However, from Table 1-1 it can be seen that the average tyre stiffness measured during the acceleration tests is 76kN/m. This can be explained through the fact that the tyre deflected far more than 4mm during the tests, resulting in the higher measured stiffness. Also, the curve fit is based on an estimated static mass of 9.9kg; no dynamic effects were accounted for. The effective mass of the dynamic system will in all probability differ. The non-linearities in the tyre also play a part.

When considering the damping as determined by the transfer function curve fit (with a ζ of 0.036), it can be seen that this value is lower than what is predicted by the damping ratio of 0.054. Both damping estimates are strongly dependent on the estimated mass. The damping coefficient determined using the logarithmic decrement is 50% larger than that determined using the curve fit. Even when assuming different masses this 50% gap persisted between the curve fit and damping coefficient given by ζ. This could be due to the fact that the tyre deflected much more during the logarithmic decrement tests, and only the higher amplitude data was used – even the data measured for use with the decrement method showed strong non-linear damping effects.

It has to be mentioned that major discrepancies arose due to the fact that the tyre's stiffness and damping is non-linear, while it was attempted to fit it to a linear spring-mass-damper system's transfer function. It is thus expected that the correlation won't be perfect, and the transfer function test can only serve as a check to see if the stiffness and damping values are of the same order of magnitude – a "ball-park" value, in essence.

These inconsistencies proved troublesome when analysing the motorcycle rear wheel geometry as discussed in Chapter 4. The stiffness used in the simulations will be discussed then.

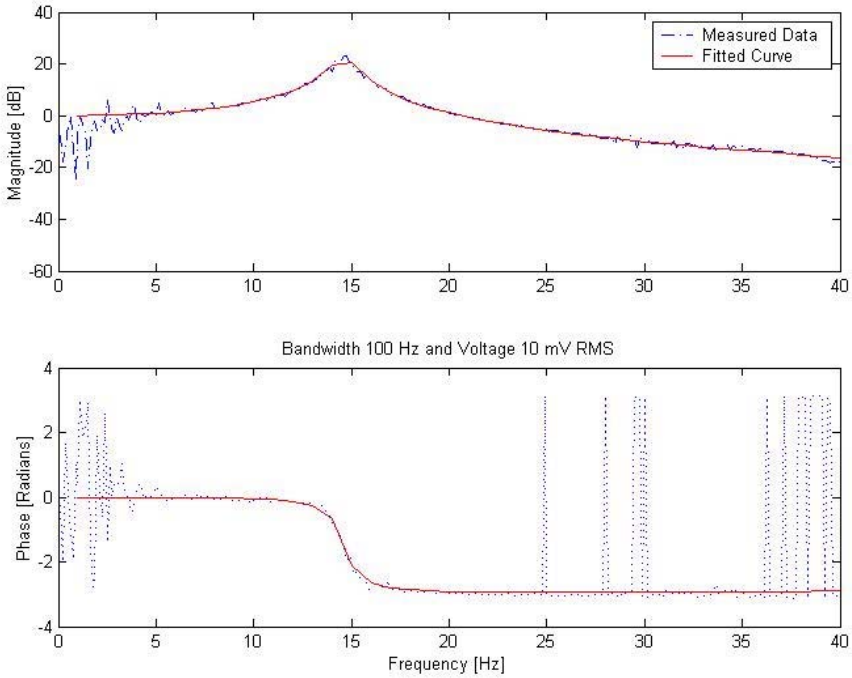

Figure 1-26: Fitted transfer function data for 100Hz bandwidth, 10mV RMS excitation

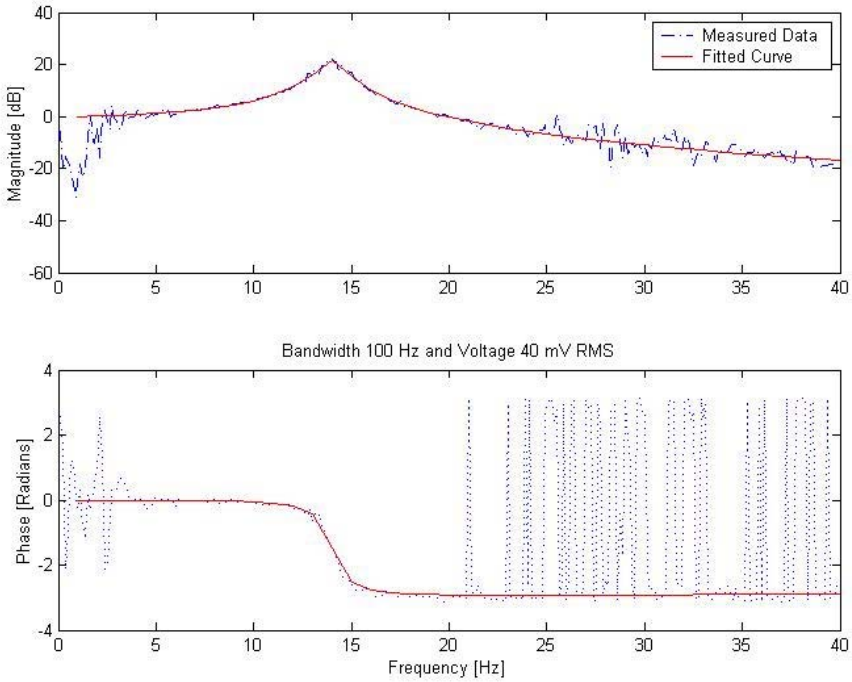

Figure 1-27: Fitted transfer function data for 100Hz bandwidth, 40mV RMS excitation

1.5. Hardware Used in This Study

An overview of the main hardware used in the study will be given in this section, as there are numerous ways to implement hardware-in-the-loop simulations using different hardware configurations. Already, a method using an A/D&D/A card coupled with a 386 PC running custom C code has been discussed. As computer technology advances along with I/O methods and protocols, HiL will become increasingly easier to implement.

Every engineer has access to a computer capable of simulation. This can be done with either custom code running on the PC, like C or C++, Pascal or Fortran, or with purpose-developed off-the-shelf applications like MatLab's Simulink or National Instruments' LabView. Control engineers can design control algorithms and run software simulations much faster than the real system on their PCs. Similarly, many embedded software engineers first test the embedded code by running a reasonable facsimile of it on a desktop PC before porting it to the final micro controller. They emulate the embedded system's I/O and environment with custom code executing on their PC. Of course, there are differences between this kind of pure software simulation and HiL:

- Software simulations give device outputs as numbers stored in memory bytes ready for the next CPU computation, not real hardware signals with noise, conductor resistance, etc.;
- HiL simulations run in real time;
- HiL simulations use the real product or part that will eventually be built into the completed system, not an imaginary part running on a workstation.

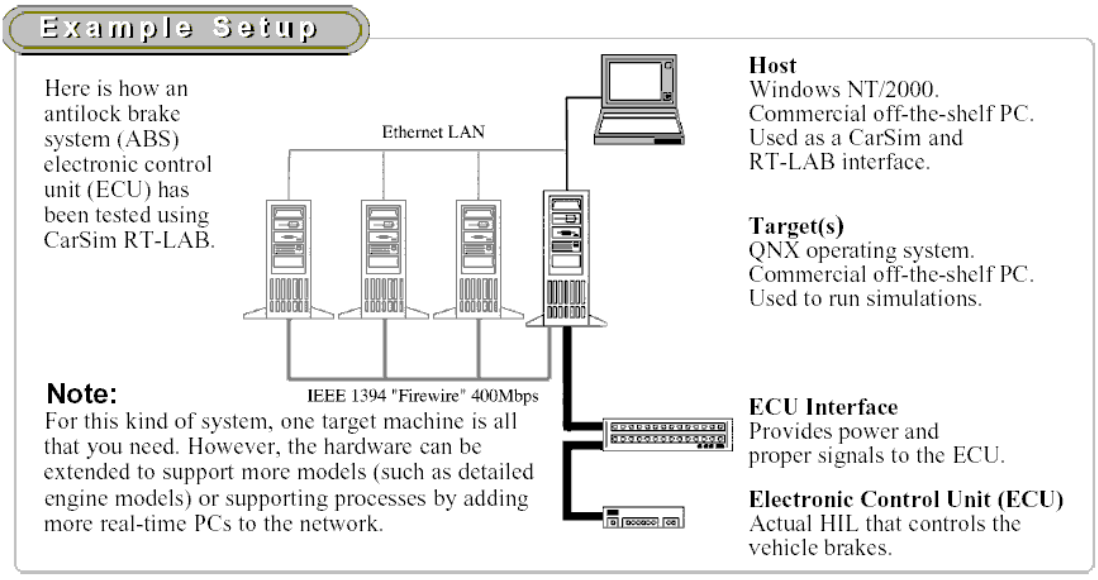

Figure 1-28: Example of the CarSim system

According to Gomez [2], there are no real off-the-shelf HiL tools available. This is understandable, since different products will require different approaches when using this kind of simulation. He led a team in designing a custom HiL system having 100 inputs and outputs, capable of iterating a fairly complex model at 70 Hz. The first unit cost $100 000 (in the mid 1990's) while the second unit cost only $25 000. This was significantly less than the Unmanned Aerial Vehicles that the company was developing, and more importantly, it allowed the development of various systems to be used on the UAVs before a lot of the hardware needed for conventional flight-testing was available. Recently, however, more and more ECU HiL setups have become commercially available. Systems like CarSim by Mechanical Simulation Corporation (an example of which is shown in Figure 1-28) and an interface to the MSC.ADAMS software for HiL and driver-in-the-loop by "IPG Automotive GMBH" are available. DSP board manufacturers dSpace have also introduced specialist ECU HiL simulators. It must be said that these

products are usually aimed at a specific application, and none are readily usable for the simulation of mechanical systems.

Two commercially available systems do have potential for HiL testing and simulation. Firstly, dSpace creates various DSP-based I/O boards that interface either directly with a PC slot or through a chassis connected to a PC using Ethernet. The boards are fitted with Texas Instruments DSPs, which provide computing power that a conventional CPU-I/O device is hard-pressed to keep up with. Coupled to this is the fact that dSpace also provides software to allow the porting of Simulink models to the DSP hardware, making it considerably more user-friendly than the norm. DSPs are notoriously difficult to use for the inexperienced. The software takes care of that problem by compiling C code from the Simulink model and downloading it to the board automatically. The second potential system is the before mentioned LabView package which can interface with a large variety of National Instruments I/O devices. The PC supplies the processing power in this case, but the interface between hardware and software is optimised sufficiently by NI to allow implementation in a HiL environment. It is user-friendlier than the dSpace boards with its ability to develop virtual instruments, however, when implementing more complex models and with other applications running in the background (like data capturing software accessing the hard drive) it doesn't achieve the performance that can be given by the DSP-based systems. (The dSpace boards store the compiled C code locally, so once the program is started it requires none of the PC CPU's computational power. This means that it can be implemented on a slow PC without adversely affecting the DSP.)

In this study a dSpace DS1102 DSP board was used to run the HiL control software, while a separate CDAS equipped computer handled the data capturing. A Schenck actuator/controller combination supplied the motion.

1.5.1. The dSpace DSP Card

The DSP board used is a dSpace DS1102. This board has an ISA port interface, and was installed in a 100MHz Pentium PC equipped with 16MB of RAM. Even with this inferior PC the DSP performed admirably. The drawback of this "slow" PC is that it ran Windows 3.1 and MatLab 4.2, which are somewhat outdated, and this restricted the model generation. (Some Simulink blocks aren't available for C translation when using the older Simulink and RTW versions. The new dSpace software is available, enabling more features and blocks to go with MatLab 5.3 under a later Windows version, but a more powerful PC is needed for this software.) Still, using the older Simulink version together with the block library as supplied by dSpace, sufficiently complex models were implemented and executed at an incredible pace. Simple SISO filtering models can be implemented at over 30kHz; that's a time step of about 0.03ms! The coding and implementation phase also requires MatLab's Real Time Workshop, even though the user does not have direct contact with it.

The dSpace board's performance comes form the onboard Texas Instruments TMS320C31 DSP chip. Coupled with a fast I/O controller and A/D & D/A converters, as well as sufficient on-board memory to store rather complex models, this board has more than adequate performance for the application at hand. There is also digital I/O ports available on the board, but only the four analogue-to-digital and four digital-to-analogue channels were used. The interface to the DSP card is via a 62-pin high-density sub-D connector, and there are more connections other than the digital and analogue inputs and outputs, like pins to connect to a slave DSP. These are not used in this study and will not be discussed. As a standalone the DS1102 board offers the following:

- 4 channels each for A/D and D/A conversion,
- 10 digital I/O,
- 6 independent channels for PWM generation,
- One incremental encoder interface,
- One hardware interrupt.
- 128kb on-board memory, with 2kb memory on the chip

Later versions of the dSpace software include applications like ControlDesk and Cockpit, software used to simplify the creation of user-friendly DSP-based control systems and applications.

1.5.2. Texas Instrument's DSK

There are several TI Developer Software Kits (DSKs) available at the UP. Before the availability of the dSpace board with which to handle the HiL simulations, it was proposed to use some of these DSKs. Even though each kit only has one output and one input, the hardware can easily be "daisy-chained" using some easy to implement custom wiring. However, from a mechanical engineer's point of view, the software supplied with the DSKs is woefully inadequate when considering modelling and compiling of mathematical models and control systems. Every program needs to be custom written in C and compiled, linked and downloaded to the DSK using a black-box set of commands. No information is given on how to program for chained DSKs, and a software debugging tool is also absent. The C code, along with the memory pointers and interrupts, has to be programmed and compiled without testing the code in its final form first. It is the opinion of the author that it would be easier for anyone not fluent in C to learn assembler code directly, and to implement programs in that way. Of course, every time a new model is used, it must be programmed and implemented from the start, so even changing a model parameter like the mass entails a reprogramming of the DSP.

1.5.3. Other dSpace Products

As already mentioned, dSpace introduced a range of products for the exclusive task of ECU HiL simulation. These products differ from small PC-based units to cabinet-installed, 50 channel multi-purpose hardware units. For HiL simulation of mechanical systems, there are a lot of boards similar to the DS1102 on offer; these boards use DSPs varying from the TMS320C30 to the newest TMS320C5x and C6x chips. Some of these chips, like the C32, have the ability to interface with external SDRAM, due to its small internal memory.

dSpace products' strong suite is the high-level interface it offers to users; the DS1102 board, for instance, is a DSP board that can be used by anyone who knows a little about Simulink, a MatLab add-on that is intuitive to learn. In contrast to Simulink, assembler code and object manipulation is best left to professionals – it is not something that is intuitive or easy to learn, and DSP usage in this context is out of reach for most mechanical engineers.

1.5.4. Actuator/Controller Combinations

The Sasol Laboratory is fortunate to have several hydraulic actuators available for use; these range from high-stroke high-velocity 40kN actuators to a 630kN load test actuator. For repeatability and availability reasons, most of the tests were done using a relatively small actuator with dynamic response as given in Figure 2-13. This figure shows the natural frequency and useful bandwidth of the particular actuator/controller combination. The controller's PID settings were such that good dynamic response with acceptable overshoot and settling times were obtained. This was done so that the actuator could keep up with the HiL simulation without unacceptably large phase lags, while staying stable.

Unfortunately, due to the LVDT used in the controller's displacement feedback loop, phase lag other than that caused by the PID control is present. This is due to the fact that the LVDT is energised with a high-frequency carrier signal, and displacement (or rather changes in it) is detected by induction. The displacement signal given as output by the controller is a filtered version of that which physically leaves the LVDT. This process causes additional phase lag – it is visible in the plot of Figure 2-12.

The actuator dynamics will be discussed further when the hardware-in-the-loop simulation for the single degree of freedom system is set up, in Section 2.3.

1.5.5. MGC Bridge Amplifier

The strain gauges as used in the load cell and the external displacement transducer are amplified using a MGC-model digital bridge amplifier by HBM. The advantages of using this digital bridge amplifier is great – it is very easy to switch the amplification ratios, zeroing is done with the touch of a button, and there are reconfigurable digital filters built in. Furthermore, each input channel has two output channels (front panel and back) each of which can be filtered independently through the available Butterworth and Bessel filters. A calibration chart for the load cell, as compiled using the MGC, is shown in Figure 1-29.

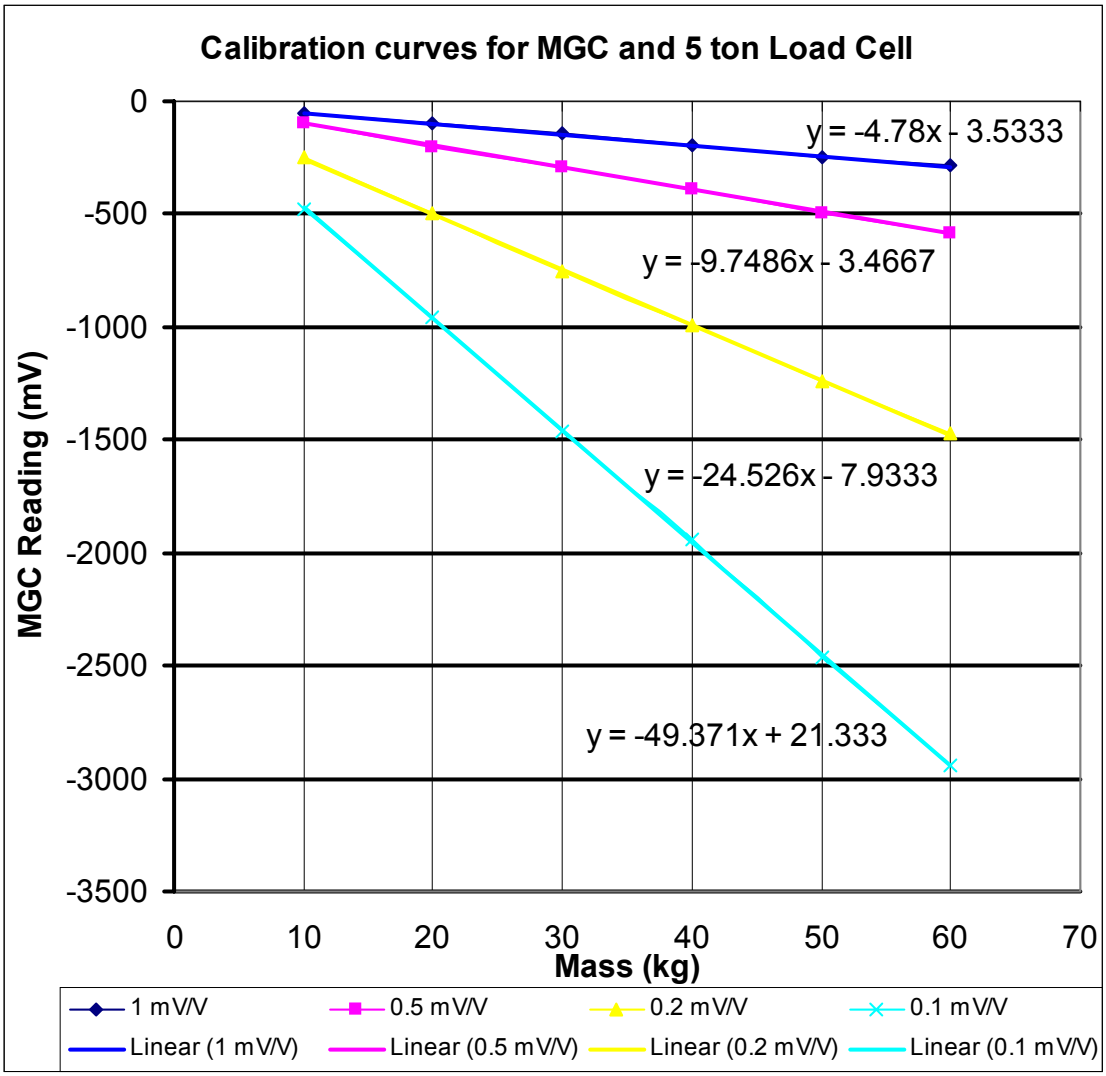

Figure 1-29: MGC calibration chart

The load cell was operated at a 0.2mV/V amplification setting, because this enabled a maximum in-range force of 4kN to be measured at a sufficient accuracy. A 5-ton / 50kN load cell was used as it granted the most versatility during tests, and was used solely for all the HiL simulations, giving good continuity throughout all the tests. Throughout the tests 100Hz or 400Hz Bessel filters was used (usually the former), due to the superior phase behaviour of this type of filter. Due to the relatively low frequencies of interest in all the tests, the 100Hz cut-off frequency was sufficient. The MGC allows for various types of sensors, not just strain gauges.

2. Single Degree of Freedom Testing

In this chapter both a single degree-of-freedom (SDOF) spring-mass and a spring-mass-damper setup will be investigated to determine the validity of hardware-in-the-loop simulations and to show its applicability to suspension tests. Although a SDOF setup is the simplest test setup that one can use to test dynamic systems, it has been employed in the testing of suspension components and the development of active and semi-active suspension control algorithms. An example of this is the levered mass test as used by Deakin et al [26], as shown in Figure 1-20.

The chapter will start with the derivation of general equations of motion, and focus will then move to software simulation, HiL simulation and a comparison of the results.

2.1. Mathematical Model

The single degree of freedom model is very simple to implement. It consists of a single body mass for which its vertical displacement is the only sought state. It is shown graphically in Figure 2-1 for forces acting on the body, and more appropriately, for a spring and damper suspending it above a reference input. This reference input is the excitation input of the system, the road excitation or road vertical disturbance.

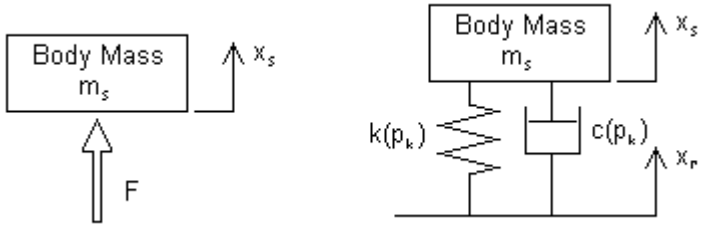

Figure 2-1: SDOF model

2.1.1. Equation of Motion

The equations of motion are derived using Newton's second law of motion, i.e.

$$F = ma$$

Using this equation on a SDOF system with a general spring and damper, and with velocity the first derivative of displacement and acceleration the second derivative of displacement, we get

$$k(p_k)\times(x_r - x_s) + c(p_c)\times(\dot{x}_r - \dot{x}_s) = m\ddot{x}_s$$

with p_k the parameters of the spring stiffness coefficient model and p_c the parameters of the damping coefficient model. Alternatively, the two terms on the left side of the equation can be written as $F_k(p_k)$ and $F_c(p_c)$, where p_k and p_c are appropriate parameters for the spring and damper forces F_k and F_c. (Remember that Segel and Lang described an 82-parameter model, so the parameters can be numerous!) Using the equation above, and assuming constant stiffness and damping coefficients, the equation of motion becomes

$$m\ddot{x}_s - k(x_r - x_s) - c(\dot{x}_r - \dot{x}_s) = 0$$

This is the form of the equation that is used throughout this chapter to calculate the displacement due to x_r, the road input excitation.

2.1.2. Analytical Harmonic Solution

It is possible to easily determine the solution of the equation of motion for a harmonic input, that is, input in the form of

$$x_r = A\sin(\omega t)$$

where A is the signal amplitude (max road displacement) and ω is the angular frequency of the harmonic input in radians/s. The solution of x_s will have a transient

part due to the initial conditions, and a harmonic part due to the excitation. With the road input as given above, the equation of motion becomes

$$m\ddot{x}_s + kx_s + c\dot{x}_s = kx_r + c\dot{x}_r = kA\sin\omega t + c\omega A\cos\omega t$$
$$= B\sin(\omega t - \psi)$$

with

$$B = A\sqrt{k^2 + (c\omega)^2} \quad and \quad \psi = \tan^{-1}\left(-\frac{c\omega}{k}\right)$$

This equation implies that the road motion will give a response similar to that obtained when a harmonic force is directly applied to the mass. The steady-state harmonic response of the mass is then

$$x_b = \frac{A\sqrt{k^2 + (c\omega)^2}}{\sqrt{(k - m\omega^2)^2 + (c\omega)^2}}\sin(\omega t - \psi - \alpha)$$

where α is another phase shift,

$$\alpha = \tan^{-1}\left(\frac{c\omega}{k - m\omega^2}\right)$$

The simplified result can be given as

$$x_b = X\sin(\omega t - \theta)$$
$$X = A\sqrt{\frac{k^2 + (c\omega)^2}{(k - m\omega^2)^2 + (c\omega)^2}}$$
$$\theta = \tan^{-1}\left[\frac{mc\omega^3}{k(k - m\omega^2) + (c\omega)^2}\right]$$

Harmonic excitation is not the sole input, however. It has been stated by various authors that there is a need to determine responses due to transient phenomena – various different obstacles will be used as road inputs. The theoretical derivation of such a response will not be discussed here, but would be simple enough if the problem of the transient road inputs is broken up into smaller problems containing ramp and step inputs with various initial conditions.

2.2. Software Simulation

Software simulation is done so that an idea of the response of the system to a certain input can be given. The simulations are run using models for the springs and dampers to be used – the accuracy of said simulations are to a very large degree dependent on the component models employed. Even though the more complex models are more accurate than their simpler counterparts, they require much more time to implement and run in simulations. Simple linear models of the suspension components are used, which enables fast implementation and simulation, and enables the skipping of the numerous characterisation tests that are necessary when using more complex models. The spring and damper models used are discussed below.

2.2.1. Model Parameters Used

While it may be tempting to use complex models for the damper and spring, it certainly isn't recommended, as the amount of tests that are required to determine the parameters for a lot of the models are impractical. Furthermore, many damper models rely on the availability of information on the damper's layout, valve architecture and size, and the type of damper. It was decided to use linear models for both the spring and damper that is to be used in this part of the study. Accuracy was in this case sacrificed at the expense of efficiency, since the aim of the SDOF tests are to verify qualitatively that HiL can be employed, and to prove that the hardware

available was sufficient. It is for this reason that the software simulations and the HiL tests aren't quantitatively compared, as in the later chapters.

The implementation of a bilinear spring model is actually very accurate, as the spring characteristic diagram given in Figure 2-2 shows. The linear curve fit corresponds excellently to the measured data, as one would expect. Visual investigation of the spring showed that it was, in fact, designed to be a bilinear spring. Other non-linearities would only come into effect when the spring is greatly compressed and the spring's end conditions play a role, but to protect the spring and other hardware, displacement limits on the actuator controller doesn't allow this motion.

It should be noted that the convention used in this thesis differs from standard engineering practise, in that tensile force is not taken as positive when considering suspension units (springs and dampers) but rather as negative. The convention used could be summarised as follows:

- Compression leads to positive force and displacement values
- Extension (rebound) leads to negative force and displacement values
- Compression leads to negative velocity values (and negative damper forces)
- Extension (rebound) leads to positive velocity values (and positive damper forces)

The convention as described here can be explained with the help of Figure 2-2. A positive displacement on the x-axis means that the suspension component is compressed or shortened – this leads to a positive force. (The zero position of the force measurement will always depend on the load cell amplifier calibration and zeroing, but the convention remains intact.)

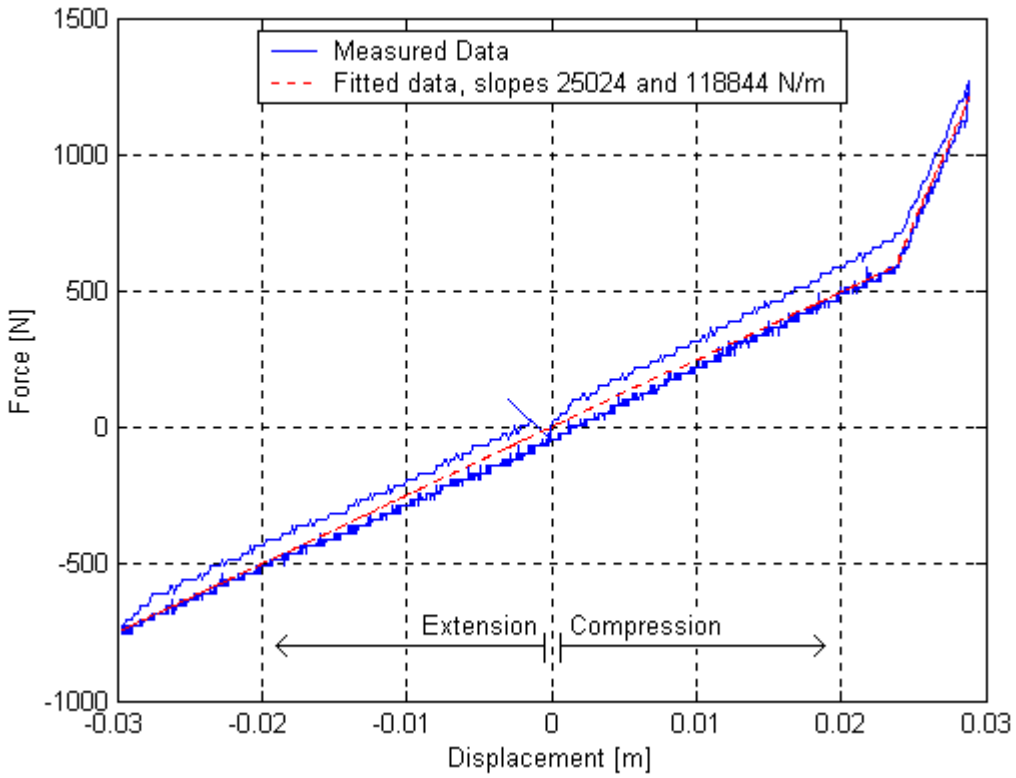

Figure 2-2: Spring characteristic used SDOF study

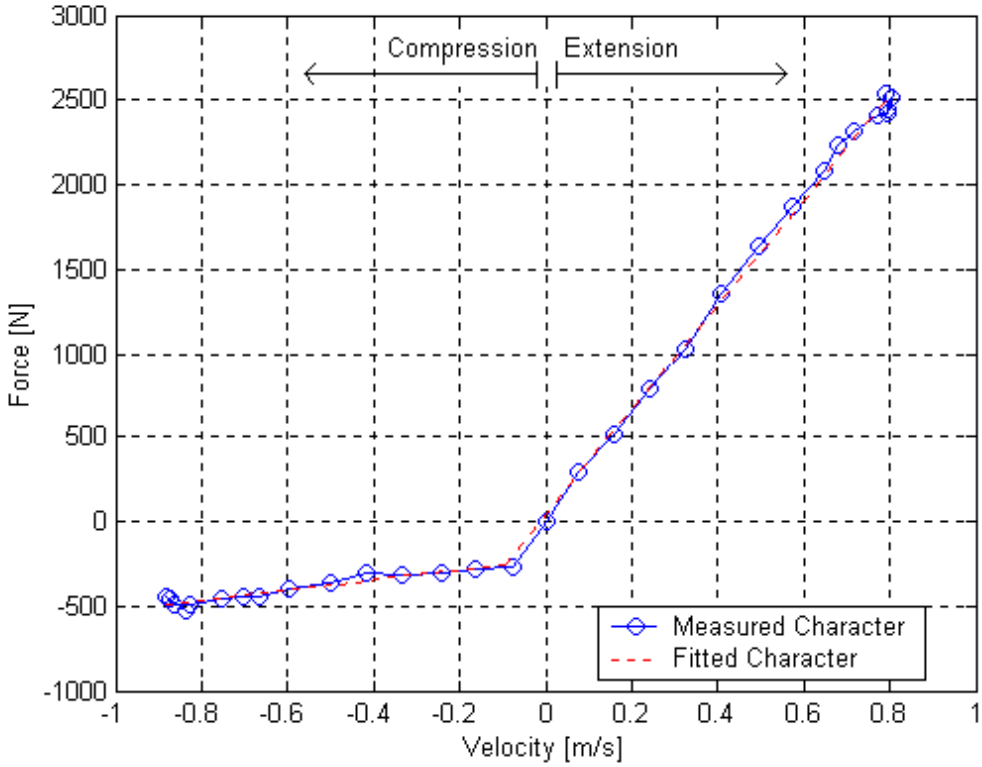

Figure 2-3: Damper characteristic used in SDOF study

The slight hysteresis in the measured data is due to the way the spring was fastened during characterisation – it was free to rotate, and apparently did so, even though slightly. This hysteresis is relatively small, however, and will be ignored.

The damper's characteristic is also in the form of a multi-linear curve, so that there exist a definite non-symmetry between the compression and rebound forces. This curve is determined through various harmonic-excitation tests, and even though the hysteresis can be determined with the tests, the damper is incorporated without hysteresis. The damper's characteristic diagram is shown in Figure 2-3.

When implementing the abovementioned curves in a software simulation, one must bear in mind that the model does not regard the working space required for physical hardware or realistic spring and damper minimum and maximum displacements. For instance, the spring-damper unit can be compressed in such a way that the mass body is at a lower displacement than the road; it is theoretically "in" the ground, and the top and bottom mounting points of the suspension unit have passed each other. Also, during certain motions (like excitation close to the SDOF model's natural frequency) the spring and damper may elongate to exorbitant lengths, which are totally unrealistic. It is for this reason that it was decided to implement the spring and damper models in the form of lookup tables giving a force output for a suitable input, so that wheel hop and bump through can be simulated as well. While wheel hop may be easy to implement in the form of a zero force when suspension deflection reaches a certain maximum level, it is more difficult to implement bump, because the bump-stops of the suspension unit acts as a high-rate spring and a damper at the same time (they are usually made of rubber). For the purpose of this study, the bump-stops are modelled as springs with high stiffness coefficients, while their damping is zero – this is still handled by the conventional damper. The lookup tables used in the SDOF simulations are shown graphically in Figures 2-4 and 2-5.

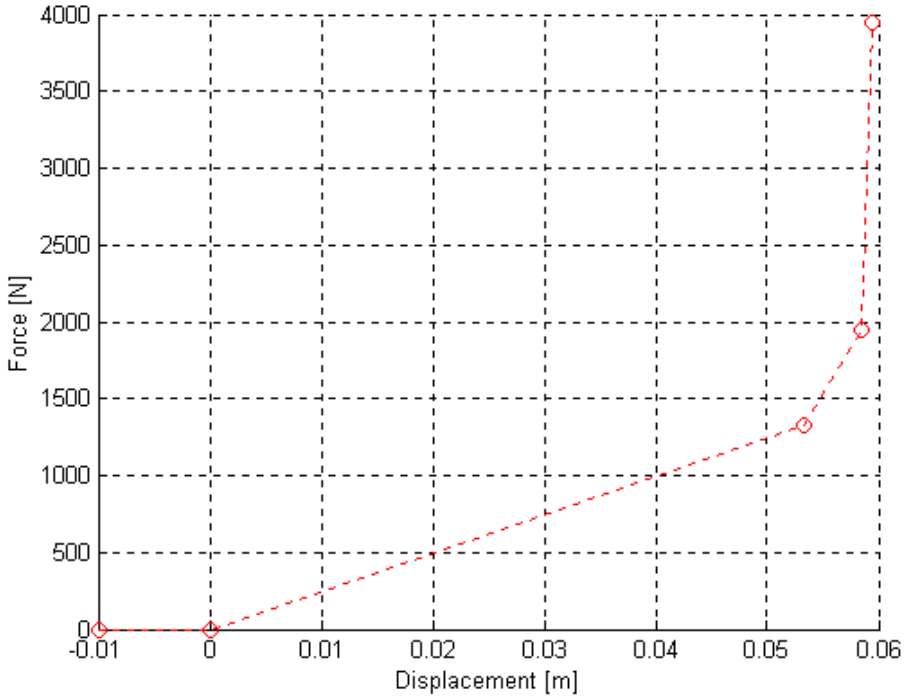

Figure 2-4: Spring force lookup table

The spring force lookup table is a simple two-dimensional table giving a force value for a prescribed spring compression value. When the spring is at the maximum elongation, and thus no spring compression, the force becomes zero as it loses contact with the ground. When the spring is sufficiently compressed, the bump stop comes into play, and a higher spring rate is called into effect. Extrapolation is used for spring elongation and compression values not in the range of the shown lookup table.

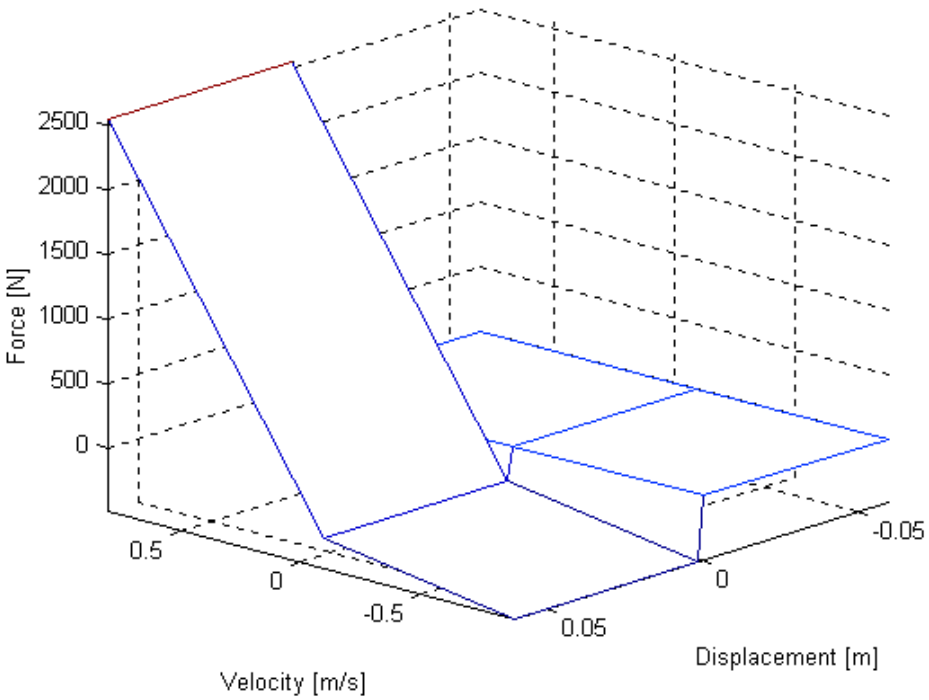

Figure 2-5: Damper force lookup table

The damper force lookup table follows the same line of reasoning, except for the fact that this three-dimensional lookup table gives a damper force for a certain damper velocity as long as it is in contact with the ground. This check is done with the third table axis being a displacement axis, and when the displacement is below a certain level, the damper force becomes zero (this situation corresponds to maximum damper extension for the SDOF model). The plateau in the negative displacement region shows this characteristic. In essence, the spring force lookup table gives force as a function of spring elongation, while damper force is a function of damper velocity and body position relative to the road.

To allow for the static deflection of the spring, the equation of motion needs to be adapted to allow for the weight of the body, *W*. The equation worked with becomes

$$m_s \ddot{x}_s = F_k + F_c - W$$

2.2.2. Fixed-Step Simulation

Fixed-step simulation was done as well as normal adaptive numerical integration, as they may have slightly different results (Simulink can vary its integration step sizes dynamically to increase calculation accuracy, if need be). Also, since HiL is run at a fixed time step, this type of integration is more similar to the HiL setup. For the purpose of this study, and for the accuracy required, it was found that the difference between the fixed-step simulations as done by Simulink and the iterative simulations as done by ODE45 was negligible for time steps of 0.001s. The Simulink model used for the simulation is shown in Figure 2-6.

Since fixed-step simulation was possible using Simulink, a comparison of the fixed-step and ODE results were handy in that it served as a check to determine a suitable time step for the DSP running the HiL simulation. The model shown in Figure 2-6 was run using ODE45 integrations with a tolerance set at 10^{-6}, which is very accurate, and fixed-step simulations with step sizes ranging from 0.1s to 0.001s. The results of these fixed-step integrations were compared quantitatively with the variable-step integration using the Error Coefficient of Variance (ECOV) as mentioned in Chapter 1 (page 1-19) – it is described further in Section 3.2.2. This measure was used by Besinger et al [12] to determine the suitability of a HIL setup compared to a software simulation. Apart from the varying time steps, different fixed-step integration algorithms were investigated as well.

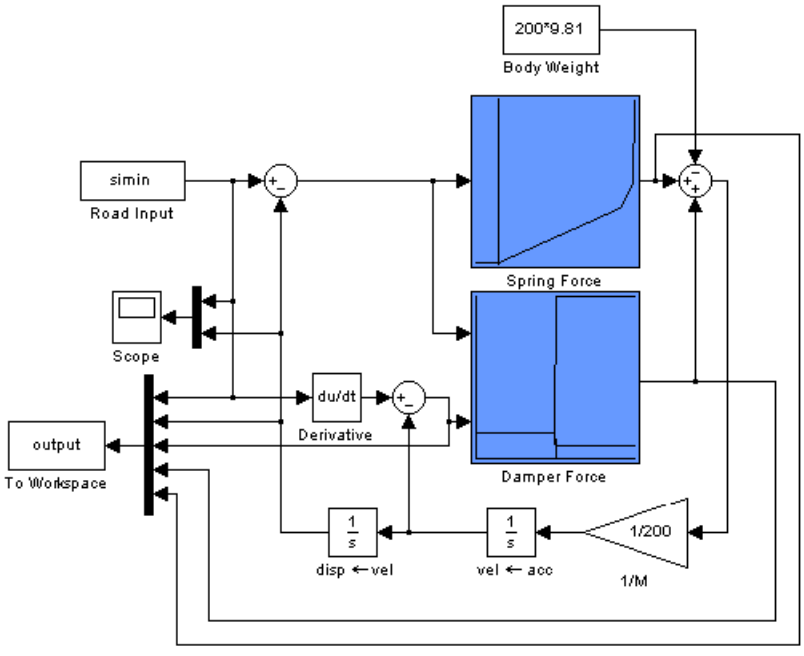

Figure 2-6: Simulink model for fixed-step SDOF solution

The result of the integration investigation is shown in Figure 2-7, where curves show how the ECOV values differ for step time size and integration method. The integration methods ODE1 through ODE5 are based on different schemes, namely Euler, Huen, Bogacki-Shampine, Runge-Kutta and Dormand-Prince respectively.

The ECOV curves all showed the same tendency to decrease a little bit as step sizes increased from 0.001 to 0.005 seconds, and then to increase rapidly with increasing step sizes, so much so that no integration scheme performed well above time steps of 0.01 seconds. At time steps smaller than 0.001 seconds, the ECOV values showed little signs of deviation. Time steps of 0.001 to 0.005 seconds are thus in range to give good integration results while still having a sampling frequency (200 Hz to 1 kHz) high enough to include the model's higher-frequency behaviour. These sampling times are easily attainable using the dSpace hardware.

2.2.3. ODE45 Simulation

One of MatLab's bundled functions is the integration function ODE45, which has been used extensively by the author in the past and has proven to be a reliable and accurate integration scheme. There are a few integration schemes in the ODE suite of MatLab, notably ODE45, ODE15 and ODE23. ODE45 and ODE23 are the two explicit Runge-Kutta codes that have replaced their namesakes in older versions with new code to address some of the deficiencies in the design and to take advantage of developments in the theory and practice of Runge-Kutta methods. Shampine and Reichelt studied the MatLab ODE suite [34]. They summarized and discussed some of the schemes.

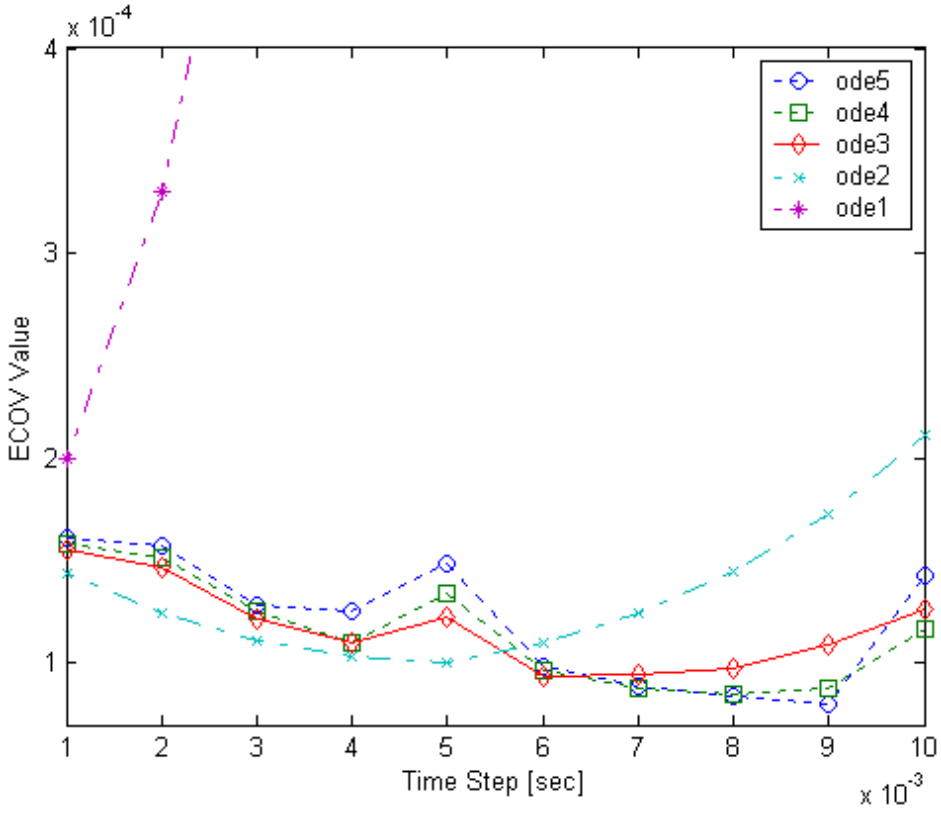

Figure 2-7: ECOV Values for different integration schemes

The new ODE23 is based on work by Bogacki-Shampine and the new ODE45 is based on Dormand and Prince's work. The latter is the one mostly used. Using quantitative measures, Shampine determined that both these integration schemes are of high quality. ODE45 uses interpolants as well, to improve the integration scheme's resolution. In fact, four points are calculated for each natural specified time step. The experiments done by Shampine suggest that except in special

circumstances, ODE45 should be the code tried first; if there is reason to believe the problem to be ill conditioned, or if the problem turns out to be unexpectedly difficult for ODE45, the ODE15s code should be tried.

Shampine et al [34] compared custom-defined problems in their research, to determine the properties of the ODE schemes (Schemes considered were ODE23s, ODE15s, ODE113, ODE23 and ODE45). ODE45 performed best for all the problems when considering the time to solve the problem and the number of time steps necessary. Even though it is not universally the most stable integration scheme, it performed well enough to justify its usage. ODE23s took the longest to solve in all cases, and did the most function and derivative function evaluations.

The ODE simulation of the SDOF model was done using recursive integration and adaptive time steps. It was implemented using the same lookup tables as used in the fixed-step integration.

2.3. HiL Simulation

In this section real hardware-in-the-loop simulation will be introduced for the first time. As discussed in the previous chapter, HiL testing and simulation has been implemented in a variety of situations, from multi-parameter ECUs to multi-degree-of-freedom dynamic systems. The SDOF model of Figure 2-1 is now used as the dynamic model, and a HiL simulation is built around it. Where one PC is necessary for software simulation, HiL simulation requires a control PC, a data capturing PC (which can be the same as the control PC if a DSP card is used), an actuator/controller combination, and of course the component to be tested.

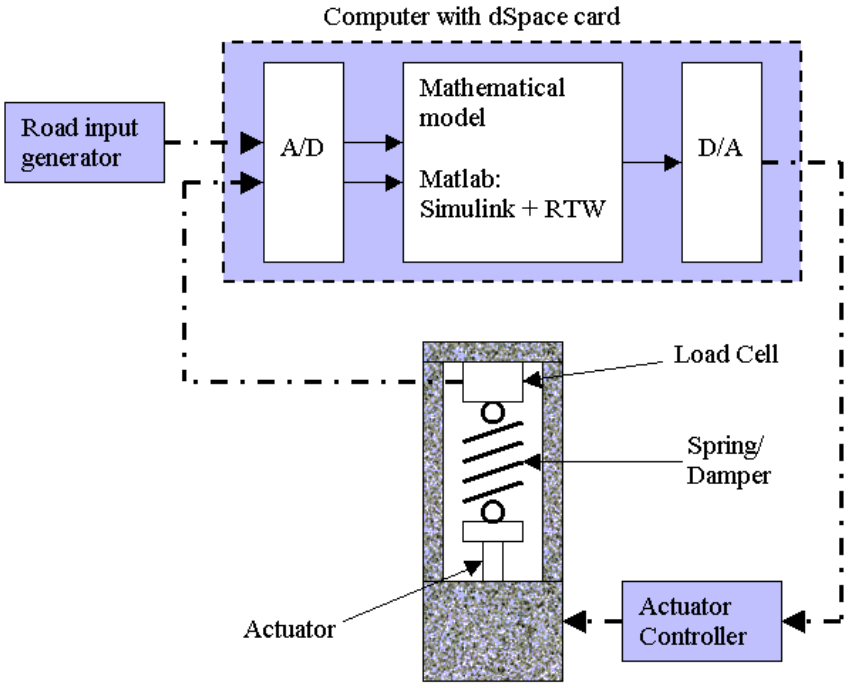

Figure 2-8: Schematic HiL setup

Additional sensors and peripherals like oscilloscopes, accelerometers and bridge amplifiers also form part of the HiL setup. The amount of equipment used is comparable to the actual building of a SDOF dynamic setup using a real mass on linear bearings (or something similar). Schematically, the HiL setup is shown in Figure 2-8.

The setup of Figure 2-8 doesn't show all the hardware that was used in this study. There is still a MGC bridge amplifier for the load cell, a measurement computer, and at times, a filter to lessen digitisation noise present.

2.3.1. Simulink Model Implementation

The beauty of the dSpace DSP system is its ease of use, even for those that have never programmed DSPs. The familiar Simulink interface acts as middleman between the user and the DSP. New Simulink blocks, supplied by dSpace, are used to facilitate the input and output of signals through the card's A/D and D/A channels. Plugs for the input and output terminate each signal in Simulink (in- and out plugs). The model implemented on the dSpace card is shown in Figure 2-9, where the DS1102AD and DS1102DA blocks as well as the in- and out plugs are shown.

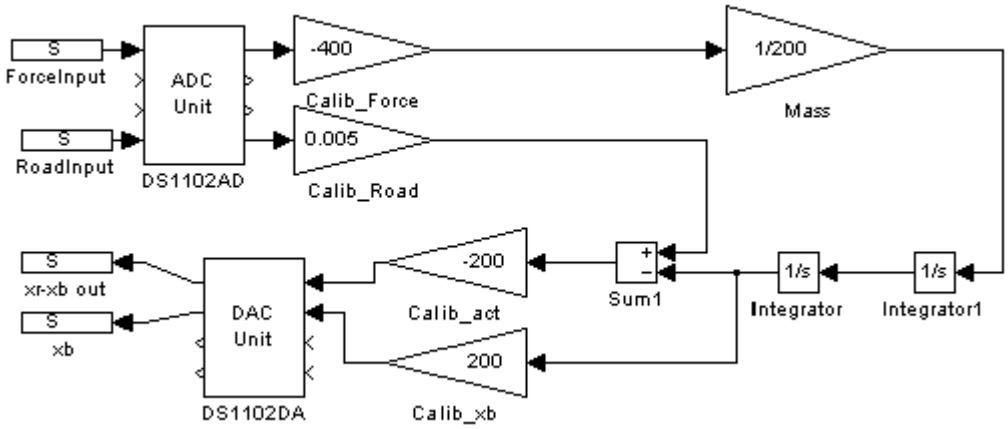

Figure 2-9: Simulink model implemented on the dSpace DSP card

(Note: "Calib_act" in Figure 2-9 contains the calibration gain for the suspension deflection output from the model, which is used as the actuator input. Since the actuator is set up with a sign convention opposite to that of the mathematical model, the sign of the gain is reversed to account for this hardware-software interaction.)

There exists a remarkable resemblance between models used for software simulations in Simulink (like the SDOF model in Figure 2-6) and those intended for HiL simulations on the dSpace card. The dividing factor is the calculation of the force that affects the body mass, m_s. In software simulation gains or lookup tables can give the forces as generated by the spring and damper during motion, by monitoring the suspension deflection and damper velocity. In HiL configuration, however, the suspension deflection is fed from the model to the actuator while the integration scheme determines the response of the mass in real time. The load cell measures a force at the same time and feeds it back into the model. The velocity component of the suspension motion is not explicitly needed, as the motion of actuator accounts for it. This method may invite phase lags that wouldn't be present in either a software simulation or a conventional SDOF test, but as stated previously, these lags are very short and have negligible impact on the results.

2.3.2. Test Results

Some of the results from HiL testing of the SDOF model are given below. These results were generated using the model of Figure 2-9, with a spring or a spring-damper unit in the actuator. Figures 2-10 and 2-11 show some of the measurements taken during the HiL tests.

Any suspension component can be placed in the actuator, albeit spring, damper, spring-damper unit, semi-active damper or fully active suspension components. This is because the HiL setup doesn't care what generates the force – it is more concerned with the force itself. If only a damper was to be tested, the supplementary spring force can easily be generated in the Simulink model.

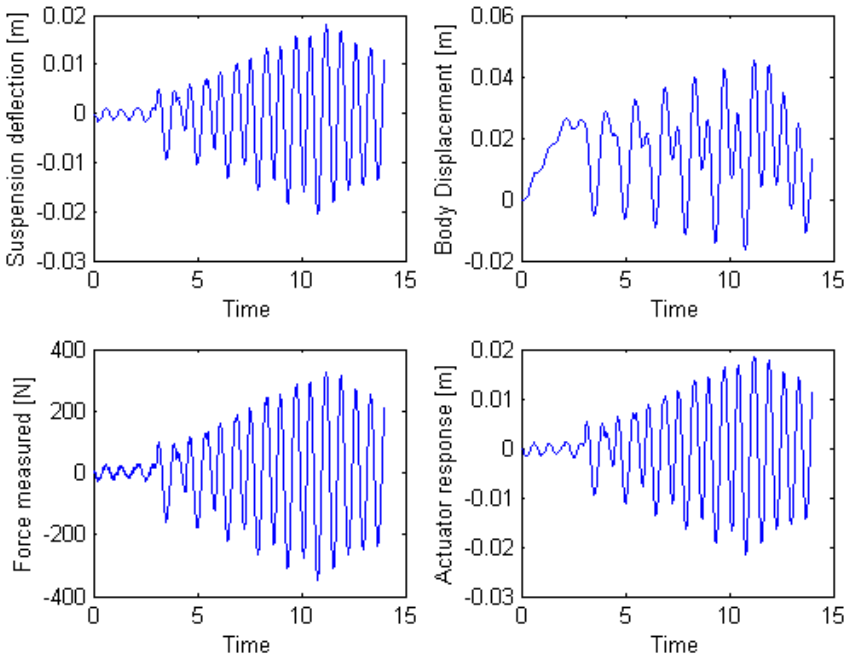

Figure 2-10: HiL test of spring-mass system with bump inputs

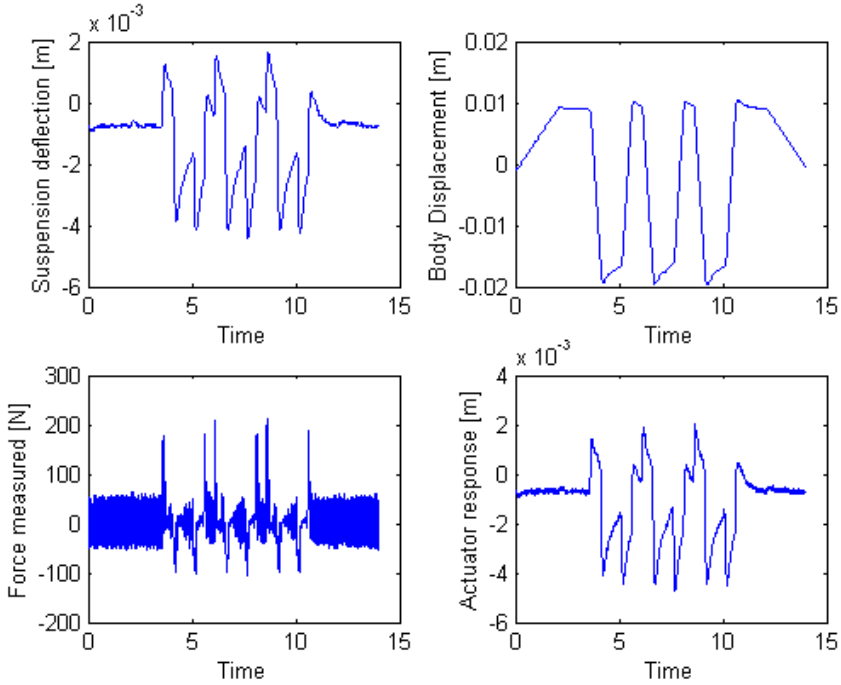

Figure 2-11: HiL test of spring-mass-damper system with ramp inputs

The data in Figures 2-10 and 2-11 is raw and needs to be compared with a known solution. This solution is a numerical one, generated using ODE45 and spring and damper models where applicable. The result comparison will be discussed in Section 4. The signals used as inputs are defined in Appendix A: Input Motions Used in HiL Tests.

2.3.3. Considerations for HiL Testing

When considering the use of HiL as a test method, there are some considerations that need to be made which will affect the setup's performance. They include hardware and software considerations, hardware availability, etc. A few of these considerations are discussed below.

2.3.3.1. Phase Lag of Actuator/Controller Combination.

There will definitely be a phase lag in the HiL setup due to the dynamics of the actuator and the control applied by its controller. Tuning the PID controller is necessary as the gains have quite a large influence on the system, and hence its performance and the errors generated. Also of interest is the manner in which the controller measures the feedback signal, either for force or displacement control.

Strain gauge based sensors (like load cells) and resistive displacement transducers can operate without filtering the signal, which minimises the controller's lag. LVDTs working on an inductive principle need filters to demodulate or condition the return signal. This adds to the phase lags. For the actuator controller used in this study, the phase lag was determined by letting the unloaded actuator follow a reference signal. The plot is shown in Figure 2-12.

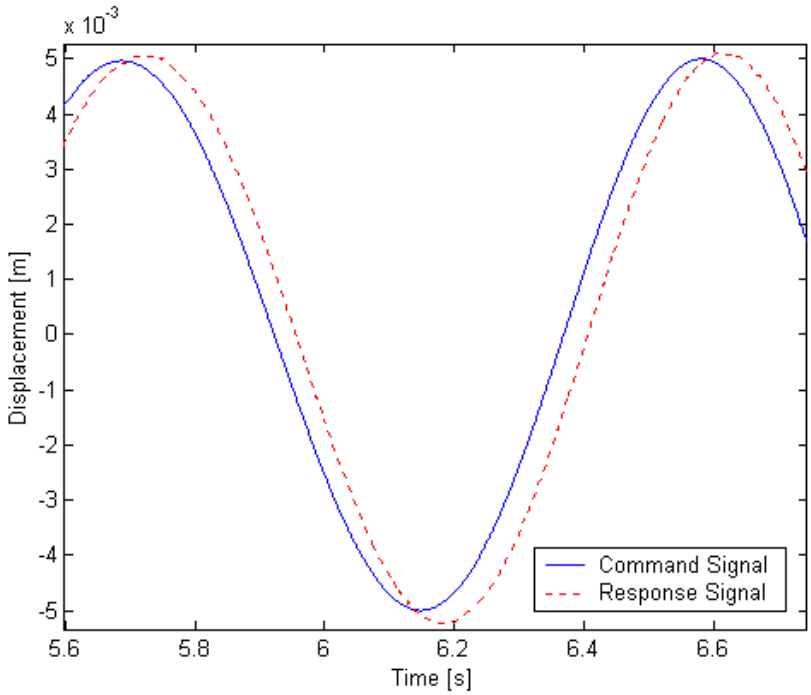

Figure 2-12: Actuator response to show phase lag

Also of interest concerning the actuator is its dynamic performance. Deakin et al [26] tested on a conventional SDOF test rig because the equipment they had didn't perform sufficiently to implement HiL. The bandwidth of the actuator used can be determined using a sweeping harmonic excitation at constant amplitude, and measuring the actuator response. A magnitude envelope calculated using such data is shown in Figure 2-13. The sudden drop at about 20Hz is due to the software that was used to generate the excitation signal. There is, however, enough data to suggest that the actuator in question has sufficient dynamic properties.

Figure 2-13 was created using a 5mm sine sweep signal, varying linearly from 1Hz to 20Hz over the 120 second signal time span. Comparing the command signal and response signal magnitude envelopes do, however, reveal some of the actuator's dynamic properties. One can also see the prominent natural frequency of the actuator, which lies at just over 10Hz. The command signal had a maximum amplitude of 5mm (equivalent to 1V for the actuator/controller combination) while the response peaked at a maximum displacement of 7mm.

The phase properties of the actuator as given in Figure 2-13 was considered in larger detail only upon completion of the experimental HiL tests, as ways were sought to reduce the phase lags. Before the execution of the HiL tests, the controller's PID was set up using accepted methods, and otherwise yielded good

results. It should be kept in mind that the actuator/controller is primarily used for fatigue testing of components, and as such may not have ideal dynamic properties for HiL testing. (Refer to Besinger [12] for an investigation of the effect of the PID on HiL tests.) The PID settings selected resulted in large damping of the system, and hence large phase lags at high frequencies. Reducing the damping may have reduced the phase lags at the body (or sprung mass) natural frequency, but would also have lead to larger displacements at the actuator natural frequency. However, large reductions in phase lags on the actuator used, by adjusting the PID controller considered, are unlikely. While the results obtained using the PID settings selected were satisfactory, it was decided to implement the HiL system on an actuator/controller combination with better dynamic properties, such as those on the Sasol Laboratory's actuator block, as a future task.

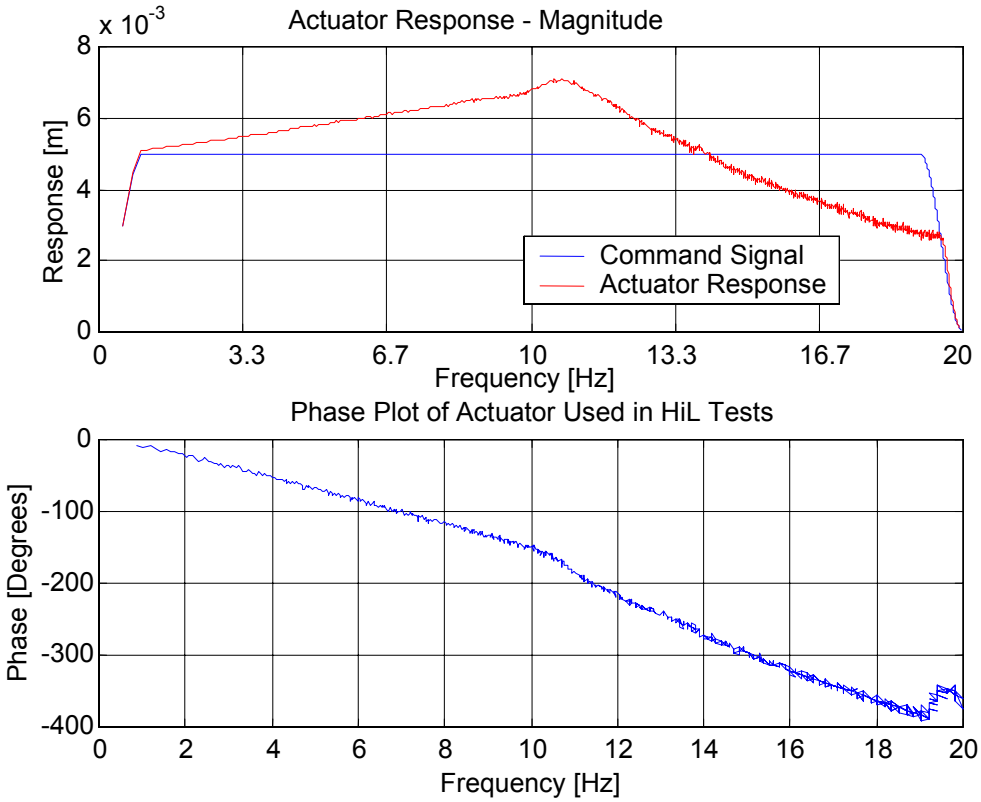

Figure 2-13: Measured Actuator Response

2.3.3.2. Integration Scheme

The integration scheme that is to be used can be one of a vast variety employing a fixed-step method. Fixed-step integration has been highlighted previously, but when using custom C code, for example, many more schemes become available. The dSpace DSP software allows several integration codes to be used – Runge-Kutta 3rd and 5th order schemes, Euler and Huen. From the work of Besinger [12 and 21] it is clear that the scheme of choice is Runge-Kutta's 5th order scheme. This integration scheme stayed stable throughout testing, unlike the Euler and Huen schemes that broke down at lower sampling frequencies.

2.3.3.3. Sampling Frequency

The sampling frequency was chosen as 1000Hz for all the tests, as it has a good enough resolution to detect all the frequency and magnitude phenomena and has a sampling time sufficiently small to update the model regularly. Furthermore, considering the phase lag of the actuator/controller of 8 ms, a sampling frequency of more than 125Hz is required to ensure that data is trustworthy. Coupled with

the “ten times more than highest frequency” advice given by Gomez [2], where a frequency of more than 200 Hz is needed, a sampling frequency of 1 kHz was selected. This frequency is high enough to allow the reliable use of many integration schemes as well.

2.3.3.4. Actuator Limits

All actuator controllers have limits or breakpoints that can be set for either a maximum measured force or displacement, whether in force control or displacement control. These limits protect the tested object, and are thus an important consideration when looking at HiL testing. The object in question, the spring/damper unit, must be sufficiently protected because the range of the actuator used, 100mm, is potentially larger than the allowed deflection of the suspension unit. For the tests done in this chapter, for instance, a spring-damper unit with maximum deflection of 80mm was used. This resulted in limits being set to allow only motion smaller than 80mm. The dynamics of the actuator is also such that, when the motion goes beyond the breakpoint, it seldom stops dead (i.e. the limit stops the actuator displacement the moment it crosses the threshold value) but rather scales down the input and returns the actuator to zero. This implies that, firstly, the zero force position of the actuator should be such that the spring-damper unit is at a comfortable position (not an extreme) when the controller is at zero input, and secondly that the limits should be set to allow for some margin of error at maximum and minimum suspension deflection. If there is enough inertia present as the actuator goes through the limit, it may damage the suspension unit if the limit is at the unit’s extreme deflection.

It is for this reason that there was decided to abort the use of a potential model incorporating wheel-hop for the single-degree of freedom system, as the suspension unit could potentially deflect from minimum to maximum (bump stop) during a bouncing motion, damaging the suspension unit. The “wheel”, in this case, is basically taken as the bottom of the suspension unit instead of an unsprung mass as found in quarter-car models.

The points discussed above affect the HiL simulations in various ways, from the damper stroke length that can be tested, to the model that will be used. While a DSP card will run large model simulations with very small step sizes (smaller than 0.5 ms) when installed in just about any computer, an ordinary A/D D/A interface card needs a fast computer to achieve decent results. Also, it might be tempting to use filters to smooth out the responses (in frequency ranges far above system frequencies) and to diminish noise, but the lag introduced by the filters are unacceptable. The best results are obtained when using no filters.

2.4. Result Comparison and Discussion

In the previous sections various different topics relating to HiL simulation was discussed – the mathematical SDOF model was described, the spring and damper models to be used, the HiL setup and the hardware used, and its implementation. Now we can look at the generated results and compare and discuss it. (Note: In the following figures, the “Measured” signals are those as obtained from the HiL tests.)

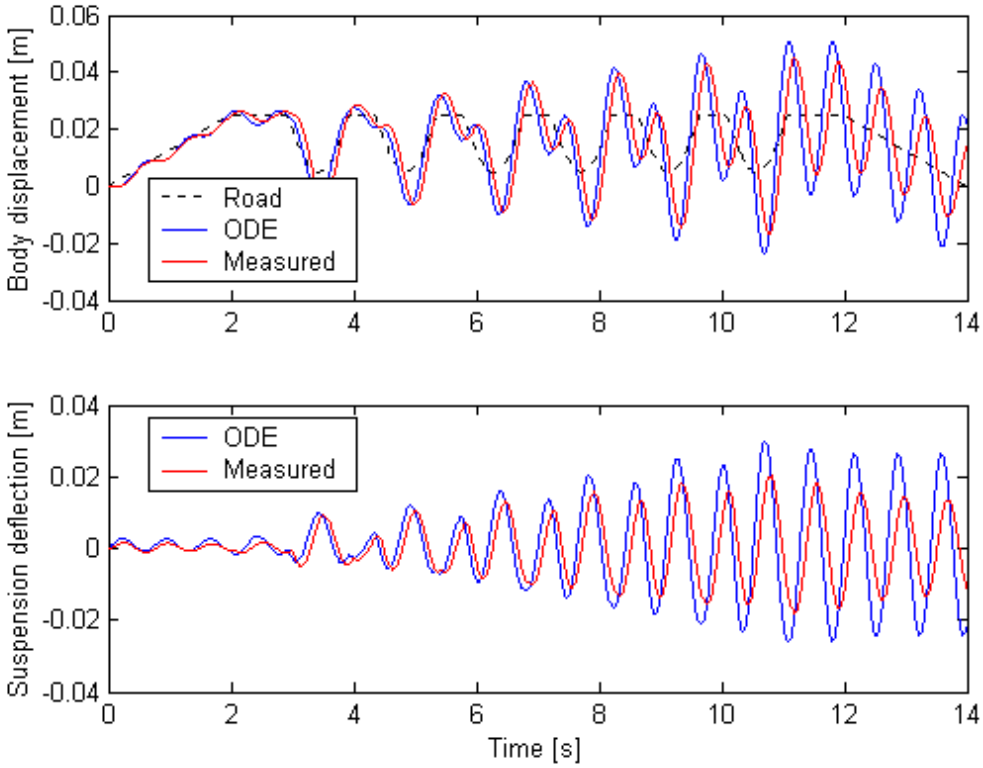

Figure 2-14: HiL and ODE45 response for speed bump inputs

At first, consideration will be given to the simplest setup, i.e. the spring-mass setup. No damper is present in this simulation, so the software model used to solve the software integration doesn't have the damper given in the equation of motion; obviously, this is equivalent to damping coefficient c = 0. For the HiL simulation no alterations are necessary.

A spring-mass system was chosen to begin with because this is the easiest to implement in both the hardware and software environments. What makes it valuable is the lack of a damper model in the software simulation – even though the damper would make the setup more complete and realistic, the model used is of inferior quality to the real damper's behaviour and the software simulation will give results biased by this discrepancy. Gaining confidence in HiL was considered important and hence a software system model, sans damper, was chosen because it gives reliable results to compare the initial HiL results with.

Figure 2-14 shows the superimposed results of the HiL and software solutions – the results will be given in this fashion for the rest of the chapter. The top graph, "Body displacement" gives the displacement of the body mass above the reference zero displacement, compared to the road input (labelled "Road"). The bottom graph gives the "Suspension deflection", calculated with $x_{road} - x_{sprung\ mass}$. It can be seen that there is excellent correlation between the HiL simulation (labelled "Measured") and the ODE45 simulation results. For the first half of the test the responses are virtually identical, and after that there seems to be a loss of accuracy. Even in the test's second half, there is a good correlation with regards to both frequency and magnitude response. The deviation is caused by phase lags in the actuator and load cell bridge amplifier, noise on the input and output signals and delays in the A/D and D/A conversions. Other minor causes include drift in the load cell, which should be negligible, and motion of the actuator other than that requested by the controller (i.e. due to valve stick, actuator dynamics or controller noise).

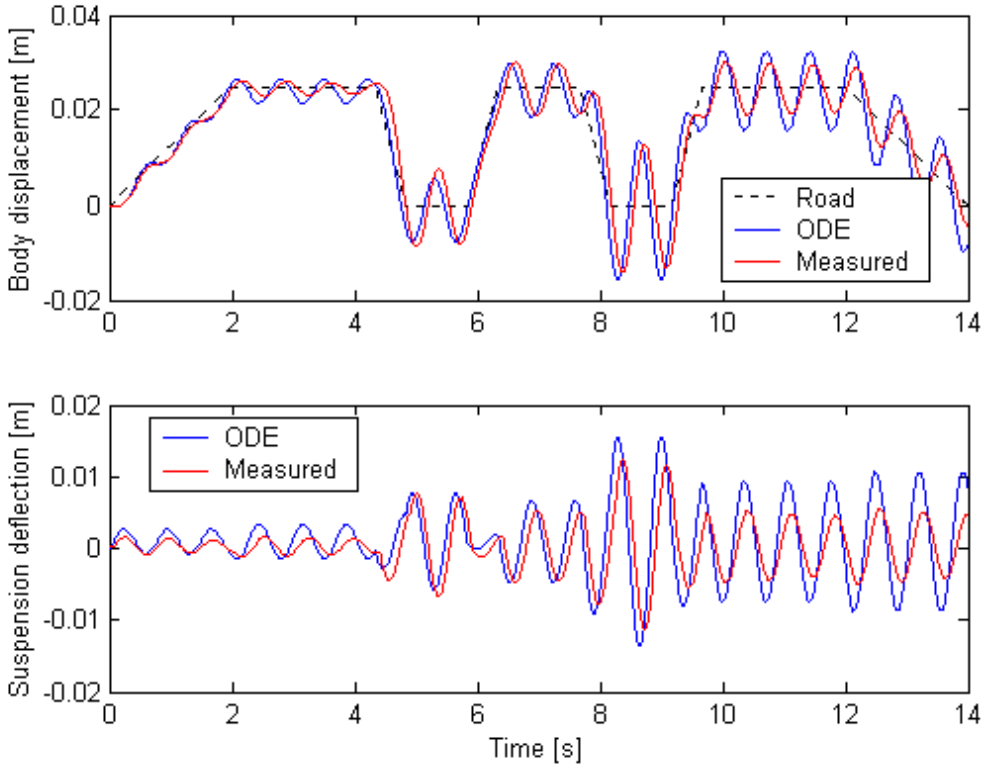

Figure 2-15: HiL and ODE45 response for ramp inputs

In Figure 2-15 the responses for a different type of input, a ramp input, is given. This figure shows the same tendencies as Figure 2-14, and shows good correlation in general. The amplitude of the suspension deflection for the ODE simulation is much higher than that for the HiL simulations, but even this difference doesn't cause any adverse effects on the body displacement. The body follows the road input, with a lower oscillatory component than the ODE's. Figures 2-16, 2-17 and 2-18 show some more results for a spring-mass system using various other road inputs. These figures indicate that HiL does indeed show great promise.

Now that spring-mass systems have been considered and shown to be well suited to HiL testing, spring-mass-damper systems will be considered. In the mathematical model the simple addition of a damper is needed, while the HiL hardware is exactly the same as that used for the spring-mass tests, with the spring replaced by a spring-damper combination. All the tests executed for the spring-mass system is repeated for the spring-mass-damper system, with some of the comparative results given in Figures 2-19 to 2-23.

The difference in response is immediately obvious, with the amount of overshoot greatly diminished and oscillatory motion absent. Considering the body displacement graph, it can be seen that the measured data shows characteristics of larger damping than that predicted by the purely software model. While it may seem that the unproven HiL method is at fault, the simulation is more likely to be in error because of the damper model, which is very basic and contains no transition or hysteresis effects. The real damper itself may also contain low-velocity stick-slip effects which aren't modelled by the software (Discussed in Appendix C: Determination of Stick-Slip Effect).

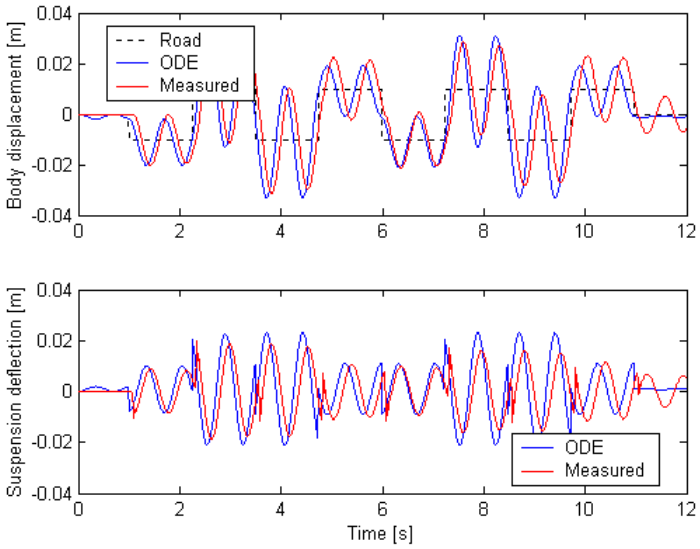

Figure 2-16: HiL and ODE response for SM system with step input

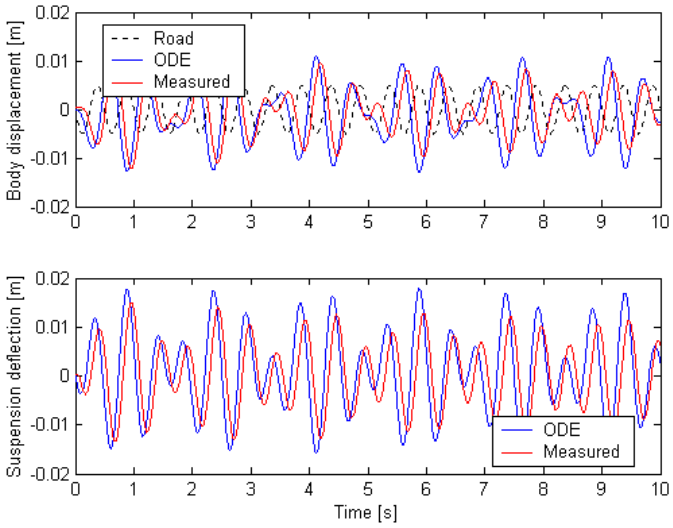

Figure 2-17: HiL and ODE response for SM system with harmonic input

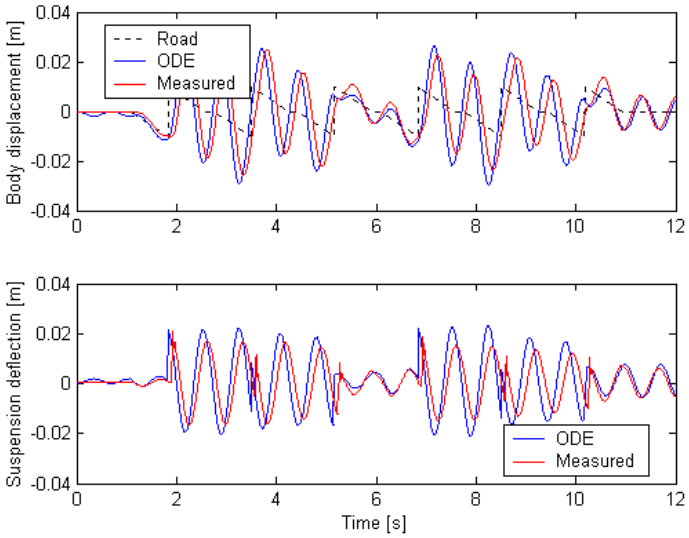

Figure 2-18: HiL and ODE response for SM system with sawtooth input

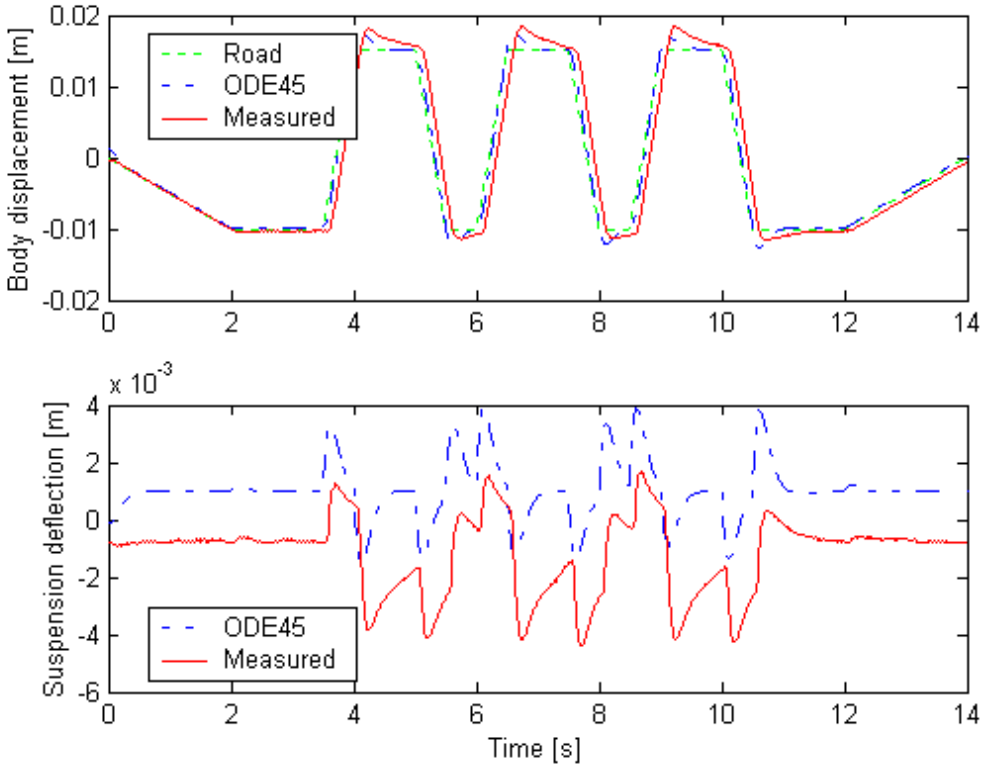

Figure 2-19: HiL and ODE responses for SMD system with ramp input

When looking at the suspension deflection graph, an offset between the measured and calculated responses is obvious. This is due to the zeroing of the load cell and displacement LVDT, which has different zeros for internal and external signals, and the static deflection of the model because of the pretension imposed on the spring during its mounting in the spring-damper unit housing. (When switching the actuator controller to external input, the displacement reading drifts to a different value. Resetting the zero effectively induces this offset due to an artificial shift in the road-mass equilibrium positions.) Even thought the readings doesn't line up, it can be seen that they have the same character and magnitudes. It would thus be easy to compute ride and handling characteristics by removing the signal offset in the software, where necessary.

The comparative HiL and software simulation results showed in Figure 2-21 for step inputs also show deviant behaviour, in that the software simulation in this case gives a response very different from the measured response. At the first input event the measured response shows the body displacement that one would expect, with severe overshoot that is damped on its return to obtain a statically deflected position, before the next step input. The calculated response, on the other hand, follows the road input more closely, with very little overshoot.

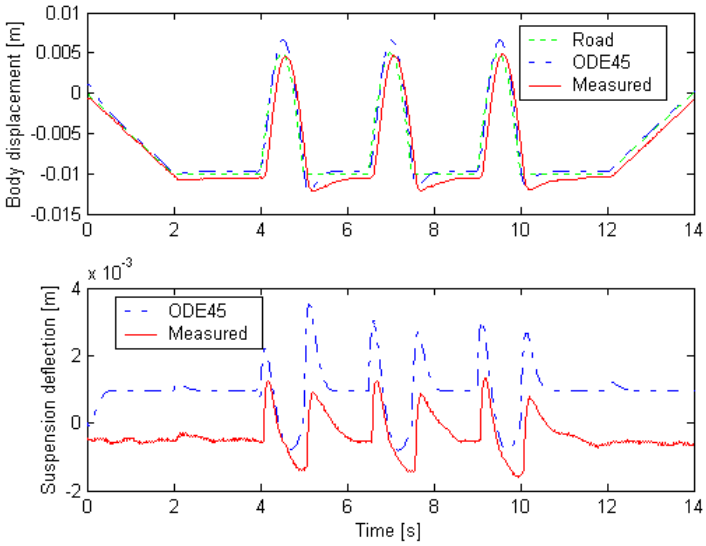

Figure 2-20: HiL and ODE responses for SMD system with speed bump input

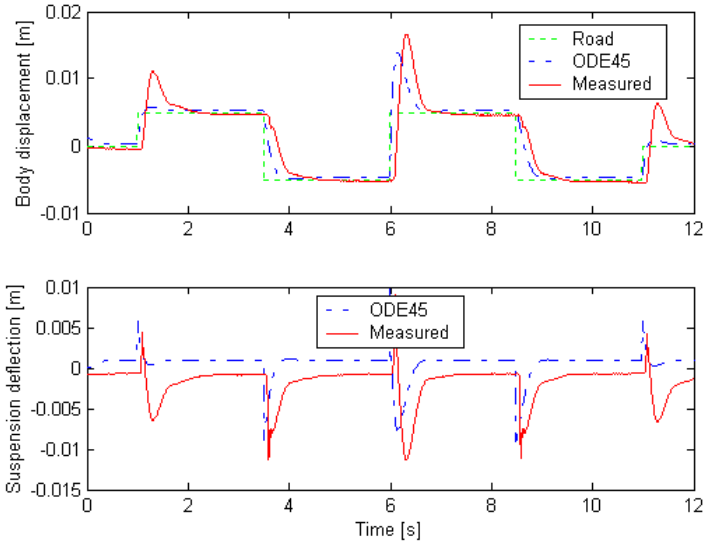

Figure 2-21: HiL and ODE responses for SMD system with step input

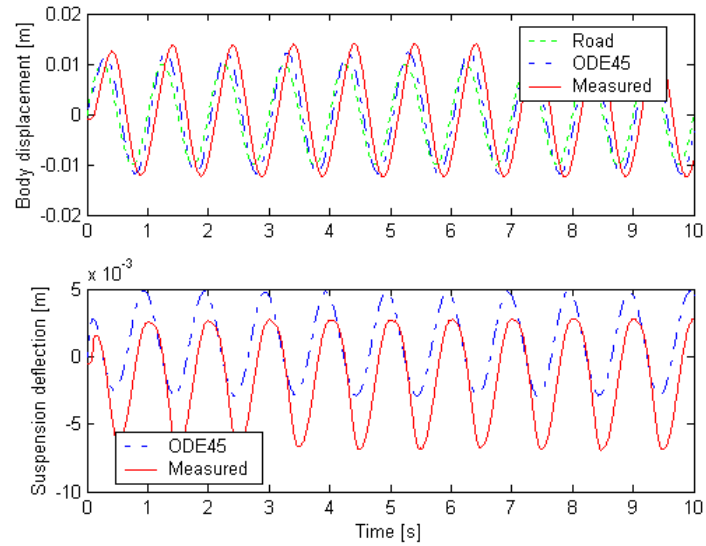

Figure 2-22: HiL and ODE responses for SMD system with harmonic input

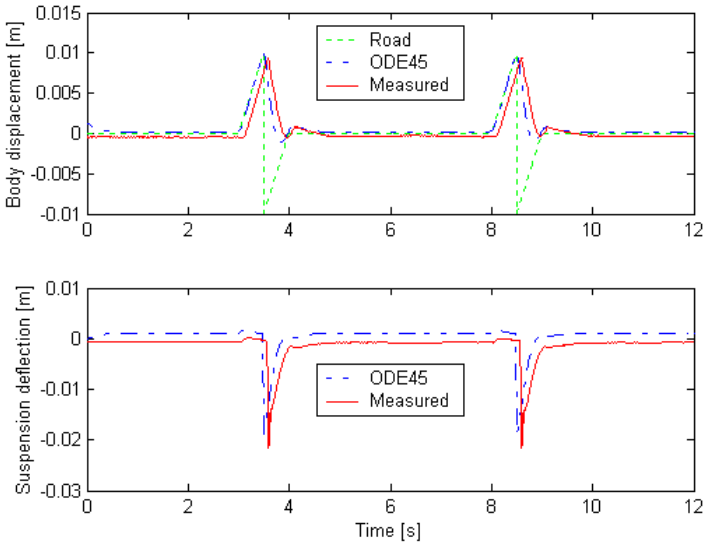

Figure 2-23: HiL and ODE responses for SMD system with sawtooth input

At the second step input the measured and calculated responses behave similarly and normally, but the third step again shows the deviant behaviour. In this case it seems as if the software simulation using the damper model is insufficient for the task at hand, i.e. suspension testing.

Figures 2-19 through 2-23 shows the responses that can be expected from different excitation inputs for HiL and software simulations. While HiL may have some known drawbacks (notably phase lags and its reliance on actuator dynamics), software simulations fare even worse than HiL in many circumstances. When testing new or uncharacterised suspension components for their suitability of use, HiL provides a valuable tool.

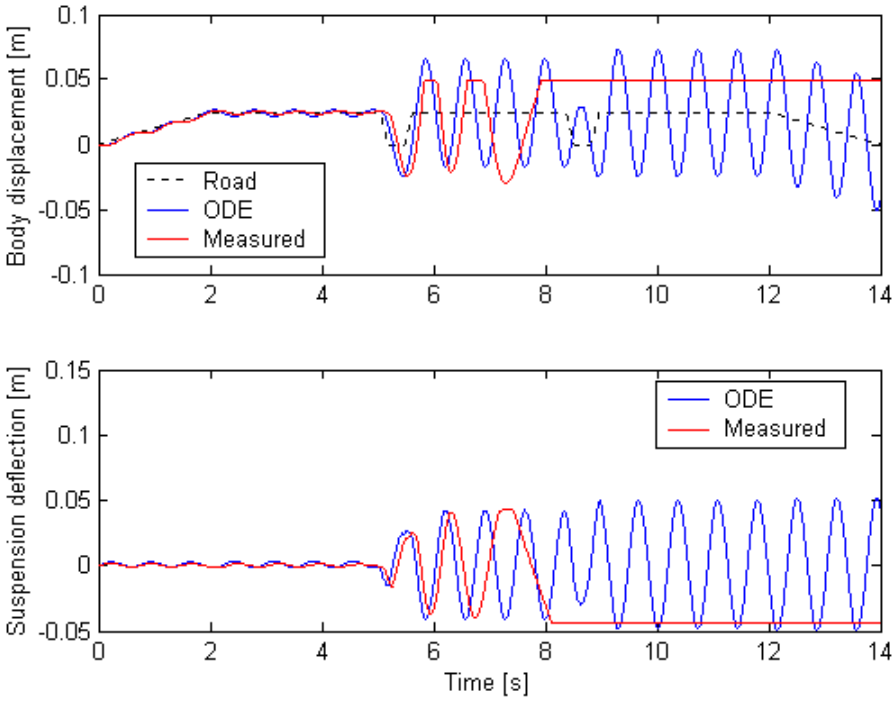

Figure 2-24: HiL simulation during which actuator limits are triggered

A final note on the measurements as afforded by HiL, concerning the wheel hop model. Due to the need for limits on the actuator to protect the suspension unit with its relatively short working space, the wheel hop model wasn't used for tests of the SDOF system. Figure 2-24 shows the kind of readings obtained when the limits are triggered. This situation could potentially harm the suspension unit being tested. If an actuator with physical stops instead of input scaling is used, or the suspension unit is placed in a frame to stop excessive elongation and compression, a model incorporating bounce can be used.

3. Two Degree of Freedom Testing

In Chapter 2 a simple single-degree-of-freedom (SDOF) system was selected as a test and first verification of the hardware-in-the-loop simulation method. The results indicated that HiL is indeed a valid testing and simulation tool, even though bouncing motion wasn't tested due to hardware constraints. In this chapter, a more complex two-degrees-of-freedom (2DOF) model, as indicated in Figure 3-1, will be used.

The advantage that a 2DOF system offers over a SDOF system is the ability to model the body mass, called the sprung mass (the vehicle body or chassis) along with an unsprung mass representing a wheel station. This setup has been used extensively in the past, and is referred to as a quarter car model. This model allows not only sprung mass displacement to be monitored, but also unsprung mass displacement and hence also tyre deflection and tyre forces. The latter two measurements are of importance in the testing of vehicle suspension systems.

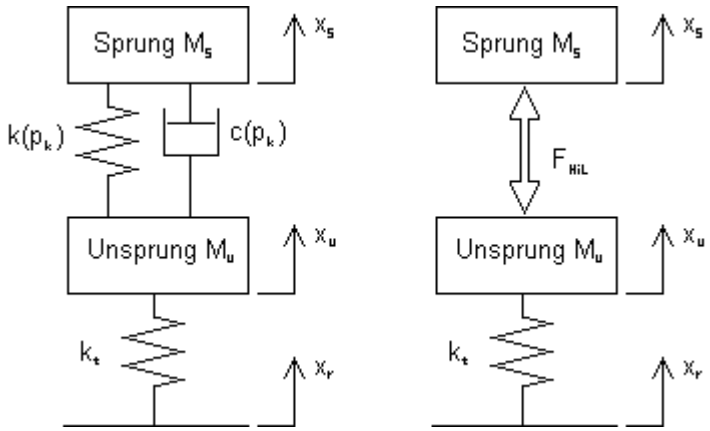

Figure 3-1: Two-degree-of-freedom system

The tyre of the 2DOF system can be modelled as a spring and damper, but due to the low damping usually afforded by tyres, it is here modelled as a spring only. This model is used throughout this chapter, again leading to a comparison between HiL and software simulations.

3.1. Mathematical Model

The mathematical model of the 2DOF system is derived in a similar fashion as to the SDOF model of Chapter 2. Now, since there are two bodies, two equations need to be satisfied:

$$m_s \ddot{x}_s = \sum F_s$$
$$m_b \ddot{x}_b = \sum F_u$$

Considering the tyre stiffness to be k_t and the suspension stiffness and damping to be *k* and *c* respectively, these equations become

$$m_s \ddot{x}_s = k(x_u - x_s) + c(\dot{x}_u - \dot{x}_s) - m_s g$$
$$m_u \ddot{x}_u = k(x_s - x_u) + c(\dot{x}_s - \dot{x}_u) + k_t(x_r - x_u) - m_u g$$

In the above equations x_s is the displacement of the sprung mass, x_u the displacement of the unsprung mass, and x_r the road input. The values of k, c and k_t are assumed to be constant for the purpose of this idealised derivation, even though they may well be deflection, velocity and time dependent in real hardware. Implementing the equations in ODE45 integration is just as easy, as it takes but a small adaptation to obtain a suitable form:

$$\frac{\partial}{\partial t}\begin{bmatrix}\dot{x}_s\\ x_s\\ \dot{x}_u\\ x_u\end{bmatrix}=\begin{bmatrix}-\frac{c}{m_s} & -\frac{k}{m_s} & \frac{c}{m_s} & \frac{k}{m_s}\\ 1 & 0 & 0 & 0\\ \frac{c}{m_u} & \frac{k}{m_u} & -\frac{c}{m_u} & -\frac{(k+k_t)}{m_u}\\ 0 & 0 & 1 & 0\end{bmatrix}\begin{bmatrix}\dot{x}_s\\ x_s\\ \dot{x}_u\\ x_u\end{bmatrix}+\begin{bmatrix}-g\\ 0\\ \frac{k_t}{m_u}x_r-g\\ 0\end{bmatrix}$$

Constant coefficients cannot be used if good results are sought, so the coefficients are determined during the simulation.

In the case of applying the equations to the hardware-in-the-loop experiments, the theoretical stiffness and damping of the suspension components become redundant, and the force term of the suspension, *F*, is used (as shown schematically in Figure 3-1):

$$m_s\ddot{x}_s = F - m_s g$$

$$m_u\ddot{x}_u = -F + k_t(x_r - x_u) - m_u g$$

These equations are very easy to implement in a HiL environment using Simulink in tandem with the dSpace hardware.

3.2. Software Simulation

In the software simulation, both Simulink and ODE45 were again employed to establish whether the fixed-step simulation would be adequate for HiL implementation. However, using the command window ODE45 interface became redundant, and only the Simulink model was used, as it offers full ODE45 and fixed step integration.

Apart from using two degrees of freedom in the model, it also contains wheel-hop capability through the use of a check to see if the wheel centre isn't too far off the road. The check is simple: if the wheel's displacement is higher than the road's by a distance equal to the amount that the tyre would deflect under static loading, it is considered to be off the ground. The returning force for the system would then be gravity, which is incorporated into the model at a constant value of g = 10 m/s^2. This will be discussed more thoroughly when the Simulink model is discussed.

3.2.1. Simulink Model Used

In the case of the 2DOF system the Simulink model, in various guises, will serve as the integration interface for fixed step, variable step and hardware-in-the-loop integration. In fact, a comparison of the fixed and variable step integrations will be given using the "Error Coefficient of Variance" (described in the next section), using the same model for both integration processes. The model is shown in Figure 3-2, with similar lookup tables as used in the SDOF tests, because the same spring-damper unit was used in the 2DOF tests. (The lookup tables used for 2DOF simulation do not include wheel-hop phenomena.) Using the look-up tables of a known component enabled a relatively easy investigation into the effect of changes in the damping curve's break point. This was accounted for in the actual model execution and the results calculated.

The advantage of using the same model, adapted for different uses, is that the model debugging can be done quickly, and adaptation is a menial task. Automation of a lot of the tasks can also be achieved, since MatLab allows the calling of a Simulink model using the "`sim`" command, and the simulation parameters (integration type, algorithm, step size/error tolerance) can be set beforehand. This allows the automation of a loop to calculate the ECOV values of a particular road input using a single command. The largest change that was made to the model was the incorporation of the dSpace interface blocks and the calibration gains needed to correctly couple the load cell and LVDT with.

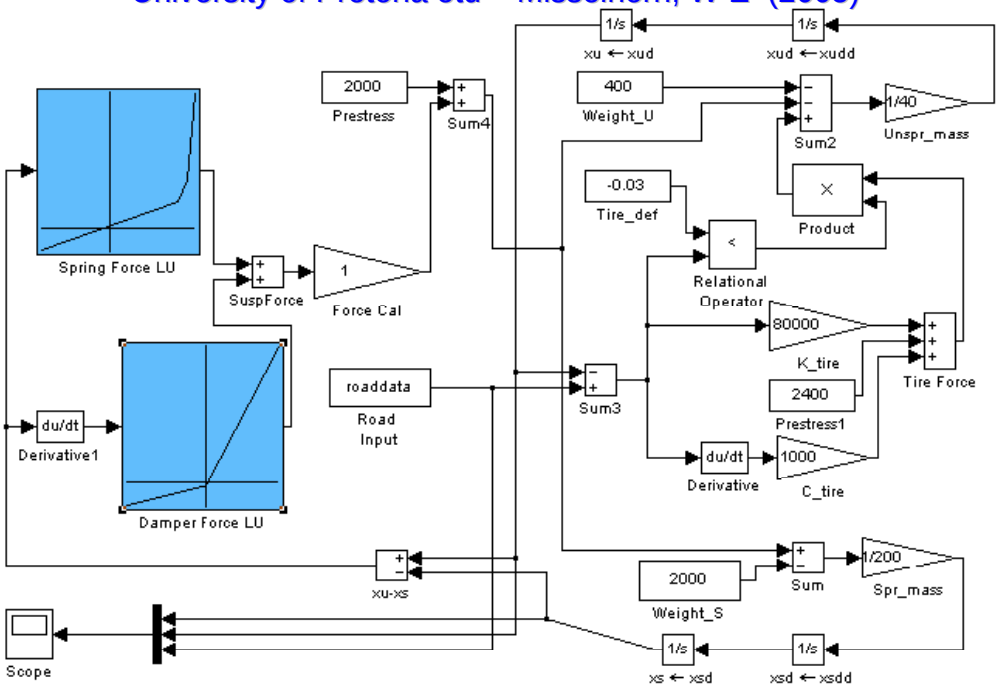

Figure 3-2: Simulink model used for software integration

While it may be sufficient to specify initial parameters of zero for all the displacements and velocities for the software simulations ran, it proved disastrous to let the system masses move to statically deflected positions from a zero spring force position during the HiL simulation. This is because the actuator must be "primed" to follow an external signal by the time the DSP board, with its suspension deflection and body displacement outputs, is started. If the system isn't in static equilibrium when the DSP is started, and it must reach static equilibrium from an elevated displacement, the result is unnecessary jolting of the suspension unit in the actuator rig and more often than not a triggering of one of the displacement limits. (During SDOF testing the mass was not subjected to gravity, hence the starting position became, in effect, the static position.)

The approach followed to circumvent this problem was to assume that there are initial forces in the springs and account for the static deflections of the suspension unit's spring and the tyre with these initial forces. The same mass for the sprung mass was used as was in the SDOF tests, namely 200 kg, while an unsprung mass of 40 kg was used. That means that the suspension unit must bear a 200 kg, or 2000 N, load when the simulation is started, while the tyre must bear the entire model's load, i.e. 240 kg or 2400 N. The check of tyre contact was initially a check to see if the unsprung mass is displaced more than the road at a certain increment (in the model that would deflect to reach equilibrium). However, with the spring pretensions applied, it was modified in such a way that the 30mm static deflection that the tyre has under loading, is used in addition to this zero displacement; when the tyre deflects –30mm from the new equilibrium, the tyre force is –2400 N, which cancels out the tyre pretension and effects the wheel hop mode. This situation corresponds to *30 – 30 = 0mm* wheel deflection, and hence *2400 – 2400 = 0N* tyre force.

Similar provision was made for the suspension unit's spring, whereby the lookup table was modified so that it would act as though the spring started the integration from a zero force position. The damping force lookup table was left unaltered, as starting the integration from a different height wouldn't affect it – the force is only proportional to velocity.

The blocks in Figure 3-3 (found in the models of Figures 3-2 and 3-11) perform the check for wheel hop. When the unsprung mass is more than 0.03 m above the road, the tyre is essentially off the ground – conversely, when the road input is –0.03 m

from the unsprung mass displacement, the wheel is off the ground. This check allows for a tyre force to exist while $x_{road} - x_{unsprung} > -0.03$, as the relational operator outputs a "1" in this case, and the tyre force (multiplied by 1) forms part of the forces acting on the unsprung mass. In the case of $x_{road} - x_{unsprung} < -0.03$, i.e. the tyre is off the ground, the relational operator outputs a "0", which causes the tyre force transmitted to be zero. The 0.03 m cut-off allows tyre forces from 0N to infinity.

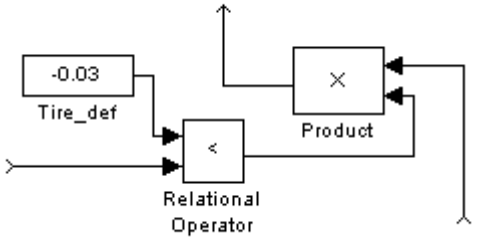

Figure 3-3: Blocks used to check for wheel hop

3.2.2. Error Coefficient of Variance

The Error Coefficient of Variance (ECOV) is a quantitative measure used to compare signals with each other. The values can be expressed as a fraction or as a percentage. Mathematically, the equation is

$$ECOV = \sqrt{\frac{\int_0^T (x(t) - y(t))^2 \, dt}{\int_0^T x(t)^2 \, dt}} \times 100\%$$

The numerator inside the square root is the square of the difference between the signal to be tested against (the one assumed correct) and the signal that is compared (the quality of which is unknown). The denominator contains the square of the trusted signal. From the equation it should be clear that certain phenomena that arise during testing could have large effects on the ECOV value - factors included are phase lags, incorrect scaling, DC offsets due to hardware or difficulties during zeroing, and signal noise. To quantify the effect of several of these phenomena, and to illustrate the sensitivity of the ECOV equation, some examples are given below.

In Figure 3-4 a harmonic base signal of magnitude one and frequency 2 Hz is compared to a similar signal, deformed in some way. Changes were made to the signal in terms of magnitude scaling, an offset was applied, and a phase shift was incorporated. The signal changes consisted of a magnitude amplification to 1.3, an offset of 0.3, and a phase shift of 40^O. This led to the seemingly high ECOV values of 30%, 42% and 68%, respectively. Another signal, in which all these combined effects were applied, resulted in an ECOV value of 94% when compared to the original. Some remarks about the ECOV value can thus be discussed.

Firstly, the ECOV doesn't superimpose the effect of potential signal deviations – the ECOV value of a comparative signal with offset and phase shift is not the same as the sum of the ECOV values for comparative signals, one having a phase shift and the other an offset. Secondly, it can be seen visually that the signals (base and modified) in the graph demonstrating phase lag compare favourably, however, the ECOV value is very high. This shows that ECOV is very sensitive to phase distortion and lag, which is unfortunate – the HiL setup contains definite lags, which doesn't bode well. For these reasons the ECOV value should be viewed in perspective, it should be known what curves are compared, and a plot or some other kind of visual representation should preferably back up the ECOV values.

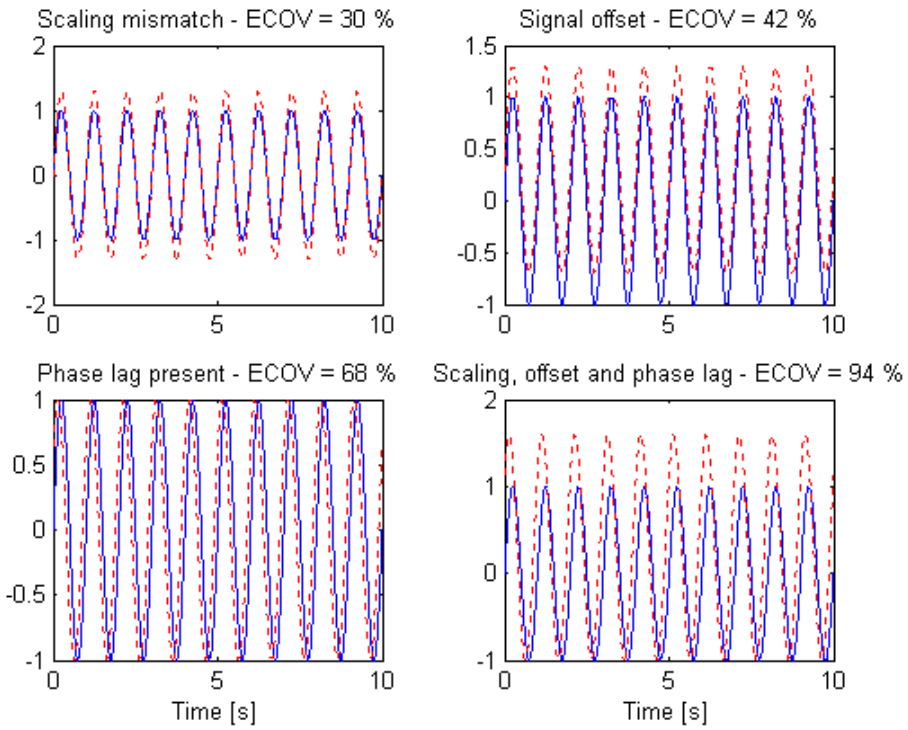

Figure 3-4: Effect of signal imperfections on ECOV value

3.2.3. Simulation Comparison

When the fixed- and variable step integration schemes are compared, it is necessary to compare both the sprung (body) mass and the unsprung (wheel) mass motions. The ECOV values for both were determined, and it was found that the input to the system played some part in the results. Variable-step integration is taken as the reference.

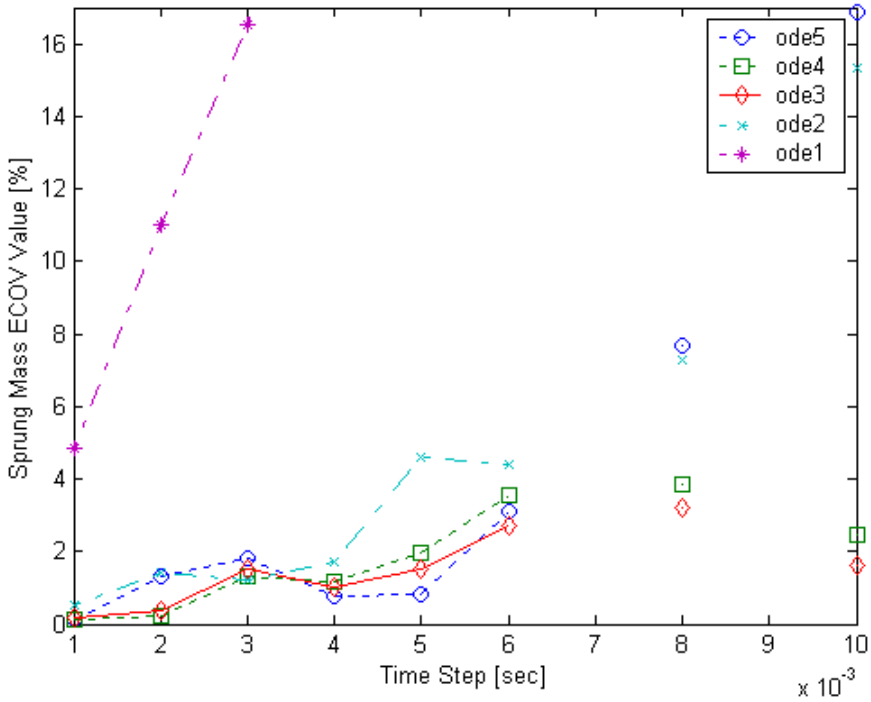

Figure 3-5: ECOV values of sprung mass motion, sawtooth input motion

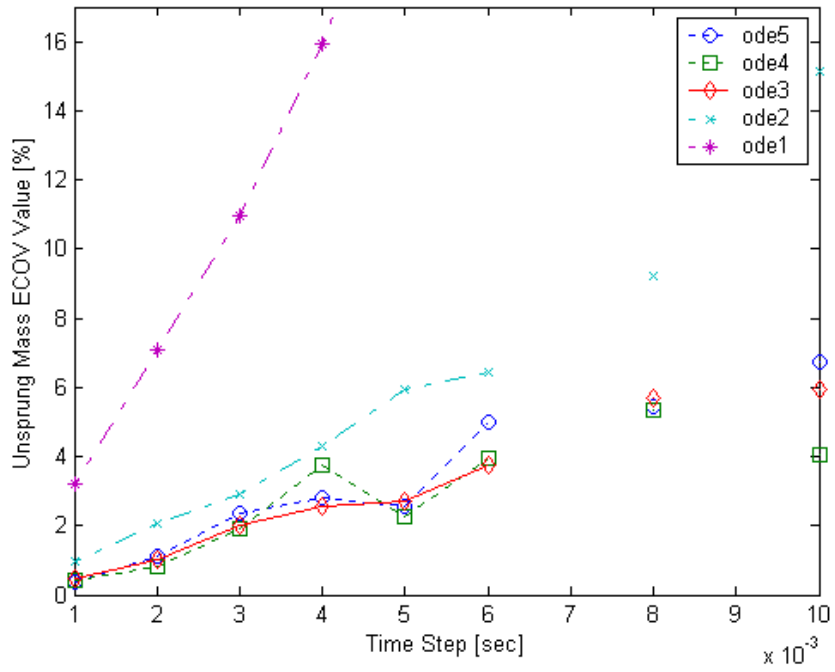

Figure 3-6: ECOV values for unsprung mass, sawtooth input motion

In Figures 3-5 and 3-6 the ECOV values for the sprung and unsprung masses are determined through integration using a sawtooth as road input. From these figures a clear indication of the trend concerning the ECOV can be seen, as all the fixed step integration schemes tend to perform better as step sizes decrease. Also, the sprung mass motion seems to be predicted more accurately when using a sawtooth input. This trend is reversed when using a square wave road input, as shown in Figures 3-7 and 3-8. Here, the unsprung mass is more accurately predicted. Looking at Figures 3-5 through 3-8, it can be concluded that a step size of 1ms would be sufficient, as the ECOV is less 1% in each of these cases. The integration step size is thus 0.001 seconds for the 2DOF HiL simulation as well.

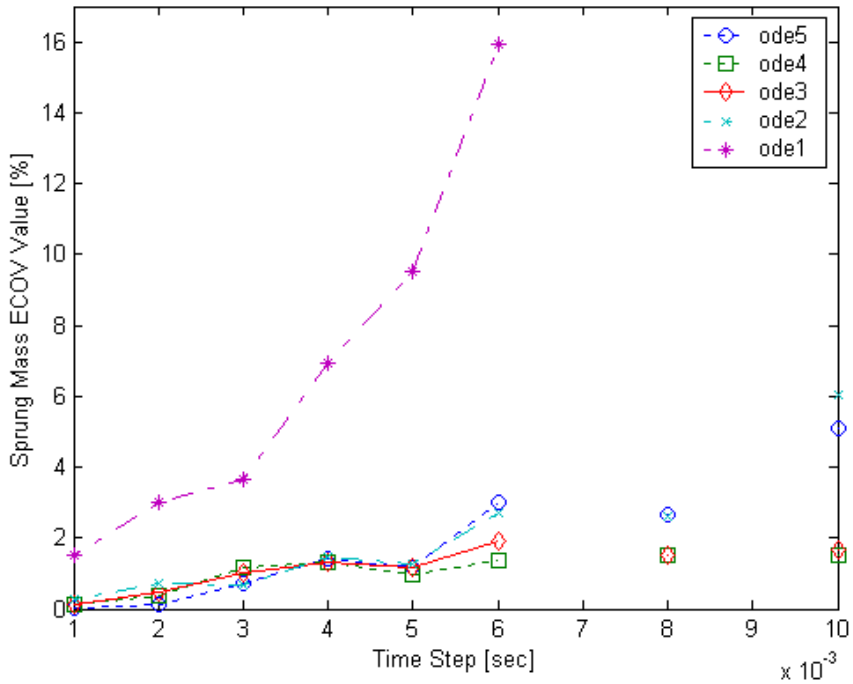

Figure 3-7: ECOV values for sprung mass, square wave input motion

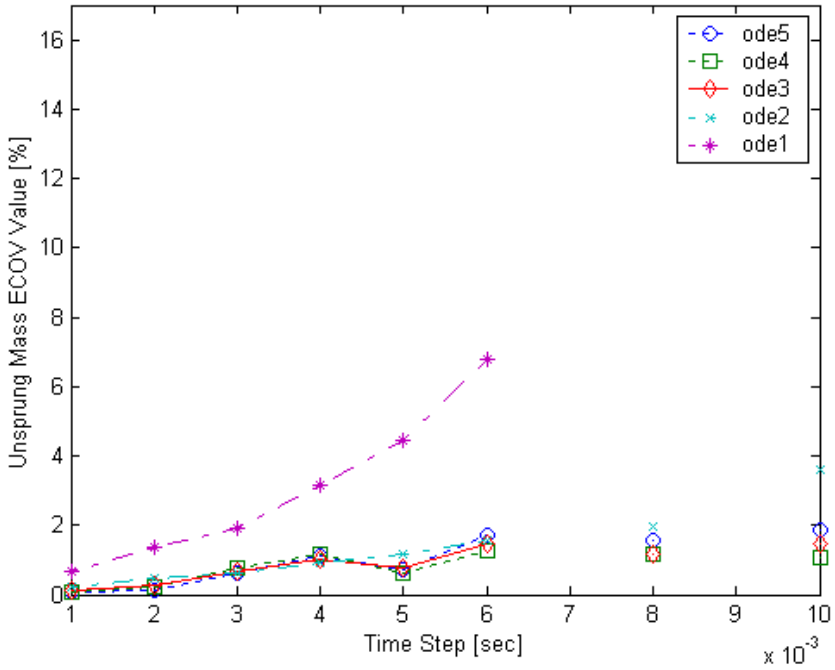

Figure 3-8: ECOV values for unsprung mass, square wave input motion

The lines on the graphs of Figures 3-5 to 3-8 connect the successive points as the ECOV values were calculated for successively larger time steps; however, fixed step integration wasn't stable or possible at all the time steps, as the break in the lines for time steps of 0.007 and 0.009 show. The omitted points occurred because the ECOV's numerator value was either ridiculously large, or the simulation wasn't completed due to the unstable response being out of MatLab's bounds. It is not known why the integration scheme returned results for some step sizes above 0.007 seconds, when a step size of 0.007 seconds proved unstable.

3.2.4. The Tyre Model

The choice of the tyre model was a simple process, as it was only used in a theoretic space and wasn't compared to any real tyre, hence no model corruption. Normally, the unsprung mass' natural frequency (i.e. the frequency at which the unsprung mass resonates) is ten times higher than that of the sprung mass, and since the latter is about 1.5Hz according to the parameters used in the model, one would assume a tyre model resulting in an unsprung mass natural frequency of about 15Hz. It was decided to use a tyre model that results in a lower frequency, as the actuator dynamics and the fact that the actuator's displacement limits aren't positive will create a situation in which the suspension unit can be damaged. (The actuator goes through the limit by some way before stopping, and the actuator may be excited through its natural frequency; this is a recipe for damage.)

Also of interest was the application of the wheel-hop model, and some concerns that goes with it. The static deflection of the wheel is directly proportional to tyre's stiffness, which is a factor in the unsprung mass natural frequency. By decreasing the tyre stiffness, a larger static deflection is obtained, meaning more leeway before the wheel hops – it must travel the equivalent of 30mm higher than the road surface before it breaks ground contact. This is preferable to a tyre model with a high stiffness coefficient that moves just a little to break contact, and causes excessive tyre and suspension deflection.

It was considered, at one point, to employ the Fiala tyre model as used in the MSC.ADAMS dynamics software. However, due to the amount of extra parameters needed, like wheel rotational velocity, contact patch length, rolling resistance

coefficient, and radially directed frictional force per unit angle of revolution, it was decided to use a simple tyre model consisting of a basic spring and damper.

A change in the tyre's damping coefficient has very little effect on the ECOV value of a model using this changed coefficient as compared to a model using the standard damping coefficient, that being a tyre damping coefficient of 1000 Ns/m. Even when two models utilising different damping coefficients are used (500 and 1000 Ns/m), does the ECOV calculate only a 2,24% and 2,7% difference in the sprung and unsprung mass responses, respectively. This is very little when viewed in the context of the experiments done, but it must be remembered that these values are calculated in both cases with ODE45 integration schemes. When the lesser damping is used in HiL testing, a completely different picture presents itself. A ripple of about 14 Hz is detected on the measured unsprung mass displacement. This means that the wheel is in fact oscillating continuously on a level road surface, even with damping in the tyre and suspension strut. This ripple is shown in Figure 3-9. This zoomed plot shows the software simulation's unsprung mass response.

The small ECOV values as generated by the comparison of two tyre-damping models suggest that the sprung and unsprung masses should behave similarly in the two simulations, in spite of the change of damping coefficient. This is excellent from a HiL point of view, as it means that the HiL simulation of a system with little tyre damping can be undertaken with added tyre damping without adversely affecting the results. Of course, as the ripple of Figure 3-9 shows, more damping is preferable since this case leads to fewer ripples in the unsprung mass response.

The matter of the tyre hop will be discussed further when the HiL simulation is discussed.

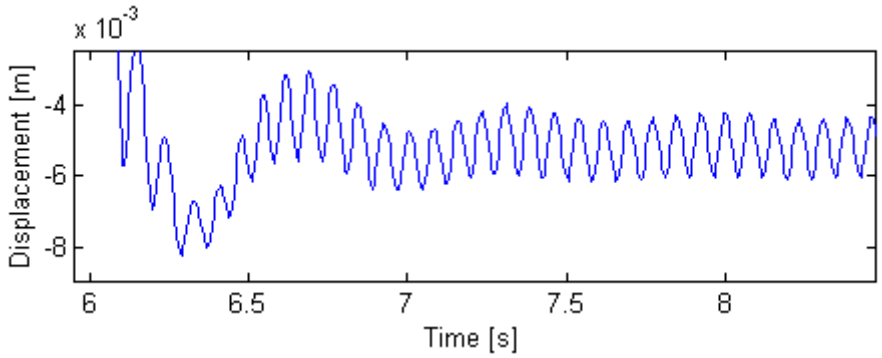

Figure 3-9: Ripple present for HiL unsprung mass response with tyre damping coefficient at 500 Ns/m.

3.3. HiL Simulation

The HiL simulation was done using the exact same hardware setup as was used in the SDOF HiL setup. This shows the flexibility of the method – a single hardware setup can be used to characterise the suspension components, and to run any number of tests using different HiL models. The spring-damper unit mounted in the actuator is shown in Figure 3-10.

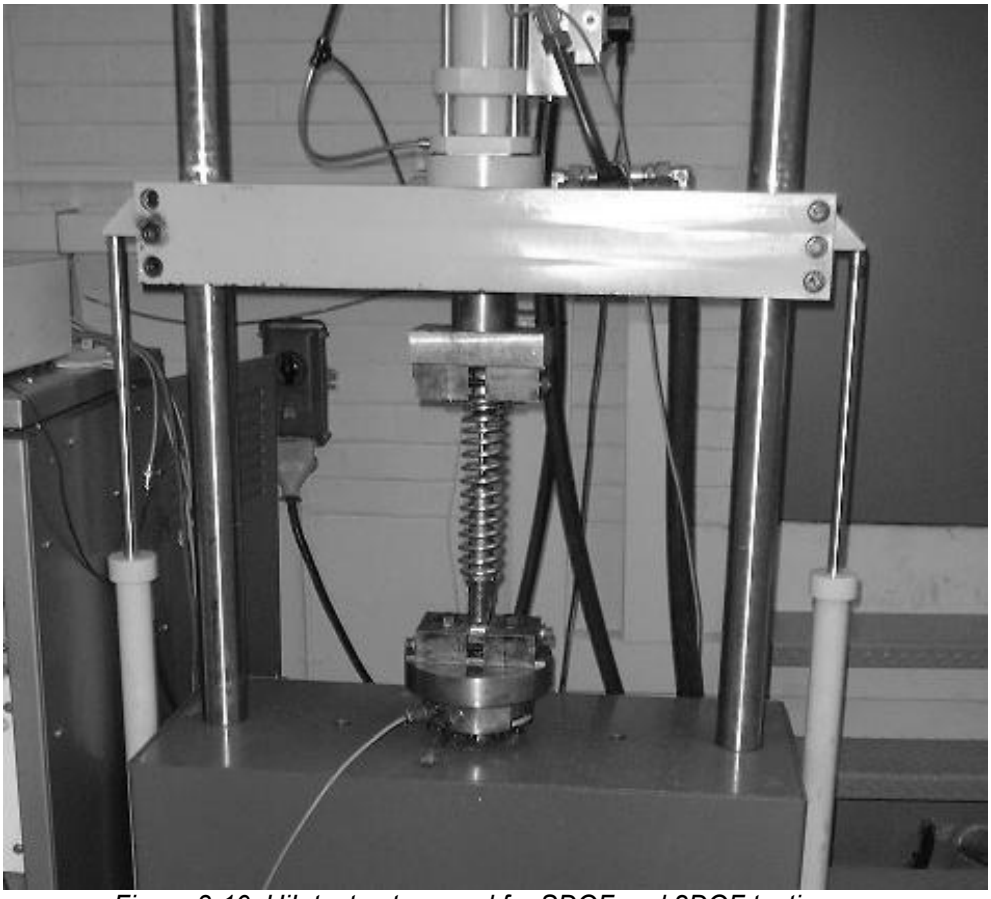

Figure 3-10: HiL test setup used for SDOF and 2DOF testing

3.3.1. Modelling for Wheel Hop Motion

The software Simulink model used a tyre model that allowed wheel hop. With the tyre and suspension parameters as used, the wheel-hop frequency was at between 8 and 9 Hz, which was chosen to be lower than the actuator/controller combination's natural frequency. The wheel hop model allows for road inputs of sufficient frequency content and magnitude to let the wheel, or unsprung mass, reach this hopping mode. Even with this hopping motion, the hardware can be used without triggering the limits on the actuator and thus jeopardising the suspension unit by resetting the actuator and thus the test.

The HiL simulation model thus allowed road excitations that would otherwise have caused the suspension deflection to exceed its limit to be used, even if the suspension limits offered only 70mm travel. Due to the little travel afforded by the spring-damper unit, the limits were reached easily even without excessive road inputs, but it was found that near the wheel hop frequency the wheel did break contact with the ground. At these relatively high frequencies the sprung mass did not displace excessively and some wheel hop phenomena was possible. Unfortunately the input motions used were mostly small and had little high frequency content, and so the bouncing motion wasn't induced. (It should be noted that even though the inputs are relatively small, most research into suspension and seat vibration utilises even smaller magnitude input excitations.)

3.3.2. dSpace Model Used

As can be seen from Figure 3-11, the model used in the real HiL simulations is an adaptation of that used in the software simulations. The calibration factors used are so that the actuator and load cell communicate the right signal magnitude – the load cell, calibrated to 400N = 1V, measures a real force of 400N for each volt read, while the controller LVDT has a scaling of 1V = 5mm, hence the gain of 200.

Some comments regarding the sign convention used in the model of Figure 3-11 is in order. The controller/actuator is set up in such a way that the maximum actuator extension (thus minimum suspension deflection) is achieved at the most positive control value accepted by the controller. This means that for the suspension unit to extend, the actuator must retract, and hence move to a smaller control voltage – hence the negative gain employed for the D/A plug feeding the controller (marked "xu-xs").

The same negative gain used at the force input ("Force Cal") to the HiL simulation model is due to the fact that the load cell measures compressive force as a negative value. For the orientation to be correct (refer to Figure 3-1) according to the equations of motion, the sign of the measured value must be changed, so that compressive suspension forces are positive.

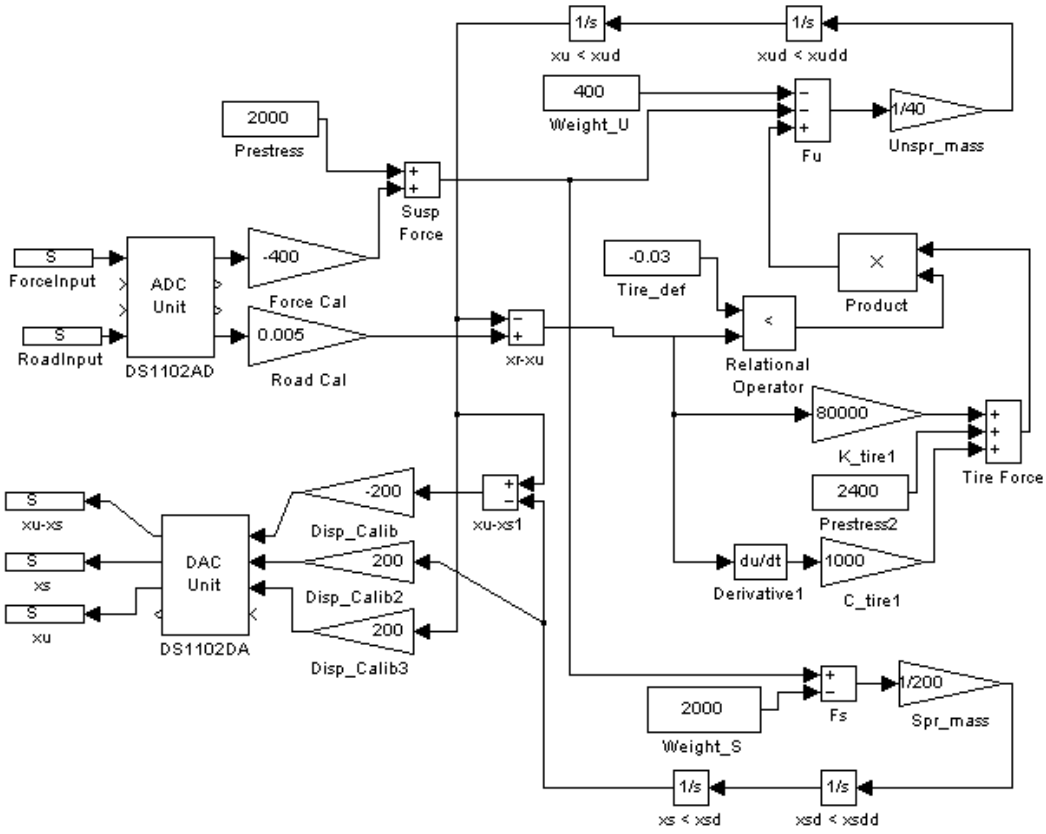

Figure 3-11: Simulink model used for HiL simulation

The addition of forces in the form of mass weights and spring pretensions enables the HiL simulation to start from the zero (equilibrium) position – since the load cell amplifier is zeroed before the simulation is started, the force present in the spring due to the sprung mass reaching the equilibrium position must be replaced by this "dummy" force or pretension. When the actuator is started and the external input is enabled, it immediately follows this external signal, because the "dummy" force that replaced the real spring force (due to compression) now balances the sprung mass in equilibrium. Hence, this signal must conform to the actuator limits. Starting the 2DOF system from a position of zero spring deflection (without using additional or "dummy" forces) will cause the masses to displace downward to the equilibrium position under the gravitational force, which is needed when the wheel hop model is to be used. This downward displacement is more than the actuator allows for in the limits, and hence the actuator cannot be started using this method.

An alternative to this method is to give the DSP board a constant output with some software model object other than the HiL simulation code to be loaded. When the HiL software is loaded, the actuator starts not at its own zero position but at a position representative of a deflected suspension unit at equilibrium (with an external input value as given by the previously loaded object). The simulation is thus primed so that the HiL code starts running when the model is already at equilibrium, and the suspension unit is already deflected. The transition from one DSP model to another can then be safely undertaken. This method has drawbacks in that every time the actuator needs to be restarted, the DSP object having the constant outputs must be loaded before the HiL object, and these constants must be accurately determined beforehand. (This can be troublesome since the internal zero and external zero aren't the same for the actuator controller.) Also, zeroing of the load cell can only be done at max suspension elongation using this method, whereas the load cell is zeroed at equilibrium even when the HiL simulation is running when using the method of spring pretensions and gravity forces.

3.3.3. HiL Results

Figures 3-12 and 3-13 show some of the results obtained from HiL testing. Both figures were generated using a 5mm amplitude square wave as input excitation. The difference is in the tyre damping used – Figure 3-12 was measured using a modelled 1000 Ns/m tyre damping coefficient, while Figure 3-13 was measured using a tyre damping coefficient of 500 Ns/m. There are some clear differences between the two responses – the oscillation caused by the inadequate tyre damping in the latter model results in inaccurate estimates of all the parameters measured, as the force measured, and hence the mass motions, are affected. In fact, while the simulation is running without any input (the signal value is zero) the actuator still oscillates at 14 Hz. This is due to the phase lags and the actuator's dynamics, but is easily remedied by applying more tyre damping to the model.

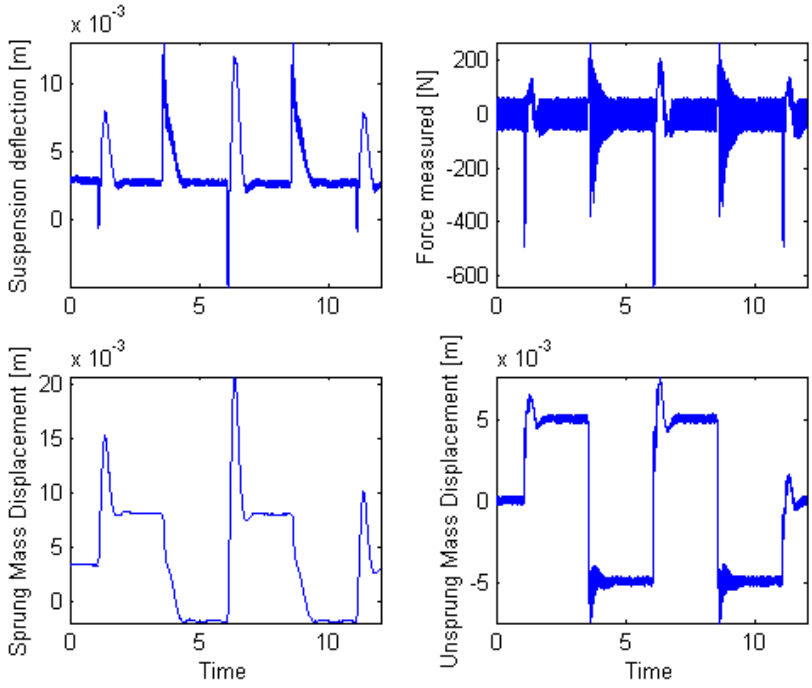

Figure 3-12: HiL results as measured for a square wave input, high tyre damping

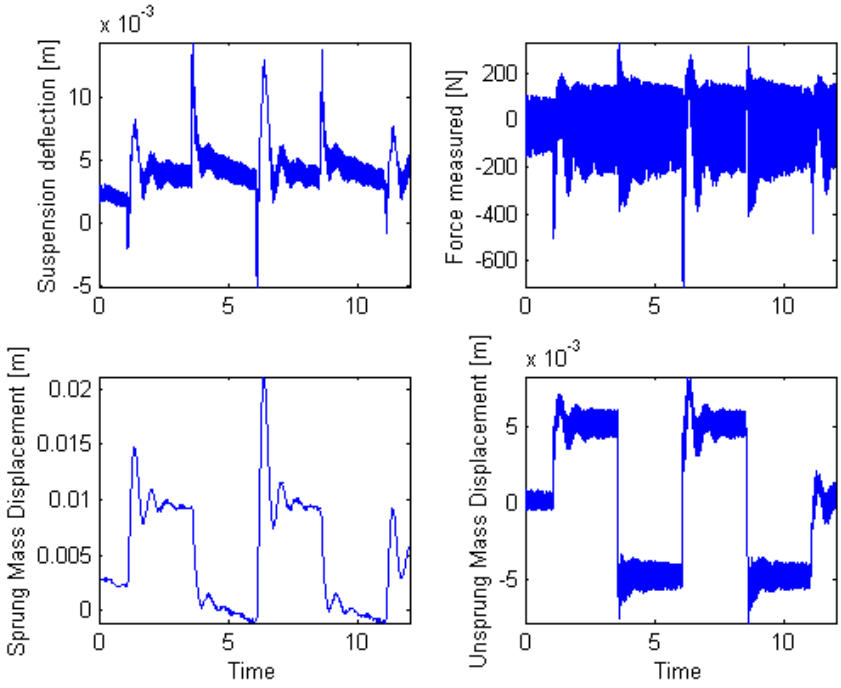

Figure 3-13: HiL results as measured for a square wave input, low tyre damping

Comparing Figures 3-12 and 3-13 shows the extent of the ripple's effect – the sprung mass shows a lot more oscillatory behaviour, while the force signal measured seems more like noise than a resultant signal. This behaviour justified the use of a tyre-damping coefficient of 1000 Ns/m.

3.4. Result Comparison

The results obtained through HiL testing must be compared to some other set of data to determine if the simulation did indeed achieve what it set out to do. Again the comparison will be between the HiL and ODE simulations, both run with essentially the same model. Also, the ECOV value will be determined as a quantitative measure of the simulation's performance (software simulation is a proven method, and is used as the reference). The results obtained when using different input signals will be discussed below. The input signals are described in more detail in Appendix A: Input Motions Used in HiL Tests.

3.4.1. Harmonic Inputs

Harmonic input signals of the form $x_{road} = Asin(\omega t)$ have been used with different excitation frequencies ω and different excitation amplitudes A. While most of these tests gave acceptable, measurable responses, all the tests near the sprung mass natural frequency caused the actuator to trigger its displacement limits. This is the expected response. Figures 3-14 and 3-15 show some of the measured responses, measured with harmonic excitations of 15mm amplitude and 1Hz and 2Hz excitation frequency. The ECOV values for these and other harmonic excitations are given in Table 3-1.

When considering the ECOV values it is clear that higher frequency signals tend to perform worse than their lower frequency counterparts – the 1Hz signals has ECOV values much lower than those of the 2Hz signals. This is mainly due to the way in which the ECOV is calculated, whereby the larger phase differences between the measured and calculated responses for the higher frequency input signals are penalised. Besinger [12] also noted this. Even though the ECOV values are high, it can be seen that the suspension deflection is similar for both the 1 Hz and 2Hz in Figures 3-14 and 3-15. It should be noted that a signal offset exists between the HiL-measured displacements and the calculated (software) displacements; this was corrected, and removed in the graphical representation.

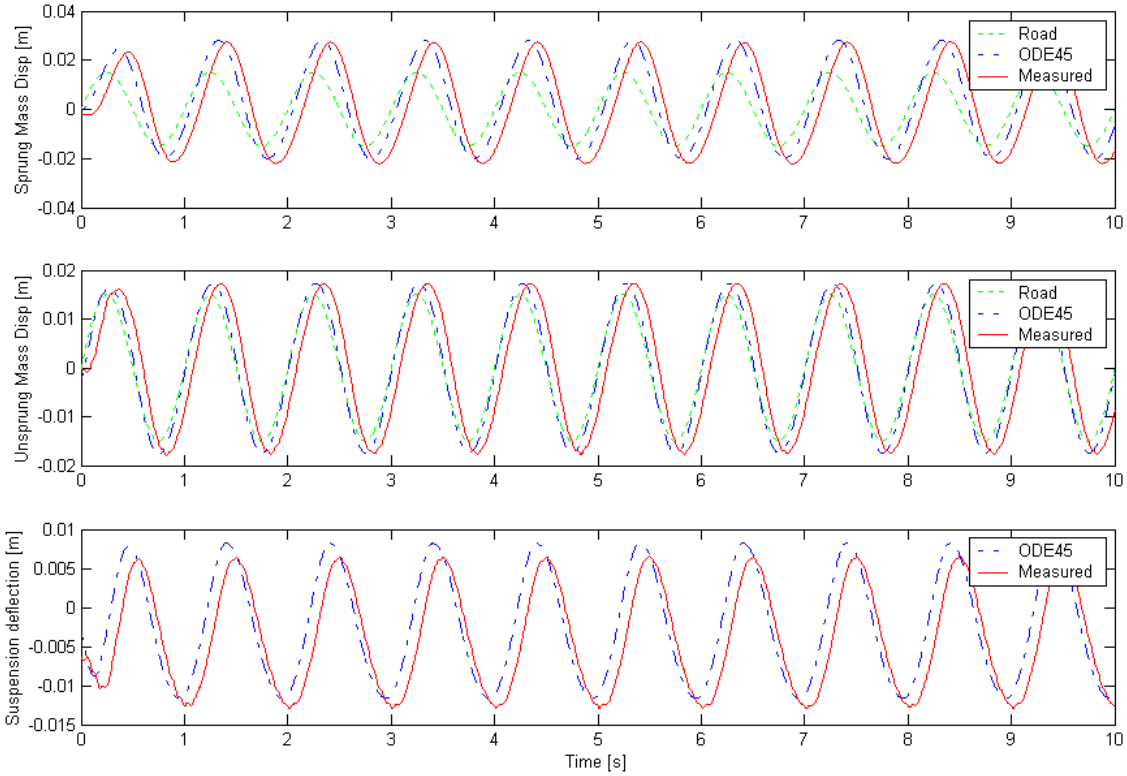

Figure 3-14: Comparative results for harmonic input of 1 Hz

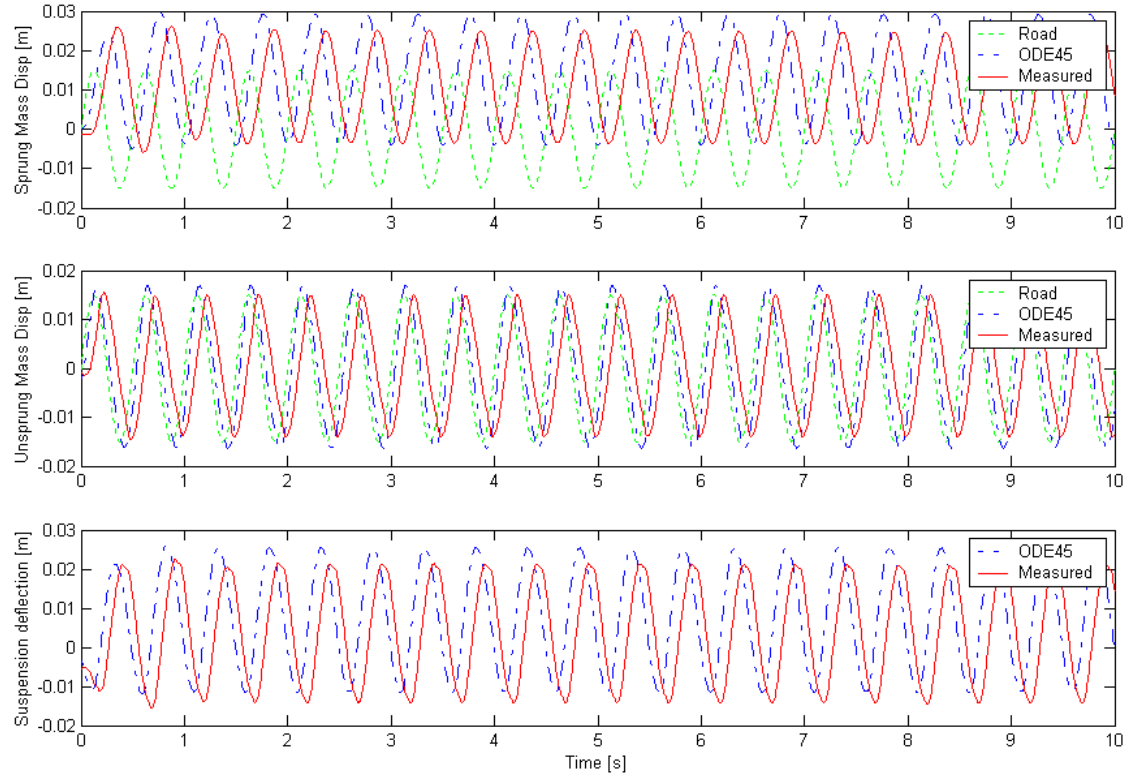

Figure 3-15: Comparative results for harmonic input of 2 Hz

Table 3-1: ECOV values for various harmonic input signals

Frequency [Hz]	Amplitude [mm]	ECOV		
		Sprung Mass [%]	Unsprung Mass [%]	Suspension Deflection [%]
1	5	58	47	37
1	10	51	48	46
1	15	51	48	52
2	5	70	93	84
2	10	71	88	90
2	15	79	81	94

3.4.2. Sawtooth Inputs

The sawtooth signals used in some HiL tests also give ECOV values that show the unsprung mass response to be far off from the calculated value, and in this case the reason for this behaviour is clear - the ripple in the measured unsprung mass response due to the oscillation of said mass causes relatively large differences between the measured and calculated displacements, as the HiL unsprung mass has a larger amplitude motion than the software equivalent. When looking at the suspension deflection, however, the picture is much better, with the ECOV and visual results indicating good resemblance. The phase lags in the HiL setup also exaggerates the sprung mass response over the discontinuity, but this doesn't have too much of an effect on the suspension deflection response. Plots comparing the measured and calculated responses are given in Figures 3-16 and 3-17.

Table 3-2: ECOV values for various sawtooth input signals

Sawtooth Duration [s]	Amplitude [mm]	ECOV		
		Sprung Mass [%]	Unsprung Mass [%]	Suspension Deflection [%]
1	10	61	92	41
0.5	10	67	128	44
0.3	10	85	157	63
0.5	10	68	129	62

3.4.3. Square Wave Inputs

A series of step inputs is handy to check the response of a system with, and can give a lot of information pertaining to a system, like damping, gains, etc when the system configuration is known. Even when the configuration is unknown, it is usually relatively easy to set a dummy system up to respond like the measurements.

Good results were also obtained when using the square wave inputs for the HiL simulations, as shown by the ECOV values in Table 3-3. In fact, the lowest ECOV value for the discontinuous road inputs (sawtooth and square waves) were obtained during the test using 5 steps. This is visually reflected in Figure 3-18, where the measured sprung mass, unsprung mass and suspension deflection responses correlate excellently with the calculated values. Figure 3-19 shows the adverse effect of the discontinuities on the phase character of the test, and this is reflected in the equivalent ECOV values – all are above 60%. Bear in mind these values stem from a test with 13 discontinuities in the road input.

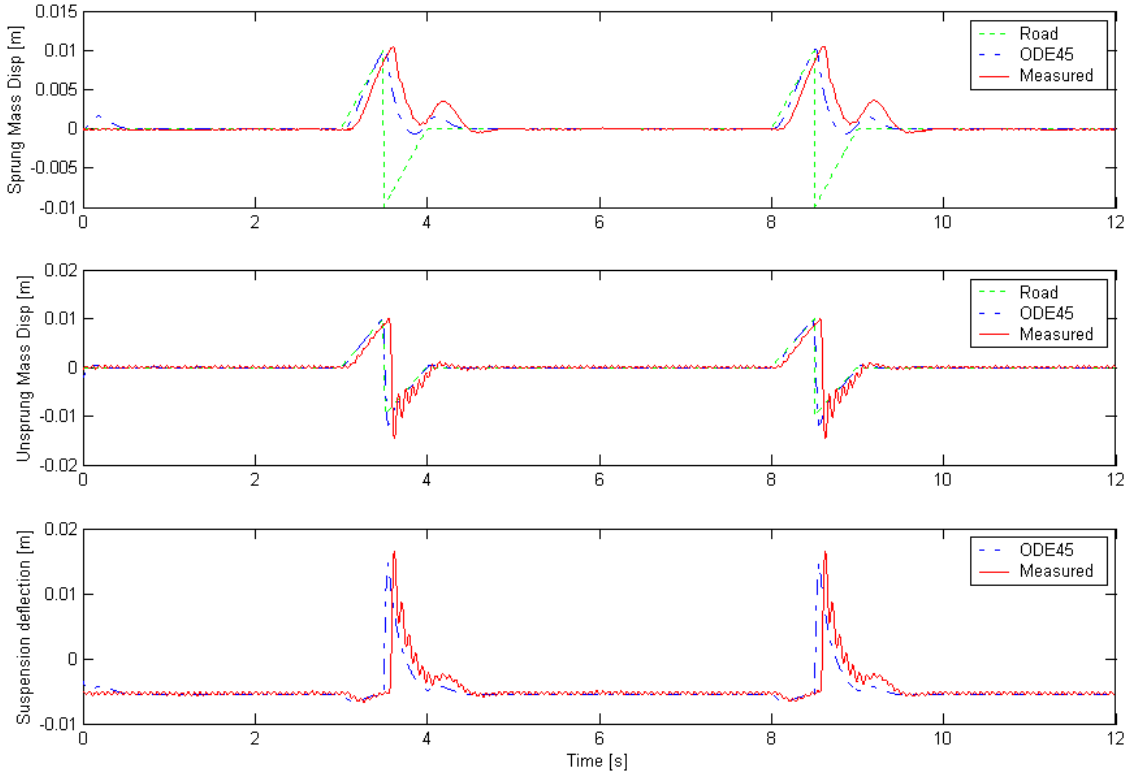

Figure 3-16: Comparative results for sawtooth input of 10mm lasting 1 second each

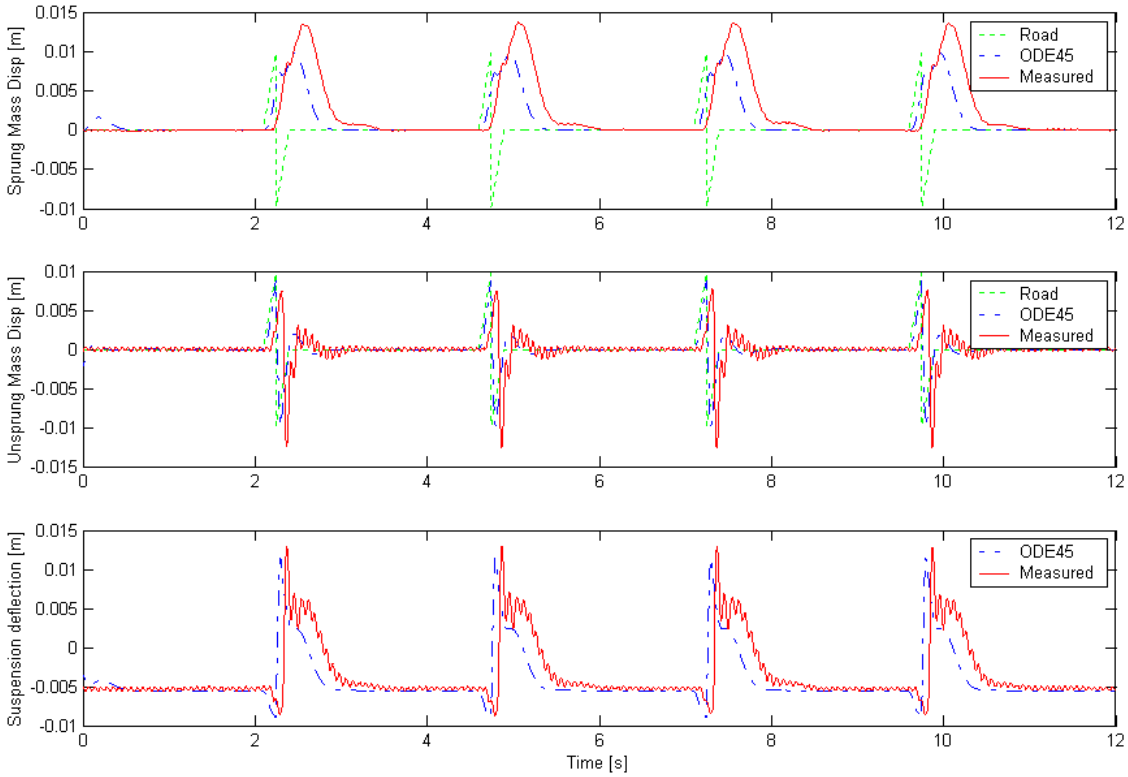

Figure 3-17: Comparative results for sawtooth input of 10mm lasting 0.5s each

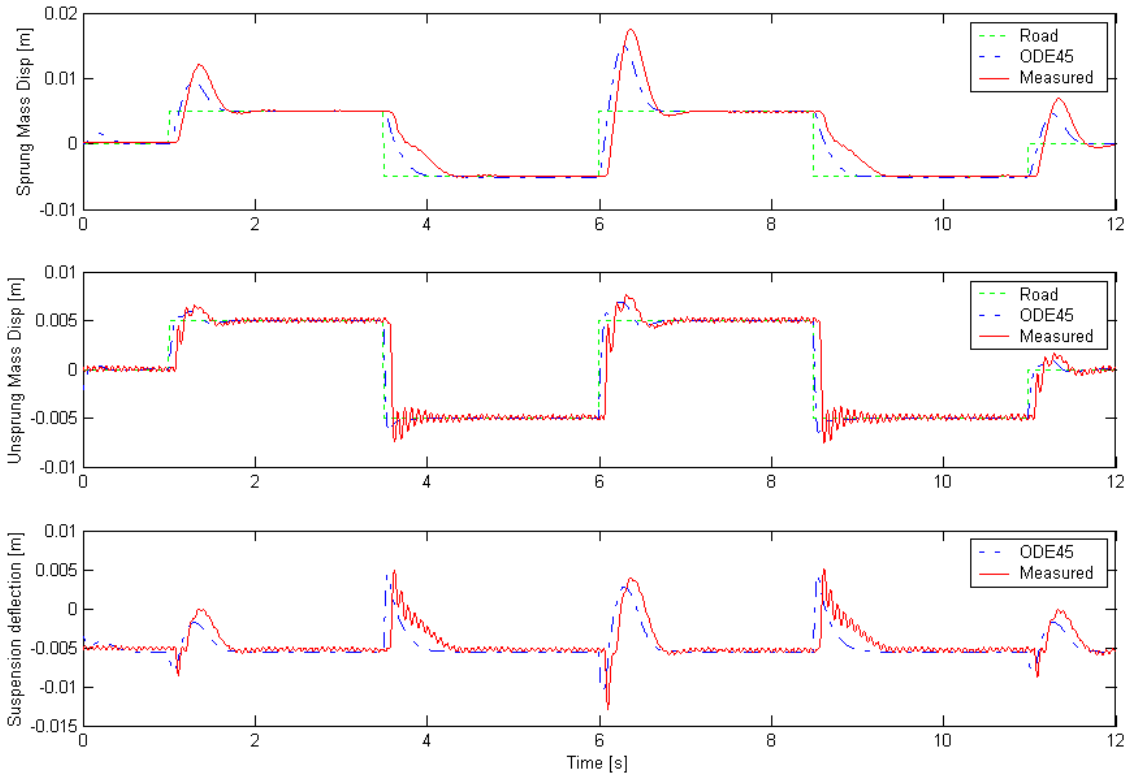

Figure 3-18: Comparative results for square wave input of 5mm

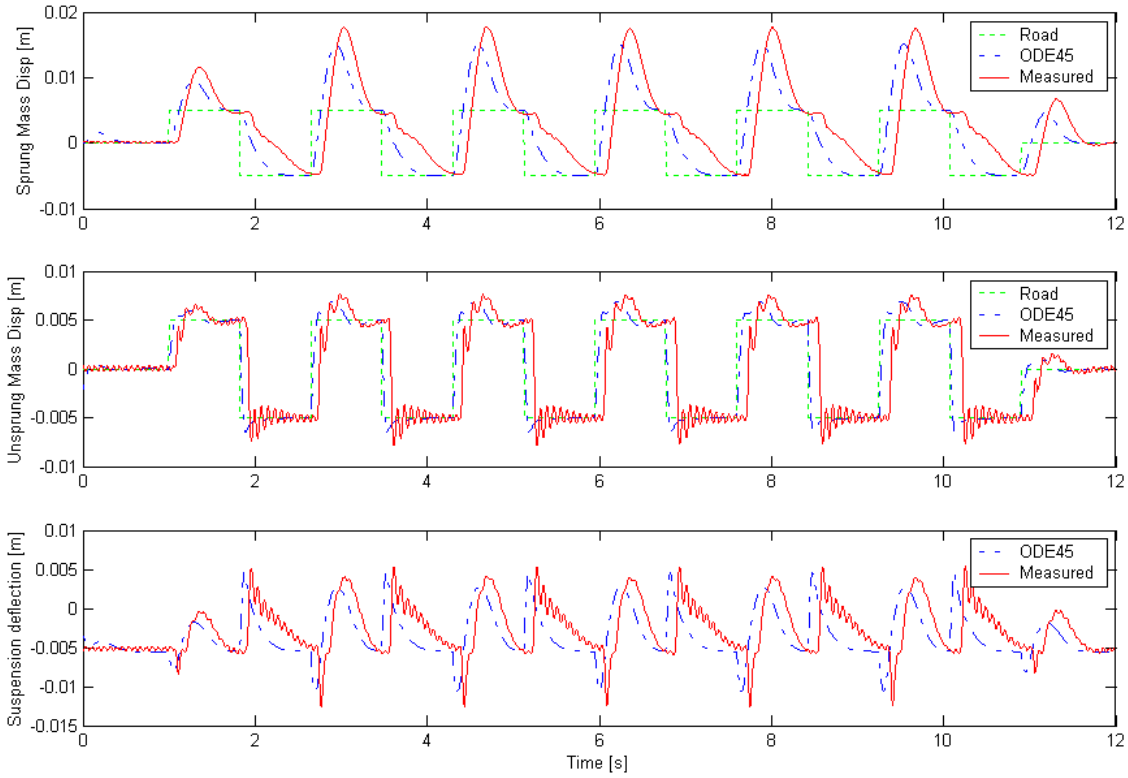

Figure 3-19: Comparative results for square wave input of 5mm

Table 3-3: ECOV values for various square wave input signals

Square Wave Duration [s]	Amplitude [mm]	ECOV		
		Sprung Mass [%]	Unsprung Mass [%]	Suspension Deflection [%]
1	5	48	65	67
5	5	34	32	32
4	5	46	45	49
3	5	66	68	79
2	5	49	61	71

3.4.4. Ramps and Speed Bump Inputs

Ramps and speed bumps make effective obstacles due to the fact that they are continuous while allowing transient motion to occur. (Even though the ramp inputs are supposed to be continuous, one of the inputs, “r3_5_20”, contains discontinuities. This is shown in Figure 3-21.)

The continuity of the input signals, unfortunately, doesn’t improve the phase behaviour of the HiL setup to such an extent that the ECOV values become less than 10%; however, from the values as given in Table 3-4, it can be concluded that the ramp and speed bump inputs give very good correlations between measured and calculated response. Figures 3-20 through 3-22 show some of the results obtained, and the excellent correlation between the two methods of determining the system response.

Table 3-4: ECOV values for various ramp and speed bump input signals

Ramp/Bump Duration [s]	Amplitude [mm]	ECOV		
		Sprung Mass [%]	Unsprung Mass [%]	Suspension Deflection [%]
1 (Ramp)	25	21	18	20
2 (Ramp)	25	14	26	46
0.5 (Ramp)	25	33	32	43
1 (Bump)	15	21	16	16

3.5 Summary of 2DOF HiL

In this chapter, it was shown that HiL is indeed suitable when testing multiple-degree-of-freedom systems since the comparison of the system response obtained using the real, physical spring-damper unit in a HiL simulation and the software simulation using spring and damper models, compared very well. Some problems did arise, though.

The use of a spring-damper tyre model is necessary. Although some research has been done using only a spring as a tyre model, the research in question was conducted using software simulations utilising models of the objects to be tested instead of incorporating the hardware into the simulation. Indeed, if the software simulations run in this chapter were run using a spring as the only tyre component, successful integration is achieved, albeit with some predictable unsprung mass motion. HiL simulation with this tyre model is impossible, as it proves to be unstable using the hardware available. The unsprung mass displacement, and hence the suspension deflection, grows progressively larger until a limit is triggered. A solution when using a spring-only tyre model may be using a different actuator-controller combination having less inherent phase lag and having better phase characteristics. That said, the incorporation of a damper in the tyre model proved to be very effective and not at all disruptive to the integration process. Comparing software models with tyre damping of 0, 500 and 1000 Ns/m indicated that the sprung mass motion, unsprung mass motion and suspension deflection differed little in these cases. Using a tyre-damping coefficient of 1000 Ns/m in this case proved a good compromise between simulation stability, accuracy and reality.

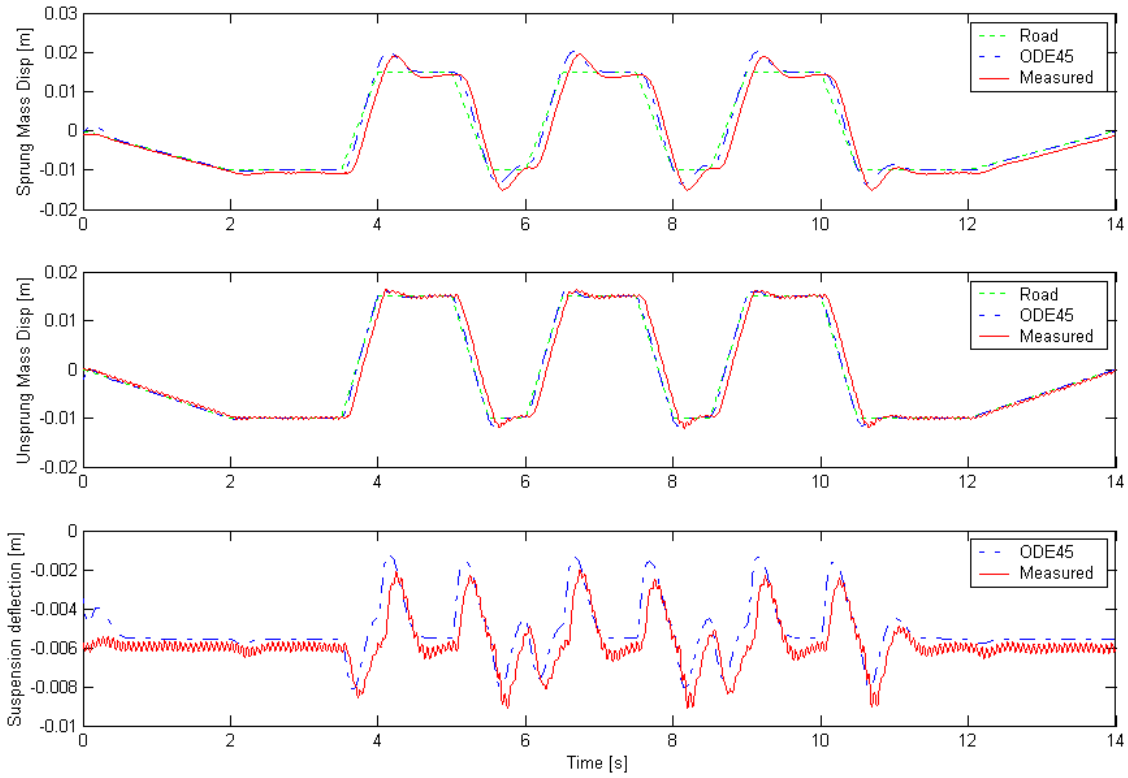

Figure 3-20: Comparative results for ramp input of 15mm

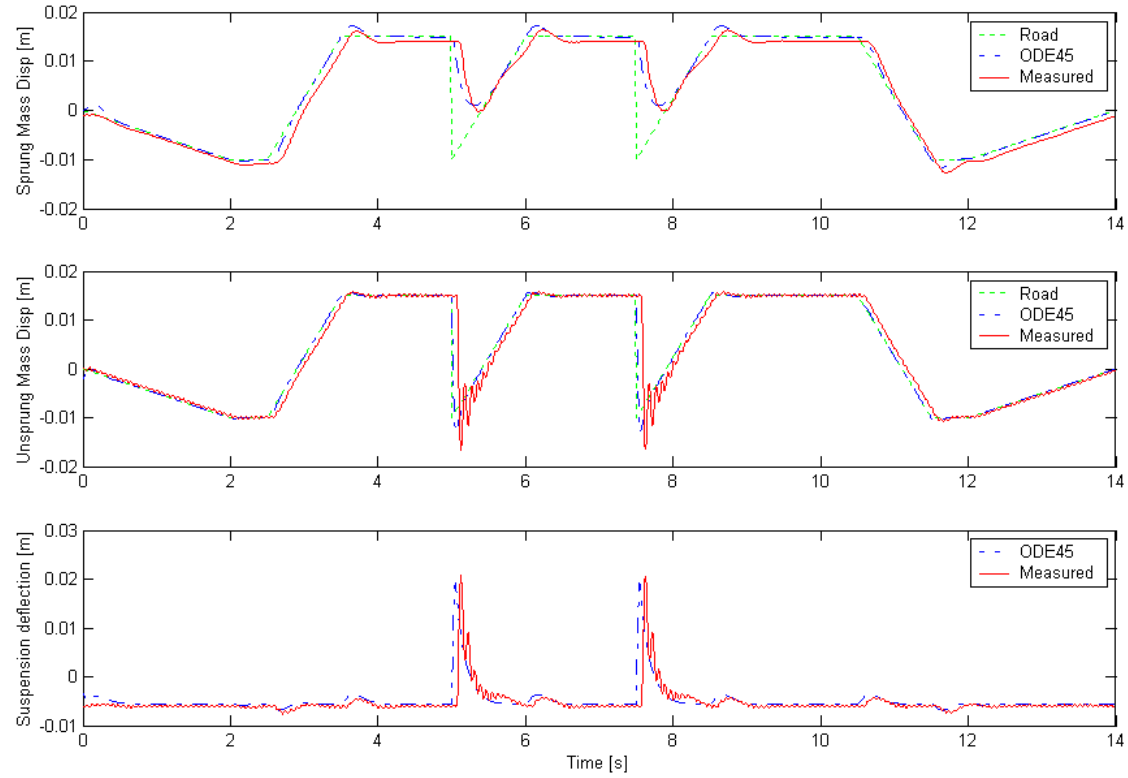

Figure 3-21: Comparative results for ramp input of 15mm

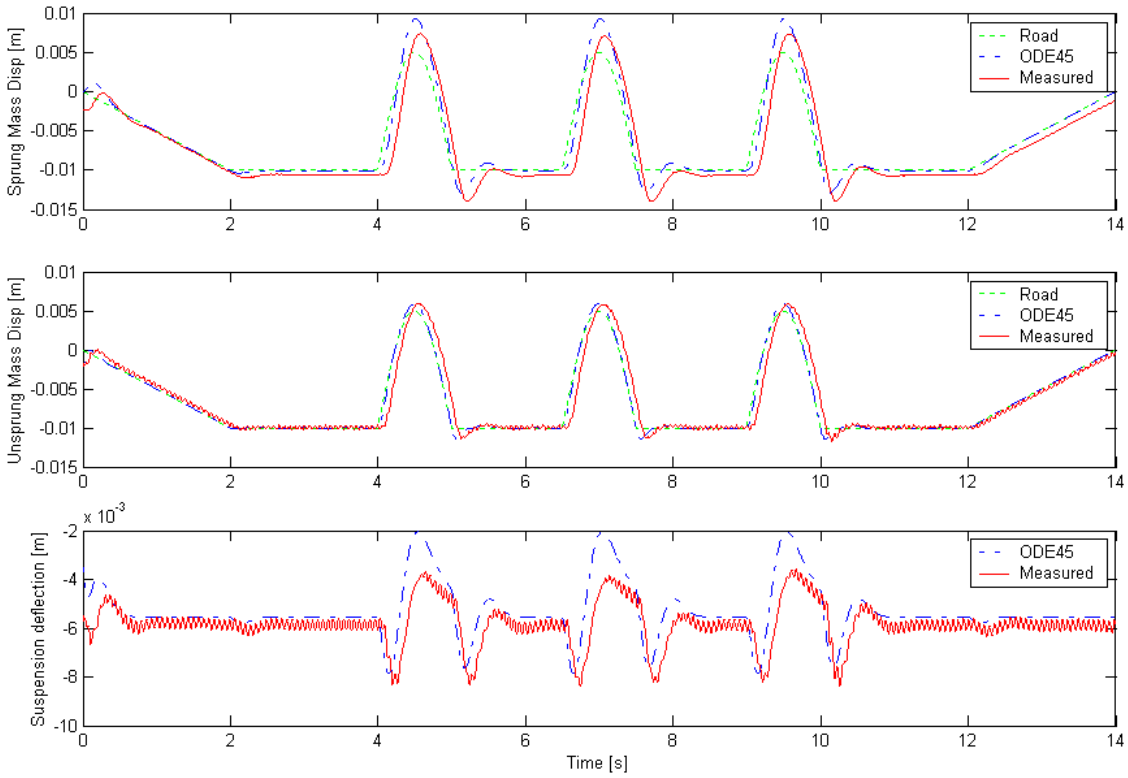

Figure 3-22: Comparative results for speed bump input of 5mm

Another problem encountered during the investigation of the 2DOF system ties in with the first, as discussed above. Introducing damping into the system leads to mechanical phase lags – coupled with the electrical phase lags incurred mostly by the controller's LVDT and filters, and the converters in the hardware, this has a detrimental effect on the ECOV values calculated for a system. It has been shown, however, that the ECOV equation is very sensitive and that the phase lags has a large influence on these error values. Considering the visual representation of the responses, it can be concluded that the HiL simulation fared well, even when the ECOV value told otherwise. It would thus be wise to consider the ECOV value in the context in which it is used when it is utilised as a quantitative measure.

4. HiL Compared to an Actual Measurement on a Non-Linear System

In the previous chapters, single- and two-degree-of-freedom systems were considered, and these utilised a “standard” geometry – the mass centres of all masses were assumed to be vertically aligned. The bodies never came into contact and the springs and dampers displaced the same value as the change in distance between two bodies (or reference points). These systems are conducive to easily derivable equations of motion, and the implementation of HiL and Simulink models for these systems are relatively easy.

In this chapter it will be attempted to prove that HiL is indeed suitable for use in situations where the system geometry and complexity is larger, so that the confidence in HiL can be justified. Also, instead of comparing the HiL simulation to some software model running inaccurate damper models, the HiL simulation will be compared to a real 2DOF setup. The setup to be used consists of the rear swingarm of a motorcycle coupled to an equivalent motorcycle body. This means that, effectively, the software inaccuracies are now transferred to the HiL Simulink model.

4.1. Test System Configuration

The test configuration of the real system as used in this chapter is a motorcycle rear swingarm connected to a sprung mass assembly, which substitutes the motorcycle chassis (Figure 4-1). The sprung mass assembly is connected to a wall using two pairs of parallel wall-mounted arms that, through their limited movement, maintain the essentially vertical motion of the sprung mass (body) of the setup. The arms also ensure that the attitude of the sprung mass stays constant – no rotation or leaning is allowed. The motorcycle rear swingarm, which makes up a part of the unsprung mass, is a “Pro-Link” swingarm as found on Honda MBX motorcycles. The rear tyre from said motorcycle is used, and provides additional mass and tyre forces at the swingarm tip. All ancillaries including the chain guides, brake assemblies, etc. have been removed to keep the setup simple.

The sprung mass is designed in such a way that the effective mass of the body can be changed through the addition or removal of metal plates. This allows the system to be used to simulate various conditions. The test setup is shown in Figures 4-1 to 4-3.

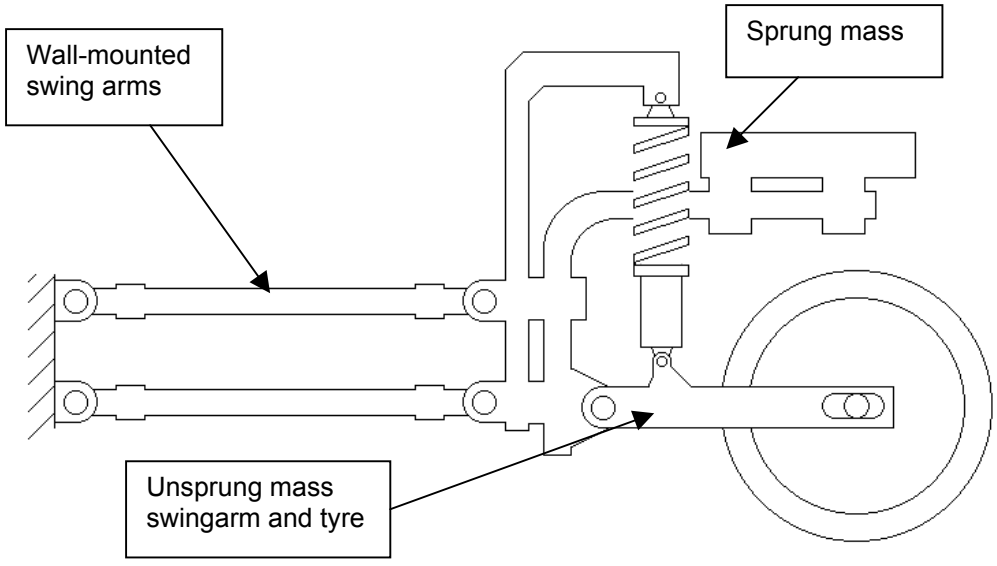

Figure 4-1: Schematic representation of 2DOF setup

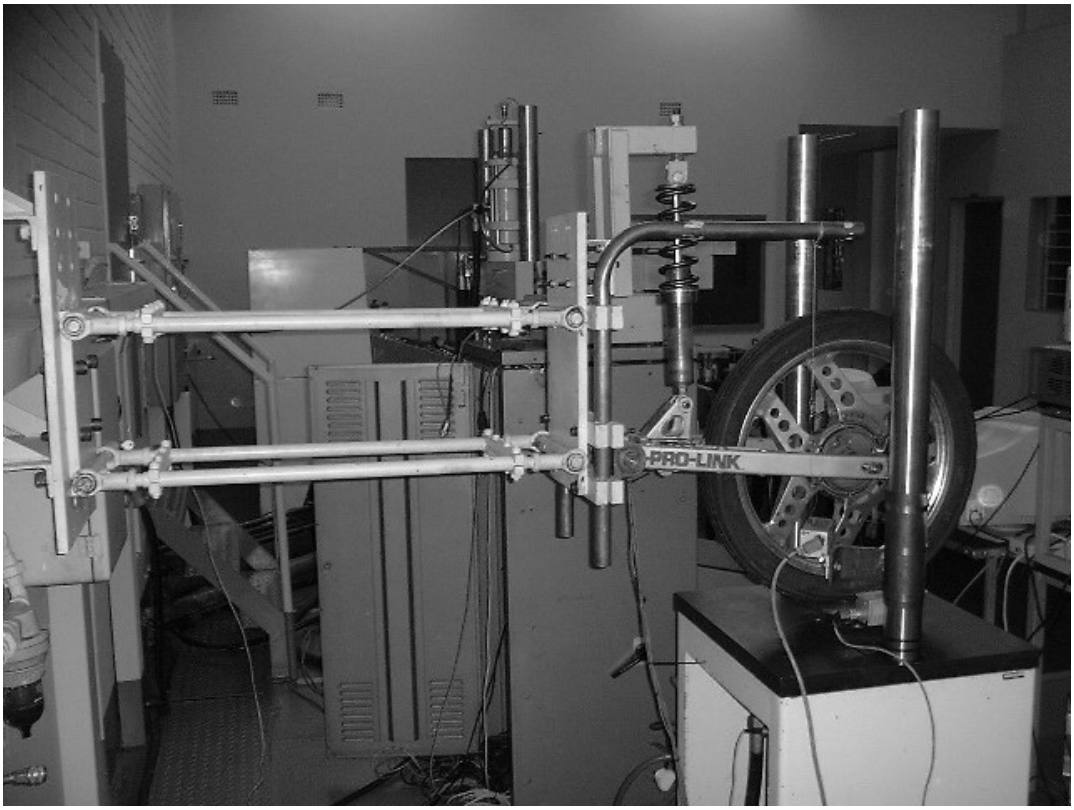

Figure 4-2: The physical system in the laboratory

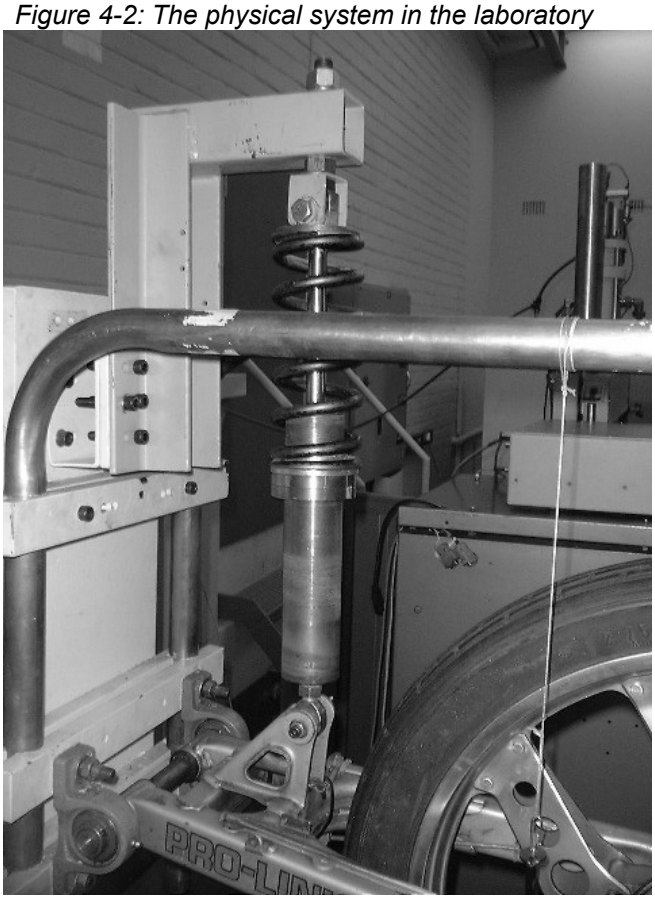

Figure 4-3: Spring-damper mounted on real system

The mounting positions of the support arms on the wall can be changed so that they are horizontal at static equilibrium for a given setup. The spring-damper unit used can be

adjusted so that the unsprung mass swingarm is horizontal as well. This allows easier modelling of the system.

4.2. Equations of Motion

The equations of motion for the motorcycle rear suspension geometry are necessary, as they will be used to implement HiL with. These equations are not as straightforward as the ones considered in Chapters 2 and 3 though, as the geometry is more complex.

4.2.1. Small Angle Assumption

It was sought to use the small angle assumption, that is $\cos(\theta) \approx 1$ and $\sin(\theta) \approx \theta$ if θ is sufficiently small. If this assumption could be justified, it would greatly decrease the complexity of the equations of motion and decrease the processing power used by the DSP running the model in the HiL setup.

Considering the working space of the real setup, it can easily be seen that the maximum and minimum wheel displacements, relative to the sprung mass, occur when the wheel touches the sprung mass and when the suspension unit, the spring-damper combination used, is elongated to its maximum length. These two deflections are 100 and 60 mm respectively from the static position, which is also taken as the zero position. The deflections equate to swingarm angles, relative to the zero, of 11.3 and 6.8 degrees, respectively.

When considering the error in the system's motion due to the introduction of the small angle assumption, one can easily determine that the minimum and maximum errors are 1.9 and 0.7% respectively. This shows that the small angle assumption is indeed valid and it is thus used.

The wall mounted swing arms, used to constrain the sprung mass in an almost vertical plane, also rotate through a finite angle during operation. The minimum and maximum angles of rotation is determined by the lowest position of the sprung mass (i.e. tyre touching ground and sprung mass) and the maximum suspension deflection. Again, the angles are relatively small, and the errors in assuming unity and linear values for cosine and sine are even smaller due to the longer swingarm: the maximum angle achieved is only six degrees, equating to a maximum error of 0.74%.

4.2.2. Derivation of the Equations of Motion

The equations of motion are derived in Appendix D. The equation of motion for the sprung mass is

$$\boxed{M_1\ddot{x}_s = F_1 + G_1F_t - G_2F_{sd}}$$

with

$$M_1 = -\left[\frac{I_O}{l_u} + \frac{I_O}{m_u l_{cg}}\left(m_u - \frac{m_u l_{cg}}{l_u} + m_s + \frac{2I_{Ow}}{l_{wm}^{\ 2}}\right)\right]$$

$$F_1 = -m_u g l_{cg} + \frac{I_O g}{m_u l_{cg}}\left(m_s + m_u\right) + \frac{2m_{wm} g l_{cgw} I_O}{l_{wm} m_u l_{cg}} + \frac{F_{cs} I_O}{m_u l_{cg}}$$

$$G_1 = l_u - \frac{I_O}{m_u l_{cg}}$$

$$G_2 = l_{sd}$$

For the unsprung mass, the equation of motion is determined to be

$$\boxed{M_2\ddot{x}_u = F_2 + G_3F_t + G_4F_{sd}}$$

with

$$M_2 = \frac{m_u l_{cg}}{l_u}$$

$$F_2 = \left[-\left(m_u + m_s - \frac{m_u l_{cg}}{l_u} + \frac{2I_{Ow}}{l_{wm}^{\ 2}} \right) \frac{F_1}{M_1} - \left(\frac{2m_{wm} g l_{cgw}}{l_{wm}} + (m_s + m_u)g + F_{cs} \right) \right]$$

$$G_3 = -\left(m_u + m_s - \frac{m_u l_{cg}}{l_u} + \frac{2I_{Ow}}{l_{wm}^{\ 2}} \right) \left(lu - \frac{I_O}{m_u l_{cg}} \right) \frac{1}{M_1} + 1$$

$$G_4 = \frac{l_{sd}}{M_1} \left(m_u + m_s - \frac{m_u l_{cg}}{l_u} + \frac{2I_{Ow}}{l_{wm}^{\ 2}} \right)$$

4.3. Characterising the System

The 2DOF motorcycle suspension system uses a spring and damper other than that used in Chapters 2 and 3. Now, a spring with larger stiffness and a damper with higher damping are used. The suspension unit is also physically larger, as the comparison in Figure 4-4 shows. Characterisation of the suspension unit will be discussed in Section 4.3.1.

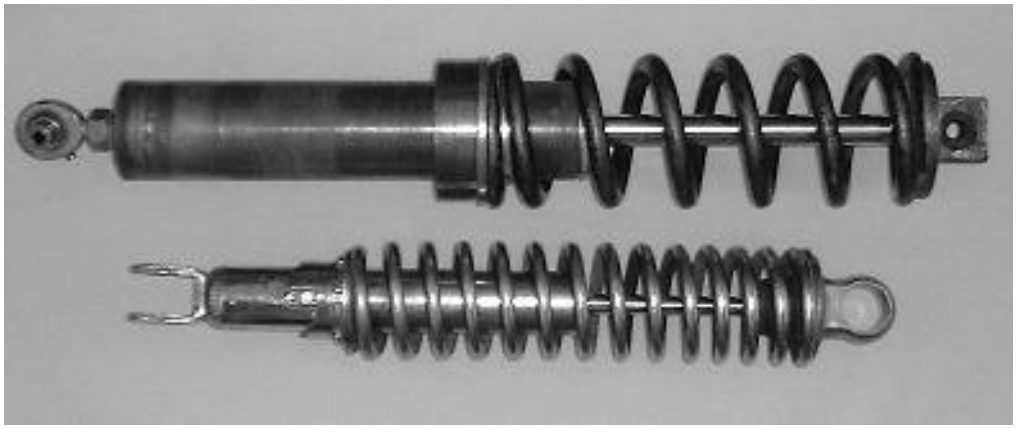

Figure 4-4: Spring-damper unit for motorcycle setup (top) and unit used for SDOF and 2DOF tests (bottom)

The equations of motion as derived in Appendix D utilises predetermined gains and constants; these values must be calculated before the simulation, and to do so, a lot of information on the system in question must be gathered. For instance, all the bodies' masses, centres of gravity, lengths, and so forth, must be determined. This information is also included in Appendix D.

4.3.1. Spring and Damper Used

The spring-damper combination used in these tests are made up of a motorcycle spring capable of supporting the sprung mass' weight, even with the lever effect of the smaller moment arm, and a damper unit specifically designed for use in a Baja Bug, a light four-wheeled off-road vehicle.

The spring's characteristic is shown in Figure 4-5, while Figure 4-6 shows the damper's characteristic. These were determined by separately characterising the spring and damper using suitable tests. Immediately the higher spring rate becomes evident, being more than four times larger than that of the spring used in Chapters 2 and 3. The damper now shows no break-off behaviour, as one can expect from a damper with just shims on the piston. The spring and damper was combined to form a single suspension unit, and the spring was installed in such a way that the unsprung mass swingarm was horizontal at static equilibrium.

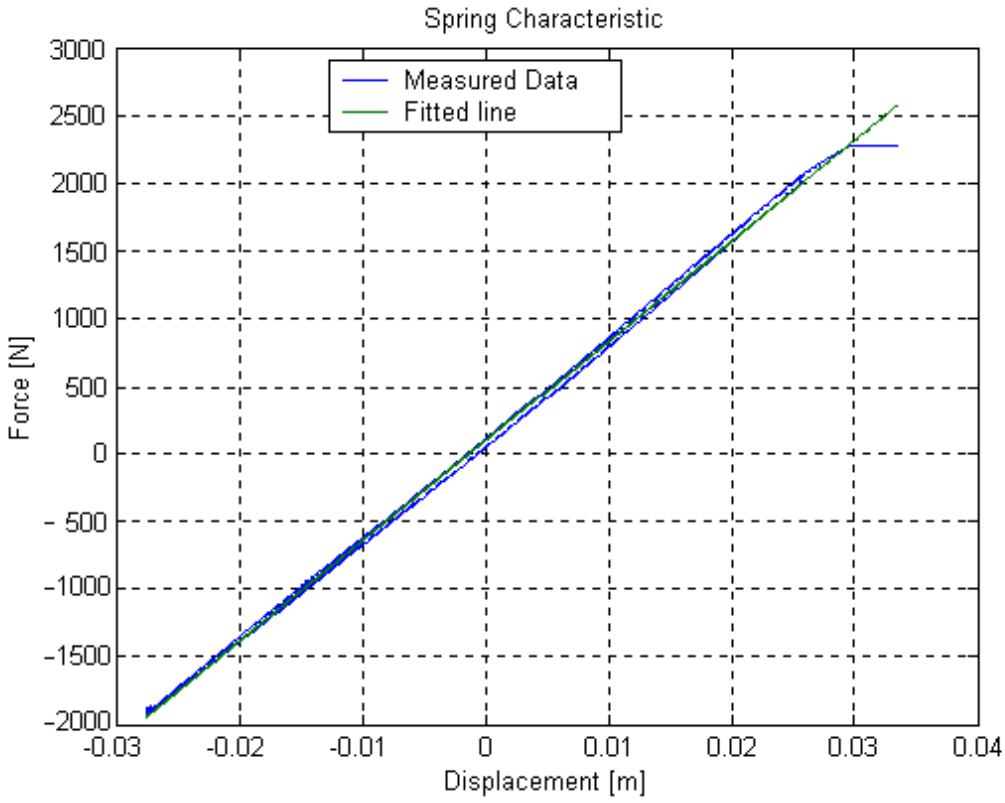

Figure 4-5: Spring characteristic

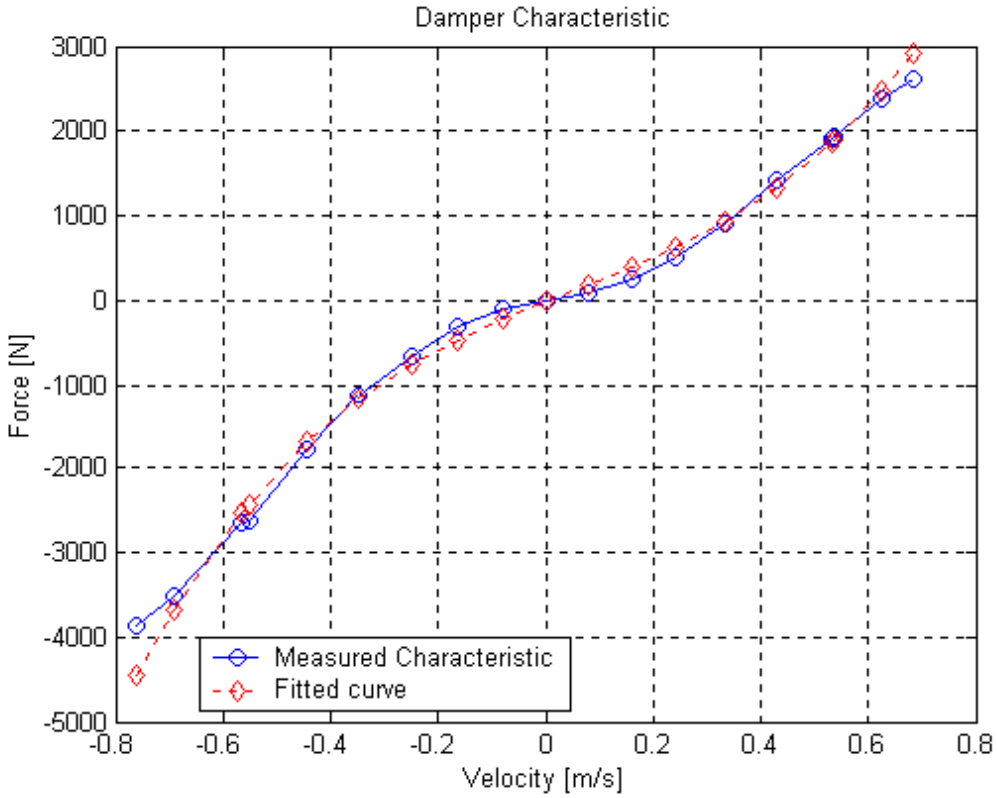

Figure 4-6: Damper characteristic

4.3.2. System Components

The non-linear 2DOF system has many components, the properties of which needed to be established so that the equations of motion could be used. This included the determination of the system components' masses, the centres of gravity, bearing friction (damping) etc. The component parameters that are used in this study are summarised in Appendix D.

4.4. System Tests

The real 2DOF motorcycle setup was tested using an actuator to supply the road input excitation – this actuator is similar to the one employed in the HiL simulations of previous chapters. The controller used was the same one as used previously, just plugged into this actuator's LVDT. This meant that the minimum of changes to the testing hardware was needed. Also, the road inputs defined and used previously are used here as well, albeit scaled up magnitude-wise due to the increased displacement that the real system can handle (there is no obstruction above the motorcycle wheel setup to bump into) and the fact that the suspension deflects only a small factor of the difference between the sprung and unsprung masses' displacement.

4.4.1. Measuring Equipment Used

Only the displacements of the sprung and unsprung masses were sought, and hence it was firstly considered to use accelerometers, the signals of which could be integrated twice to obtain the displacement. It would have been favourable to use accelerometers since they are easily attached to the physical setup without causing any changes to the physics; the accelerometers weigh little enough to be neglected. Also, the laboratory in which the tests were done is equipped with the necessary tools to easily measure, integrate and store the measured data. Unfortunately, the accelerometers available in the labs had insufficient low-frequency properties, and it was thus decided to use cable-type displacement transducers. These sensors consist of a body attached to a stationary point, and a cable running from where it is attached to the body to be measured. The transducer must be placed directly below the body (in this case, the sprung and unsprung masses) to avoid angular deflections corrupting the data. The measurement setup is shown in Figure 4-7. In Figure 4-3, the cable attached to the sprung mass is clearly visible.

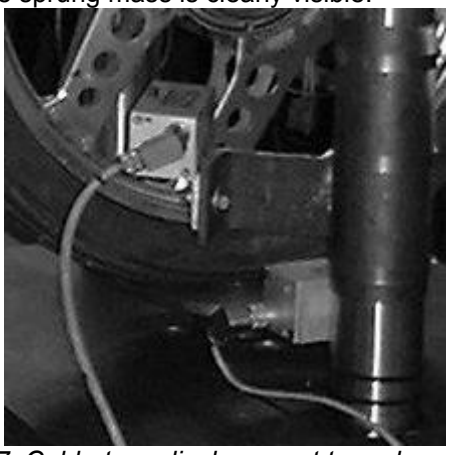

Figure 4-7: Cable-type displacement transducers

It wasn't necessary to measure the reactive forces of the tyre, as it wasn't necessary for the comparison between the HiL-simulation and real motorcycle test. It would have been of value to check the tyre model with, though, but this idea was abandoned due to the unavailability of a suitable load cell and mounting rig.

4.4.2. Modelling the Tyre

To use a tyre model in the setup of a 2DOF system is trivial – a simple spring-damper system can be used as was shown in the previous chapter. However, now a real tyre is present and a model of said tyre is needed for incorporation into the HiL simulation.

The tyre used was characterised as a non-linear spring and damper combination, the parameters of which was determined in the way described in Section 1.3.

The use of this model caused excessive wheel hop, and it was decided to use a tyre-damping coefficient of 250 Ns/m. The tyre tangent stiffness as defined in Chapter 1 was used, that being K_{tyre} = 28530 + 17.26x10$^5 x$.

The change in tyre damping coefficient removes the excessive ripple in the unsprung mass response, and the influence of the increased damping has been shown to affect the simulation negligibly.

4.4.3. System Responses

Some of the responses of the real motorcycle suspension system are shown in Figures 4-8 and 4-9. In these tests the sprung mass weight was set to 35 kg.

Initially, a sprung mass of 50 kg was to be used, but it appeared that the system damping was excessively large when this mass was used. The cause was only ascertained as the sprung mass was dismantled; the large mass seems to cause excessive stick-slip in the system's bearings. This leads to measurements characterised by motions that had no overshoot when the sprung mass velocity reached a certain level, and the motion of the sprung and unsprung masses damped out quickly. It was decided to use the lower mass instead.

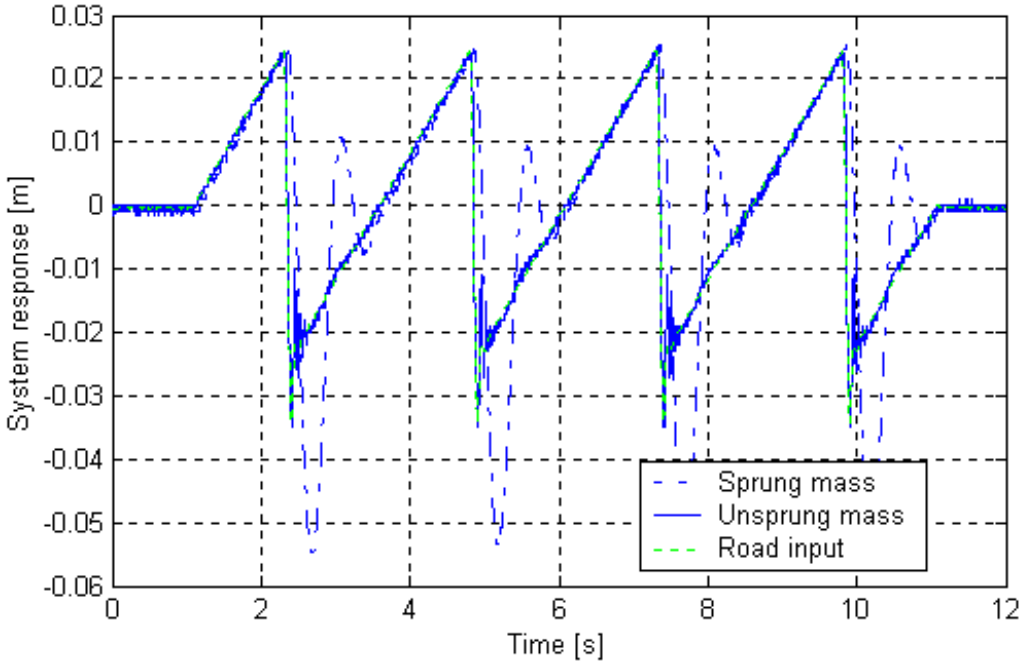

Figure 4-8: 2DOF system response for sawtooth road input

From Figures 4-8 and 4-9 the small amount of wheel deflection is evident – this is as expected. Already larger obstacles is used compared to the SDOF and 2DOF tests of Chapters 2 and 3, where much smaller obstacles were used due to the limitations of the spring-damper unit used. It can also be seen that there is some noise on the measurements, but the comparison with HiL data will show some definite trends.

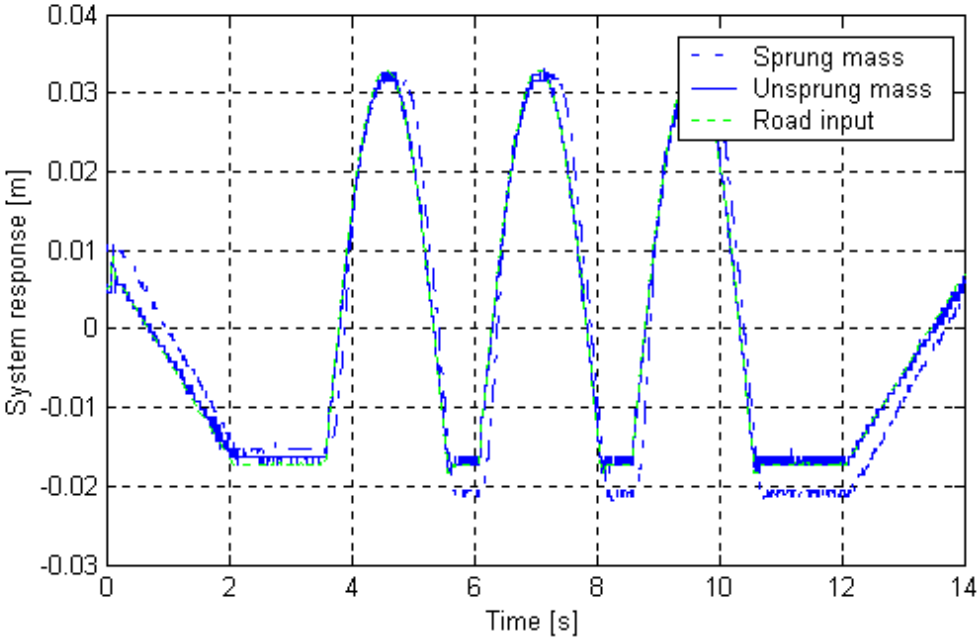

Figure 4-9: 2DOF system response for road input

4.5. HiL Tests

The HiL tests of this chapter were completed with the same setup as was used in the previous SDOF and 2DOF HiL tests – versatility is, after all, one of HiL's strong suites. The DSP was just loaded with a different model, and the correct spring-damper unit was placed in the test bench. The HiL setup used is shown in Figure 4-10, with the larger spring-damper unit installed when verifying the method using the motorcycle model.

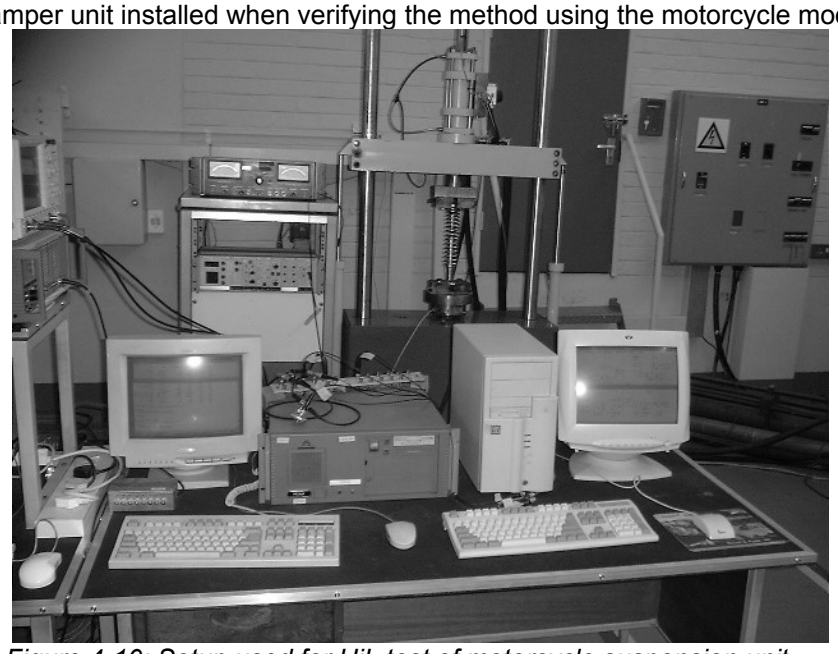

Figure 4-10: Setup used for HiL test of motorcycle suspension unit

4.5.1. HiL Simulink Model Used

The Simulink model used for the motorcycle HiL verification is shown in Figure 4-11, with its tyre force subsystem shown in Figure 4-12. Here it can be seen that the system parameters like weight, centre of gravity, etc. are implemented indirectly, with the coefficients for the forces and the force constants determined using a script file beforehand. The coefficients and constants are labelled S1 to S3 and U1 to U3 for

the simulation, the former being F_1/M_1 G_1/M_1 and G_2/M_1 while latter represents F_2/M_2, G_3/M_2 and G_4/M_2.

The use of coefficients S_1 to S_3 and U_1 to U_3 decreased the complexity of the equations of motion actually used in the Simulink model. Before this model was generated, it was attempted to use the equations of motion without relying on the coefficients, but rather using the parameters of the individual parts, like masses, distances, etc. This resulted in a model that proved difficult to debug, and the compiler gave an error when compiling this bulky model. Using the coefficients proved to be beneficial in more ways than one – compilation time was reduced, model complexity was reduced, and the amount of memory taken up in the DSP card's on-board memory was less. Reduced complexity also meant potentially shorter step times, even though it wasn't needed.

In Figure 4-11 a block called "Const Force" supplies the spring force to allow HiL simulation to start from equilibrium. The static tyre force is shown in Figure 4-12 as "Constant Tyre Force". Furthermore, the output of the DSP that gives the suspension deflection, and thus the actuator displacement signal, is scaled so as to compensate for the calibration factor and the lever at work in the suspension system. Since the suspension unit pivot point is 130 mm from the swingarm hinge, and the unsprung mass reference point 500 mm form the hinge, the lever arm equates to a suspension deflection fraction of 0.13/0.50 = 0.26 times the difference between sprung and unsprung mass deflection.

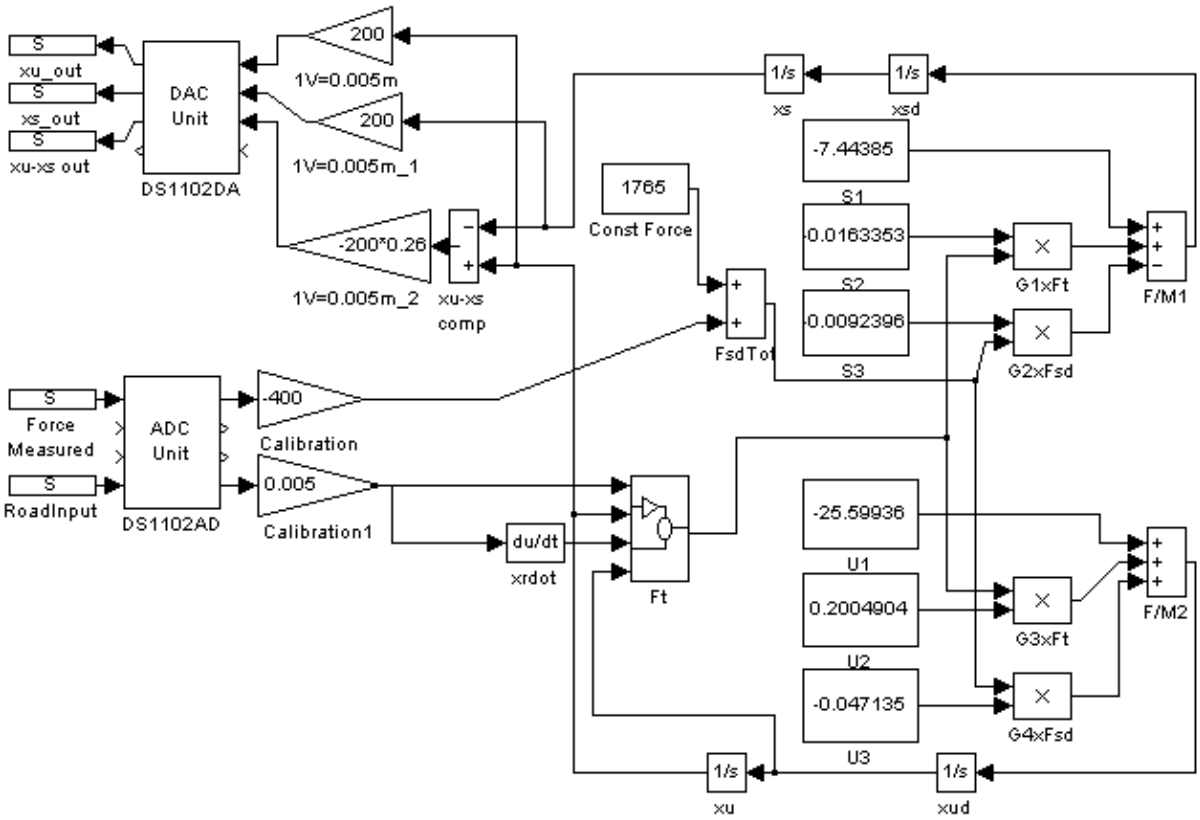

Figure 4-11: Simulink model used for motorcycle suspension HiL

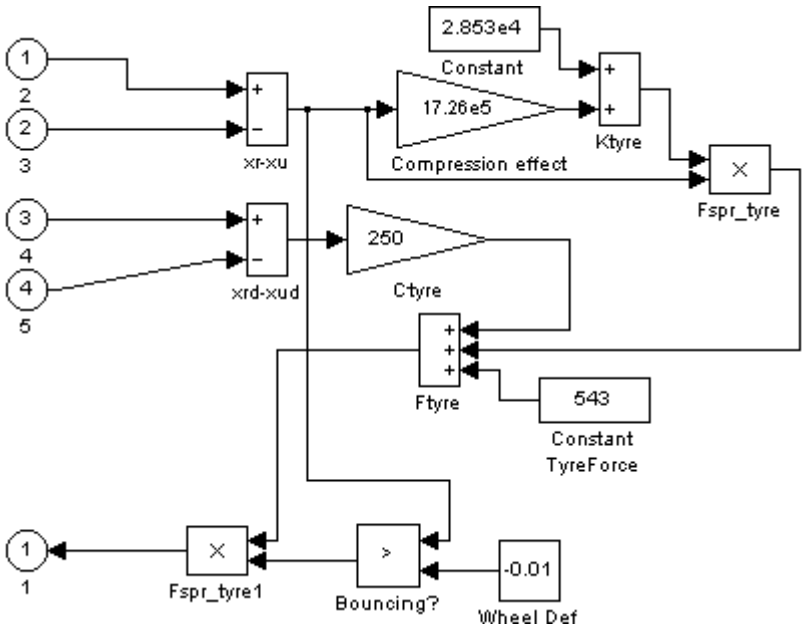

Figure 4-12: Simulink subsystem to calculate tyre force, "F_t"

It is notable that the object files downloaded to the dSpace card are relatively small – the model used here has a Simulink model size of about 25 kilobytes, while the equivalent object size is about 18 kilobytes. Thus, the size of the model, and hence the amount of blocks used in it, can be increased significantly without storage memory on the DSP card being a problem. (The dSpace card has 128kb memory on-board.)

The motorcycle suspension configuration used plays a part in the model behaviour. In general, two motorcycle rear swingarm-suspension geometries are commonly used. Two spring-damper units are placed on both sides of the wheel, mounted closer to the wheel spindle position than the swingarm pivot point, or a single spring-damper unit is placed on the motorcycle's centreline, between the wheel and the swingarm pivot. The latter is used in the test setup employed in this chapter. This configuration is dependent on a rather stiff spring and a damper with a high damping coefficient due to the lever effect on the suspension unit. The spring used in Chapters 2 and 3 was also a motorcycle unit, from a dual-unit configuration as was described first. The difference in the spring stiffness between the springs of Chapters 3 (16 kN/m) and 4 (74 kN/m) indicates the different configurations.

By using this levered spring-damper unit, only a fraction of the motion between the sprung and unsprung mass reference points is carried over to the suspension unit. This has advantages and disadvantages. Now the suspension unit maximum and minimum deflection values are not the limiting parameters in HiL testing, because even though the actuator controller limits are set to protect said unit, the unit is physically larger to accommodate the stiffer spring, and the motion is just a fraction of the referenced motion. Therefore the limiting factor might well be the actuator dynamics, which cannot keep up with the large suspension deflection displacement command values allowed by the setup.

The drawback is related to the instruments used – to obtain the same displacement measurement resolution as in the simple linear 2DOF system of Chapter 3, the measuring equipment should have better resolution. A piece of equipment may have adequate resolution to measure the difference between the sprung and unsprung masses, while measuring a fraction thereof proves problematic. This is not a problem for these tests, however, as the resolution of the measuring devices is ample to deal with all the motions.

4.5.2. Results

Some HiL simulation test results are given in Figures 4-13 and 4-14. These figures show the sprung mass, unsprung mass and actuator response. The suspension deflection is 26% of the difference between the unsprung and sprung mass displacements.

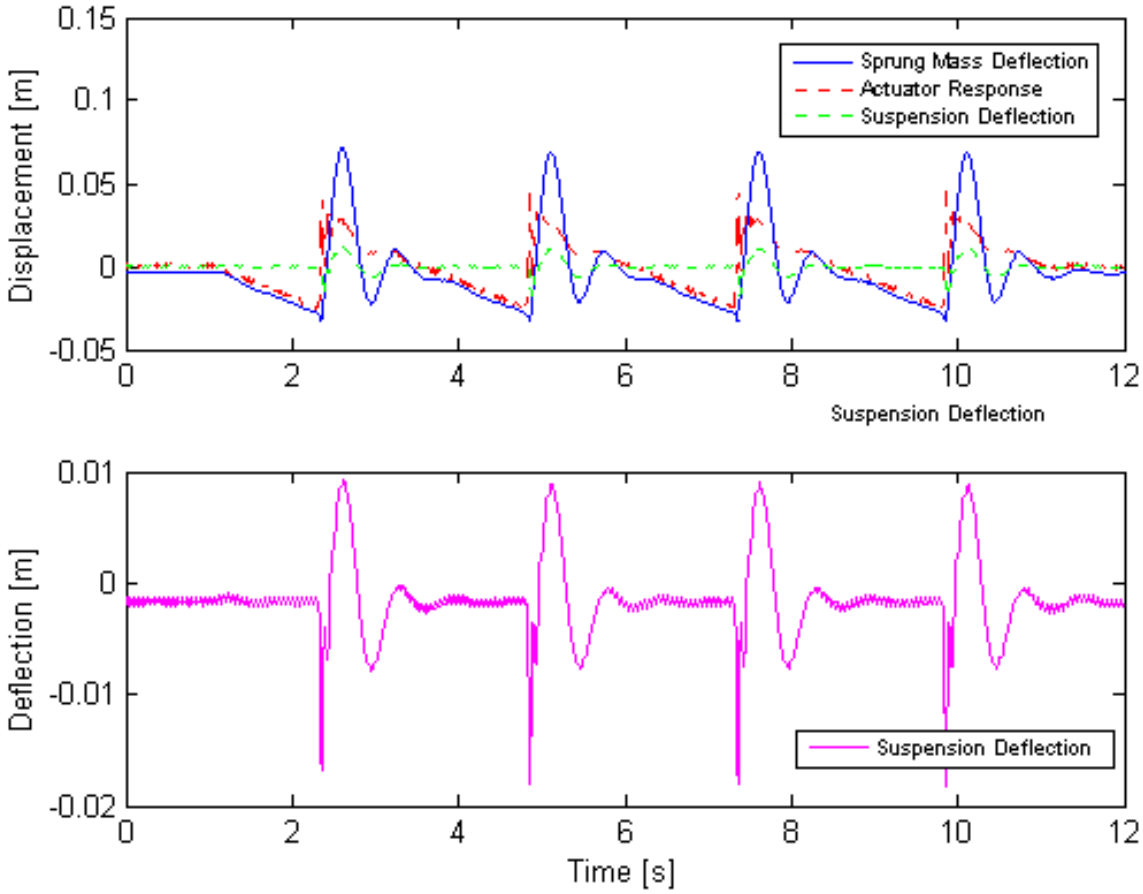

Figure 4-13: HiL raw results using a sawtooth road input

Figure 4-13 shows the actuator response, responsible for the suspension deflection motion. The sawtooth input has a first order (displacement) discontinuity that no physical system can follow identically, but the actuator PID controller is set in such a way that the response is acceptable.

Figure 4-14 illustrates the point made about the advantage of the single spring-damper unit configuration; even thought the peak-to-peak displacement of the sprung mass is more than 200 mm, the suspension unit can handle it – the maximum displacement difference between the sprung and unsprung masses is almost four times more than the maximum suspension deflection achieved.

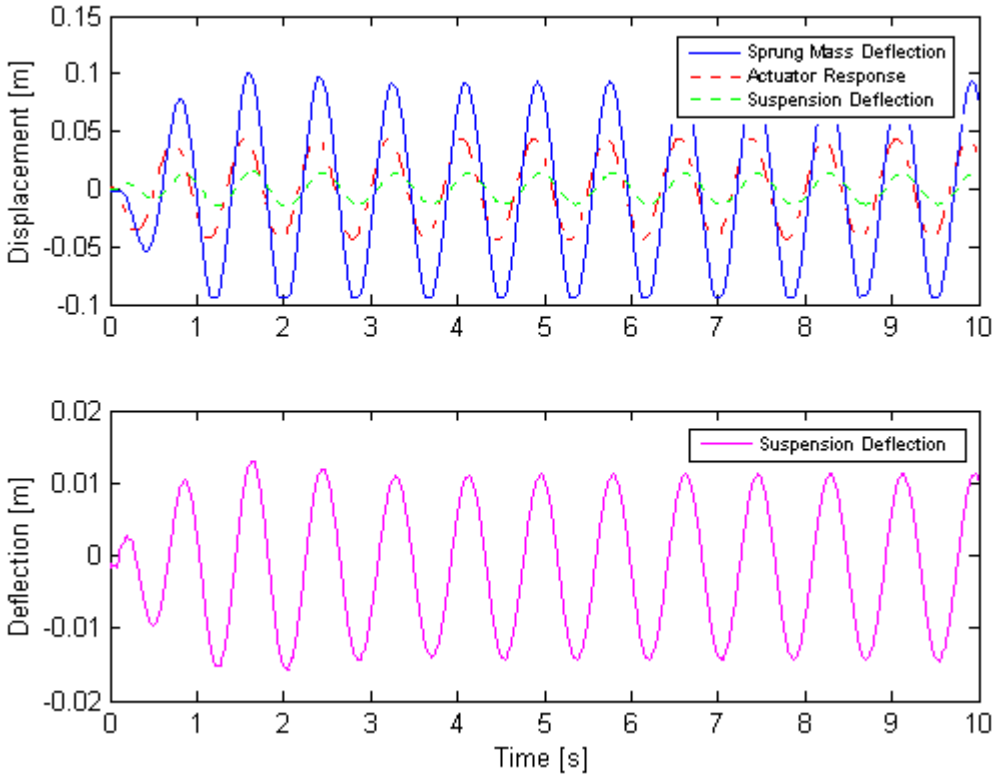

Figure 4-14: HiL raw results using harmonic road input

4.6. Comparative Results

As in the previous chapter the ECOV was used as a quantitative measure of the HiL simulation's response accuracy compared to the response of the real motorcycle test setup as seen in Figure 4-2. The values will again be determined for a certain input type, i.e. harmonic wave inputs, sawtooth wave inputs, square wave inputs, ramps and speed bumps. The variation in the input types will give different ECOV values and trends depending on the character of the wave.

4.6.1. Harmonic Inputs

Harmonic inputs are used due to their ability to induce phase lags that are easily identifiable visually. The lags are due to the inclusion of damping in the system. The ECOV values for several harmonic wave inputs are given in Table 4-1, where the real motorcycle setup response is taken as the reference response against which the HiL simulation results are compared.

Some notes on the ECOV values are necessary to put the readings in perspective. The sprung and unsprung mass values compare well, but a quick overview of the suspension deflection ECOV values indicate that the response is poor. This seems like a contradiction in the ECOV values, because one would expect good deflection correlation if the sprung and unsprung mass motions are accurately followed.

The problem is due to zero offsets in various measuring equipment; the cable-type displacement transducers used in the real motorcycle response measurements weren't zeroed to allow more positive displacement, because the negative displacement was governed by positive stops through the actuator rod and actuator rig table. This meant that a numerical zeroing had to be done after the measurements were taken, which was executed in a batch command (all the zeros were set using a specific constant). This resulted in some signals being zeroed almost perfectly while others still had some residual offset. Another source of offset is the actuator controller itself – when coupled to the motorcycle suspension setup the zero also shifted when

the external displacement command signal was selected; the zero shift differs from the shift experienced when the controller is coupled with the HiL setup.

The load cell posed another problem due to some noise experienced even when the HiL simulation wasn't running; zeroing the MGC bridge amplifier was only accurate to about 10N and led to different static equilibrium positions when the HiL simulations were running. Through the before-mentioned effects, the offset in signals measured and compared could reach relatively high values.

The signals showing the most discrepancy between the sprung and unsprung mass motion ECOV values and the suspension deflection ECOV are the 1Hz signals with 30mm peak-to-peak displacement. These signals are used in the real and HiL tests to determine if there is consistency in the tests. If the responses of these tests, intermixed into all the other tests, differ from each other it indicates that the system changes during operation. While it was found that the results when using these signals were sufficiently close to each other, the suspension deflection when using these signals are very small compared to the system's total motion – this is evident in Figure 4-14, for example. The effect of a constant signal offset is much larger when the measured signal is small. For instance, a 0.1V offset on a 1V signal equates to an ECOV of 10%, while the same offset on a 0.2V signal equates to an ECOV of 50%.

The deflection ECOV discussion above is applicable to all input types, and the results should thus be backed up with visual evidence.

Table 4-1: ECOV values using harmonic excitations

Frequency [Hz]	Amplitude [mm]	ECOV		
		Sprung Mass [%]	Unsprung Mass [%]	Suspension Deflection [%]
1	15	53	16	107
1	25	20	12	41
1	35	20	12	46
2	15	41	36	37
1	15	63	15	133
2	25	35	37	32
2	35	33	39	29
1.2	15	24	17	32
1.2	25	36	21	52
1	15	61	13	135
1.2	35	40	24	55
1	15	65	13	146
1	15	68	13	165
1	15	67	13	158
1	15	70	13	180
1	15	69	13	179

Figures 4-15 and 4-16 give some visual confirmation of the comparative signals. Figure 4-15 shows one of the responses of the 1.2Hz, 35mm amplitude harmonic signals; the HiL sprung mass amplitude is larger than the real system's response, which also contributes to the large ECOV values for the suspension deflections achieved for these signals.

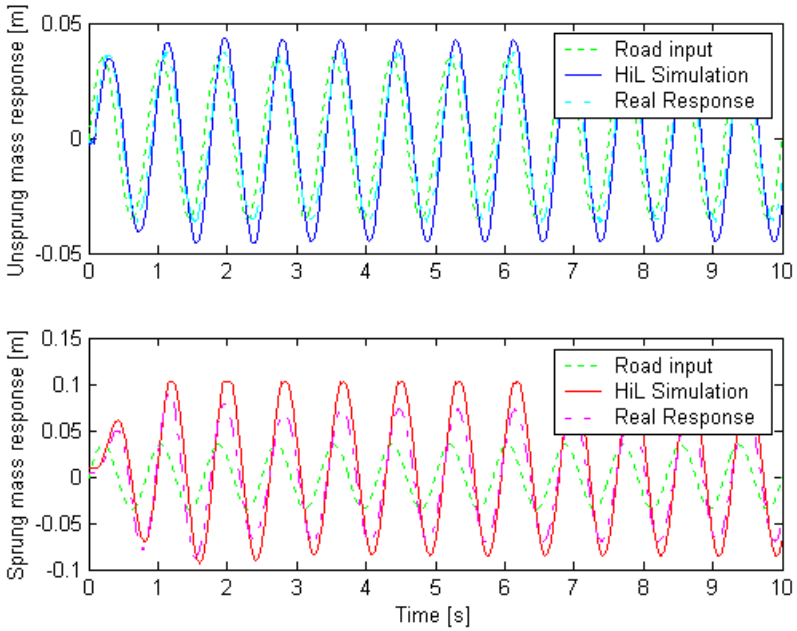

Figure 4-15: System responses for 1.2Hz, 35mm amplitude harmonic excitation

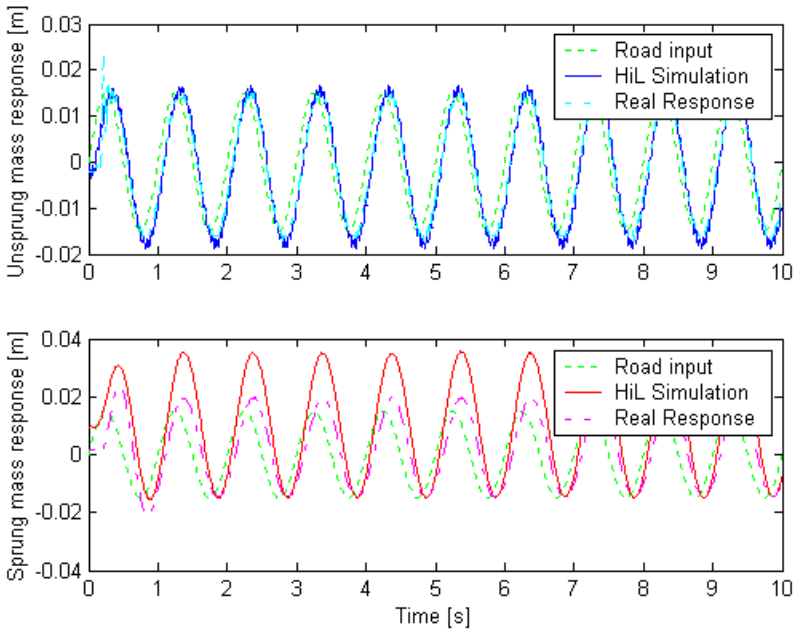

Figure 4-16: System responses for 1 Hz, 15mm amplitude harmonic excitation

4.6.2. Sawtooth Wave Inputs

As with the SDOF and 2DOF tests, sawtooth signals are again used. All the sawtooth signals have the same amplitude, namely 50mm peak-to-peak, but different amounts of discontinuities. The ECOV values calculated for the system responses are given in Table 4-2, while some graphical plots are shown in Figures 4-17 and 4-18.

It can be seen that although suspension deflection ECOV values are relatively high, the sprung and unsprung mass responses compare favourably – this is reflected in their ECOV values. From Figures 4-17 and 4-18 it can be seen that a dc offset between the signals is the main reason for the large ECOV values.

Table 4-2: ECOV values using sawtooth wave inputs

Obstacle Duration [s]	Amplitude [mm]	ECOV		
		Sprung Mass [%]	Unsprung Mass [%]	Suspension Deflection [%]
2.5	25	56	42	81
1.5	25	54	56	76
1.3	25	55	61	75
1	25	50	68	72

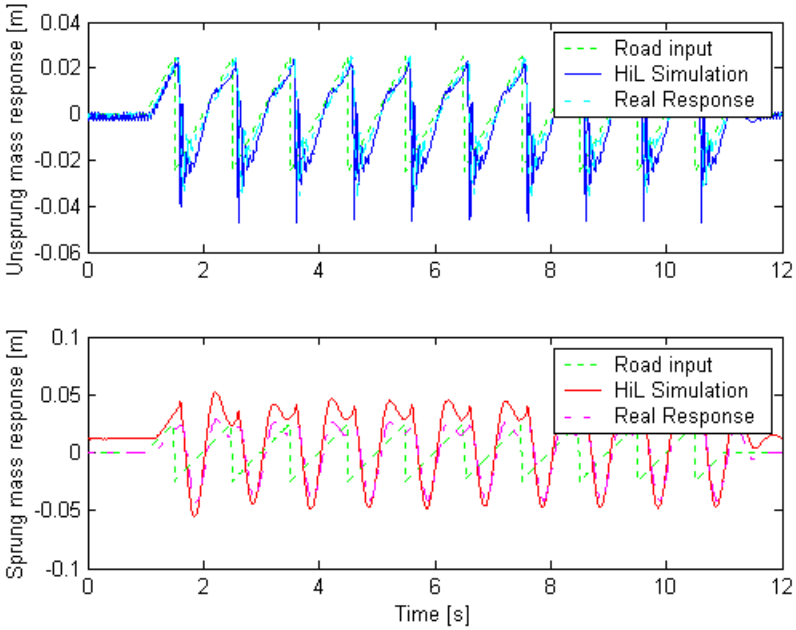

Figure 4-17: System responses for 10 teeth, allowing transient motion to persist

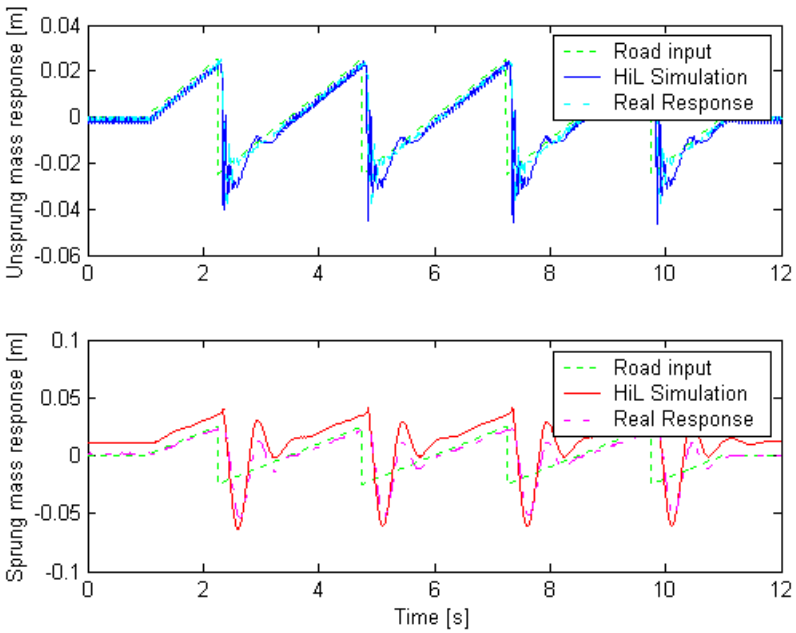

Figure 4-18: System responses using 4 teeth, allowing a return to equilibrium

4.6.3. Square Wave Inputs

The square wave inputs vary in peak-to-peak amplitude and the amount of obstacles. When there are sufficient obstacles, the sprung mass natural frequency is

approached, and the HiL system response differs much from the real system response. However, from the plot of Figure 4-19 it can be seen that the HiL sprung mass motion follows the real motion closely, with the stick-slip character of the real system again showing up.

Figure 4-20 contains the plot of the square wave, with the frequency approaching the sprung mass' natural frequency. The effect is clear on the response magnitude, and this is also shown in the ECOV values for the sprung mass – as the amount of obstacles increase, the ECOV values increase. Close to the natural frequency the excessive displacement of the real system will be damped somewhat at the maximum sprung mass displacement due to the stick-slip present at low velocities, which correspond to these displacement maximums and minimums. The additional damping present in the real system, which is lacking in the mathematical model implemented in the HiL setup, causes the real system sprung mass response to be significantly lower than its HiL counterpart. The ECOV values for the low-frequency square waves are significantly lower than those for the higher-frequency signals.

Table 4-3: ECOV values using square wave inputs

Amount of Steps	Amplitude [mm]	ECOV		
		Sprung Mass [%]	Unsprung Mass [%]	Suspension Deflection [%]
2	25	33	23	82
4	25	34	32	69
10	25	45	52	95
12	15	64	55	91
13	15	68	61	85

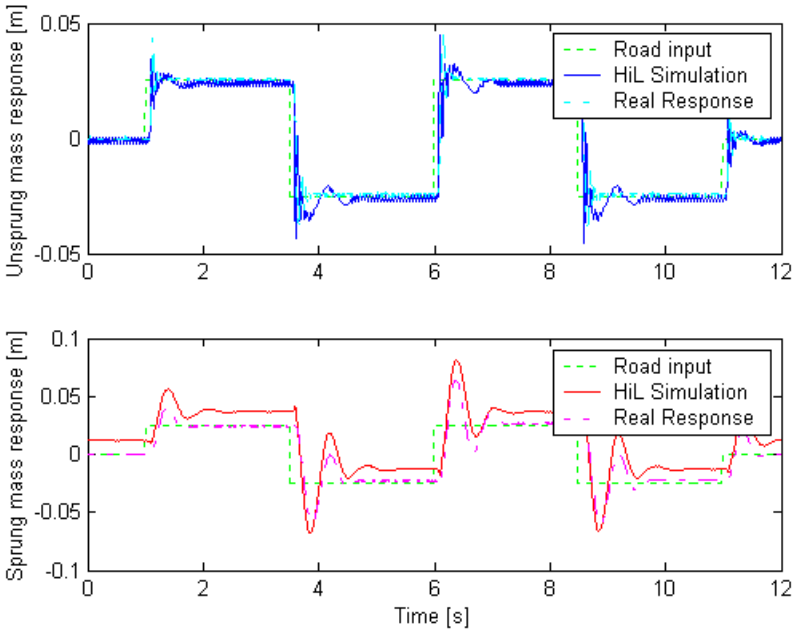

Figure 4-19: System responses for square wave road input

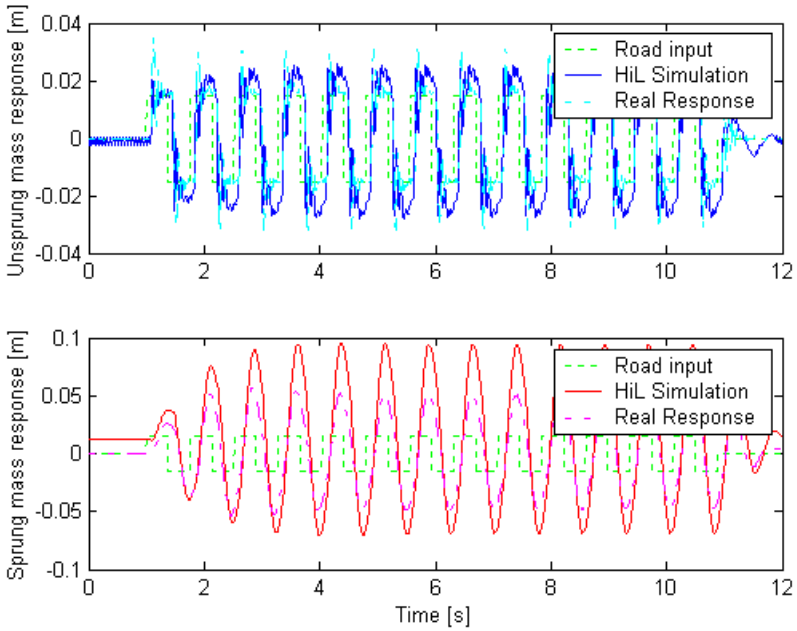

Figure 4-20: System responses for square wave, with frequency approaching natural frequency of sprung mass

4.6.4. Ramp and Speed Bump Inputs

Ramps and speed bumps are transient obstructions differing from sawtooth and square waves in that they are second-order (velocity) discontinuous instead of first-order discontinuous. Several ramps and speed bumps are used, with differing numbers of obstacles and different obstacle times. The time each obstacle lasts gives an indication of how "narrow" the obstacle is, and the shorter times thus reflect more severe obstacles.

Table 4-4: ECOV values using ramps and speed bump inputs

Obstacle Duration [s]	Amplitude [mm]	ECOV		
		Sprung Mass [%]	Unsprung Mass [%]	Suspension Deflection [%]
Speed Bumps				
2	50	30	6	146
1	70	15	7	52
0.5	70	45	25	55
0.5	70	28	18	41
Ramps				
1	70	22	5	145
0.5	70	26	8	66
0.3	70	33	13	56
0.5	70	25	10	61
0.3	70	29	18	49

Some responses for the speed bump and ramp inputs are given in Figures 4-21 through 4-24, while the comparative ECOV values are given in Table 4-4. It can be seen from the ECOV values of the sprung and unsprung mass responses that the HiL simulations followed the real setup's responses closely despite the obvious signal offsets. This can be expected due to the absence of displacement discontinuities.

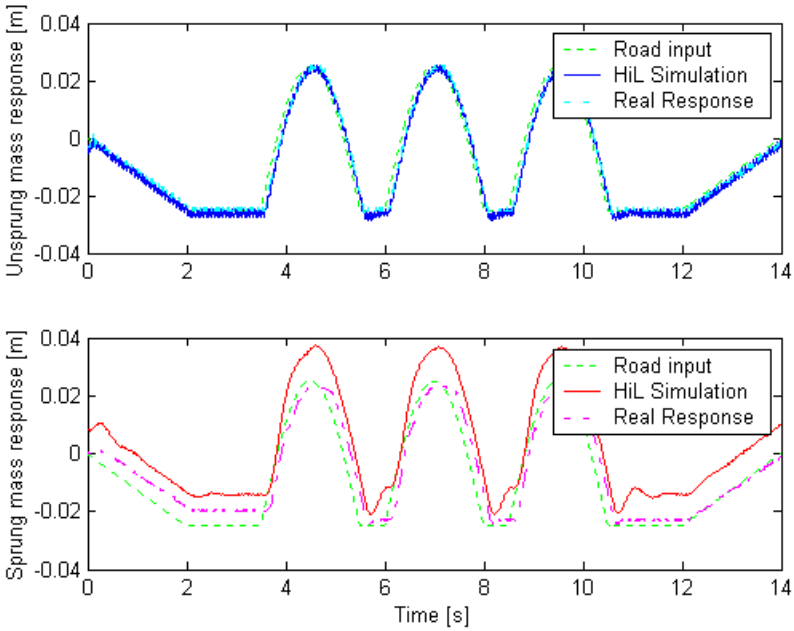

Figure 4-21: System responses for three 50mm speed bumps

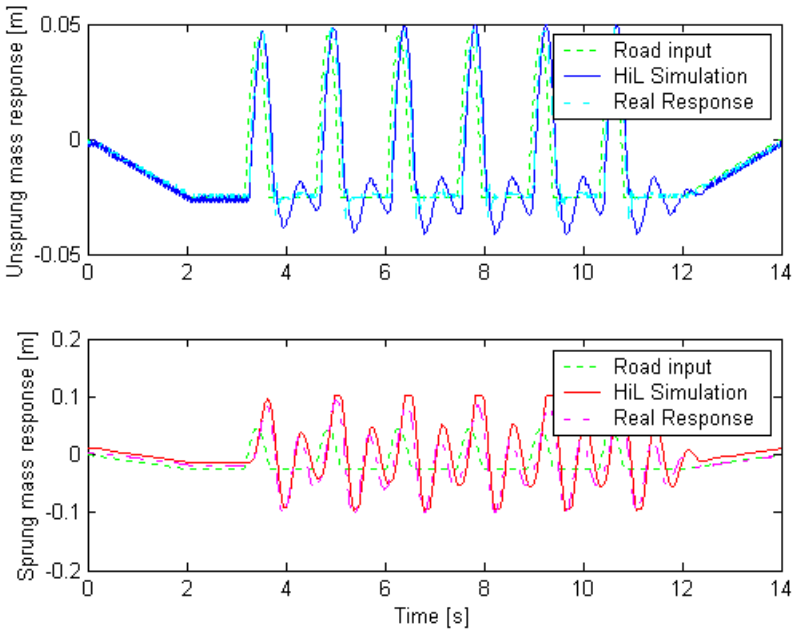

Figure 4-22: System responses for six 70mm speed bumps

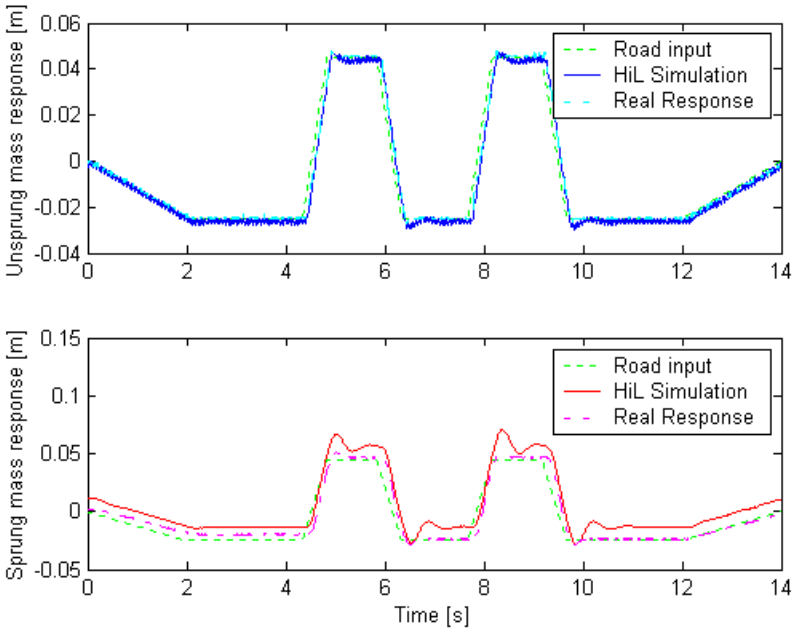

Figure 4-23: System responses for two 2 sec ramps

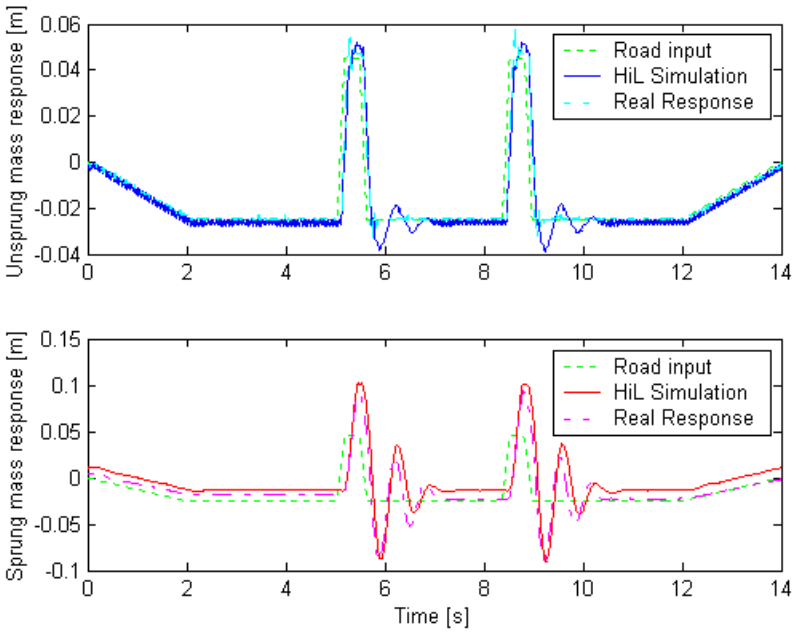

Figure 4-24: System responses for two 0.6 sec ramps

The sprung mass response shown in Figures 4-23 and 4-24 gives an indication of the effect of the input excitation's slope. In the latter, the slope is much steeper, resulting in larger overshoot, while the downward motion is amplified by an initial positive displacement. The negative overshoot is thus even more than the positive overshoot.

In general, good agreement between the physical system's motion and the HiL simulation results were obtained, despite the high ECOV values in some cases. These values were high due to the offset in the measured signals (for the real and HiL system responses), and also because the HiL system was excited at frequencies close to the system's sprung mass natural frequency, leading to erratic behaviour.

4.7. Result Summary

The results given in Figures 4-25 to 4-30 are sorted results of the tests and simulations from the various chapters. The sorting criterion (for the test number) was chosen as the suspension deflection, since this parameter has the direct influence on the suspension hardware through the actuator displacement control signal. Suspension deflection ECOV values are given from small to large; the test in which the smallest was achieved is test one, test two achieved the second best correlation, and so forth. This is done because the HiL test shouldn't be dependent on the specifics of the input signal used, and representing the data like this puts all input signals on equal foot.

In Chapters 3 and 4 ECOV values were used to compare two signals quantitatively. Although the ECOV values could theoretically be used as the sole criterion, it was found that visual evidence is necessary in these cases as well. This is because the effect of measurement discrepancies, like the zeroing of signals, lag and minor scaling differences can have massive effects on the ECOV values of compared signals. When considering HiL testing, for instance, suspension deflection is an important parameter. A minor lag between two signals, having almost no effect on the motion of the overall system, can cause large ECOV values. The same goes for DC offsets in the measuring devices, controllers and sensors. The effect on the suspension deflection is especially obvious when considering a suspension unit that deflects only a fraction of the difference between the sprung and unsprung mass displacements – the deflection signal is smaller, and the offset is proportionally larger.

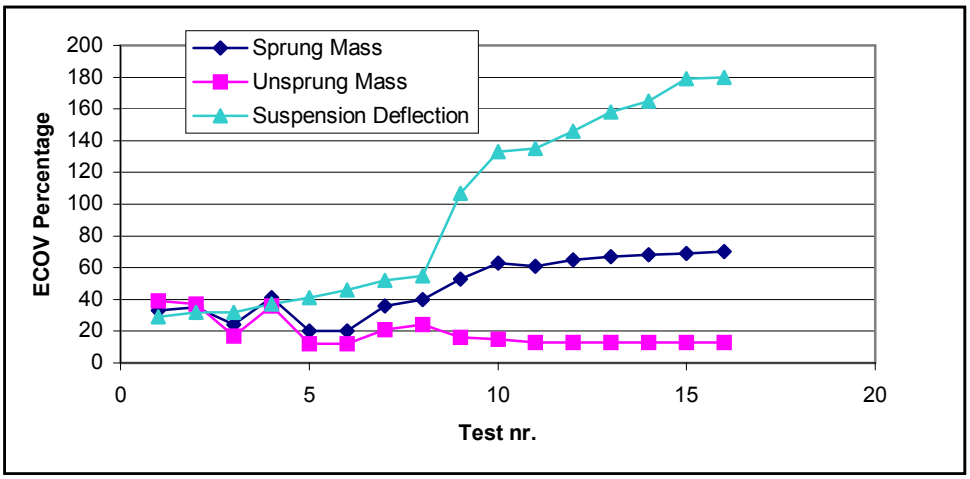

Figure 4-25: ECOV values for harmonic excitation tests, 2DOF motorcycle setup

Figure 4-25 proves this point – here, the ECOV results are sorted by suspension deflection comparison. The worst results, in tests 10 to 16, were obtained using the lowest frequency and amplitude – 15mm, 1Hz excitation signals! The sprung mass comparison performs average, while the unsprung mass comparison is very favourable. The suspension deflection ECOV values, on the other hand, is very large; this is due to the small deflection measured relative to the sprung mass motion, and thus discrepancies like offsets and lags have a much larger effect. The same is seen in Figure 4-26, where the ECOV values for square wave response is given. Here test four outperforms test three in both the sprung and unsprung mass deflection comparisons, but still test four has a higher suspension deflection ECOV value.

In general, when using the motorcycle test setup, it seems that larger input excitations result in better deflection correlations, while smaller input excitations are favourable for better unsprung mass correlations. The sprung mass motion is dependent on the physical damper or an inaccurate damper model (no advanced damper models were used in the software simulations – see the results in Figures 4-26 and 4-27) and seems to be unaffected by input magnitude.

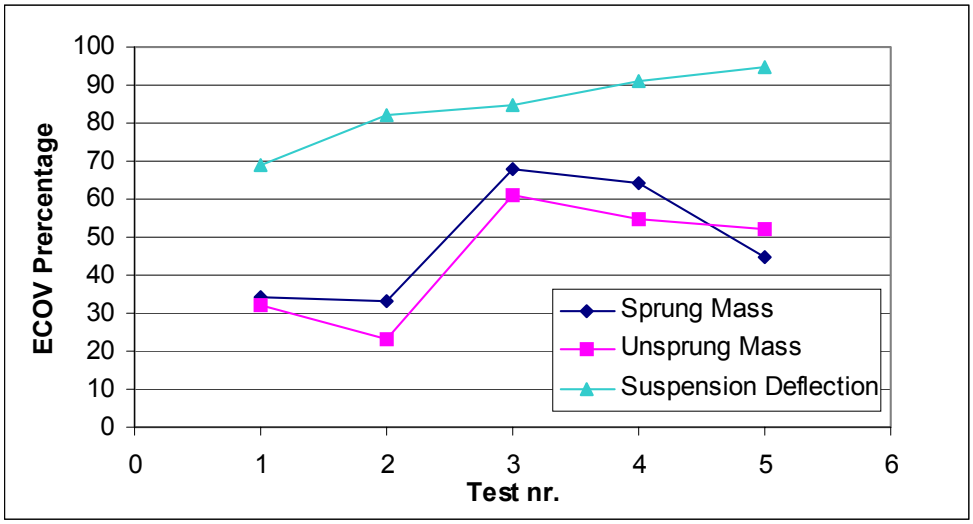

Figure 4-26: ECOV values for square wave excitation tests, motorcycle setup

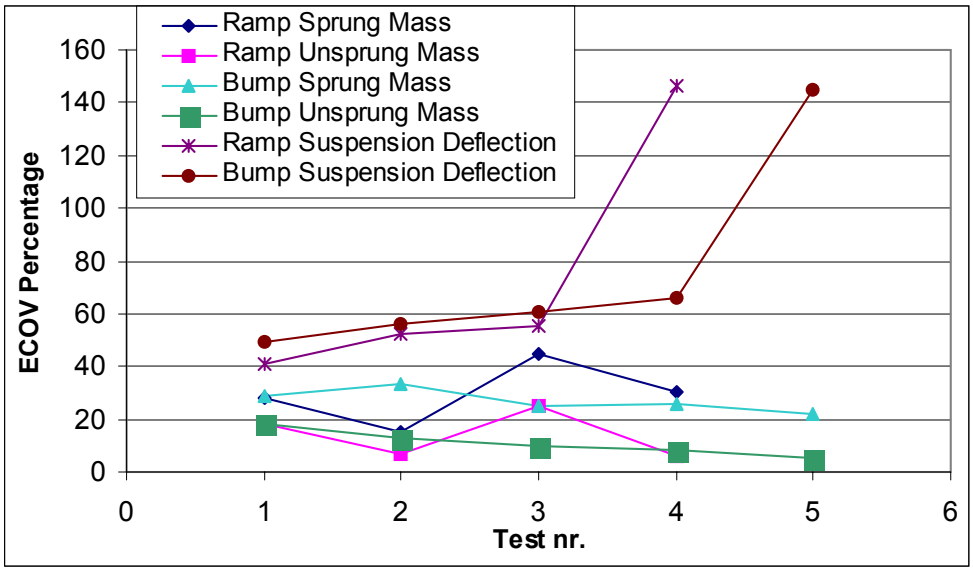

Figure 4-27: ECOV values for ramp and speed bump inputs, motorcycle setup

The ECOV correlations measured when using the linear simple 2DOF setup was much lower than those measured for the motorcycle setup. This was because a linear model was used for both the HiL and software simulations. The difference in the simulations was the mathematical spring and damper models used in the software simulation, while HiL used the real hardware. In the motorcycle test setup the entire physical system (except the suspension unit) was modelled. This leads to some inaccuracies:

- Even thought the angles used were in fact small, the small angle assumption whereby $sin\theta = \theta$ and $cos\theta = 1$ become zero and one in calculations does have an influence
- The masses and centres of gravity of the individual body masses were measured to a finite resolution, and implemented accordingly. The precise masses weren't used, as the measuring accuracy wasn't perfect
- There exists some stick-slip in the real system, which wasn't modelled in the HiL software model. The effect of the stick-slip was quantified after the tests were run and these results are given in Appendix C. The effect of the stick-slip is quite large. The sprung mass used was decreased so as to decrease its effect.

The ECOV values for the linear 2DOF model tests are given in Figures 4-28 to 4-30.

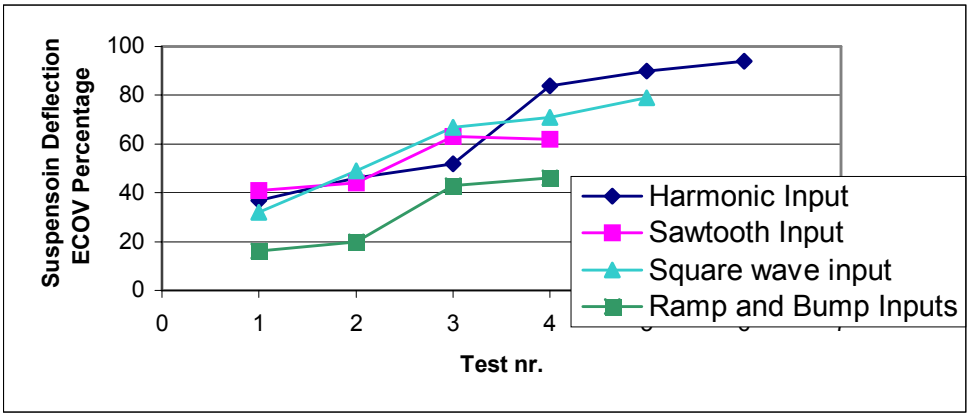

Figure 4-28: ECOV values for suspension deflection, linear 2DOF model

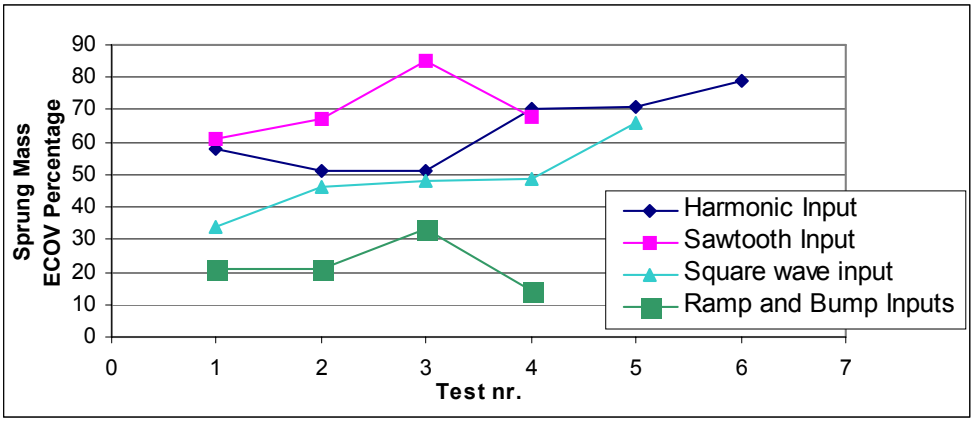

Figure 4-29: ECOV values for sprung mass displacement, linear 2DOF model

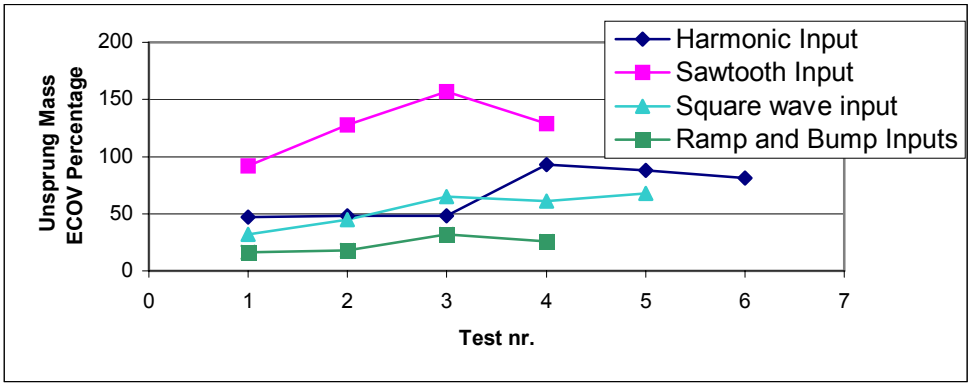

Figure 4-30: ECOV values for unsprung mass motion, linear 2DOF model

5. Summary and Conclusions

A summary of the research discussed in this thesis is given in this chapter, along with some conclusions on the results obtained in the previous chapters.

5.1. Summary

It has been stated that hardware-in-the-loop simulation as concept is not new. ECUs like ABS, traction control and autopilots have been simulated and tested this way for more than a decade, even though commercially available HiL systems for testing ECUs are only beginning to show promise now.

In the mechanical sense, as used in this research, HiL is still new and not frequently used. This could be due to the cost involved in setting up computer hardware and software of adequate performance to perform the simulations with, or to a notion that HiL simulations aren't accurate enough to run reliable simulations on. While it is true that suspension testing using hydraulic actuation requires some very expensive equipment, and not all actuators have the dynamic response characteristics suitable for HiL testing, the cost of the additional equipment to implement HiL simulations with is very small compared to the actuator/controller/hydraulic power pack cost. It would thus make sense for anybody acquiring hardware for the use in suspension testing to include the kit needed for HiL simulation, and for those with actuators already suitable, to upgrade their facilities to include this capability.

Pure software simulation does have a use in the development of suspension systems, but the models used for advanced development and prototyping are more often than not complex or based on proprietary information. While software simulations can give an indication of the relative spring and damping forces required, models of the dampers (especially semi-active and active units) become overly large and mathematically complex, leading to simulations that can take days to complete. As these models grow in complexity, the cost of the simulations goes up. This is not true for HiL, as the real suspension unit is tested directly. Of course, this would require production of a prototype, and a model of the system under investigation can also be rather complex.

When considering damper models, many have tried to create models using the valve architecture, internal diameters and valve sizes, valve characteristics, pressure fluxes and similar parameters. These models have been shown to be reasonably accurate for specific cases, but implementation in general conditions or unfamiliar layouts have proven disastrous. For instance, some models are derived specifically for mono-tube dampers. Implementation of these models on dual-tube dampers, or dampers with reservoirs, is not possible. Some damper models work very well within a limited frequency band, but poorly outside said band.

It is for this reason that the investigation into the use of HiL simulation is prompted, as it offers various advantages compared to conventional testing:

- HiL is a versatile tool that is not dependent on suspension unit type, size, geometry or peripherals. If the unit can fit into the actuator rig, it can be tested.
- It depends on mathematical models only for the mass bodies. If need be, a tyre model can be included as a mathematical model, or as a second HiL setup, thus decreasing system complexity.
- Changing the model's parameters is done in the software environment, enabling tests of different models using the same test setup. SDOF and multiple-degrees-of-freedom systems, each with various masses, can be tested using the same hardware setup.
- The time of implementation is greatly decreased compared with conventional testing, as no or very little materials are needed for test rig conversion to fit different suspension units in. Usually only small brackets need to be made, a process which is quite quick and inexpensive.

- The time saved in HiL setups also bear influence on the time taken to develop advanced suspension systems. RCP can be used while a physical prototype is unavailable, implemented using a simple model, and the control system can be tested using HiL when the prototype becomes available, allowing testing using the real valves, switches, etc.
- The initial cost of HiL capability might be higher than conventional testing, but the small amount of changes needed during different HiL simulations, as opposed to the purchase of materials to implement a sprung mass with, for instance, makes HiL a more cost effective solution in the long run.
- The cost saved using HiL is also influenced by the reduction in setup and simulation times.
- HiL simulations are reliable and due to the nature of the hardware setup, the tests can be repeated numerous times. With only small changes to the suspension unit, for instance, it can be optimised relatively quickly from a hardware point of view
- The system offers excellent repeatability, and is not affected by bearing failure, stick-slip, temperature effects (apart from changes in the damper oil viscosity) or other ambient effects.
- The inclusion of a tyre model in a system (where the tyre doesn't have a relatively small finite radius) allows the use of displacement-discontinuous input signals, which cannot be used reliably during conventional mass model testing due to actuator constraints.
- Expanding the tests to larger vehicle models is relatively easy. The HiL tests can be expanded to include the simulation of pitch-vehicle and even full car models as more suspension prototypes become available. The university has adequate resources to implement a four-actuator setup to supply the motion with, and the HiL can be implemented using only four inputs (force measurement) and four outputs (suspension deflection displacement signals). A DSP card with more I/O channels will be necessary if more model parameters are sought than the dSpace card can handle.

Some of the advantages above show that hardware-in-the-loop is indeed superior to conventional suspension testing in several ways, and is set to become the method of choice.

5.2. Chapter Summary

In Chapter 2 a single-degree-of-freedom system was analysed using hardware-in-the-loop simulation, where the suspension component in question was either a single spring or a spring-damper combination. These results were compared to a pure software simulation of the same system, in which a mathematical model of the spring and/or damper replaced the real suspension unit. A qualitative comparison of the HiL and software system responses was made visually, as a proof of concept.

In Chapter 3 the HiL simulation was expanded to include a second degree of freedom, realised by a tyre model incorporated in both the HiL and software simulations. The addition of the tyre model increased the complexity of the system, and brought the simulation model on par with that used normally in suspension testing – the quarter car two-degree-of-freedom is often used in suspension component and control system design. A quantitative comparison of the HiL simulation results and the results of a software model of the same system, implementing lookup tables for the spring and damper characteristics, was made using the error coefficient of variance, or ECOV. This value gave an indication of how closely the HiL simulation followed the software simulation. The implementation of a tyre model with wheel hop capability enabled the use of larger input excitations than those used in Chapter 2, even though the actuator displacement limits weren't altered.

Chapter 4 took the 2DOF system even further, with the HiL simulations now being compared to a real 2DOF system. This enabled the comparison of a HiL simulation running a model of the real system to be compared to measured displacements. Again

ECOV values, as fractions or percentages, were used as comparator. Here the HiL simulation was the inaccurate method, due to the modelling of real setup and the assumptions (however minor) made pertaining to said setup.

All the test results are subject to some visual and/or ECOV comparison, indicating the relevance and performance of the HiL simulation method. These results were summarised in Chapter 4.

5.3. System Requirements

Implementing HiL testing requires only a little more hardware than conventional testing. In conventional testing an actuator/controller combination supplies the excitation, while a computer or some other data-capturing device creates the actuator inputs and records the force and displacement. The HiL test method requires only an additional method to run the plant software model with – this can be accomplished using another computer fitted with an A/D D/A card and running custom software to allow suitable sampling rates to be achieved, or it can be implemented using a DSP.

Using a computer fitted with a generic A/D D/A card has been used before, however the sampling rates that can be achieved are very much dependent on the complexity of the vehicle model in the software environment and the conversion speed of the I/O device. Implementing HiL with this type of setup has the drawback that the software model must be realised using C, C++ or some low-level computing language so that it executes with sufficient speed.

Using an external DSP, or a DSP card like the dSpace DS1102, has the advantage that once the DSP object is loaded and the program is started, other applications (like the measurement application) can be run. The newer dSpace cards even have data-capturing capabilities on-board. The dSpace board, and similar DSP products, have the ability to run in real-time. This seems to be addressed best in the Simulink Real-Time Workshop that, due to the automatic code generation facility, gives the fast generation of controller code and using dSpace functionality frees the designer from the burden of writing the low-level software (drivers).

A suitable actuator and controller combination is also important when considering HiL testing. Insufficient actuator dynamics could give inaccurate results and even lead to system instability. The software model used should also be considered carefully – while a simple linear 2DOF system is very easy to implement, it may be more difficult to implement complex suspension geometries. It is still cheaper than building the geometry for testing purposes, though.

5.4. Conclusions

The results given in Section 4.7 give a clear indication of the HiL simulation setup's character. Displacement continuous input signals give the best correlation globally, as one would expect. However, even though harmonic inputs are continuous, they seem to under perform even when compared to discontinuous inputs. This is not the whole truth. The effect of the harmonic input ECOV values is amplified by the fact that the responses, in particular the suspension deflection, are small in comparison to noise, ripple and offset.

Running the simulation using either continuous or discontinuous input excitations, with large or small input magnitudes, results in responses similar to those obtained using either the software simulation of the linear 2DOF model, or the real motorcycle setup. Even though the ECOV values are large, it is a very sensitive measure (perhaps too sensitive for this application) – the visual plots of the predicted (or measured) and HiL responses show good correlation throughout the tests.

HiL is a testing method with multiple uses: it can be designed to test the suspension component and/or its control system, with the body mass motion (like acceleration of the driver, or tyre-road loads) being a secondary concern, or it can determine body mass motions for a particular suspension component, too difficult or time-consuming to model

for software simulation. When using a HiL setup, it was found that actuator dynamics play a large role on the system's performance. Filters in the system (controller and noise filters) should be avoided whenever possible, and where they are necessary, minimum phase lag and phase distortion should be paramount. Displacement transducers that work with potentiometers are preferable to LVDTs.

Discontinuous inputs, as well as harmonic (or other) inputs with frequencies near the system in question's natural frequencies, cause some deviation in the HiL results. However, operation near the natural frequency need not be avoided, since the system behaves well enough to damp out transient behaviour and excessive displacements. Since random signals of frequency content limited to a band within reach of the system dynamics, like 30 Hz, cannot be seen as displacement discontinuities, HiL simulations seem to be suited well to their use.

The fine-tuning of the actuator controller's PID does not have a major effect on the HiL test's behaviour, although it should be mentioned that it was found, for HiL testing, the settings corresponding to conventional suspension testing was sufficient to provide good results. While these values may differ from controller to controller and from test to test, the technicians and engineers performing the tests know from experience what the desired setting for the PID is. This wasn't quantified in the present research as the actuator dynamics model implemented by Besinger [12] showed little deviation from the ideal actuator dynamics in term of the HiL simulation results.

Hardware-in-the-loop simulation and testing was shown to be a valid testing method in various applications and with different types of input. It can thus be implemented in an environment where an unknown suspension component needs to be tested with confidence, barring any major actuator/controller inadequacies. The actuator used in this research is a relative "lightweight" and thus most actuators would suffice.

5.5. Future Work

The research into hardware-in-the-loop testing was prompted by the university's need for a reliable, versatile and easy to implement suspension component test method. As such, future work will predominantly pertain to the testing of suspension systems, in particular the hydro-pneumatic four-state semi-active heavy vehicle suspension unit as developed by Giliomee and Els [35]. An improved version of this unit is pictured in Figure 5-1.

The future work (not limited to HiL development) includes:

- Verifying the settings and actuator dynamics so as to use HiL testing on the hydraulic actuator/controller combination that currently houses the hydro-pneumatic suspension unit;
- Employing HiL in simulations to verify the behaviour of the system using larger road inputs than those allowed by current test setup;
- Defining a suitable random road input to serve as excitation for said suspension unit;
- Defining suitable performance criteria for the suspension unit and its control system;
- Implementing the HiL simulation using the dSpace and CDAS measuring computers, utilising the dSpace computer (or similar system) for both HiL and the control of the semi-active suspension unit.

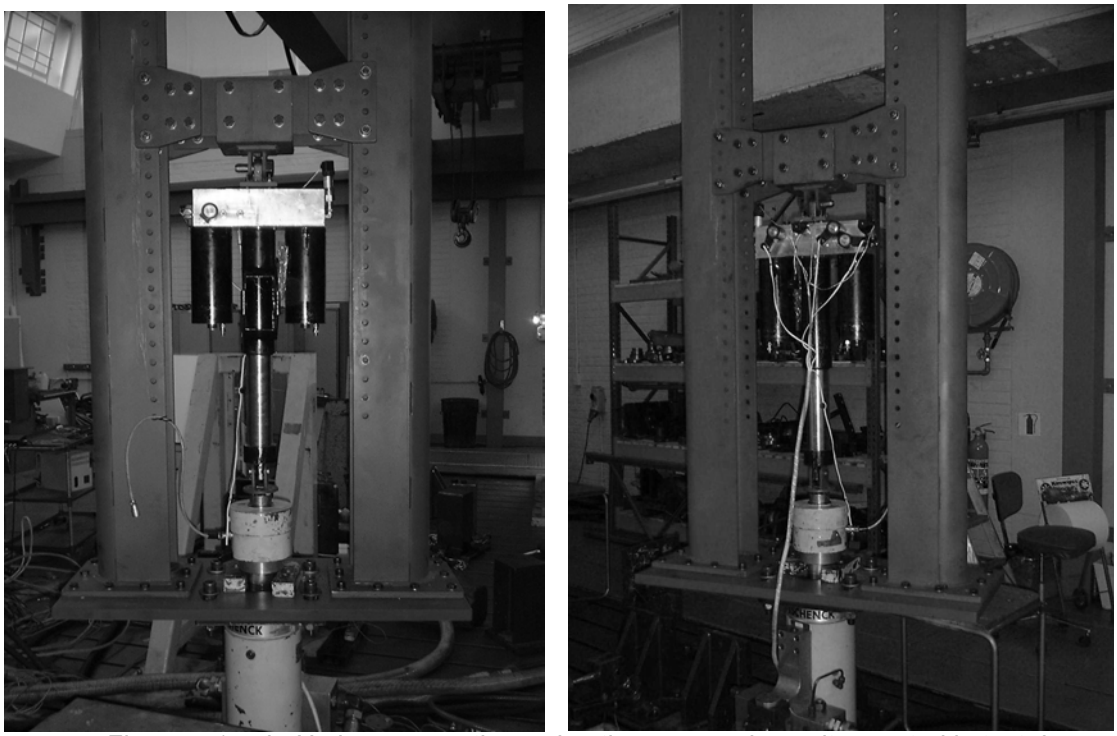

Figure 5-1 a, b: Hydro-pneumatic semi-active suspension unit mounted in test rig

6. Reference List

1 CHOI, S.B., Lee, H.K. & Chang, E.G. 2001. Field Test Result of a Semi-Active ER Suspension System Associated with Skyhook Controller. Mechatronics, Volume 11: 345 – 353.

2 GOMEZ, M. 2001. Hardware-in-the-Loop Simulation. *Internet*: http://www.electronicengineering.com/features/software/OEG20011129S0054 Access: October 2002.

3 HANSELMANN, H. 1996. Hardware-in-the-Loop Simulation and Testing and its Integration into a CACSD Toolset. *The IEEE International Symposium on Computer-Aided Control System Design*, September 15-18, 1996. Dearborn, Michigan, United States of America.

4 JEDRKOWIAK, A., Hesselbarth, J., Bartels, H. & Miller, H. 1998. Implementation of Real Time Simulation with Hardware in the Loop on a Dec Alpha Workstation. *Procedures of the 4th International Conference on Motion and Vibration Control MOVIC '98,* Volume 1.

5 JACKSON, A., Brown, M., Crolla, D., Woodhouse, A. & Parsons, M. [S.a.]. Co-ordinated Mobility Control of a 6x6 Off-Road Vehicle with Individual Wheel Control. SAITS 01054.

6 FERREIRA, J.A., de Oliveira, J.E. & Costa, V.A. [S.a.] Modelling of Hydraulic Systems for Hardware in the Loop Simulation: A Methodology Proposal. University of Aveiro, Portugal.

7 MACLAY, D. 1997. Simulation gets into the Loop, IEE Review, May.

8 DUYM, S., Stiens, R. & Reybrouck, K. 1997. Evaluation of Shock Absorber Models. *Vehicle System Dynamics*, Volume 27: 109 – 127.

9 LANG, H.H. 1977. *A study of the characteristics of automotive Hydraulic dampers at high stroking frequencies*. PhD Thesis, University of Michigan, United States of America.

10 LANG, R., Sonnenburg, R. 1995. A Detailled [Sic] Shock Absorber Model for Full Vehicle Simulation. *10th European ADAMS User Conference*, November 14-15, Marburg, Germany. (From Fichtel & Sachs AG.)

11 SCHIEHLEN, W. & Hu, B. 2003. Spectral Simulation and Shock Absorber Identification. *International Journal of Non-Linear Mechanics*, Volume 38: 161-171.

12 BESINGER, F.H., Cebon, D. & Cole, D.J. 1995. Damper Models for Heavy Vehicle Ride Dynamics. *Vehicle System Dynamics*, Volume 24 (1): 35 – 64.

13 HALL, B.B. & Gill, K.F. 1986. The Performance of a Dual Tube Automotive Damper and the Implications for Vehicle Ride Prediction, *Procedures of the IMechE*, Part D, 200 (D2): 115 – 123.

14 SEGEL, L. & Lang, H. 1981. The Mechanics of Automobile Hydraulic Dampers at High Stroking Frequencies. *Vehicle System Dynamics*, Volume 10: 79 – 83.

15 KARADAYI, R. & Masada, G.Y. 1986. A Nonlinear Shock Absorber Model. *Procedures of the Symposium on Simulation and Control on Ground Vehicles and Transportation Systems*, pp. 149-165.
Also Published: 1990. ASME AMP Vol. 80, DSC Volume 2: 299-308.

16 RAO, M.D. & Gruenberg, S. [S.a.]. Measurement of Equivalent Stiffness and Damping of Shock Absorbers. Michigan Technological University, Houghton.

17 MORMAN K. A Model for the Analysis and Simulation of Hydraulic Shock Absorber Performance, Part I- Theoretical Development (SR-83-043), Part II- Parameter Identification and Model Validation Studies (SR-86-61). Ford Motor Company Research Staff Reports.

18 REYBROUCK, K. 1994. A Non Linear Parametric Model of an Automotive Shock Absorber. SAE Paper No. 940869, *Vehicle Suspension and System Advancements*, SP-1031: 79-86.

19 DUYM, S.W., Stiens, R., Baron, G.V. & Reybrouck, K.G. 1997. Physical Modelling of the Hysteretic Behaviour of Automotive Shock Absorbers, Society of Automotive Engineers (SAE), Paper 970101.

20 MORMAN, K.N. 1984. A Modelling and Identification Procedure for the Analysis and Simulation of Hydraulic Shock Absorber Performance. ASME Winter Annual Meeting, New Orleans, Louisiana, Dec 9-14, 1984.

21 BESINGER, F.H., Cebon, D. & Cole, D.J. 1995. Force Control of a Semi-Active Damper. *Vehicle System Dynamics*, Volume 24: 695-723.

22 KITCHING, K.J., Cole, D.J. & Cebon, D. 1998. Performance of a Semi-Active Damper for Heavy Vehicles. ASME Journal of Dynamic System Measurement and Control, June, 1998.

23 BESINGER, F.H., Cebon, D. & Cole, D.J. 1991. An Experimental Investigation into the use of Semi-Active Dampers on Heavy Lorries, *12th IAVSD Symposium on the Dynamics of Vehicles on Roads and on Railway Tracks*. Lyon: Swets and Zeitlinger.

24 RIEGER, K.J. & Schiehlen, W. 1994. Active versus Passive Control of Vehicle Suspensions – Hardware-in-the-Loop Experiments. *The Active Control of Vibration, Procedures of the IUTAM Symposium*. London: Mechanical Engineering Publications: 93 – 100.

25 BESINGER, F.H. 1992. *The Performance of Passive and Semi-Active Suspensions for Lorries*. PhD Thesis, Cambridge University, United Kingdom.

26 DEAKIN, A., Crolla, D., Roberts, S., Holman, T. & Woodhouse, A. [S.a.]. Development of a Practical Semi-Active Damper for a Combat Support Vehicle through modelling and Hardware-in-the-Loop Simulation. SAITS 01062.

27 KITCHING, K.J., Cebon, D. & Cole, D.J. 1999. An experimental Investigation of Preview Control. *Vehicle System Dynamics,* Volume 32: 459 – 478.

28 HWANG, S., Heo, S., Kim, H. & Lee, K. 1997. Vehicle Dynamic Analysis and Evaluation of Continuously Controlled Semi-Active Suspensions Using Hardware-in-the-Loop Simulation. *Vehicle System Dynamics*, Volume 27: 423-434.

29 KARNOPP D. 1995. Active and Semi-active Vibration Isolation. *Transactions of the ASME*, Volume 117, June.

30 NELL, S. 1993. *'n Algemene Strategie vir die Beheer van Semi-aktiewe Dempers vir Voertuigsuspensiestelsel*, PhD Thesis, University of Pretoria, Pretoria.

31 KIM H.J., Yang, H.S. & Park, Y.P. 2002. Improving the Vehicle Performance with Active Suspension using Road-sensing Algorithm. *Computers and Structures*, Volume 80: 1569 – 1577.

32 VENUGOPAL, R., Beine, M. & Ruekgauer, A. 2002. Real-Time Simulation of Adaptive Suspension Control using dSpace Control Development Tools. *International Journal of Vehicle Design*, Volume 29: 128 – 138.

33 ROBERTS, S.A., Deakin, A.J. & Crolla, D.A. [S.a.]. Rapid Control Prototyping for a Semi-Active Suspension System to be fitted to Heavy Off-Road Vehicles. SAITS 01050.

34 SHAMPINE, L.F. & Reichelt, M.W. 1997. The MatLab ODE Suite. *SIAM Journal on Scientific Computing*, Volume 18 (1): 1-22.

35 Giliomee, C.L. & Els, P.S. 1998. Semi-Active Hydropneumatic Spring and Damper System. Journal of Terramechanics, Volume 35:109 – 117.

36 RAO, S.S. 1995. *Mechanical Vibrations*. 3rd edition. New York: Addison-Wesley.

Appendix A: Input Motions Used in HiL Tests

In all the HiL simulations and software/hardware tests, a single Matlab script file supplied input motions. This script file generated all the road inputs used, which lead to repeatability.
In all, four types of input motions were used – harmonic (sine) waves, square waves, ramp waves and continuous transient obstacles, namely ramps and speed bumps.

The harmonic inputs are necessary to determine the phase behaviour of the system, and to see what effects operation near the system's natural frequencies entailed. The waves used were sine waves, with the amplitude and frequency chosen beforehand. Since the initial values for the sprung and unsprung masses cannot be specified (they are in equilibrium at the start of the test, which entails zero velocity), the initial road displacement causes some transient behaviour that damps out quickly. This is due to the sine wave having a certain non-zero slope at the beginning of the input signal.

All the hardware-in-the-loop tests were done while the DSP was active – a "sine wave input" thus means that the system sees level road (zero input) before the application of the input motion, and level road thereafter.

Square waves were used since these highlight some of a system's characteristics – the natural frequencies can be seen, as well as the amount of damping in a system. By running consecutive steps the character, and any drift in the system, would become evident. Drift may occur due to the sudden and violent actuator motion required by the displacement discontinuous input.

Sawtooth waves have discontinuities similar to square waves, but only steps in one direction. A constant velocity part characterises the rest of the signal, giving the system time to achieve equilibrium during this constant velocity part. The motions of the sprung and unsprung masses are greatly influenced by this input. Sawtooth input signals are characterised by the amplitude, amount of "teeth" and the duration of each – a time in seconds specify the duration of a constant velocity climb from zero to the specified amplitude, followed by the step down (or up) to the negative of the amplitude, and then another climb to zero. The signal can be constructed so that the climbs follow each other directly, giving a climb-drop-climb nature.

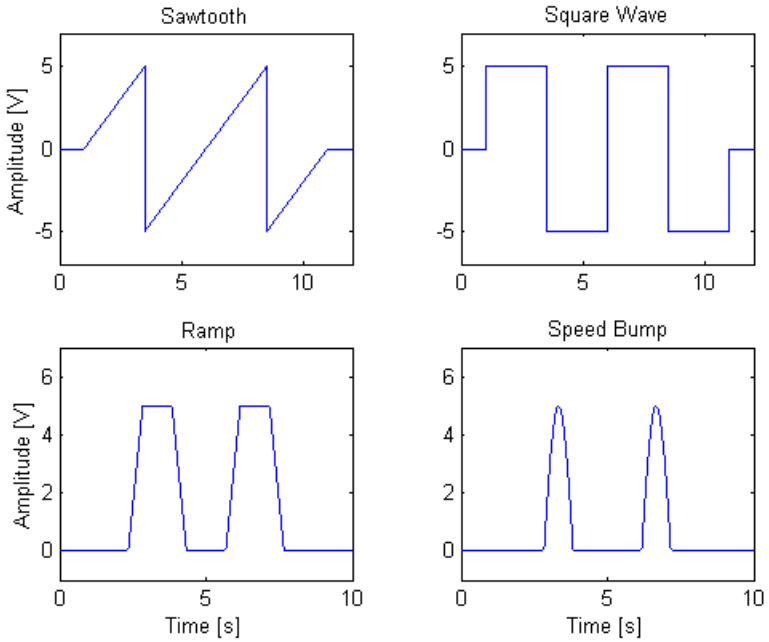

Figure A-1: Examples of the input signals used

Transient phenomena like the ramps and speed bumps used are necessary since they are displacement continuous, thereby eliminating the need for sudden displacement command signal changes for the controller. Static equilibrium can be achieved between obstacles, but the amount of obstacles seldom allows this. The speed bumps are constructed from half sine waves, the duration and amplitude of which are given. The duration given should be half of the period of the corresponding sine wave. A ramp is constructed from a constant slope incline to the specified magnitude, followed by a plateau and a constant slope decline. The obstacle duration time specified for the ramp is the time idle at the plateau, and half the time of the incline and decline ramps – in all, a ramp input (upward slope, plateau and downward slope) lasts for twice the specified time.

The time factor in all these inputs is important, as specifying shorter durations equate to faster vehicle motion. A ramp as described here may be modelled after a 3m long real ramp, over which a car drives at 6m/s. It should take the car 0.5 seconds to traverse each wheel station, and thus a similar input in the HiL setup, using the road inputs described above, should be specified using a duration time of 0.25 seconds (remember the complete obstacle duration is twice the specified time). Similarly, the speed bump's initial slope can be determined with the signal time – if a 10% initial slope is sought for a vehicle travelling 2m/s, the initial slope indicates a 0.2m climb within one second. This is done by specifying an obstacle duration (half wave period), which equates $\omega X_{amplitude}$ to the desired slope – in this case an amplitude of 20mm and a duration of 0.314 seconds.

Examples of the input signals used are shown in Figure A-1. For the most part, the magnitudes of the input signals are relatively small as compared to real road inputs typically encountered. This is due to the limitation set by the test bench, but every effort was made to use as large signals as possible – ramps and speed bumps of 70mm magnitude, sawtooth and square wave inputs of 25mm, and harmonic inputs of 35mm were used. This compares well to signals used in the literature on HiL ([12] and [22], for example).

Appendix B: Effects of Phase Lag on Damper Characterisation and HiL Simulation

Phase lag is usually the result of damping in a system, and is present in all mechanical systems to a greater or lesser degree, or it can be due to electronic signal conditioning which takes a finite amount of time from reading the signal to sending the conditioned or processed data from its output. This means that the output is a delayed version of the input. The lags occur due to filtering, system dynamics, measuring conversions, etc.

When characterising a damper (or any dynamically actuated object) filters are more often than not found in the measuring equipment. The actuator controller may also have filters, and the PID controller also introduce lags. These lags may cause erroneous results. Consider Figure B-1, where the displacement, velocity and force curves of a perfectly linear damper is shown. The damper force signal is delayed by 10 ms due to the fact that different filters are applied to the displacement (velocity) transducer and the force transducer.

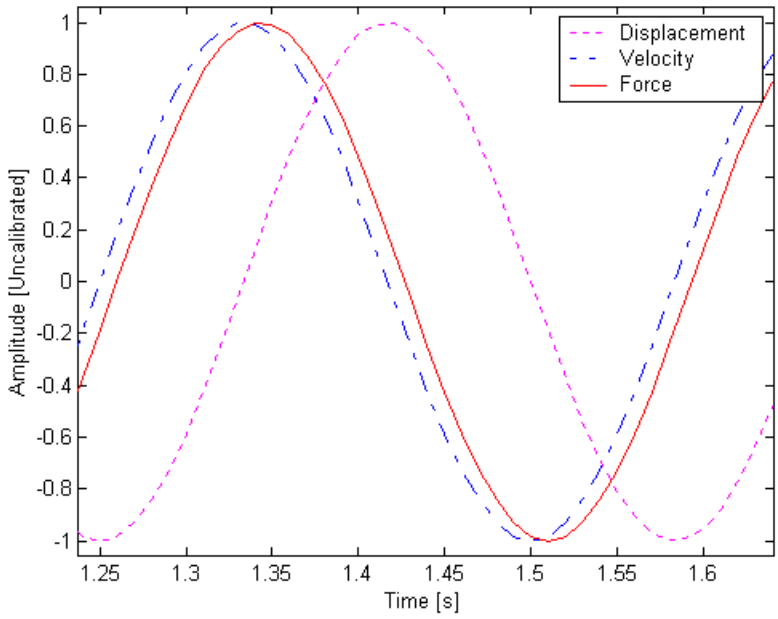

Figure B-1: Displacement, velocity and force of fictitious system

In a perfect, linear damper one would expect the maximum force to be achieved at the maximum velocity; in Figure B-1 it would appear otherwise. The lag in the system has now introduced an error. The characteristic of the system above and the perfect system is shown in Figure B-2. Here the perfect system shows its expected response – a straight line. The measured response shows signs of hysteresis, but this isn't possible – a perfect, linear damper was used. The phase lag causes the apparent hysteresis through the false "measurement". A force less than the maximum was measured when the velocity was maximum, as can be seen in Figure B-1.

For this reason it is important to either use the same filters when measuring, or to use no filters at all. The latter option may not always be possible, and so some information about the filters used should be available. The CDAS used to measure the HiL and real model simulation responses, for instance, also uses internal digital filters (for anti-aliasing) that cannot be disabled, but their type and cut-off frequencies are known.

Phase lags affect HiL simulations in the same way. The force measured is not really the immediate force for a given displacement and velocity, but rather the force for circumstances a few milliseconds before. HiL has an inherent lag, which is small in comparison to the lags found in filters and measuring equipment. (If one assumes that the A/D and D/A conversions

are done on each DSP time step, then the wanted force signal lags the displacement to generate that signal with by one time step.)

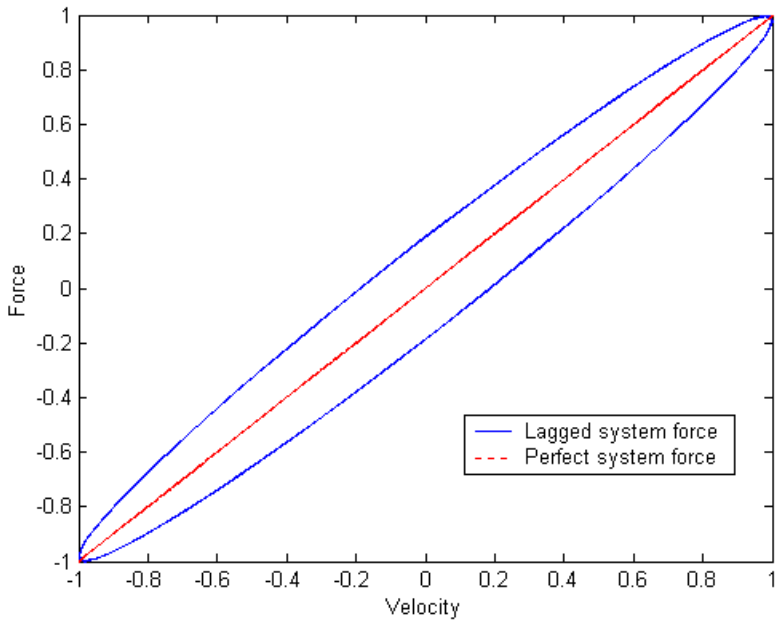

Figure B-2: Character of perfect and lagged systems

Lag is introduced into HiL simulations in various ways. The PID actuator controller introduces some phase lag even before the suspension component is excited, and facilitates control using displacement control, itself dependent on a filtered signal from the LVDT. The load cell bridge amplifier has filters, which introduce lag. Even though the effect of any one of these lags may be small, it culminates into a potentially serious situation. When using HiL one must thus always be aware of the filters and other lag sources in the system.

Another way in which phase lags complicates a system is phase distortion. The phase lag for a particular source may not be constant, but may vary with frequency. In general, low frequency excitation induces little lag, while higher frequencies are conducive to much higher lag. This means that when using signals of varying frequency, a simple shift of the measured signal to account for the phase lag induced is not viable.

Appendix C: Determination of Stick-Slip Effect

Stick-slip (also called sticktion) is a phenomenon characterised by disproportionately large resistive forces when the velocity of an object is lower than a certain break value, and much smaller resistive forces when the velocity is higher than said value. The two-degree-of-freedom motorcycle setup used in this research showed strong signs of stick-slip. While the sprung mass velocity was high there seemed to be less damping in the system than when the velocity was low. Large sprung mass overshoot resulted in some oscillation, but when the threshold level was reached, the sprung mass returned to equilibrium without any further oscillation. A small amount of overshoot was met with no oscillation, just a simple return to static equilibrium.

In an attempt to characterise the stick-slip quantitatively, elastic bands were used to support the whole setup while an impulse input was given. The response of the system was measured and analysed. The damping of the elastic bands were first characterised, and it was found that the inherent damping in the bands were negligible – a damping ratio of less than 0.01 was found. The motorcycle setup response is shown in Figure C-1.

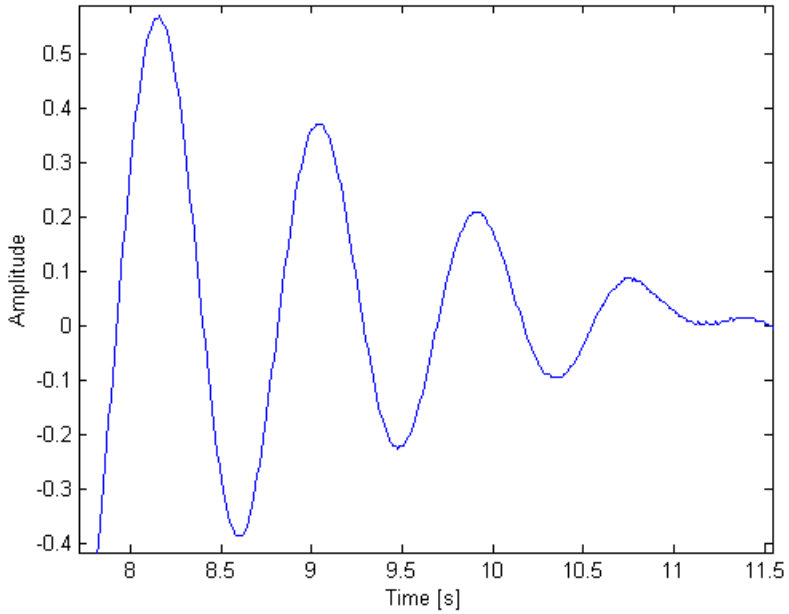

Figure C-1: Measured response of motorcycle setup suspended with elastic bands

The displacement response shown above was used to determine the damping of the system using the logarithmic decrement method. It was found that the damping as determined for the first two readings (the oscillations between the first three peaks) are about the same, i.e. a damping ratio of about 0.08. The third reading gave a damping ratio of 0.133 while the fourth gave the system's damping ratio as 0.3! This can be confirmed from Figure C-1 – the damping of the system increases as the oscillation amplitude (velocity) decreases.

The effect of stick-slip can be seen in many instances of the results shown in Chapter 4, and accounts heavily for the discrepancies in the responses. The ECOV values for the comparative measured signals are also larger than they should be because of the stick-slip. The response in Figure C-1 was measured using a sprung mass of 35 kg – higher sprung masses resulted in even higher damping ratios!

Appendix D: Derivation of Equations of Motion for Motorcycle Rear Suspension

When deriving the equations of motion for the system under investigation, it is useful to start by modelling the suspension unit and tyre as a force, and considering each body as its equivalent free-body diagram. The bearing forces and moments are omitted due to their small force contribution.

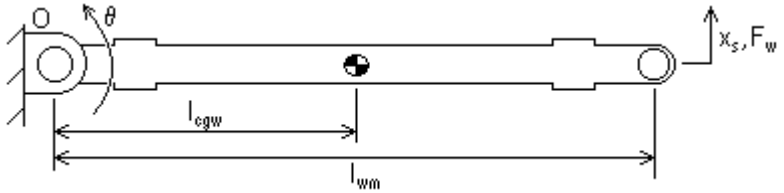

Figure D-1: Wall mounted swing arm parameters

Figure D-1 shows the parameters of importance in the wall-mounted swingarm. These are the hinge point "O", mass m_{wm}, angle of rotation θ, length l_{wm}, tip vertical displacement x_s, and tip vertical reaction force F_w. The distance to the arm's centre of mass is l_{cgw}, while the moment of inertia of the swingarm is I_{Ow}. Only the vertical components are considered, as the motion and forces sought for the sprung and unsprung masses will be vertical. However, the swingarm only rotates. The equation of motion used for the wall-mounted arm is

$$\sum M_{Ow} = I_{Ow}\alpha$$

The angle of rotation θ and the sprung mass displacement are directly proportional, thus

$$\theta = \frac{x_s}{l_{wm}} \quad \therefore \quad \ddot{\theta} = \frac{\ddot{x}_s}{l_{wm}}$$

Now the sum of the moments about the pivot point yields

$$-m_w g l_{cgw} + F_w l_{wm} = I_{Ow}\frac{\ddot{x}_s}{l_{wm}}$$

From this equation, it is possible to obtain the reactive force F_w present during the sprung mass' motion:

$$F_w = \frac{I_{Ow}\dfrac{\ddot{x}_s}{l_{wm}} + m_{wm} g l_{cgw}}{l_{wm}} = I_{Ow}\frac{\ddot{x}_s}{l_{wm}^{\,2}} + \frac{m_{wm} g l_{cgw}}{l_{wm}} \qquad (1)$$

The sprung mass is considered next; the free-body diagram is shown in Figure D-2.

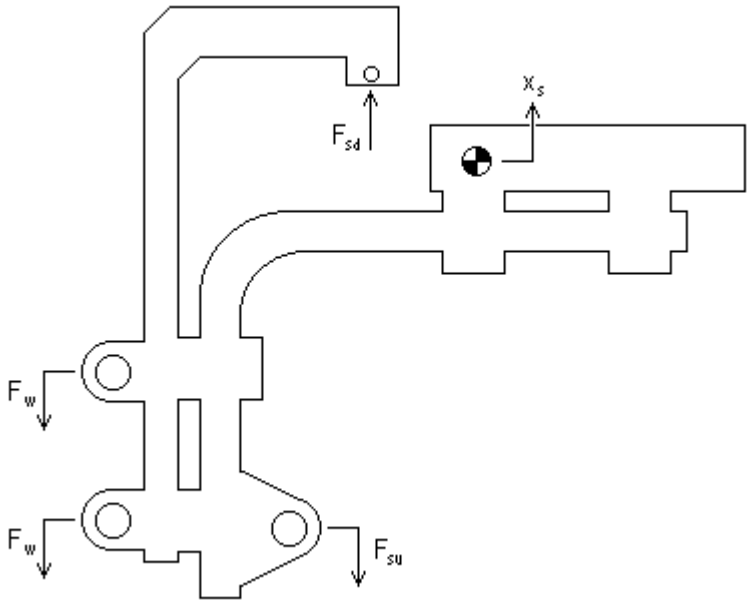

Figure D-2: Sprung mass parameters

Here, the relevant parameters are again the wall-mounted swing arm's transmitted force F_w, as well as the bearing force at the sprung-unsprung mass interface F_{su}, the force in the spring-damper suspension unit F_{sd}, the sprung mass itself, m_s, and the sprung mass displacement, x_s. A linear equation of motion is derived, as the mass is assumed to move vertically only.

Substituting all the external forces into the familiar equation of linear motion, it becomes

$$m_s \ddot{x}_s = -2F_w - F_{su} + F_{sd} - m_s g - F_{cs}$$

F_{cs} is the force introduced through the use of spring-loaded wire displacement transducers, used to measure both the sprung and unsprung mass displacements. Adding the equation for F_w, equation (1), gives

$$m_s \ddot{x}_s + 2\left[I_{Ow} \frac{\ddot{x}_s}{l_{wm}^{\,2}} + \frac{m_{wm} g l_{cgw}}{l_{wm}} \right] = -F_{su} + F_{sd} - m_s g - F_{cs} \qquad (2)$$

Equation (2) is now the equation of motion for the sprung mass.

When considering the unsprung mass, both rotation and translation occurs, meaning that two equations of motion can be derived. The unsprung mass is schematically shown in Figure D-3, and the required parameters are again x_s, F_{sd} and F_{su}, as well as the mass m_u, tyre force F_t, unsprung mass motion x_u, swingarm length l_u, and centre of mass length and displacement l_{cg} and x_{cg}. The moment of inertia of the unsprung mass swingarm about its pivot is I_O, and the moment arm of the spring-damper unit is l_{sd}.

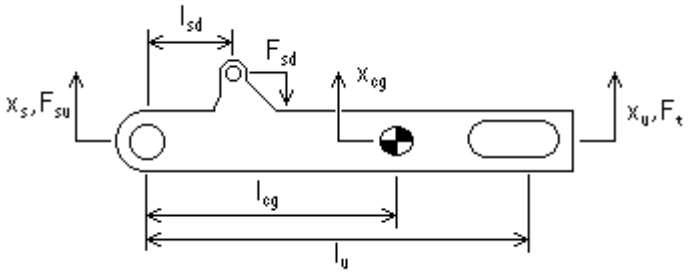

Figure D-3: Unsprung mass parameters

Using the linear equation of motion, one gets

$$m_u \ddot{x}_{cg} = F_{su} - F_{sd} + F_t - m_u g$$

However, the centre of mass displacement x_{cg} can be given as

$$x_{cg} = x_s - \frac{l_{cg}}{l_u}(x_s - x_u) = \left(1 - \frac{l_{cg}}{l_u}\right)x_s + \frac{l_{cg}}{l_u}x_u$$

thus

$$\ddot{x}_{cg} = \left(1 - \frac{l_{cg}}{l_u}\right)\ddot{x}_s + \frac{l_{cg}}{l_u}\ddot{x}_u$$

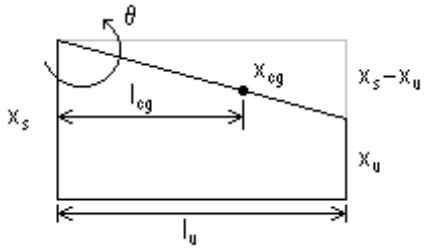

Figure D-4: Centre of mass displacement for certain x_s and x_u

Using the centre of mass displacement in terms of the sprung and unsprung displacements, the equation becomes

$$m_u\left(1 - \frac{l_{cg}}{l_u}\right)\ddot{x}_s + m_u\frac{l_{cg}}{l_u}\ddot{x}_u = F_{su} - F_{sd} + F_t - m_u g \qquad (3)$$

Using the rotational equation of motion:

$$\sum M_O = I_O\alpha + m_u\ddot{x}_{cg}l_{cg}$$

$$\theta = \frac{x_u - x_s}{l_u} \quad \therefore \quad \ddot{\theta} = \frac{\ddot{x}_u - \ddot{x}_s}{l_u}$$

$$F_t l_u - m_u g l_{cg} - F_{sd}l_{sd} = \frac{-I_0 - m_u l_{cg}l_u - m_u l_{cg}^2}{l_u}\ddot{x}_s + \frac{I_0 + m_u l_{cg}^2}{l_u}\ddot{x}_u \qquad (4)$$

From (2)

$$-\left[\ddot{x}_s\left(m_s + \frac{2I_{Ow}}{l_{wm}^2}\right) + 2\frac{m_{wm}gl_{cgw}}{l_{wm}} - F_{sd} + m_s g + F_{cs}\right] = F_{su} \qquad (5)$$

(5) into (3)

$$m_u\left(1 - \frac{l_{cg}}{l_u}\right)\ddot{x}_s + m_u\frac{l_{cg}}{l_u}\ddot{x}_u = -\left(m_s + \frac{2I_{Ow}}{l_{wm}^2}\right)\ddot{x}_s - \frac{2m_{wm}gl_{cgw}}{l_{wm}} + F_{sd} - m_s g - F_{sd} + F_t - m_u g - F_{cs}$$

$$\therefore \quad \left(m_u\left(1 - \frac{l_{cg}}{l_u}\right) + m_s + \frac{2I_{Ow}}{l_{wm}^2}\right)\ddot{x}_s + m_u\frac{l_{cg}}{l_u}\ddot{x}_u = -\frac{2m_{wm}gl_{cgw}}{l_{wm}} - (m_s + m_u)g + F_t - F_{cs} \qquad (6)$$

Get unsprung mass acceleration from (6):

$$\ddot{x}_u = \frac{l_u}{m_u l_{cg}}\left[-\left(m_u - \frac{m_u l_{cg}}{l_u} + m_s + \frac{2I_{Ow}}{l_{wm}^2}\right)\ddot{x}_s - \frac{2m_{wm}gl_{cgw}}{l_{wm}} - (m_s + m_u)g + F_t - F_{cs}\right] \qquad (7)$$

Substitute unsprung mass acceleration (7) into (4):

$$F_t l_u - m_u g l_{cg} - F_{sd} l_{sd} =$$
$$\frac{I_O + m_u l_{cg}^2}{m_u l_{cg}} \left[-\left(m_u - \frac{m_u l_{cg}}{l_u} + m_s + \frac{2I_{Ow}}{l_{wm}^2} \right) \ddot{x}_s - \frac{2m_{wm} g l_{cgw}}{l_{wm}} - (m_s + m_u) g + F_t - F_{cs} \right]$$
$$+ \frac{-I_O + m_u l_u l_{cg} - m_u l_{cg}^2}{l_u} \ddot{x}_s$$

This equation can be rewritten to obtain the sprung mass acceleration:

$$F_t \left(l_u - \frac{I_O + m_u l_{cg}^2}{m_u l_{cg}} \right) - m_u g l_{cg} - F_{sd} l_{sd} - \frac{I_O + m_u l_{cg}^2}{m_u l_{cg}} \left(\frac{-2m_{wm} g l_{cgw}}{l_{wm}} - (m_s + m_u) g - F_{cs} \right) =$$
$$\left[\frac{-I_O + m_u l_u l_{cg} - m_u l_{cg}^2}{l_u} - \frac{I_O + m_u l_{cg}^2}{m_u l_{cg}} \left(m_u - \frac{m_u l_{cg}}{l_u} + m_s + \frac{2I_{Ow}}{l_{wm}^2} \right) \right] \ddot{x}_s$$

Let

$$M_1 = \left[\frac{-I_O + m_u l_u l_{cg} - m_u l_{cg}^2}{l_u} - \frac{I_O + m_u l_{cg}^2}{m_u l_{cg}} \left(m_u - \frac{m_u l_{cg}}{l_u} + m_s + \frac{2I_{Ow}}{l_{wm}^2} \right) \right]$$

and

$$F_1 = -m_u g l_{cg} + \frac{\left(I_O + m_u l_{cg}^2\right) g}{m_u l_{cg}} \left(m_s + m_u\right) + \frac{2m_{wm} g l_{cgw} \left(I_O + m_u l_{cg}^2\right)}{l_{wm} m_u l_{cg}} + \frac{F_{cs} \left(I_O + m_u l_{cg}^2\right)}{m_u l_{cg}}$$

$$G_1 = l_u - \frac{I_O + m_u l_{cg}^2}{m_u l_{cg}}$$

$$G_2 = l_{sd}$$

to obtain the sprung mass equation of motion

$$\boxed{M_1 \ddot{x}_s = F_1 + G_1 F_t - G_2 F_{sd}}$$

This equation can be substituted into equation (7) for the unsprung mass acceleration:

$$\ddot{x}_u = -\frac{l_u}{m_u l_{cg}} \left(m_u - \frac{m_u l_{cg}}{l_u} + m_s + \frac{2I_{Ow}}{l_{wm}^2} \right) \left(\frac{F_1 + G_1 F_t - G_2 F_{sd}}{M_1} \right)$$
$$- \frac{l_u}{m_u l_{cg}} \left[\frac{2m_{wm} g l_{cgw}}{l_{wm}} - (m_s + m_u) g + F_t - F_{cs} \right] \qquad (8)$$

Rewriting equation (8) into a more manageable form:

$$\frac{m_u l_{cg}}{l_u}\ddot{x}_u = \left[-\left(m_u + m_s - \frac{m_u l_{cg}}{l_u} + \frac{2I_{Ow}}{l_{wm}^{\ 2}}\right)\frac{F_1}{M_1} - \left(\frac{2m_{wm} g l_{cgw}}{l_{wm}} + (m_s + m_u)g + F_{cs}\right)\right]$$

$$- F_t\left(\frac{\left(m_u + m_s - \frac{m_u l_{cg}}{l_u} + \frac{2I_{Ow}}{l_{wm}^{\ 2}}\right)\left(lu - \frac{I_O}{m_u l_{cg}}\right)}{M_1} - 1\right) + F_{sd}\left[\frac{l_{sd}}{M_1}\left(m_u + m_s - \frac{m_u l_{cg}}{l_u} + \frac{2I_{Ow}}{l_{wm}^{\ 2}}\right)\right]$$

Now let

$$M_2 = \frac{m_u l_{cg}}{l_u}$$

and

$$F_2 = \left[-\left(m_u + m_s - \frac{m_u l_{cg}}{l_u} + \frac{2I_{Ow}}{l_{wm}^{\ 2}}\right)\frac{F_1}{M_1} - \left(\frac{2m_{wm} g l_{cgw}}{l_{wm}} + (m_s + m_u)g + F_{cs}\right)\right]$$

$$G_3 = -\left(m_u + m_s - \frac{m_u l_{cg}}{l_u} + \frac{2I_{Ow}}{l_{wm}^{\ 2}}\right)\left(lu - \frac{I_O}{m_u l_{cg}}\right)\frac{1}{M_1} + 1$$

$$G_4 = \frac{l_{sd}}{M_1}\left(m_u + m_s - \frac{m_u l_{cg}}{l_u} + \frac{2I_{Ow}}{l_{wm}^{\ 2}}\right)$$

This gives the unsprung mass equation of motion

$$\boxed{M_2\ddot{x}_u = F_2 + G_3 F_t + G_4 F_{sd}}$$

The forces F_t and F_{sd} are dependent on various parameters; in general,

$$F_t = f(x_u, x_r, \dot{x}_u, \dot{x}_r)$$

$$F_{sd} = f(x_s, x_u . \dot{x}_s, \dot{x}_u)$$

where x_r is the road (input) excitation.

Two equations have now been derived, which will be used in the simulations. The external forces due to motion will be multiplied by a gain, given by G_1 to G_4, and the effective masses and body external forces are given by M_1, M_2, F_1 and F_2. These gains, masses and forces will be constant for a certain set of parameters, and can be determined before the simulation starts. It can thus be seen that the implementation of the equations of motion is similar to that of a linear 2DOF system.

The parameters used in this study are now discussed. Determining the mass of all the constituents of the system was the first task – this was done using a relatively small load cell (1000N) and an analogue bridge amplifier, a HBM amplifier, model KWS. The load cell was first calibrated using known weights, which was double-checked using the MGC, and the component weights were then measured. The load cell was also used to determine the centre of gravity of the components, due to the fact that the load cell, when measuring the tension in a light cable, will read a value identical to the mass of the component when the cable tension force is applied at the centre of gravity. Thus, the two rotational components (the wall-mounted and unsprung mass swing arms) had their centres of gravity determined in this fashion. The centre of gravity of the unsprung mass swingarm was adjusted mathematically to account for the mass of the wheel with the equation

$$l_{com} \times \sum m_i = \sum (l_i m_i)$$

where m_i is the individual component masses, l_i is the distance to the component's centre of mass, and l_{com} is the distance to the assembly's centre of mass.

The centre of gravity of the wall-mounted arm was determined to be midway between its connecting bearings, which is obvious from its symmetric layout. Table D-1 has the results of the characterising tests.

The sprung mass has four fixtures that are used to secure additional mass to the assembly. These fixtures were weighed separately, as well as the additional mass added. The sprung mass can thus be changed to suit the test/purpose. The weight of any connecting bolts, washers and nuts are included in the relevant assembly mass.

Table D-1: System component masses

Component	KWS Reading	Mass [kg]
Wheel and tyre	-285	6.64
Wall-mounted swingarm	-509	11.86
Sprung mass Fixture	-92	2.14
"ProLink" Swingarm plus two bearings	-250	5.82
Sprung mass assembly minus 4 fixtures	-1371	32.0
Bearing (each)		1.45
Swingarm mass		2.93
Sprung mass with 10kg ballast		53.42
Notes: Bearing mass taken from catalogue KWS reading times -0.0233 gives mass in kg Wheel and tyre mass excludes spindle mass		

The moment of inertia of a body can be determined if the body's centre of gravity, natural frequency of its pendulum motion and its mass are known. This follows from the general pendulum equation of small motion

$$I_O\ddot{\theta} + mgd_{cg}\theta = 0$$

which yields the natural frequency of

$$\omega_n = \sqrt{\frac{mgd_{cg}}{I_O}}$$

Rewriting in a suitable form, the equation gives the moment of inertia as

$$I_O = \frac{mgd_{cg}}{\omega_n^{\,2}}$$

Here, I_O is moment of inertia about its pivot point, and d_{cg} is the distance form said point to the centre of gravity. The moments of inertia of the wall-mounted and unsprung mass arms were determined in this fashion – the results are given in Table D-2.

To determine the friction in the bearings used, and the friction they caused, the logarithmic decrement was again employed. The bearings were held so that the relevant swingarm could rotate freely below it; the successive rotation angles, θ, were then determined, as well as the time to complete three oscillations. This gave the damping of each bearing, as well as the (damped) natural frequency as used in Table D-2. Each test was performed at least three times to gain consistent results.

Table D-2: System swingarm moments of inertia

Swingarm	Total mass [kg]	d_{cg} [m]	ω_n [radians/s]	I_{Hinge}
Wall mounted (per pair)	11.86	0.41	3.85	3.22
Unsprung	9.9	0.43	5.33	1.47

Table D-3: Swingarm properties

	Unsprung	Wall mount
θ_{Start}	36.9°	37°
θ_1	33.6°	37°
θ_2	30.7°	36.9°
δ_1	0.095	-
δ_2	0.090	-
δ_{Ave}	0.092	-
ζ	0.015	0
Times [s]	3.53 3.55 3.53 4.97	4.88 4.91 4.83 -
T_{ave}	3.54 s	4.90 s
τ_{damped}	1.18 s	1.63 s
$\tau_{natural}$	1.18 s	1.63 s
ω_n	5.33 rad/s 0.85 Hz	3.85 rad/s 0.63 Hz

As can be seen from Table D-3, the damping in the bearings has very little influence on the system, and their omission in the equation of motion derivation is justified.

The parameter values determined in this section were used in the software Simulink model to be implemented in the HiL simulation. Some detail is necessary, since a lack thereof may cause large differences between the measured HiL and real motorcycle tests, leading to an erroneous conclusion that HiL isn't suited to complex geometry systems, or that geometric non-linearities (as accounted for by the small angle assumption) causes the method to fail.